MODELLING NUCLEOCYTOPLASMIC TRANSPORT WITH APPLICATION TO THE INTRACELLULAR DYNAMICS OF THE TUMOR SUPPRESSOR PROTEIN P53

Luna Dimitrio

Université Pierre et Marie Curie — Università Sapienza

Modelling nucleocytoplasmic transport with application to the intracellular dynamics of the tumor suppressor protein p53

Ph.D. Thesis

by

Luna Dimitrio

In Partial Fulfillment of the Requirements
the Degree of Doctor of Philosophy of

L' UNIVERSITÉ PIERRE ET MARIE CURIE - Paris VI

Spécialité : Mathématiques Appliquées

and

L' UNIVERSITÀ SAPIENZA

Indirizzo : Modelli e Metodi Matematici per le Scienze Applicate

Thesis defended on the 5^{th} September 2012 in front of the committee composed by:

Jean Clairambault	Supervisor
Roberto Natalini	Supervisor
Pierre Magal	Reviewer
Luigi Preziosi	Reviewer
Mark Chaplain	Jury member
Robin Fåhraeus	Jury member
Marcelle Kaufman	Jury member
Benoît Perthame	Jury member

DIPARTIMENTO DI
SCIENZE DI BASE E APPLICATE PER L' INGEGNERIA
SEZIONE DI MATEMATICA

Thèse préparée au sein de l'équipe-projet BANG
Centre de Recherche INRIA Paris-Rocquencourt
Domaine de Voluceau, BP 105
78153 Le Chesnay CEDEX
Tesi preparata presso il dipartimento SBAI
Sezione di Matematica
Via Antonio Scarpa 16
00161-Roma

Acknowledgements

I am glad to have the opportunity to thank all the members of my Ph.D. committee, Professors Mark Chaplain, Robin Fåhraeus, Marcelle Kaufman, Benoît Perthame, and my referees Professors Alberto Gandolfi, Pierre Magal and Luigi Preziosi. I am heartily grateful to all of them for having accepted to be part of my Ph.D. committee, for the time spent on my manuscript and for the time taken to travel to Paris, or simply to Jussieu! I want to thank especially Professors Alberto Gandolfi, Robin Fåhraeus and Luigi Preziosi for the helpful discussions and comments about my work. Finally I also want to thank them for the time spent to read all my emails...

Remerciements

J'ai decidé de faire mes remerciements en français et en italien. Car cette thèse s'est passée entre la France et l'Italie , entre le francąis et l'italien, et surtout avec les personnes qui habitent ces deux Pays, si chers pour moi.

Tout d'abord, j'adresse mes remerciements à mon directeur de thèse à Paris, Jean Clairambault. Je le remercie de m'avoir donné la possibilité de travailler entre Rome et Paris, enrechissant ainsi mon bagage culturel. Je le remercie de m'avoir « initié» à la p53, et de m'avoir incité à travailler sur ce sujet, malgré mes craintes d'aborder une thématique si complexe mais, sans aucun doute, stimulante. Je le remercie aussi pour sa présence constante, sa disponibilité et sa patience. Finalement, un grand merci pour avoir apprecié, à plusieurs reprises, les produits et le soleil italien ! En tant qu'étrangère à Paris, cela m'a fait un grand plaisir !

Un merci de tout mon cœur aux amis et collegues du batîment 16 ! Je tient à remercier toutes les personnes qui sont passées par le batîment, depuis le début de ma cotutelle. L'histoire de ces années de thèse a été écrite en grande partie grâce à vous ! Merci pour les conseils, les discussions scientifiques, mais aussi pour le soutien, l'écoute et les verres bus ensemble !

Aussi, je veux remercier les doctorants du LJLL pour le nombreux conseils scientifiques, pour l'aide et le soutien en fin de parcours. Un grand merci à tout le laboratoire, pour la belle et accueillante ambiance qui m'a accompagné pendant deux ans. Merci pour les pauses cafés, les conseils et les discussions. Et de l'aide qui m'a été donné à plusieurs reprises !

Merci aux Italiens à Paris, avec lesquelles j'ai partagé des dîners inoubliables autour des discussions sur la bouffe italienne et sur le soleil qu'on voit pas à Paris. Malgré si, en fin, on reste tous ici ! Merci aussi aux français et aux allemands (...) qui ont rejoint ces dîners et qui ont rendu cet histoire de trois ans (plus ou moins...) si précieuse.

Merci à tout ceux qui ont fait une partie de ce chemin avec moi et à ceux qui ont transformé ces rencontres en amitiés speciales.

Pour terminer, je fais un gros calin à mon père, qui est sûrement en partie responsable de ce choix «français» ! Merci à Angela pour les recettes au téléphone (et les repas à la maison !) à Sara pour être venue me voir et à Deanna pour le bonheur qu'elle a amené à la famille.

Ringraziamenti

Vorrei poter includere in questi ringraziamenti tutte le persone che ho incontrato in questi anni e che hanno condiviso con me una parte, anche se piccola, di questo lungo, interessante, entusiasmante percorso di crescita professionale e personale. Per non rischiare di dimenticare nessuno, ringrazierò qui solo le persone senza le quali questa tesi non sarebbe proprio esistita!

Per primo, ringrazio il mio primo (in ordine temporale) direttore di tesi, Roberto Natalini. Lo ringrazio innanzitutto per avermi proposto un tema di ricerca che mi ha appassionato in questi anni e che sono riuscita a fare mio. E per avermi guidato su questo progetto scientifico con attenzione e pazienza. Da un punto di vista meno scientifico, lo ringrazio per tutto il suo sostegno, di cui ho avuto bisogno in questi anni passati tra Roma e Parigi e in questi ultimi mesi in particolare. Infine lo ringrazio per quel pallino sempre verde di gtalk che ha rappresentato un'ancòra di salvezza più di una volta!

Ringrazio il MeMoMat, i Professori e i Dottorandi, senza il quale questo percorso non avrebbe avuto inizio.

E in ultimo, ringrazio la mia famiglia che mi ha sostenuto moralmente (ma anche economicamente!) e che ha sempre creduto in me. Ringrazio per primi e in particolare i Dileonardelli, che ci sono SEMPRE e OVUNQUE: al telefono, dal vivo, in Italia o in Francia, insomma dove serve. Ma anche zie, zii, nonni e cugini che sono il mio tesoro più grande e più vero. Un forte abbraccio ai nonni per il loro sostegno ed entusiasmo nei miei progetti. Un grazie speciale a Nonno Franco per i suoi saggi consigli e perché mi è sempre vicino.

Ringrazio anche le mie amiche più strette (loro si riconosceranno), con cui condivido tutto che mi hanno incoraggiato e sostenuto nelle scelte di questi ultimi anni.

Abstract

In this thesis, I discuss two main subjects coming from biology and I propose two models that mimic the behaviours of the biological networks studied.

The first part of the thesis deals with intracellular transport of molecules. Proteins, RNA and, generally, any kind of cargo molecules move freely in the cytoplasm: intracellular transport as a consequence of Brownian motion is classically modelled as a diffusion process. Some specific proteins, like the tumour suppressor p53, use microtubules to facilitate their way towards the nucleus. Microtubules are a dense network of filaments that point towards the cell centre. Motor proteins bind to these filaments and move along, bearing a cargo bound to them. I propose a simplified bi-dimensional model of nucleocytoplasmic transport taking into account the kinetic processes linked to microtubule transport. Unlike in other models we know, I represented the position of a single MT filament. This model is given by a system of partial differential equations which are cast in different dimensions and connected by suitable exchange rules. A numerical scheme is introduced and several scenarios are presented and discussed to answer to the question of which proteins benefit from microtubule transport, depending on their diffusion coefficients.

In the second part of the thesis, I design and analyse a physiologically based model representing the accumulation of protein p53 in the nucleus after triggering of the sentinel protein ATM by DNA damage. The p53 protein plays an essential role in the physiological maintenance of healthy tissue integrity in multicellular organisms (regulation of cell cycle arrest, repair pathways and apoptosis). Firstly, I developed a compartmental ODE model to represent the temporal dynamics of the protein. Since the p53 protein is known for its oscillatory behaviour, I performed a numerical bifurcation study to verify the existence, in the model, of stable periodic solutions. Next, I have expanded the model by the addition of a spatial variable and analysed the spatio-temporal dynamics of p53. After checking the existence of oscillations in the spatial setting, I have analysed the robustness of the system under spatial variations (diffusion and permeability coefficients, cell shape and size).

Keywords: Mathematical Models, Cellular biology, Intracellular dynamics, Partial Differential Equations, Signalling Pathways, p53

Riassunto

In questa tesi ci interessiamo a due diversi sistemi biologici, per ciascuno dei quali introduciamo un modello matematico, al fine di riprodurne il comportamento.

Nella prima parte della tesi, ci interessiamo al trasporto intracellulare. Proteine, RNA e, in generale qualsiasi tipo di cargo si muove liberamente nel citoplasma: il trasporto intracellulare come conseguenza del moto browniano viene classicamente modellizzato come un processo di diffusione. Alcune specifiche proteine, come la proteina soppressore del tumore p53, utilizzano, oltre alla diffusione, il trasporto lungo i microtuboli. I microtubuli costituiscono una fitta rete di filamenti che si espande nel citoplasma in modo radiale da un punto situato vicino al nucleo della cellula. Alcune proteine, dette proteine motore, si legano a questi filamenti e li percorrono trasportando un carico che rilasciano in prossimità del nucleo. Per rappresentare questo tipo di comportamento, proponiamo un modello di trasporto bidimensionale tenendo conto dei processi cineteci legati al trasporto lungo i microtubuli. Rispetto ad altri modelli della letteratura, definiamo la posizione di un singolo filamento. Il nostro modello è composto da un sistema di equazioni differenziali, definite su più dimensioni e accoppiate attraverso appropriate regole di scambio. Introduciamo uno schema numerico attraverso il quale simuliamo diversi scenari per cercare di capire quali proteine possono trarre beneficio dal trasporto lungo i microtubuli, a seconda del loro coefficiente di diffusione.

Nella seconda parte della tesi, introduciamo ed analizziamo un modello, basato sulla fisiologia, che rappresenta l'accumulo della proteina p53 nel nucleo dopo l'attivazione di ATM, dovuta a danni subiti dal DNA. La proteina p53 gioca un ruolo essenziale nel mantenimento dei tessuti sani e dell'integrità degli organismi pluricellulari (regolazione dell' arresto del ciclo cellulare, dei processi di riparazione e di apoptosi). In primo luogo, sviluppiamo un modello ODE a compartimenti per descrivere le dinamiche temporali della proteina. Poiché la proteina p53 è nota per il suo comportamento oscillatorio, svolgiamo, numericamente, un'analisi delle biforcazioni del sistema, in modo da verificare l'esistenza, per il nostro modello, di una soluzione periodica stabile. Successivamente, espandiamo il modello aggiungendo la variabile spaziale, cosa che ci permette di analizzare la dinamica spazio-temporale di p53. Verifichiamo l'esistenza di oscillazioni nel contesto spaziale e analizziamo la robustezza del sistema rispetto a variazioni dei parametri spaziali (coefficienti di diffusione, di permeabilità, dimensioni della cellula).

Parole chiave: Modelli Matematici, dinamiche intracellulari, equazioni differenziali alle derivate parziali, pathways di segnalazione, p53.

Résumé

Dans cette thèse, je me suis intéressée à deux systèmes biologiques différents, pour chacun desquels j'ai introduit un modèle mathématique, afin d'en reproduire les comportements observés expérimentalement.

Dans la première partie de cette thèse, j'ai étudié le transport intracellulaire des molécules. Les protéines, les ARN et, en général, tout type de molécule-cargo, se déplacent librement dans le cytoplasme : le transport intracellulaire à la suite du mouvement brownien est classiquement modélisé comme un processus de diffusion. Certaines protéines, telles la protéine p53 'suppresseur de tumeur', utilisent, en plus de la diffusion, le transport le long des microtubules. Les microtubules forment un réseau dense de filaments dans le cytoplasme qui s'étend radialement à partir d'un point situé près du noyau de la cellule. Certaines protéines, connues sous le nom de protéines motrices, se lient à ces filaments et les parcourent longitudinalement en transportant une cargaison qu'elles relâchent près du noyau. Pour représenter ce type de comportement, je propose un modèle de transport à deux dimensions qui prend en compte les processus cinétiques liés au transport le long des microtubules. Comparé à d'autres modèles connus de la littérature, je précise la position d'un filament unique. Ce modèle est composé d'un système d'équations différentielles définies en plusieurs dimensions et couplées par des appropriées règles d'échange. J'introduis ensuite un schéma numérique à l'aide duquel je résous plusieurs scénarios dont les résultats sont présentés et discutés dans cette partie. Le but de ces différentes simulations est de mieux comprendre quelles protéines peuvent bénéficier du transport le long des microtubules, en fonction de leur coefficient de diffusion.

Dans la deuxième partie de la thèse, j'introduis et j'analyse mathématiquement un modèle, basé sur la physiologie, qui représente l'accumulation de la protéine p53 dans le noyau après activation de l'ATM par des dommages à l'ADN. La protéine p53 joue un rôle essentiel dans le maintien de l'intégrité des tissus sains dans les organismes multicellulaires (régulation des processus d'arrêt du cycle cellulaire, de réparation et apoptose). En premier lieu, j'ai développé un modèle EDO par compartiments pour décrire la dynamique temporelle de la protéine. Puisque la protéine p53 est connue pour son comportement oscillatoire, j'ai procédé à une analyse théorique et numérique des bifurcations du système, afin de vérifier l'existence dans le modèle de solutions périodique stables. Par la suite, j'ai étendu le modèle en ajoutant une variable d'espace, ce qui permet d'analyser la dynamique spatio-temporelles de p53. Vérifiant l'existence d'oscillations dans un contexte spatial, j'ai examiné la robustesse du système par rapport aux variations des paramètres spatiaux (coefficients de diffusion et de perméabilité, forme et taille des cellules).

Mots-clés: modèles mathématiques, dynamique intracellulaire, équations aux dérivées partielles, voies de signalisation, p53.

Contents

Introduction

Nowadays, biology increasingly needs mathematical models to simulate phenomena which occur on a microscopic scale. Mathematics provides the main framework to collect and organize data. Furthermore, mathematical models can be used to test and suggest new models that can explain biological phenomena. Mathematical systems can also provide clues for experimental studies, based on the model results.

In this Thesis we will work on some biological problems, approaching them from a mathematical point of view. In particular, we will focus our attention on problems related to the dynamics of biological pathways at the single cell level.

Signals and space

In biology, a signalling pathway is a process by which one or more molecules pass a signal within the cell. For example, an external stimulus received by the secretion of hormones or other chemical factors, must be transduced through the cell in order to obtain a change in cell function. Also internal signals, like a damage signal, must be translated and produce a cellular response, like promoting repair mechanisms or activating mitosis or apoptosis. All these different signals are transmitted through pathways which consist in a series of chemical reactions. Enzymes catalyse these reactions and produce molecular modifications of their substrates. Biological pathways may be elaborate since they may involve several proteins or may be activated by different stimuli. We report, in Figure 1, a generic example of pathway induced by an external stimulus.

If we look at the current modelling literature that faces problems of signalling pathways, the main method used to explore the subject is based on the analysis of the temporal dynamics of the network [56, 105, 115]. In these models, the cell is commonly represented as a homogeneous environment where proteins and enzymes are distributed everywhere. Therefore, the reactions between proteins can occur at each point of the cell and the localization of processes is not taken into account. This approach corresponds to the use of ordinary differential equations, that allow the analysis of the temporal evolution of complexes systems. Indeed, ODEs can be quite easily treated numerically. Therefore large ODE systems, modelling complex networks, can give some insights about the possible cellular responses. Sometimes, of course, qualitative properties of those systems can be investigated also analytically.

In recent years, however, more and more studies have revealed the importance of dealing with problems of intracellular signalling considering their evolution both in space

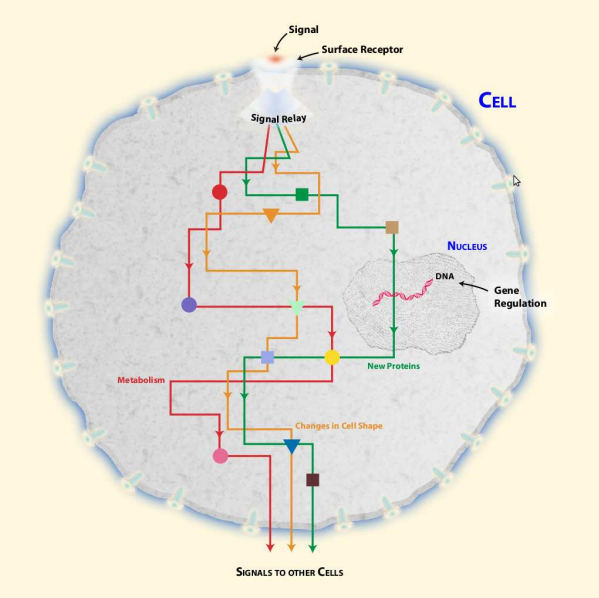

Figure 1: Biological pathways. ©National Human Genome Research Institute

and time.

Emerging evidences of the spatial organizations of enzymatic reactions and the spatial gradients that can arise, were recently discussed [4, 64]. A relevant example is signal transduction: a signal arrives at the cytoplasmic membrane and, often by phosphorylation cascades, must be transmitted over long distances, for instance to the nucleus [101]. Meyers *et al.* proved through mathematical modelling, that cell signalling pathways can be turned on and off in response to changes in cell shape and size [88]. Indeed, when dealing with activators (i.e. kinases) bound to the plasma membrane, versus cytoplasmic de-activator (i.e. phosphatases), cell growth leads to a decreased proximity to the activator and the substrate is deactivated. This type of gradients have been experimentally observed by Nalbant *et al.* [94]. Cell polarization due to protein gradients and propagation of fronts can also explain cell motility, as it has been shown in [92]. We also refer to the works of Veglio *et al.* [133] and of Goehring *et al.* [42] that deal with cell polarization. The spatial features of intracellular signalling that can explain such global behaviours, as cell motility, are thus becoming an attractive subject of study.

In this Thesis we follow this line of research and will consider intracellular phenomena as spatially localised.

The main contributions of this Thesis

This work is divided into two parts. In the first part we deal with transport of proteins towards the nucleus. We are interested, on the one hand, in the import pathway that allows molecules to access the nucleus. On the other hand, we want to test which proteins may benefit of active transport through *motor proteins* that walks along the

cell cytoskeleton, in particular along microtubules. A few models exist that treat each of these subjects, together or separately, as [15, 28, 29, 121, 122]. We introduce a new model and analyse various possible scenarios by numerical simulations.

In the second part of this work we focus on the cycle of a specific nuclear protein, the tumour suppressor factor p53. Also in this case, there are some mathematical models that reproduce the temporal dynamics of the p53. Very recently, Sturrock *et al.* begin to investigate the spatial dynamics of the protein [128, 129]. Here, we propose a new model that accounts for localizations of the reactions and directionality of transport. We approach it at two different levels. We study the temporal dynamics of the network through a compartmental system of ordinary differential equations. This let us analyse different scenarios, the existence of bifurcations and test the validity of our model in a simpler way. Then, we introduce the spatial variable and we propose a numerical analysis of the response of the system over variations of the spatial constraints.

In the following of this introduction we detail further the themes approached in this thesis, we summarize the principal results and we give a sketch of the methods we used to obtain them. We will stick to the essential information with the purpose to present only the main ideas and contributions of this work.

Part I - Nucleocytoplasmic transport

First we investigated the cellular transport from two different points of view. We considered proteins that are directed to the nucleus and we took into account the pathway necessary to their import. We also considered the embedded structural support that the cell provides, represented by the cytoskeleton.

The signalling pathway that allows molecules to access the nucleus has been by now identified. Molecules having a molecular mass larger than $\sim 40kDa$ are actively transported into the nucleus, by means of chaperones that carry through the nuclear membrane the proteins that are too big to passively diffuse through the pores of the nuclear envelope (Nuclear Pores). This process is based on a complex signalling pathway that 1) controls which proteins are imported into the nucleus, 2) dictates the directionality of transport and 3) supplies the energy necessary for active transport.

Before gaining the access to the nucleus, nuclear proteins have to diffuse within the cytoplasm, covering large distances, in order to approach to the nuclear membrane. This is because proteins are synthesised by ribosomes, that are located in a homogeneous manner within the cytoplasm. The localization of molecules within the cytoplasm is partially handled by the cytoskeleton of the cell. Depending on protein molecular mass, the mobility of a molecule can be highly reduced. Therefore the cytoskeleton of the cell represents a structural support for proteins displacements. The cytoskeleton is composed by two main kinds of filaments: actin filaments and microtubles. Microtublules are organized in a radial network that span the whole cytoplasm and has its centre next to the nucleus. Large proteins, organelles and viruses are known to use microtubules as a high-road to move faster in the cytoplasm.

So, In the first part, we try to understand if this microtubules transport is effective

and also which proteins, among those supposed to move towards the cell nucleus, may benefit of transport along microtubules. To do this, we propose a model that take into account a generic cargo protein that is able to diffuse and to bind to motor proteins that walk along the microtubule. Let $\Omega = \Omega_c \cup \Omega_n$ be a rectangular domain, divided into two sub-domains, as in Figure 2. Let us consider Ω_c as the cytoplasmic domain and Ω_n as the nuclear one. Let us suppose Ω_c thin enough to contain a unique microtubule filament.

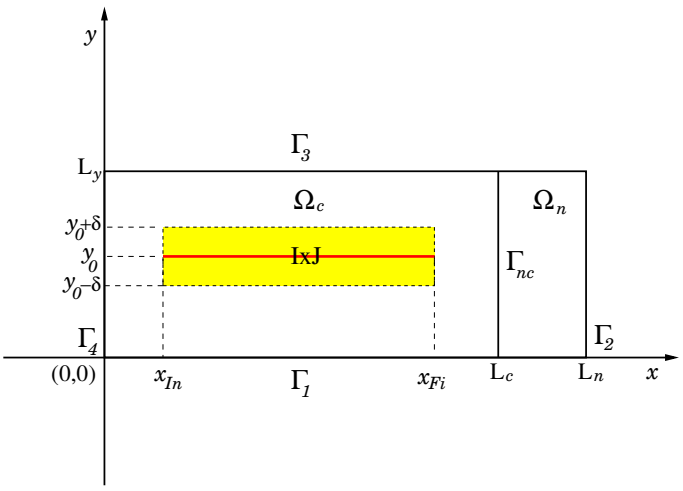

Figure 2: Area of the cell where intracellular transport is modelled: $\Omega_c \cup \Omega_n$, cytoplasm and nucleus. $\Gamma_{nc} = \partial\Omega_c \cap \partial\Omega_n$ is the common boundary of the two compartments. The yellow rectangle ($\mathbf{I} \times \mathbf{J} = [x_{In}, x_{Fi}] \times [y_0 - \delta, y_0 + \delta]$) represents the attraction area of the microtubule filament, the red strip is the microtubule, positioned in y_0.

We localize the microtubule by defining an *attraction area* where proteins can bind to it, that we coloured in yellow in figure 2. Let us introduce the following variables: let u be the concentration of the free cargo protein, v the concentration of cargo bound to the motor protein and W the complex cargo+motor protein bounded to the microtubule. We cast u and v in two dimensions and we suppose that both species are able to freely diffuse. On the other hand, we consider W in one-dimension and we suppose that it moves exclusively by transport, towards the nuclear compartment. We suppose that the exchange between different species is regulated by kinetic reactions that we model using the Mass Action Law. Under the previous assumptions, the u and v species satisfy a reaction-diffusion equation, while W is controlled by a convection equation modelling the

transport along the microtubule with a steady velocity $c > 0$. Our model reads:

$$\begin{cases} \dfrac{\partial u}{\partial t} = d_u \Delta u - ku + k_- v, & \text{in } \Omega_c, \\ \dfrac{\partial v}{\partial t} = d_v \Delta v + ku - k_- v - k_1 v \mathbb{1}_{\mathbf{IxJ}} + k_{-1} w \frac{\mathbb{1}_{\mathbf{IxJ}}}{|\mathbf{J}|} \\ \qquad\qquad + cW(x_{Fi})\delta_0(x - x_{Fi}, y - y_0), & \text{in } \Omega_c, \\ \dfrac{\partial W}{\partial t} + c\dfrac{\partial W}{\partial x} = -k_{-1} W + k_1 \int_{\mathbf{J}} v dy, & \text{in }]x_{In}, x_{Fi}[. \end{cases} \tag{1}$$

Here d_u and d_v are the diffusion coefficients of the diffusive species and the k, k_-, k_1, k_{-1} are the kinetic constant of the reactions. More details about the notations and the choice of parameters will be given in Section 2.1.2. The equations assure the conservation of the mass. We impose periodic boundary conditions on the long sides of the domain and we close the system by imposing the boundary conditions:

$$\begin{cases} \dfrac{\partial u}{\partial n} = 0, \ \dfrac{\partial v}{\partial n} = 0, & \text{on } \Gamma_4, \\ d_u \dfrac{\partial u}{\partial n} + p_u u = 0, \ d_v \dfrac{\partial v}{\partial n} + p_v v = 0, & \text{on } \Gamma_{nc}, \\ w(x_{In}) = 0. \end{cases} \tag{2}$$

By this boundary conditions we suppose that on Γ_4 (the *plasma* membrane) no flux is allowed, while on Γ_{nc} (the *nuclear* membrane) there is a flux proportional to the species concentration. We developed a numerical approximation scheme based on finite differences. We tested the accuracy of the proposed scheme and we analysed, by numerical simulations, different possible scenarios.

Principal results

System (1)-(2) is defined only on the domain Ω_c. This is because, as a first step, we were interested in understanding which molecules increase their flow in the direction of the nucleus, if transport along microtubules is allowed. We differentiated *molecules* by their *diffusion coefficient*, while the velocity along the microtubules is fixed and is the same for every molecule, since it depends on the speed of motor proteins. We also considered different detachment rates from the microtubule, in order to quantify the increase on the total flow with respect to the ability of the molecule to stay *on* the microtubule. We found, as expected, that the longer the cargo is bound to the microtubule, and the lower its diffusive mean time, the higher flow towards the nucleus is observed. Thus the benefit of microtubule transport depends on the mobility of the cargo, expressed by its diffusion coefficient, and on its capability to attach and stay on the filament. We found that the delivery towards the nucleus is enhanced for proteins having a diffusion coefficient $< 6\mu m^2 s^{-1}$ (which corresponds to a mass of about $200kDa$ [55]), if the detachment rate is low enough. More technical and quantitative details about our results, as well as several figures of our simulations, can be found in chapter 2.

As a next step, we considered the whole pathway of nuclear import, thus inscribing our model in the bi-compartmental domain $\Omega_c \cup \Omega_n$ represented in Figure 2. The model of the import pathway that we used in this thesis and that we do not detail here for sake of simplicity, has been proposed by Cangiani *et al.* [15]. Unlike the model in [15], where the transport along microtubules is described by a vector field, we coupled this model with system (1) and the result is a system of eight reaction-diffusion equations cast in two dimension and coupled with the one-dimensional convection equation of system (1). It is important to say that the boundary conditions expressed in (2) changes in the new model. On Γ_{nc}, the flux of u and v is set to zero, since by now, only the imported molecules traverse the nuclear membrane. In order to be imported, proteins have to bind to a chaperone (*importin protein*) and only the complex cargo+importin is able to traverse the nuclear membrane Γ_{nc}. Furthermore, the coupling of the two models has been done supposing that the cargo u binds exclusively to the motor protein (giving v) or to the importin protein. Using these different boundary conditions we observed that the cargo concentration that accumulates inside the nucleus is lower when the cargo proteins are transported along the microtubule. Indeed, since the cargo can be carried on the microtubule, or outside the cytoplasm by different carriers, a competitive mechanism is established and the import of the cargo is delayed. Only proteins having a very low mobility ($> 1\mu m^2 s^{-1}$) benefit of enhanced transport towards the nuclear membrane. These results are detailed and discussed in chapter 3.

Part II - The protein p53

In the second part of the Thesis we introduced a model for a specific cargo protein, called "p53". This protein is known for its biological relevance in cell survival. Indeed, when a damage to DNA is detected, p53 is activated. This protein has multiple roles but in general, one can say that it acts as a controller. Indeed, p53 blocks the cell cycle in order to avoid cell division, starts reparation pathways and, if needed, triggers apoptosis (*cell suicide*).

The protein p53 is a nuclear protein. When it is in an active state, it accumulates in the nucleus, where acts as a transcription factor and regulates the expression of many genes. When it is inactive, it is quickly degraded and, generally, poorly imported into the nucleus.

Notably, when activated, the level of p53 starts oscillating [70]. Initially the p53 accumulates in the nucleus and its half-life rises. This can be observed 30 minutes after the damage has been induced to the cell. After 5-6 hours the concentration of p53 in the nucleus decreases again, but if the damage has not been repaired, a second cycle starts over. These oscillations are due to the negative feedback that p53 has with its major antagonist, the protein Mdm2. On the one hand, Mdm2 is responsible of the degradation of p53, on the other hand, p53 produces the mRNA of Mdm2. Together with this negative feedback, we need a second trigger for the oscillations. Indeed, mathematical models show that, in order to produce sustained oscillations in a negative-feedback system, a positive feedback or a delay on the negative one is needed. There exist several mathematical

models of p53 and each of them propose an explanation for the oscillations either by a positive feedback, either with an explicit time delay. Most of the existing models use ordinary differential equations to represent the network of p53. One of the main weakness of these models is the absence of a localization of the different reactions. Few models consider at least one species (p53 or Mdm2) localised in the nucleus and in the cytoplasm. But none of these models distinguishes a nuclear and a cytoplasmic variable for each considered species. On the contrary, our "spatial" point of view brought us to consider, for each variable, a nuclear and a cytoplasmic form. This let us 1) to localize every process, 2) to represent the *nuclear* accumulation of p53 and 3) to include the directionality of transport between the nucleus and the cytoplasm. Furthermore, thinking to possible future extension of the model, in terms of therapeutic applications, it is important to represent the nucleus, i.e. the location where p53 acts and how long it takes to accumulate and to exit from it.

Let us introduce the variables of the system we propose. We consider concentrations for p53, Mdm2, the mRNA of Mdm2 and the phosphorylated form of p53, $p53_p$. We set $\bar{u}_0 = [p53]$, $\bar{u}_1 = [Mdm2]$, $\bar{u}_2 = [Mdm2_{RNA}]$, $\bar{u}_3 = [p53_p]$. We distiguish the nuclear and cytoplasmic concentrations by means of the indexes $^{(n)}$,$^{(c)}$. Let us set a nuclear and a cytoplasmic compartment that we will call Ω_n and Ω_c. The two compartments have a common boundary that we call Γ_{nc}. Every species is supposed to diffuse freely in both compartments. We also suppose that every species is produced and degraded in the appropriate compartment. Finally we represent several enzymatic reactions that are known to occur between the different species considered. We used the classical quasi Steady State approximation to obtain the expression of the enzymatic reactions. In the nuclear compartment Ω_n, the model reads:

$$\begin{cases} \frac{\partial \bar{u}_0}{\partial \tau} = \bar{D}_0 \Delta \bar{u}_0 - k_{ub}\bar{u}_1 \frac{\bar{u}_0}{(K_{ub}+\bar{u}_0)} - \overline{ATM}\frac{\bar{u}_0}{(1+\bar{u}_0)} + \bar{k}_{ph}\frac{\bar{u}_3}{(\bar{K}_{ph}+\bar{u}_3)}, \\ \frac{\partial \bar{u}_1}{\partial \tau} = \bar{D}_1 \Delta \bar{u}_1 - \bar{d}_1 \bar{u}_1, \\ \frac{\partial \bar{u}_2}{\partial \tau} = \bar{D}_2 \Delta \bar{u}_2 + \bar{k}_{pm} + \frac{\bar{u}_3^h}{(\bar{K}_{Sp}^h+\bar{u}_3^h)} - \bar{d}_2 \bar{u}_2, \\ \frac{\partial \bar{u}_3}{\partial \tau} = \bar{D}_3 \Delta \bar{u}_3 + \overline{ATM}\frac{\bar{u}_0}{(1+\bar{u}_0)} - \bar{k}_{ph}\frac{\bar{u}_3}{(\bar{K}_{ph}+\bar{u}_3)}, \end{cases} \tag{3}$$

and in the cytoplasm Ω_c we have:

$$\begin{cases} \frac{\partial \bar{u}_0}{\partial \tau} = \bar{D}_0 \Delta \bar{u}_0 + \bar{k}_{tp} - k_{ub}\bar{u}_1 \frac{\bar{u}_0}{(K_{ub}+\bar{u}_0)} - \overline{ATM}\frac{\bar{u}_0}{(1+\bar{u}_0)} + \bar{k}_{ph}\frac{\bar{u}_3}{(\bar{K}_{ph}+\bar{u}_3)}, \\ \frac{\partial \bar{u}_1}{\partial \tau} = \bar{D}_1 \Delta \bar{u}_1 + \bar{k}_{tm}\bar{u}_2 - \bar{d}_1 \bar{u}_1, \\ \frac{\partial \bar{u}_2}{\partial \tau} = \bar{D}_2 \Delta \bar{u}_2 - \bar{k}_{tm}\bar{u}_2 - \bar{d}_2 \bar{u}_2, \\ \frac{\partial \bar{u}_3}{\partial \tau} = \bar{D}_3 \Delta \bar{u}_3 + \overline{ATM}\frac{\bar{u}_0}{(1+\bar{u}_0)} - \bar{k}_{ph}\frac{\bar{u}_3}{(\bar{K}_{ph}+\bar{u}_3)}, \end{cases} \tag{4}$$

We set $\bar{D}_i$, $i = 0, \ldots, 3$, for the diffusion coefficients of the $i-th$ species, expressed in $\mu m^2 min^{-1}$. Following [15] and [121] we fix Kedem-Katchalsky [62] boundary conditions at the common boundary Γ_{nc} for the species that cross the nuclear membrane from both sides:

$$\begin{cases} \frac{\partial \bar{u_0}^n}{\partial \mathbf{n}} = \frac{\bar{p_0}}{\bar{D_0}}(\bar{u_0}^c - \bar{u_0}^n) = \frac{\partial \bar{u_0}^c}{\partial \mathbf{n}} \quad \text{on } \Gamma_{nc}, \\ \frac{\partial \bar{u_1}^n}{\partial \mathbf{n}} = \frac{\bar{p_1}}{\bar{D_1}}(\bar{u_1}^c - \bar{u_1}^n) = \frac{\partial \bar{u_1}^c}{\partial n} \quad \text{on } \Gamma_{nc}, \end{cases} \tag{5}$$

meaning that the flux of each species through the nuclear envelope is proportional to the difference between the concentrations at the two sides of the membrane. Notice that the normal vector $\mathbf{n}$ is pointing outwards from the nucleus and that fluxes are continuous. We fix the following boundary conditions for $\bar{u}_2$ (mRNA of Mdm2) and $\bar{u}_3$ ($p53_p$):

$$\begin{cases} \frac{\partial \bar{u_2}^n}{\partial \mathbf{n}} = -\frac{\bar{p_2}}{D_2}\bar{u_2}^n = \frac{\partial \bar{u_2}^c}{\partial \mathbf{n}} & \text{on } \Gamma_{nc}, \\ \frac{\partial \bar{u_3}^n}{\partial \mathbf{n}} = \frac{\bar{p_3}}{D_3}\bar{u_3}^c = \frac{\partial \bar{u_3}^c}{\partial \mathbf{n}} & \text{on } \Gamma_{nc}, \end{cases} \tag{6}$$

because their transport through the nuclear envelope is unidirectional.

In order to analyse this system we proceeded in two different ways: in Chapter 5, we reduced the reaction diffusion system (3)-(4)-(5)-(6) to an ODE system of equations, by supposing the concentration of each species homogeneous in each compartment and setting appropriate exchange rules. In the ODE case we investigated the existence of bifurcations, and we tested the validity of the system over a wide range of parameters. Besides to this approach, we focused more to the spatial case which is described in Chapter 6, by the reaction-diffusion system (3)-(4)-(5)-(6). This system was solved by finite element methods.

Main results

Through a numerical bifurcation analysis, we verified in Chapter 5 the existence of sustained oscillations for our model. The interesting aspect of this result is, on the one hand, the reproduction of the biologically observed behaviour of p53 that attests the validity of our model. On the other hand, we showed that by the simple distinction between nuclear and cytoplasmic compartment we could reproduce sustained oscillations avoiding the use of positive feedback or time delay. This result shows that the core network of p53 (its negative feedback with Mdm2) and the localization of each process is sufficient to obtain an oscillating signal. However, we cannot exclude the existence of a positive feedback that would reinforce the oscillatory behaviour.

In Chapter 5 we also tested the existence of bifurcations depending on several parameters, verifying the existence of oscillations for a large range of parameters and we investigated how the oscillations *change* qualitatively, with respect to variations of parameters (both period and amplitude).

In Chapter 6 we obtained the oscillations of the p53-Mdm2 system in the spatial environment. We set the biophysical parameters corresponding to diffusion and permeability coefficients in the range of the known values, for p53, Mdm2 and the mRNAs and we reproduced the observed behaviour of p53. We observed the rise of the nuclear concentration of p53 after 30 minutes from the beginning of the simulations. Then we tested the robustness of the oscillatory response changing the spatial coefficients as the diffusions and permeabilities, but also the total volume and the ratio between cytoplasmic to nuclear volume. We also noticed that the period of oscillations depends strongly on spatial coefficients such as diffusion and permeability. We verified that the oscillations of the p53-Mdm2 network are observed over a wide range of spatial parameters. This led

us to speculate that the oscillatory response of the network has a deep biological meaning, since we could reproduce it, in several different spatial environments. An interesting information that we obtained through the use of spatial modelling is that activation of p53 after the damage (which is described by the transformation transformation of $p53$ in $p53_p$ in our model) must occur in both compartments. Indeed, if only one compartment is *activated*, we can observe an isolate pick of p53, but no undamped oscillations.

Plan of the Thesis

This thesis is organized as follows:

- in Chapter 1 we introduce some biological elements about nucleocytoplasmic transport within eukaryotic cells. To help the reader understanding the biological notions presented, we report some figures that illustrate complex biological situations. In the same chapter, we discuss existing mathematical models that have been proposed in recent years to reproduce transport mechanism at the cellular level.

- In Chapter 2 we introduce a model of cytoplasmic transport, assisted by motor proteins along a single microtubule. We justify our modelling choices and we discuss the differences with respect to existing models in literature. The numerical scheme used in our simulations is presented and its numerical accuracy verified. Finally the numerical results are presented and discussed. Tables and figures illustrate our results.

- In Chapter 3 we describe the model of nucleocytoplasmic transport proposed in [15]. Then we couple this model with the model proposed in chapter 2 and we evaluate the differences with respect to the simple form discussed in chapter 2. A discussion about the main differences with other known model in the literature is also present.

- Chapter 4 is devoted to the description of the role of protein p53. A detailed biological introduction is given as well as a discussion about existing models in literature.

- In chapter 5 we propose our p53 model in its ODE form. We analyse the model through a numerical bifurcation analysis and we discuss our results proposing a biological interpretation of what we observe.

- Chapter 6 contains the main results about our model containing a spatial characterization of p53. Firstly, we introduce the Partial Differential System

describing the p53 cycle. Then we start its analysis by studying the behaviour of the system in a simplified one-dimensional domain. Next, we analyse, by means of numerical simulations, the behaviour of the system in a more realistic two dimensional domain. In this environment, we vary all the spatial parameters of the system (diffusion and permeability coefficients, volume and shape of the cell) and we observe the qualitative change of the responses of the system (existence of oscillations, amplitude and period of oscillations). We end the chapter with a discussion about our results and the possible extensions of the model.

Part I

A mathematical model for the enhanced cytoplasmic transport: how to get (faster) to the nucleus

Chapter 1

Nucleocytoplasmic transport in eukaryotes

In this chapter we will discuss transport within eukaryotic cells. After a brief description of the characterizing features of the eukaryotic cell, we will explain how certain macromolecules manage to reach the nucleus and gain access to it.

Contents

1.1 Eukaryotic cell. A few distinguishing elements.

Eukaryotic cells make up plants, mushrooms, animals and human beings. One of the principal characteristic of eukaryotes is the strict partitioning of different functions to various locations of the cell. Specialized compartments, called organelles, perform different tasks that are critical to life. For instance, mitochondria provide energy from food molecules and, in plant cells, chloroplasts are responsible of photosynthesis. Nearly every organelle is surrounded by a lipid bilayer, its membrane, that separate them from the rest of the cellular space. Through this specific distinction of locations and roles, the cell accomplishes all its various functions, despite the crowded environment in which it is enclosed by the plasma membrane.

Among all the organelles, the nucleus is the most important. It contains the DNA and all the information critical to cell genetic maintenance. Within the nucleus the RNA is build and exported in the cytoplasm, where it is translated into proteins by the ribosomes. Proteins then locate to the cellular sub-compartment where their function is required, or transported outside of the cell. The nuclear envelope, besides protecting the

DNA, accomplishes a strict regulation of what can access to or exit from the nucleus. Homogeneously spread among the membrane, small pores, called nuclear pores (NP), selectively control the crossing of the envelope. Nuclear pores are large protein channels and they are composed of proteins known as nucleoporins. In mammals, a single pore complex (NPC) has a molecular mass of about $120MDa$.

A sketch of an eukaryotic cell, compared to a prokaryote, is represented in Figure 1.1.

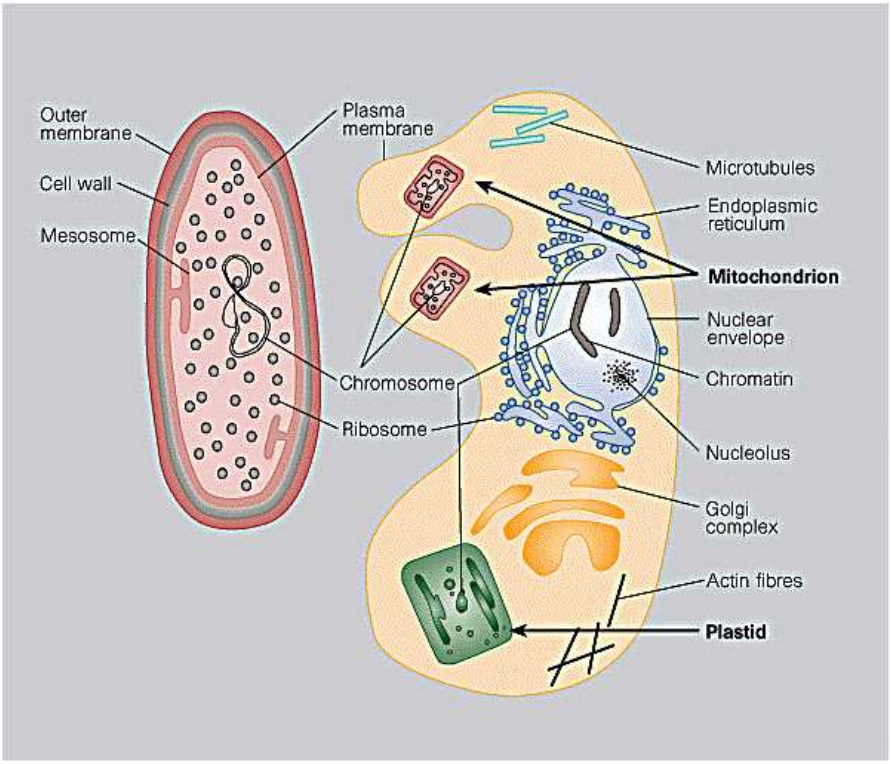

Figure 1.1: In prokaryotes, the DNA (chromosome) is in contact with the cellular cytoplasm and is not housed in a membrane-bound nucleus. In eukaryotes, however, the DNA takes the form of compact chromosomes separated from the rest of the cell by a nuclear membrane (also called a nuclear envelope). Eukaryotic cells also contain a variety of structures and organelles not present in prokaryotic cells. Throughout the course of evolution, organelles such as mitochondria and chloroplasts may have arisen from engulfed prokaryotes ©Nature Education [32].

1.2 Active transport along microtubules

The eukaryotic cytoplasm is a crowded environment. Several tasks are performed in different locations, at the same moment. For instance, some proteins are synthesised by the ribosomes, others are degraded by the proteasomes, others bind to form macromolecu-

lar complexes. Concurrent events take place in each sub-cellular compartment leading towards healthy cell survival and division. The exact regulation of all the events that maintain cell life is required and the good localization of each process is also necessary. A pivotal role in the organization of cytoplasmic activities is played by microtubules. Microtubules compose, with microfilaments and intermediate filaments, the cytoskeleton of the cell and help maintaining the cell structure.

Microtubule structure

Microtubules (MTs) are filaments, with a diameter of about 24 nanometers, composed by tubulin dimers that constitute the cytoskeleton together with actin filaments and intermediate filaments. The building block of a microtubule is the tubulin subunit, a heterodimer of α- and β-tubulin [76]. These subunits organize themselves in long strands called protofilaments. In turn, protofilaments tie up and form a microtubule filament (see Figure 1.2). Microtubules rapidly grow or shrink in size. At both ends of the filaments

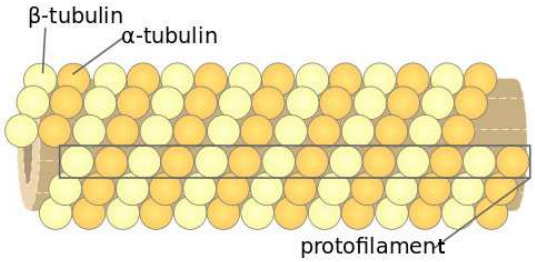

Figure 1.2: Tubulin subunits (α and β), onrganized in protofilaments, form a microtubule. ©Wikimedia Commons .

the tubulin bricks are added or removed by chemical reactions. One of the ends, called the plus end, grows more rapidly and, during interphase, can extend widely towards cell periphery. The other end, called the minus end, is anchored to the microtubule organizing centers (MTOC). The primary MTOC, the centrosome, is positioned near the cell nucleus. In most cells, during interphase, microtubules are nucleated from the centrosome. Thus, microtubules are organized in a radial structure pointing towards the nucleus and irradiate from the cell centre to the cell periphery.

Microtubule functions

Microtubules are involved in many cellular process, in particular they are responsible for vesicles and organelles transport within the cell, they are required in cellular motility and they maintain the cellular structure. They are also critical during mitosis. In Figure 1.3 it is shown how, during the cell cycle, microtubule activity is critical in cell division. The violet filaments represent the microtubules.

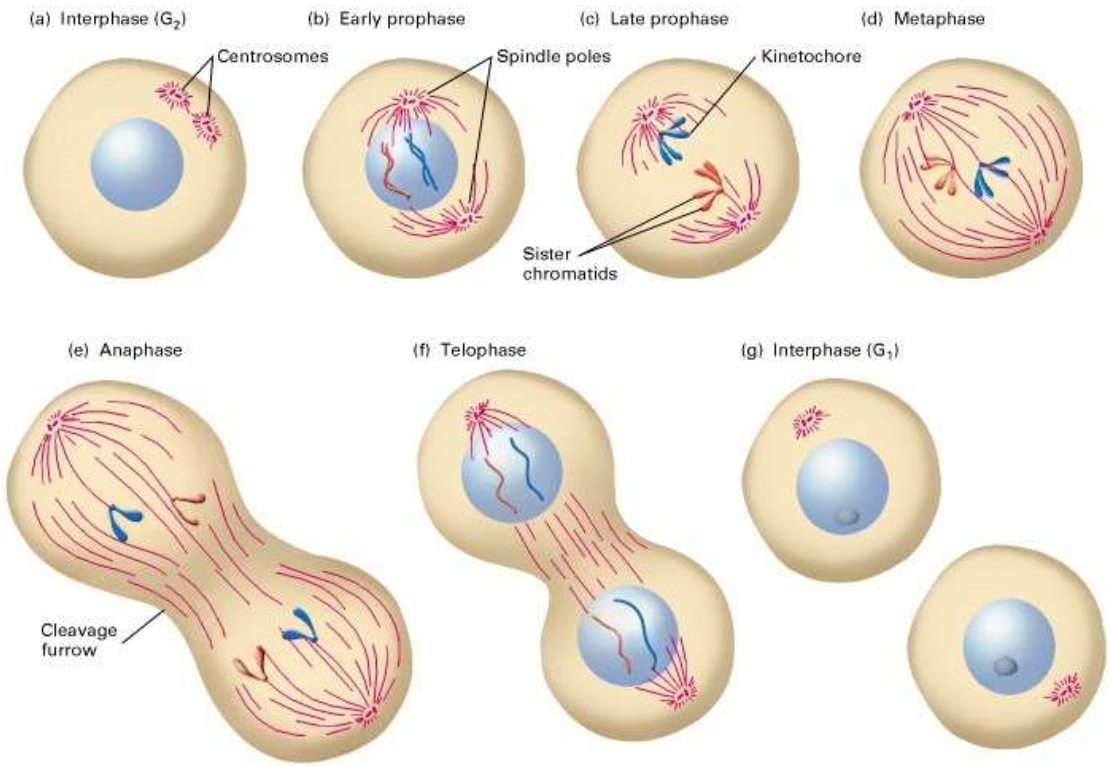

Figure 1.3: Microtubules during the cell cycle [76].

Microtubules and transport

During interphase, microtubules span into the cytoplasm in a radial structure. Since each filament has a plus and a minus end, microtubules have a polarity which permits to dedicated proteins to move towards the nucleus or towards the cell outer membrane. Because of their radial organization, microtubules play a critical role in intra-cellular trafficking. For instance, viruses use microtubules as a highway to get close to the nucleus [14]. During cell interphase, vesicles and organelles are positioned within the cytoplasm by motor proteins bound to microtubules, as shown in Figure 1.4 Two families of motor proteins associate to the MTs: dynein, which permits transport from the plus end to the minus end of the filament, and kinesin, whose members are (+) end-directed microtubule motor proteins [76]. Both motor proteins use energy from ATP hydrolysis [51] to move along the microtubule through discrete steps. Kinesin is a two-headed protein and takes hundreds of steps by walking along the microtubules before detaching [144]. It is a tiny protein compared to dynein whose mass can be greater than $1MDa$. Dynein has two heavy chains with globular heads with two elongated structures, the stalk and the stem, emerging from them [11]. These two structures bind the microtubule track and cargoes respectively. See Figure 1.5.

Researchers have shown that kinesin bound molecules fulfil distances of several mi-

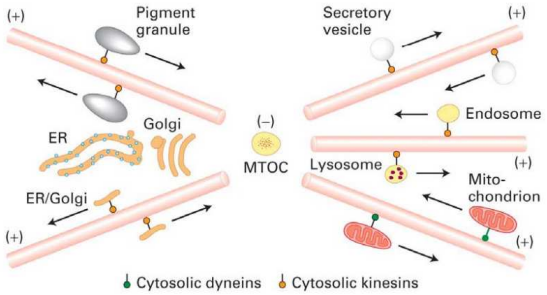

Figure 1.4: During interphase, motor proteins transport along the microtubules vesicles and organelles to position them within the cytoplasm.

crometers [130] at a speed $\sim 1\mu ms^{-1}$ [12]. *In vitro* the study of dynein motion has shown that a single dynein motor moves only along limited distances ($\sim 800nm$), although *in vivo* observations tracked longer distances (several microns [79]). More recent studies proved that multiple dynein proteins can bind to the same cargo and perform longer distances *in vitro* [81], thus explaining the *in vitro* observations (Figure 1.5). Dynein motor velocity can span betwen $0.5\mu ms^{-1} - 1.5\mu ms^{-1}$ [81, 79].

Even if the use of microtubules for intracellular transport is mainly reserved to macromolecules or organelles, that have low mobility within the cells, recent studies demonstrate that some small proteins use this network to facilitate their way towards the perinuclear region [41, 113, 72, 43, 114]. Some examples are the p53 and the PTHrP proteins [113], that both are cancer regulatory proteins. These findings enhance the hypothesis that some proteins that regulate important cellular pathways, and need to accumulate rapidly in the nucleus, use the microtubules as a preferential way to approach faster the nuclear envelope [137, 14].

1.3 Facilitated nucleocytoplasmic shuttling: the Ran pathway

In order to regulate the complex cellular activities of eukaryotes, nucleus and cytoplasm need to exchange information. Many proteins and macromolecules need to shuttle between these two compartments, at every moment of cell life. The RNAs, synthesised in the nucleus, need to be exported in the cytoplasm where they take part to the translation processes. Ribosomal proteins are assembled in the nucleus and exported to the cytoplasm. Nuclear proteins, as for instance transcription factors, gain access to the nucleus in order to play their roles.

Not all proteins are entitled to access to the nucleus and those that may, use different transport mechanisms. Some small proteins ($< 40kDa$) and ions can cross the nuclear membrane freely, but others need a chaperone to get through [47]. Indeed the nuclear pores, which are protein-lined tunnels through the nuclear envelope, consent the access

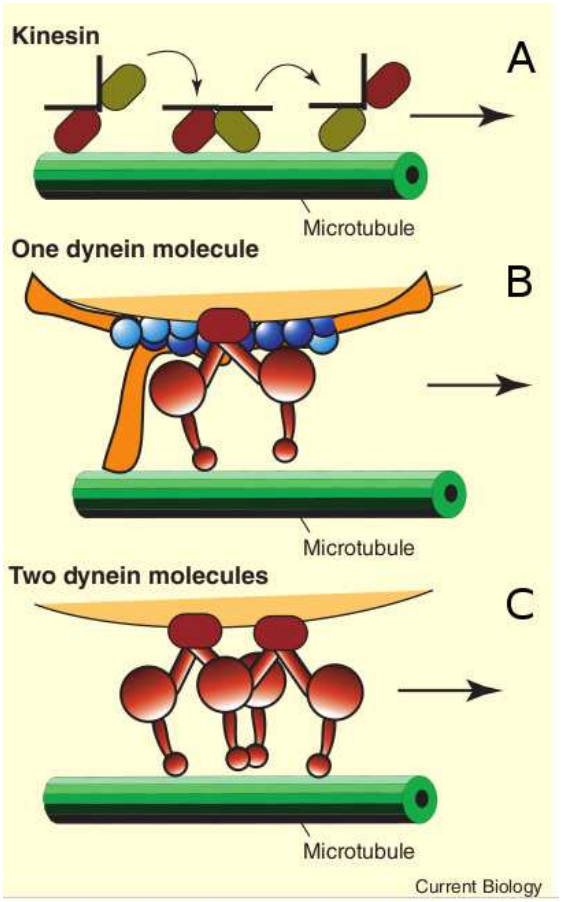

Figure 1.5: Cytoskeletal motors have multiple mechanisms for taking long walks along filaments. (A) Kinesin is a highly processive molecule that walks hand-over-hand remaining in contact with the microtubule through-out motion. (B) Single dynein molecules are not very processive, but they become more processive when bound to the accessory molecule dynactin, which provides an additional attachment to the microtubule. (C) The addition of a second dynein molecule to a cargo, even in the absence of dynactin, allows transport along microtubules for several microns [85].

to the nucleus, or to the cytoplasmic compartment, only to entitled proteins. The tag that identify proteins allowed to enter the nucleus is a signal, called Nuclear Localization Signal (NLS) [27]. Proteins that have this tag, are detected by members of the importin protein family. As a first step, an adapter protein called importin-α recognizes the signal and binds to the NLS-bearing protein. Then, the newly formed complex binds to a molecule of importin-β that is the actual carrier: the ternary complex is thus able to traverse the nuclear pore and the cargo is then released in the nucleus [46] (for a review about nuclear import see e.g. [45]).

In a similar way, proteins that have a Nuclear Export Signal (NES) can shuttle

outside of the nucleus. A member of the exportin family, called Crm1, recognizes the signal and escorts the NES-protein to the cytoplasm. The binding of exportins to the cargo protein is cooperatively activated by the protein Ran, that plays a critical role in nuclear import and export.

The role of Ran

The protein Ran is a GTPase and hydrolyses bound GTP into GDP. The GTP bound form is considered active (RanGTP), while RanGDP is inactive. The protein Ran can shuttle between the nucleus and the cytoplasm. In the nucleus another protein (RCC1) promotes the formation of RanGTP [9]. In the cytoplasm proteins of the group of RanGAP (GTPase-activating protein) and RanBPs (Ran-binding proteins: RanBP1 and RanBP2) enhance the formation of RanGDP [7, 8], see Figure 1.6. As a result, RanGDP is mostly cytoplasmic, while RanGTP is nuclear. The unpaired distribution of Ran between nucleus and cytoplasm has an essential role in nucleocytoplasmic transport. Indeed in the nucleus, RanGTP binds to the Importin-β-cargo complex and allows the cargo dissociation in the nucleus, thus concluding the import cycle. Once the cargo is released the Importin-Ran complex traverses the nuclear membrane so that Ran and importin move back in the cytoplasm, to recycle. In the cytoplasm the cycle is closed by the conversion of RanGTP to RanGDP. Ran is also involved in the export cycle: it mediates the binding of exportins to NES bearing protein. The cargo is thus exported in the nucleus in a ternary complex composed by a molecule of RanGTP, an export protein, and the cargo itself. The hydrolysis of RanGTP into RanGDP in the cytoplasm dissociates the ternary complex and the cargo is thus released. Ran gets back again into the nucleus escorted by the nuclear transport factor NTF2 that bind to RanGDP with high affinity.

In the process described above proteins move from a region of higher concentration to one of lower concentration and use carrier proteins to get to the nucleus. This process is known as facilitated diffusion. Ran is thus responsible of the existence of a concentration gradient so that facilitated diffusion can occur. For a complete review of nucleocytoplasmic transport see [80].

1.4 Existing models in literature

The mathematical formulation of the biological processes of intracellular transport is a useful tool to determine if a biological model, designed through the interpretation of experimental events, reproduce the observed behaviour. Easily, through the use of differential equations, the dynamics of a complex biological model can be predicted by simulations and, sometimes, by the mathematical analysis of the system. This tool has already been used to model transport along microtubules [122, 15] and to reproduce the facilitated translocation through the nuclear pores of NLS proteins [48].

For instance, Görlich *et al.* [48] modelled the transport mechanism mediated by

the protein Ran with an ODE system of equations and reproduced the experimental behaviour observed *in vitro*. From the one hand through this quantitative analysis the authors could verify that the biological model of nuclear import based on the Ran gradient is reliable. From the other hand the authors could observe that, during mitosis, the Ran gradient can be maintained only in sufficiently large cytoplasms. They could thus represent a behavioural feature of the Ran cycle, depending on cell size.

In [121] the authors reproduced nuclear import of NLS proteins through the Ran pathway with a PDE system of equations, considering the spatial variable and representing a nuclear membrane. They used the Virtual Cell Software[1] to compare their experimental results with a 3D simulation of the system model, see Figure 1.7(a). They predict that the steady state flux across the NPC is regulated by the Ran gradient and not by the flux capacity of a single pore. They also provided a first estimate of the total in vivo flux: 520 molecules per NPC per second.

A first pioneering work that combines the modelling of nuclear import pathway mediated by the Ran gradient, and the microtubule activity as an enhancer of nuclear import is the paper of Cangiani and Natalini [15]. The authors propose a three-dimensional model of the import pathway, reproducing the facilitated diffusion through the NE due to the Ran gradient. Furthermore they consider a vector field, acting as microtubule network, that transports NLS proteins towards the nuclear membrane, thus improving the total mass import. The authors could confirm the behaviour experimentally obtained in [113]. In Figure 1.7(b) we report one of the simulation results of [15].

Microtubule transport has been modelled for the first time in a theoretical manner by Smith *et al.* [122]. The authors provide a one-dimensional reaction-advection-diffusion model, that takes into account bi-directional transport along the microtubules and reproduces qualitatively the transport characteristics of different biological systems, as organelle transport in neurons or in melanophores[2]

A step further in the direction of models of motor assisted transport within the cytoplasm, has been done by Dinh *et al.* [28, 29]. The authors relate biochemical and biophysical aspects of organelle transport in the cytosol. In [29] a model for the kinetics of Melanophores is described. In Melanophores, microtubules and actin filaments work together in order to distribute pigment granules (melanosomes) within the cell. Melanosomes can either aggregate at the cell center or disperse throughout the cytoplasm and the switch between the two states depends on biochemical signalling pathways. Assuming radial distribution, the authors develop a model of partial differential equations that take into account transport along microtubules and actin filaments and the biochemical activation pathway that changes the status of the system. Their results agree reasonably with experimental data.

Many other works exist about the parallel aspects of microtubule activity as the molecular regulation of motor transport. Other authors study the microtubules in dif-

[1] The Virtual Cell is a computational environment for modelling and simulation of cell biology, vcell.org developed by the Center for Cell Analysis & Modeling (CCAM) at the University of Connecticut Health Center.

[2] Microtubules (MTs) and actin filaments (AFs) work together in order to distribute pigment granules (melanosomes) in Melanophores (fish and amphibian epithelial cells).

ferent phases of the cell state and their role during mitosis. See e.g. [77].

1.5 Outline of the Work

In the next Chapter we develop a simple model of motor-assisted transport in the cytoplasm. We will consider a subregion of the cytoplasm where we assume that a single microtubule is present. A diffusive species will be included in our model. This species will be able to bind to motor proteins and to attach to the modelled microtubule. We will locate in the space the attraction area of this unique microtubule, and transport along it will be modelled using a mono-dimensional transport equation. Thus we will couple a two dimensional reaction-diffusion system with a mono-dimensional transport equation. The next step will be to couple this model with the model of nucleocytoplasmic transport proposed in [15], in Chapter 3, to compare in a more quantitative manner the enhanced accumulation of proteins in the nucleus, supported by the cytoplasmic faster translocation due to MT activity.

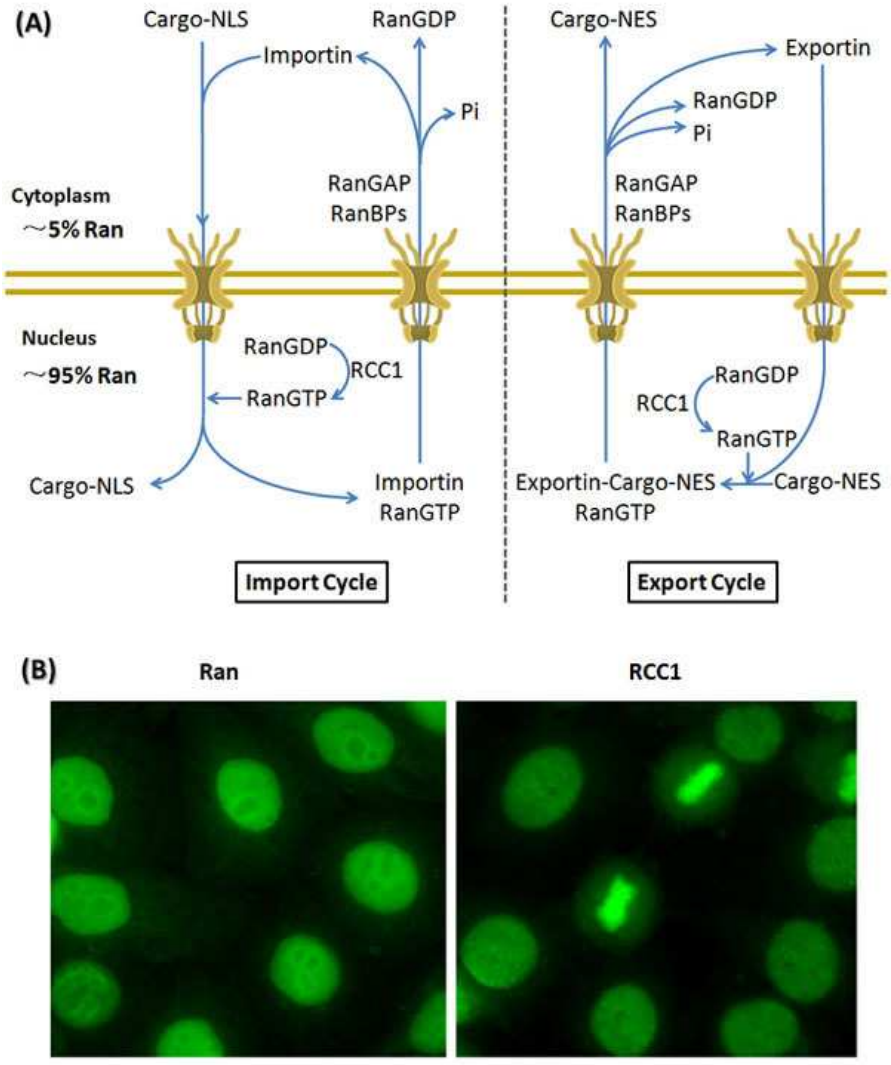

Figure 1.6: (A) Ran shuttles across the Nuclear Envelope (NE), with about 95% in the nucleus and 5% in the cytoplasm. A high concentration of RanGTP in the nucleus is maintained by RCC1, which catalyzes the formation of RanGTP. RanGDP is prevalent in the cytoplasm due to RanGAP and RanBPs that increase its GTPase activity. During import (left), importins bind to NLS-containing cargoes in the cytoplasm and translocate them into the nucleus through NPCs. RanGTP in the nucleus binds to importins and releases the cargoes from the complex. The RanGTP-importin complex is then recycled to the cytoplasm, where it is disrupted after RanGTP hydrolysis. During export (right), NES-containing cargoes in the nucleus bind to exportins and RanGTP, and translocate out of nucleus. In the cytoplasm, the cargoes are released from the complex by RanGTP hydrolysis ([21, 124, 142, 126]). (B) Images of immunofluorescence in HeLa cells. The green staining shows the location of Ran and RCC1 in these cells. Each circular shape is a cell. RCC1 appears to be located near the nucleus and chromosomes, whereas Ran appears more diffusely around the cell, both inside and outside the NE. ©Nature Education .

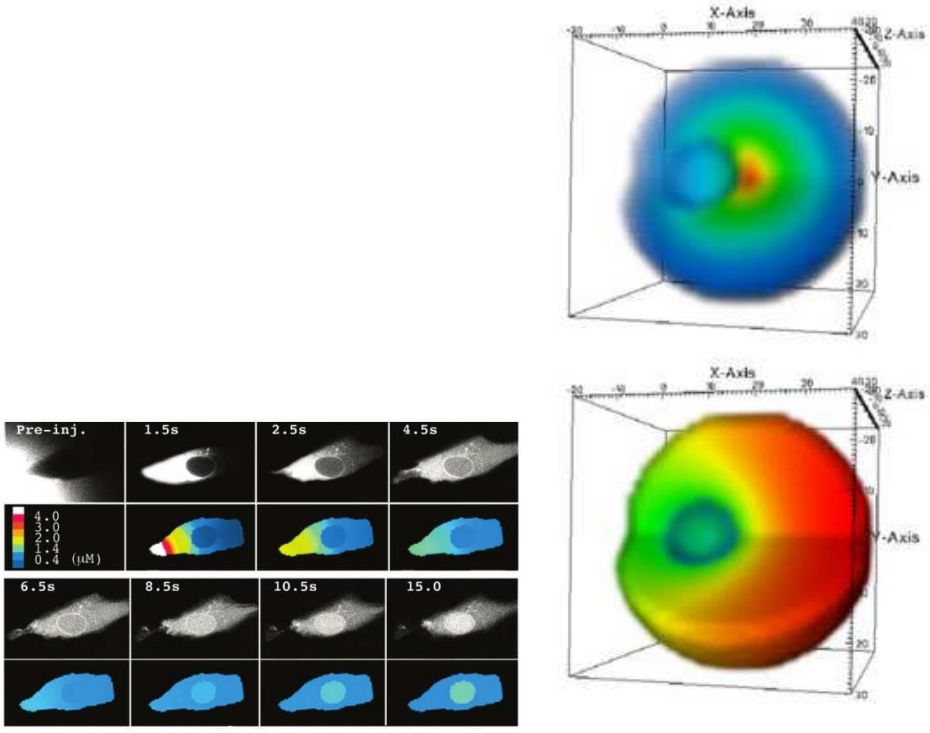

(a) (b)

Figure 1.7: (a):Ran transport is compared in a time series for Fluorescent Ran *in vitro* (grayscale) and for a sample plane from a 3D spatial model of Ran transport that simulates the same cytosolic microinjection of Ran [121]. (b) : Cargo and receptor spatial distribution with microtubule activity (above) and inhibited binding (below) [15].

Chapter 2

A model of active transport using advection-reaction-diffusion equations

In the previous chapter we introduced some elements of the biology of intra-cellular transport. In this chapter we propose a model of transport along microtubules and we predict which molecules, depending on their diffusion coefficients, could benefit of motor-assisted transport throughout the cytoplasm. In Section 2.1 we introduce the biological model and its mathematical formulation. In Section 2.2 we provide a numerical scheme with which we simulate the system proposed. Finally in Section 2.3 we show and discuss the results of the numerical simulations.

Contents

2.1 A model of active transport

Proteins are synthesised in a fairly homogeneous manner inside the cytoplasm. Each protein has a specific function and, given the spatial organization of eukaryote, a specific location where to carry it out. In particular, the nucleus is the most important organelle

of the cell and many proteins need to reach it. Transcription factors have to bind to nuclear DNA to transcribe genes, ribosomal proteins need to get to the nucleus to be assembled into ribosomes. In the event of cellular damage, the cell answers promptly, by sending signals that begin the process of repair and by arresting the cell cycle to allow the complete repair. Many of these events occur by means of the production or degradation of proteins and, for this reason, a continuous exchange of information between the nucleus and the cytoplasm is essential.

Import of proteins into the nucleus is regulated by the Ran pathway. Proteins admitted to the nucleus are labelled with a signal, called the nuclear localization signal (NLS). Importin proteins recognize this signal and carry the NLS-proteins to the nucleus, passing through the nuclear pores complexes. The protein Ran breaks the complex importin-NLS-protein and releases the cargo in the nucleus. The unbalanced concentration of the protein Ran between the nucleus and the cytoplasm dictates the directionality of transport (for further details see Section 1.3 and references therein).

Several NLS proteins have been found to interact with the cytoskeletal microtubules in their way towards the nucleus. Such examples are the protein p53 [41, 113], the parathyroid hormone-related protein PTHrP [72], the Rb retinoblastoma protein [113] and also NFκB in a complex with DNA, through the recognition of the NFκB NLS [87]. In cell-free Xenopus egg extract, a nuclear localization signal triggers active transport along microtubules [114]. Using the microtubule filaments as a highway, those proteins approach faster to the nucleus and their import results enhanced. Cytoskeletal-assisted nuclear transport can be thus considered as a simple variation of nuclear import [137], which is conventionally regulated by the Ran pathway.

With the aim to mimic such behaviour, we suggest a simplified bidimensional model of cytoplasmic trafficking where nuclear import is enhanced by active transport along microtubules.

2.1.1 Main assumptions and biological interpretation

In this model we consider a diffusive species capable of binding motor proteins. Our purpose is to evaluate if the flux towards the nucleus is enhanced when protein diffusion is supported by unidirectional transport along microtubules. For this reason, we take into account only the motor protein dynein, that is the motor that walks along the microtubules in the direction of the nucleus. This choice does not represent a limitation to the model, since the species to which we are interested are known to attach only to dynein. The diffusive species, once bound to dynein, can diffuse or bind the microtubules and be actively transported. We set C, for *cargo*, the diffusive species. The *product* of the kinetic reaction giving the complex cargo-dynein is defined as P_f (f for 'free'), while the cargo-dynein complex transported along the microtubules is defined as P_t (t for 'transported').

We model a single domain, only the cytoplasmic one, and we consider a thin area of the cytoplasm where we suppose that a *single* microtubule (MT) lies, as in Figure 2.1. We assume that motor proteins are abundant in this area and we consider dynein concentration constant and uniformly distributed. The reactions we model are the fol-

lowing: the formation and the dissociation of the cargo-dynein complex and the binding and unbinding to the microtubule. The specific feature of this model is the choice of locating the microtubule: an area of attraction, where the attachment to it is allowed, defines its location. Along the microtubule, the transport velocity is constant: dynein is known to walk along the filaments at a speed of about $1\mu m s^{-1}$ [96] and see Section 1.2.

The kinetic reactions we take into account are schematically represented by:

$$D + C \underset{k_-}{\overset{k'}{\rightleftharpoons}} P_f, \tag{2.1}$$

$$P_f \underset{k_{-1}}{\overset{k_1}{\rightleftharpoons}} P_t \qquad \text{on } \mathbf{I} \times \mathbf{J}. \tag{2.2}$$

Here k', k_-, k_1 and k_{-1} correspond to the rates of reaction. The symbol $\rightleftharpoons$ indicates that the reactions are reversible. The reaction (2.2) occurs only in the area of attraction of the microtubule, here denoted by $\mathbf{I} \times \mathbf{J}$ (see Figure 2.1).

2.1.2 Mathematical formulation

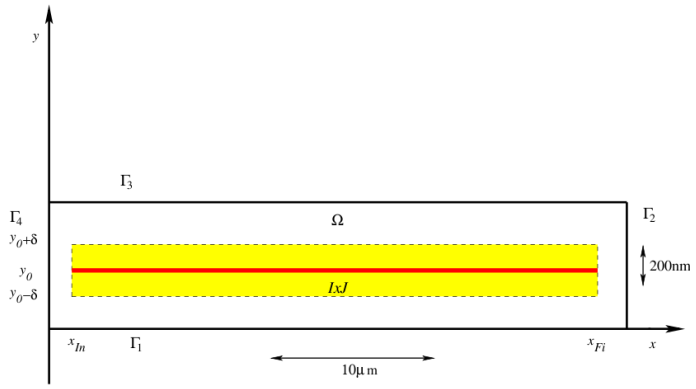

Figure 2.1: Area of the cytoplasm where intracellular transport is modelled: $\Omega = [0, L_x] \times [0, L_y]$. The yellow rectangle ($\mathbf{I} \times \mathbf{J} = [x_{In}, x_{Fi}] \times [y_0 - \delta, y_0 + \delta]$) represents the attraction area of the microtubule filament, the red strip is the microtubule, positioned in y_0.

Let $u = [C]$, $v = [P_f]$, $W = [P_t]$ be respectively the cargo, cargo-dynein complex and transported particle concentrations. We cast u and v in two-dimensions and we fix their unit to $mol/\mu m^2$. The variable W is mono-dimensional and its unit is expressed in $mol/\mu m$. The Law of Mass Action states that the rate of a reaction is proportional to the product of the concentrations of the reactants. Applying the Law of Mass Action to reactions 2.1 and 2.2 leads to the following differential equations:

$$\frac{du}{dt} = -k'[D]u + k_- v = -ku + k_- v, \tag{2.3}$$

$$\frac{dv}{dt} = ku - k_{-}v - k_1 v + k_{-1}W, \tag{2.4}$$

and

$$\frac{dW}{dt} = k_1 v - k_{-1}W. \tag{2.5}$$

In equation (2.3) we have fixed $k = k'[D]$, since we assume dynein concentration to be constant.

In order to describe spatially the dynamics of the modelled processes, let us define the simulation domain. We consider a rectangular domain Ω, represented in Figure 2.1, which we imagine to be a cytoplasmic area influenced by a single microtubule. We denote by $\mathbf{I} = [x_{In}, x_{Fi}]$ the actual length of the microtubule and $\mathbf{J} = [y_0 - \delta, y_0 + \delta]$, the width of the attraction area of the filament, positioned in y_0. The cargo and the cargo-dynein complexes, u and v, diffuse within all the domain Ω, while the transported particles W obey a one dimensional advection equation. To model diffusion we use the classical Fick's law of diffusion. This law says that the flux of a given material is proportional to the gradient of the concentration of the material; then by a conservation argument, the spatio-temporal evolution of the diffusive material is calculated [93].

We set d_u and d_v the diffusion coefficients of the u and v species respectively and c the motor velocity for the transported particles. Under the previous assumptions the u and v species satisfy a reaction-diffusion equation, while W is controlled by an advection equation modelling the transport along the microtubule with a steady velocity c. Our model reads:

$$\begin{cases} \dfrac{\partial u}{\partial t} = d_u \Delta u - ku + k_{-}v, & \text{in } \Omega, \\ \dfrac{\partial v}{\partial t} = d_v \Delta v + ku - k_{-}v - k_1 v \mathbb{1}_{\mathbf{IxJ}} + k_{-1} W \dfrac{\mathbb{1}_{\mathbf{IxJ}}}{|\mathbf{J}|} \\ \qquad\qquad + cW(x_{Fi})\delta_0(x - x_{Fi}, y - y_0), & \text{in } \Omega, \\ \dfrac{\partial W}{\partial t} + c\dfrac{\partial W}{\partial x} = -k_{-1}W + k_1 \displaystyle\int_{\mathbf{J}} v dy, & \text{in }]x_{In}, x_{Fi}[. \end{cases} \tag{2.6}$$

Notice that, in order to localize reaction (2.2), we introduced the characteristic function of the sub-domain $\mathbf{I} \times \mathbf{J}$, denoted by $\mathbb{1}_{\mathbf{I}\times\mathbf{J}}$, where $\mathbb{1}_{\mathbf{I}\times\mathbf{J}} : \Omega \to \{0, 1\}$. We also suppose that the molecules transported along the filament are freed when they reach its end. The term $cW(x_{Fi})\delta_0(x - x_{Fi}, y - y_0)$, in the equation for v, represents the contribution due to those molecules: the outgoing flux of the transported particles at the end of the MT filament. The $\delta_0(x, y)$ stands for the Dirac mass at the origin. This term guarantees the conservation of the mass, as will be shown below. Let us first close the system by imposing the boundary conditions:

$$\begin{cases} \dfrac{\partial u}{\partial n} = 0, \ \dfrac{\partial v}{\partial n} = 0, & \text{on } \Gamma_4, \\ d_u \dfrac{\partial u}{\partial n} + p_u u = 0, \ d_v \dfrac{\partial v}{\partial n} + p_v v = 0, & \text{on } \Gamma_2, \\ W(x_{In}) = 0. \end{cases}$$

Since the structure of the MTs network is homogeneous within the cell, as in Figure 2.2, we choose periodic boundary conditions on the long sides of the domain, Γ_1 and Γ_3, see figure 2.3. On Γ_4, the Neumann homogeneous boundary conditions is a zero flux condition, meaning that proteins cannot cross the membrane layer. On Γ_2 we consider an outgoing flux proportional to the species concentration, as if the species where traversing the nuclear membrane. For the transported cargo W we suppose that there is no upcoming flux at the beginning of the microtubule and we fix $W(x_{In}) = 0$.

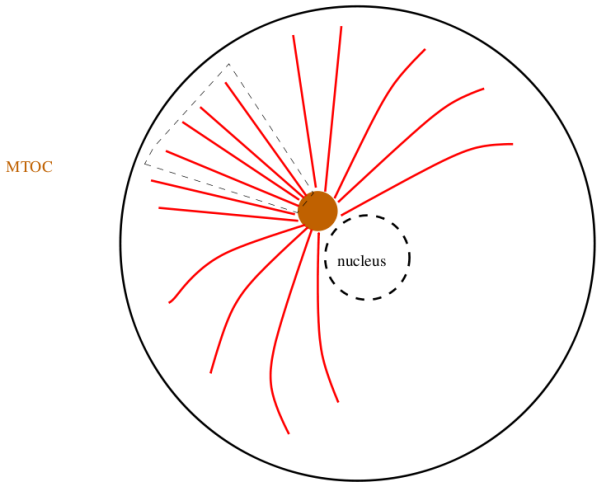

Figure 2.2: *Schematic model of the cell with its microtubules structure.*

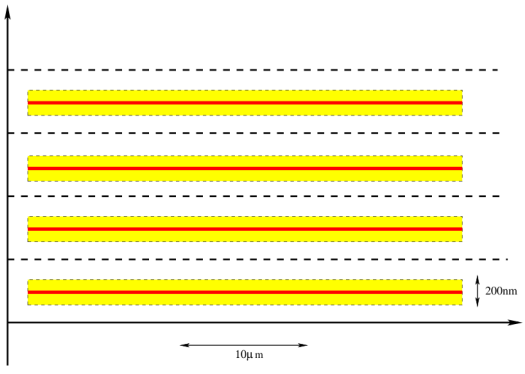

Figure 2.3: Periodic boundary conditions on the long side of the domain (see figure 2.1) in system (2.6) make the cell a homogeneous environment. This means that the strip where we model the system is a "zoom" on a single microtubule. We suppose that the same reactions take place in the rest of the cell.

Let us introduce the function, defined on the whole domain Ω:

$$w(x,y) = W(x)\frac{\mathbb{1}_{\mathbf{I}\times\mathbf{J}}(x,y)}{|\mathbf{J}|}, \tag{2.7}$$

in such a way that

$$\int\int_{\Omega} w\,dxdy = \int_{\mathbf{I}} W dx.$$

The total mass of system (2.6) is given by:

$$\int\int_{\Omega}(u+v+w)dxdy. \tag{2.8}$$

Let us write a general conservation equation which says that the rate of change of the amount of a material in a region is equal to the rate of flow across the boundary plus any that is created within the boundary [93].

Proposition 2.1.1. *The conservation of system (2.6) yields:*

$$\frac{\partial}{\partial t}\int\int_{\Omega}(u+v+w)dxdy = d_u\int_{\Gamma_2}\frac{\partial u}{\partial n}d\sigma + d_v\int_{\Gamma_2}\frac{\partial v}{\partial n}d\sigma. \tag{2.9}$$

Proof. Using the equations of system (2.6) and applying the Green's first identity, we get for u:

$$\begin{aligned}\frac{\partial}{\partial t}\int\int_{\Omega} u\,dxdy &= \int\int_{\Omega}(d_u\Delta u - ku + k_-v)dxdy \\ &= \int\int_{\Omega}\overbrace{(-ku+k_-v)}^{D+C\rightleftharpoons P_f}dxdy + d_u\int_{\Gamma_2}\frac{\partial u}{\partial n}d\sigma,\end{aligned} \tag{2.10}$$

and for v:

$$\begin{aligned}\frac{\partial}{\partial t}\int\int_{\Omega} v\,dxdy &= \int\int_{\Omega}(d_v\Delta v + ku - k_-v - k_1v\mathbb{1}_{\mathbf{I}\times\mathbf{J}} + k_{-1}w)dxdy + \\ &\quad + \int\int_{\Omega} cW(x_{Fi})\delta_0(x-x_{Fi},y-y_0)dxdy \\ = d_v\int_{\Gamma_2}\frac{\partial v}{\partial n}d\sigma &+ \int\int_{\Omega}\overbrace{(ku-k_-v)}^{D+C\rightleftharpoons P_f}dxdy + \int\int_{\Omega}\overbrace{(-k_1v\mathbb{1}_{\mathbf{I}\times\mathbf{J}}+k_{-1}w)}^{P_f\rightleftharpoons P_t}dxdy \\ &\quad + \int\int_{\Omega} cW(x_{Fi})\delta_0(x-x_{Fi},y-y_0)dxdy.\end{aligned} \tag{2.11}$$

And finally the mass of w writes:

$$\begin{aligned}\frac{\partial}{\partial t}\int\int_{\Omega} w\,dxdy &= \int\int_{\Omega}\left(-c\frac{\partial W}{\partial x}\frac{\mathbb{1}_{\mathbf{I}\times\mathbf{J}}}{|\mathbf{J}|} + \frac{k_1}{|\mathbf{J}|}(\int_{\mathbf{J}} v\mathbb{1}_{\mathbf{I}\times\mathbf{J}}dy) + k_{-1}w\right)dxdy \\ \underset{\text{Integration by parts}}{=} &-\int_{\mathbf{J}}\frac{c}{|\mathbf{J}|}\left(W(x_{Fi}) - \overbrace{W(x_{In})}^{=0}\right)dy + \int\int_{\Omega}\overbrace{(k_1v\mathbb{1}_{\mathbf{I}\times\mathbf{J}}-k_{-1}w)}^{P_f\rightleftharpoons P_t}dxdy.\end{aligned} \tag{2.12}$$

Summing up equations (2.10), (2.11) and (2.12) we find equation (2.9), i.e. system (2.6 conserves the mass. □

We conclude this section by some modelling remarks. In this model, we consider advective and diffusive processes to represent the motion of molecules inside the cytoplasm. The first and second equation represent the variables for which motion is regulated by diffusion. They lie in two-dimensions: $u = u(x, y, t)$ and $v = v(x, y, t)$ represent the species concentration per unit surface area at time t in $(x, y) \in \Omega$. On the other hand, we consider the MT dependent transport to be one-dimensional. The advection equation that model the evolution of the transported cargo concentration, W, is one-dimensional and uni-directional. Another approach to model transport along microtubules, used for example by Cangiani *et al.* in [15] and by Sturrock *et al.* in [129], is to consider a velocity field $\mathbf{v} : \Omega \to \mathbb{R}^n$, where n depends on the dimension of the modelled domain ($n = 2, 3$). Through this approach the influence of microtubules is averaged in the whole domain and no localization is allowed: at each point of the domain particles can attach to microtubules and be transported following the vector field.

Motor proteins attach to microtubules and walk along them in a given direction. As a result, transport along microtubules is mono-dimensional. Furthermore, microtubules are single filaments that span the cytoplasm of cells. Our choice was to consider both these features: we localize a single microtubule filament by fixing a tiny attraction area. Next, we consider the transport of proteins along microtubule to be uni-dimensional by coupling a one-dimensional advection equation with a two-dimensional reaction-diffusion system. Our goal is, on the one hand, to be more realistic, on the other hand, to emphasize the differences of the two transport mechanisms used by proteins to move inside the cell (diffusion and motion along cytoskeletal filaments).

2.2 Numerical approximation

In this section we propose a numerical scheme in order to solve the system presented above. Let us introduce a space discretization of the x and y axes. Our domain Ω is the rectangle $[0, L_x] \times [0, L_y]$ (see Fig. 2.1). We denote by Δx, Δy the discretization steps in the x and y directions respectively and we divide the intervals $[0, L_x]$ and $[0, L_y]$ in N_x+1 and $N_y + 1$ points. The mesh points will be $(x_i, y_j) = (i\Delta x, j\Delta y)$ with $0 \leq i \leq N_x + 1$, $0 \leq j \leq N_y+1$. Let Δt be the time discretization step and t_n the n^{th} step, i.e. $t_n = n\Delta t$, $n \in \mathbb{N}$. According to these notations $u^n_{i,j}$ will be the approximation of the solution of u in (x_i, y_j) at time t^n, while $v^n_{i,j}$ and W^n_i denote respectively the approximations of v and W. We remark that W lies in $[x_{In}, x_{Fi}]$, so that W^n_i is well defined only for certain values of i, in particular we need $x_{In}/\Delta x \leq i \leq x_{Fi}/\Delta x$.

We first solve the transport equation of system (2.6), i.e. the third equation of the system. First, let us introduce the numerical approximation of the transport term of the equation, and omit to contribution of the degradation and of the flux terms in the right side of the equation. Since the equation is linear, we can use an upwind scheme and

directly write it in its viscous form:

$$W_i^{n+1} = W_i^n - \frac{\nu}{2}(W_{i+1}^n - W_{i-1}^n) + \frac{\nu}{2}(W_{i+1}^n - 2W_i^n + W_{i-1}^n), \tag{2.13}$$

where $\nu = c\frac{\Delta t}{\Delta x}$. This scheme needs to satisfy the CFL condition $0 \leq \nu \leq 1$, that assure its convergence. Then, we consider a flux limiters to add an antidiffusive term [75]. The flux limiters we consider are TVD, *Total Variations Diminishing*, which means that the total variation of the mesh solution W^n, defined by

$$TV(W^{n+1}) = \sum_i |W_{i+1}^n - W_i^n|,$$

verify

$$TV(W^n) \leq TV(W^{n+1}). \tag{2.14}$$

We define, for the mesh function the ratios:

$$r_{i+1/2} = \frac{W_i^n - W_{i-1}^n}{W_{i+1}^n - W_i^n} \quad \text{and} \quad r_{i-1/2} = \frac{W_{i-1}^n - W_{i-2}^n}{W_i^n - W_{i-1}^n}, \tag{2.15}$$

and we introduce a *flux limiters* function $\phi(r)$ [131]:

$$\phi(r) = \max\{0, \min\{r, 1\}\}. \tag{2.16}$$

The antiviscosity term that we add to equation (2.13) reads:

$$-\frac{\nu(1-\nu)}{2}\left[\phi(r_{i+1/2})(W_{i+1}^n - W_i^n) - \phi(r_{i-1/2})(W_i^n - W_{i-1}^n)\right]. \tag{2.17}$$

Finally, let us set

$$\psi_{i+1/2} = 1 - (1-\nu)\phi(r_{i+1/2}),$$

and sum the antiviscosity term (2.17) to (2.13). We obtain the TDV-satisfying, second order accurate transport scheme:

$$W_i^{n+1} = W_i^n - \frac{\nu}{2}(W_{i+1}^n - W_{i-1}^n) + \frac{\nu}{2}\left(\psi_{i+1/2}(W_{i+1}^n - W_i^n) - \psi_{i-1/2}(W_i^n - W_{i-1}^n)\right). \tag{2.18}$$

To use the flux limiters at the last point of the grid, we need to add a fictitious point, so that we can calculate the ratio $r_{i+1/2}$. Let us call M the i point on the grid for x such that $M\Delta x = x_{Fi}$, i.e. the last point of the grid where w is defined. We set:

$$W_{M+1}^{n+1} = 2W_M^n - W_{M-1}^{n-1}, \tag{2.19}$$

in such a way that we can calculate at each time step the quantity $\phi(r_{i+1/2})$ and solve the transport equation with the same accuracy in the interior points and at the border. Formula 2.19 is referred to as quasi-characteristic extrapolation, since the extrapolation uses points near the characteristics [127].

Then, we look at the right hand side of the transport equation that is made by two parts. The degradation term $-k_{-1}W$ is stiff, and we approximate it by an implicit discretization. For the source term $F := \int_{\mathbf{J}} v(x_i, y)dy$, we use an upwinding scheme [112], which improves the resolution near the asymptotic states, and besides, we approximate the integral using a trapezoidal rule. Summing up these considerations, we obtain the following scheme for W:

$$\begin{aligned}(1+\Delta t k_{-1})W_i^{n+1} = W_i^n - \frac{\nu}{2}(W_{i+1}^n - W_{i-1}^n) + \frac{\nu}{2}\big(\psi_{i+1/2}(W_{i+1}^n - W_i^n) \\ -\psi_{i-1/2}(W_i^n - W_{i-1}^n)\big) + \frac{1}{2}\Delta t k_1(F_i^n + F_{i-1}^n).\end{aligned} \tag{2.20}$$

In oder to solve the reaction diffusion system, i.e. the first and second equations in (2.6), we use a IMEX Midpoint scheme that is a second order scheme [10]. An IMEX scheme consists in a balance of implicit and explicit terms. Here we treat implicitly the diffusion terms, to avoid a parabolic CFL condition that would require $\Delta t \sim \Delta x^2$ [95]. Instead, the IMEX Midpoint requires $\Delta t = O(\Delta x^{4/3})$ [10]. We treat explicitly the sources terms and we obtain:

$$u_{i,j}^{(1)} = u_{i,j}^n + d_u\frac{\Delta t}{2}\left(\frac{\delta_x^2 u^{(1)}}{\Delta x^2} + \frac{\delta_y^2 u^{(1)}}{\Delta y^2}\right) - k d_{dyn}\frac{\Delta t}{2}u_{i,j}^{(1)} + k_-\frac{\Delta t}{2}v_{i,j}^n,$$

$$v_{i,j}^{(1)} = \begin{cases} v_{i,j}^n + d_v\frac{\Delta t}{2}\left(\frac{\delta_x^2 v^{(1)}}{\Delta x^2} + \frac{\delta_y^2 v^{(1)}}{\Delta y^2}\right) - k_-\frac{\Delta t}{2}v_{i,j}^{(1)} + k d_{dyn}\frac{\Delta t}{2}u_{i,j}^n, \\ \qquad\qquad -k_1\dfrac{\Delta t}{2}v_{i,j}^{(1)} + k_{-1}\dfrac{\Delta t}{2}\dfrac{W_i^{n+1}}{|\mathbf{J}|} & \text{if } i,j \in \mathbf{I}\times\mathbf{J}\ , \\ v_{i,j}^n + \dfrac{\Delta t}{2}\left(\dfrac{\delta_x^2 v^{(1)}}{\Delta x^2} + \dfrac{\delta_y^2 v^{(1)}}{\Delta y^2}\right) - k_-\dfrac{\Delta t}{2}v_{i,j}^{(1)} + k d_{dyn}\dfrac{\Delta t}{2}u_{i,j}^n - k_1\dfrac{\Delta t}{2}v_{i,j}^{(1)} \\ \qquad\qquad +c\dfrac{\Delta t}{2\Delta x}\dfrac{W_{i-1}^{n+1}}{|\mathbf{J}|} & \text{if } (i,j)|(x_i,y_j) = (x_{Fi+1}, y_0) \\ v_{i,j}^n + d_v\dfrac{\Delta t}{2}\left(\dfrac{\delta_x^2 v^{(1)}}{\Delta x^2} + \dfrac{\delta_y^2 v^{(1)}}{\Delta y^2}\right) - k_-\dfrac{\Delta t}{2}v_{i,j}^{(1)} + k d_{dyn}\dfrac{\Delta t}{2}u_{i,j}^n & \text{otherwise.} \end{cases} \tag{2.21}$$

$$u_{i,j}^{n+1} = u_{i,j}^n + d_u \Delta t (\frac{\delta_x^2 u^{(1)}}{\Delta x^2} + \frac{\delta_y^2 u^{(1)}}{\Delta y^2}) - k d_{dyn} \Delta t u_{i,j}^{(1)} + k_- \Delta t v_{i,j}^{(1)},$$

$$v_{i,j}^{n+1} = \begin{cases} v_{i,j}^n + d_v \Delta t (\frac{\delta_x^2 v^{(1)}}{\Delta x^2} + \frac{\delta_y^2 v^{(1)}}{\Delta y^2}) - k_- \Delta t v_{i,j}^{(1)} + k d_{dyn} \Delta t u_{i,j}^{(1)} \\ \qquad\qquad - k_1 \Delta t v_{i,j}^{(1)} + k_{-1} \Delta t \dfrac{W_i^{n+1}}{|\mathbf{J}|} & \text{if } i,j \in \mathbf{I} \times \mathbf{J}\ , \\ v_{i,j}^n + \Delta t (\frac{\delta_x^2 v^{(1)}}{\Delta x^2} + \frac{\delta_y^2 v^{(1)}}{\Delta y^2}) - k_- \Delta t v_{i,j}^{(1)} + k d_{dyn} \Delta t u_{i,j}^{(1)} - k_1 \Delta t v_{i,j}^{(1)} \\ \qquad\qquad + c \dfrac{\Delta t}{\Delta x} \dfrac{W_{i-1}^{n+1}}{|\mathbf{J}|} & \text{if } (i,j) | (x_i, y_j) = (x_{Fi+1}, y_0) \\ v_{i,j}^n + d_v \Delta t (\dfrac{\delta_x^2 v^{(1)}}{\Delta x^2} + \dfrac{\delta_y^2 v^{(1)}}{\Delta y^2}) - k_- \Delta t v_{i,j}^{(1)} + k d_{dyn} \Delta t u_{i,j}^{(1)} & \text{otherwise.} \end{cases} \tag{2.22}$$

where

$$\frac{\delta_x^2 u^{(1)}}{\Delta x^2} = \frac{u_{i+1,j}^{(1)} - 2u_{i,j}^{(1)} + u_{i-1,j}^{(1)}}{\Delta x^2}$$

and

$$\frac{\delta_y^2 u^{(1)}}{\Delta y^2} = \frac{u_{i,j+1}^{(1)} - 2u_{i,j}^{(1)} + u_{i,j-1}^{(1)}}{\Delta y^2}$$

(respectively for v). Since u and v satisfy mixed boundary conditions on Γ_2 and Neumann boundary conditions on Γ_4 we use the second order derivative approximation to calculate the boundary values:

$$\frac{\partial u}{\partial n}(0, y_j) = \frac{1}{2\Delta x}(-3u_{0,j}^n + 4u_{1,j}^n - u_{2,j}^n),$$

to yield:

$$u_{0,j}^n = (\frac{4}{3}u_{1,j}^n - \frac{1}{3}u_{2,j}^n).$$

We also discretize:

$$\frac{\partial u}{\partial n}(L_x, y_j) = \frac{1}{2\Delta x}(3u_{N_x+1,j}^n - 4u_{N_x,j}^n + u_{N_x-1,j}^n),$$

which gives

$$u_{N_x+1,j}^n = \frac{d_u}{3d_u + 2\Delta x p_u}(4u_{N_x,j}^n - u_{N_x-1,j}^n).$$

Similarly we calculate the numerical approximation of v on the boundary.

Now we detail the treatment of the term corresponding to the outgoing flux from the microtubule. For the sake of simplicity, let us consider v as a function of (x,t) and set $x_k = x_{Fi+1}$. If we neglect the reactions terms, the mass traversing the volume D,

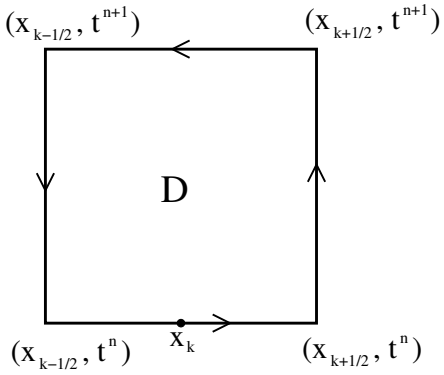

Figure 2.4: We consider the plane (x,t) and the mesh point x_{Fi+1} , called x_k.

represented in Figure 2.4, is given by the following formula:

$$\int\int_D \partial_t v + \partial_x(-\partial_x v) \underset{\text{Gauss-Green}}{=} \int_{\partial D} -\partial_x v\, dx + \int_{\partial D} -v\, dt. \tag{2.23}$$

Using formula (2.23) we obtain the expression for v:

$$v_k^{n+1} = \frac{1}{\Delta x}\int_{x_{k-1/2}}^{x_{k+1/2}} v_k^{n+1} = v_k^n - \left(\frac{1}{\Delta x}\int_{t^n}^{t^{n+1}} (-\partial_x v)_{k+1/2} - \frac{1}{\Delta x}\int_{t^n}^{t^{n+1}} (-\partial_x v)_{k-1/2}\right). \tag{2.24}$$

The flux due to the microtubule at $(x_{k-1/2}, t^{n+1})$ is cW_{k-1}^{n+1} so that if we add this flux to (2.24) we get:

$$v_k^{n+1} = v_k^n + \frac{\Delta t}{\Delta x}\left[\frac{v_{k+1}^n - v_k^n}{\Delta x} - \left(\frac{v_k^n - v_{k-1}^n}{\Delta x} + \frac{cW_{k-1}^{n+1}}{|\mathbf{J}|}\right)\right],$$

that corresponds to the formula used in the numerical scheme (2.21)-(2.22).

To verify the order of accuracy of the proposed scheme, we fix a space step $\Delta x = 0.005$, $\Delta y = \Delta x$, and, once calculated the corresponding time steps $\Delta t = \min(\Delta x/c, \Delta x^{4/3})$, we evaluate a *reference* solution $u_{ref}, v_{ref}, W_{ref}$, using the proposed scheme. We evaluate the reference solution at different final times $T = 5$, $T = 10$ and $T = 15$. Then we change the space step, and accordingly the time step, and we calculate the error evaluating the L^1 distance between the numerical solutions and the reference solution:

$$e^T(h) := \int_\Omega |u_{ref}^T - u_h^T| + |v_{ref}^T - v_h^T| + |w_{ref}^T - w_h^T| dxdy, \tag{2.25}$$

where $h = \Delta x$ is the fixed space step. We also recall that we have defined $w(x,y) = W(x)\dfrac{\mathbb{1}_{\mathbf{I}\times\mathbf{J}}(x,y)}{|\mathbf{J}|}$, thus w is well defined on Ω. Using formula 2.25, we plot, in the logarithmic scale, the numeric error at $T = 5, 10, 15$ and the h^2 curve (light blue). Looking to Figure 2.5(a) we can observe that the order of accuracy of our scheme is

h	$\|u^5_{ref} - u^5_h\|_1$	$\|v^5_{ref} - v^5_h\|_1$	$\|W^5_{ref} - W^5_h\|_1$
0.1	$1.2576 \cdot 10^{-3}$	$0.7733 \cdot 10^{-3}$	$0.4698 \cdot 10^{-3}$
0.05	$0.1963 \cdot 10^{-3}$	$0.3147 \cdot 10^{-3}$	$0.1227 \cdot 10^{-3}$
0.02	$0.0662 \cdot 10^{-3}$	$0.1016 \cdot 10^{-3}$	$0.0447 \cdot 10^{-3}$
0.01	$0.004 \cdot 10^{-3}$	$0.0131 \cdot 10^{-3}$	$0.0141 \cdot 10^{-3}$

Table 2.1: Error L^1 at different space steps.

h	$\|u^{10}_{ref} - u^{10}_h\|_1$	$\|v^{10}_{ref} - v^{10}_h\|_1$	$\|W^{10}_{ref} - W^{10}_h\|_1$
0.1	$0.8837 \cdot 10^{-5}$	$0.1287 \cdot 10^{-4}$	$0.0148 \cdot 10^{-5}$
0.05	$0.2810 \cdot 10^{-5}$	$0.0507 \cdot 10^{-4}$	$0.1260 \cdot 10^{-5}$
0.02	$0.0972 \cdot 10^{-5}$	$0.0171 \cdot 10^{-4}$	$0.0464 \cdot 10^{-5}$
0.01	$0.0145 \cdot 10^{-5}$	$0.0038 \cdot 10^{-4}$	$0.0148 \cdot 10^{-5}$

Table 2.2: Error L^1 at different space steps.

around 2, as expected. The mean error $e_m(h)$, is given by the arithmetic mean at the different time steps considered. In order to calculate more precisely the accuracy of our scheme, we consider the curve

$$log(e_m(h)) = \gamma log(h) + log(C),$$

where γ is the order of accuracy of the scheme, and we fit this curve by a least square method. We find $\gamma = 1.83$ (see Figure 2.5(b)).

The Tables 2.1, 2.2, 2.3 show the L^1 distances of solutions at different space steps, at time $T = 5$, $T = 10$ and $T = 15$. We can observe, from the values reported in the tables, that the L_1 error diminishes with h.

2.3 Simulation results

Our purpose is to evaluate for which proteins microtubule activity is a natural support for intracellular trafficking. Several proteins have been proven to use the MTs network and the motor protein dynein to facilitate their way towards the nucleus. Maybe the most notable one is the tumor suppressor protein p53, because of its crucial role in cell life regulation [41, 113]. But other proteins, such as p38 or PTHrP are known to be

h	$\|u^{15}_{ref} - u^{15}_h\|_1$	$\|v^{15}_{ref} - v^{15}_h\|_1$	$\|W^{15}_{ref} - W^{15}_h\|_1$
0.1	$0.1090 \cdot 10^{-6}$	$0.1897 \cdot 10^{-6}$	$0.4434 \cdot 10^{-7}$
0.05	$0.0406 \cdot 10^{-6}$	$0.0617 \cdot 10^{-6}$	$0.1124 \cdot 10^{-7}$
0.02	$0.0142 \cdot 10^{-6}$	$0.0212 \cdot 10^{-6}$	$0.0417 \cdot 10^{-7}$
0.01	$0.0034 \cdot 10^{-6}$	$0.0056 \cdot 10^{-6}$	$0.0135 \cdot 10^{-7}$

Table 2.3: Error L^1 at different space steps.

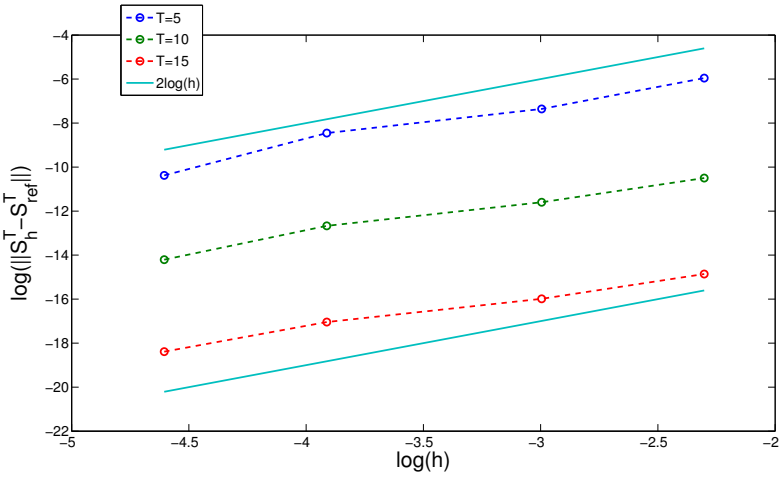

(a)

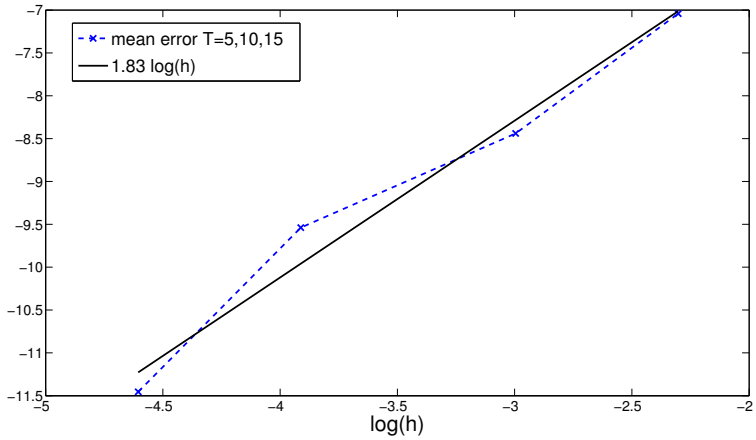

(b)

Figure 2.5: (a)L_1 error in logarithmic scale. We set $S^T = u^T + v^T + w^T$. (b) Mean error plot in logarithmic scale and its least square linear approximation.

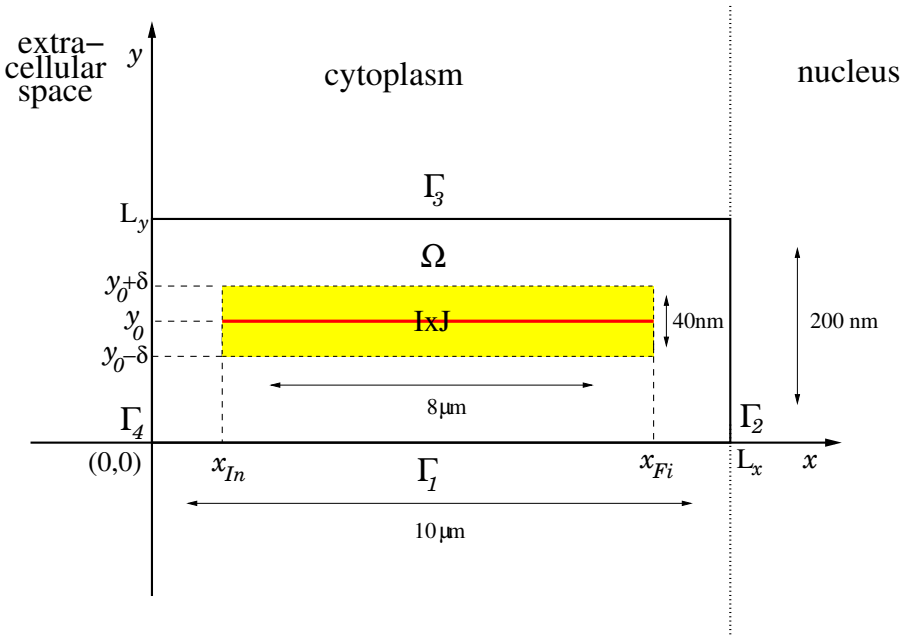

Figure 2.6: Area of the cytoplasm where intracellular transport is modelled: $\Omega = [0, L_x] \times [0, L_y]$. The yellow rectangle ($\mathbf{I} \times \mathbf{J} = [x_{In}, x_{Fi}] \times [y_0 - \delta, y_0 + \delta]$) represents the attraction area of the microtubule filament, the red strip is the microtubule, positioned in y_0.

transported by motor proteins, which can improve their nuclear accumulation [43, 72]. We solved numerically the reaction-diffusion-advection system (2.6), to calculate the total flow of particles, with and without the microtubule.

In *in vitro* experiments [113], microtubules dynamics is suppressed by the use of specific drugs that dissociate microtubules. Using numerical simulations, we can both simulate active transport, or assume that the MT is unable to perform its task because of external variation of the system, such as the infusion of a drug. Or simply assume that dynein does not bind the cargo proteins.

Model parameters and biophysical quantities

Let us recall some notations relative to the chosen domain. We consider a rectangle $\Omega = [0, L_x] \times [0, L_y]$, see figure 2.6. The attraction area of the microtubule is the subdomain $\mathbf{I} \times \mathbf{J} = [x_{In}, x_{Fi}] \times [y_0 - \delta, y_0 + \delta]$. We fix $L_x = 10$, $L_y = 0.2$, where lengths are expressed in micrometers. We suppose that in this area a single microtubule lies. The average diameter of a microtubule is $0.024\mu m$ [76], so we have chosen to fix the thickness of the attraction area $|\mathbf{J}|$ of the modelled microtubule to $0.04\mu m$. The length of a microtubule is variable and depends on the type of the cell. Here we fix its length to $8\mu m$, which means that we fix the length of the interval $\mathbf{I} = [x_{In}, x_{Fi}]$. In particular, we assume $\mathbf{I} = [0.1, 0.9]$. Finally $y_0 = 0.1$ so that the microtubule is positioned at the centre, in the y direction, of the domain Ω.

Parameter	*Unit*	*Value*	*Reference(s)*
k	s^{-1}	0.2	[15, 97]
k_-	s^{-1}	0.2	[15, 97]
k_1	s^{-1}	0.5	[122]
k_{-1}	s^{-1}	0.5	[122]
c	$\mu m s^{-1}$	1	[96, 81]
d_u, d_v	$\mu m^2 s^{-1}$	1	[117]
p_u, p_v	$\mu m s^{-1}$	1	proposed
MT length	μm	8	proposed
L_x, L_y	μm	10 and 0.2	proposed
I, **J**	μm	8 and 0.04	proposed

Table 2.4: Parameter values for system 2.6 and corresponding references in literature. Remark that the value for the permeability coefficient is not intended to be realistic, since we are not considering any import pathway. However, a permeability equal to $1\mu m s^{-1}$ corresponds roughly to the permeability of a cargo+importin complex: $1.87\mu m s^{-1}$ [121]. The length of a microtubule is variable and depends on the cell type. Microtubules can measure between less than a micrometer to hundreds of micrometers and the average diameter is $24nm$ [76].

In order to calculate the mass flow due to transport and diffusion, we fix a point $\bar{x}$, $x_{Fi} < \bar{x} < L_x$ and we calculate the net flux of each species at the end of the domain. This is to say:

$$\phi_u(t) = -d_u \int_0^{L_y} \nabla u(\bar{x}, y) \cdot \mathbf{n}(\bar{x}, y) dy, \quad \phi_v(t) = -d_v \int_0^{L_y} \nabla v(\bar{x}, y) \cdot \mathbf{n}(\bar{x}, y) dy, \quad (2.26)$$

and integrating over time we define:

$$F_u(t) = \int_0^t \phi_u(t) dt \quad \text{and} \quad F_v(t) = \int_0^t \phi_v(t) dt\,. \quad (2.27)$$

The functions F_u and F_v express the mass amount that has traversed the line $\bar{x} \times L_y$ after a time t, which makes sense since we are dealing with superficial concentrations. We fix the reaction constants for all the species, as in Table 2.4.

The total dynein concentration is assumed to be constant: $[D] = 1$. We will vary the diffusion coefficient of the cargo protein in order to determine which proteins benefit of motor-assisted transport. We fix a starting diffusion value to $1\mu m^2 s^{-1}$ that corresponds to big proteins of mass $> 1000kDa$, as it can be seen on Figure 2.8.

2.3.1 The macromolecules flow increases with MT activity

Using the numerical scheme discussed in Section 2.2 and the values of coefficients listed in Table 2.4 we perform numerical simulations of system (2.6). In particular, the diffusion values of u and v are set to $1\mu m^2 s^{-1}$. We model the combined action of diffusion

The initial values are set to:

$$
\begin{aligned}
u(x,y,0) &= \begin{cases} 10 & \text{if } 0 \le x \le x_0 \\ 10 \cdot e^{-(x-x_0)^2} & \text{if } x_0 \le x \le 10 \end{cases} \\
v(x,y,0) &= 0 \\
w(x,0) &= 0
\end{aligned}
\tag{2.28}
$$

where $x_0 = 3.3$.

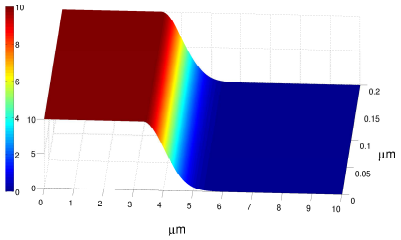

Figure 2.7: Initial data for u.

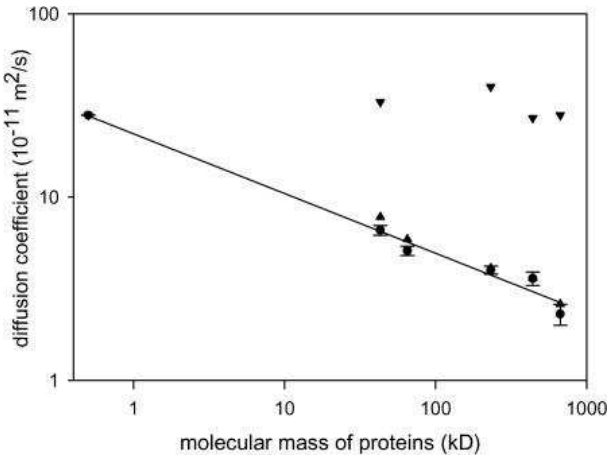

Figure 2.8: Protein diffusion coefficient and corresponding molecular mass [66]

and active transport along a single microtubule. The action of the microtubule can be observed 1) in the distribution of the total mass that accumulates around the filament and 2) in the higher velocity of the transported particles. Figure 2.9 shows the spatial distribution of total concentration $u + v + w$, at different time steps. The non-uniform distribution of the concentrations is a consequence of the microtubule activity: in the vertical direction because of localization, in the horizontal direction it is a consequence of the greater distances in the x direction travelled by the particles attached to the filament. Indeed, the displacement along the microtubule during a time t is given by

$$x_c(t) = ct = 1 \cdot t,$$

where $c = 1\mu m s^{-1}$ is the constant velocity of the motor along the filament. The mean displacement of the diffusive particles is

$$r_D(t) = \sqrt{4Dt} \sim 2\sqrt{t},$$

for $D = 1\mu m^2 s^{-1}$ [6]. Notice that the mean displacement due to diffusion underlie a displacement in $\mathbb{R}^2$, while the displacement due to the microtubule is in one direction.

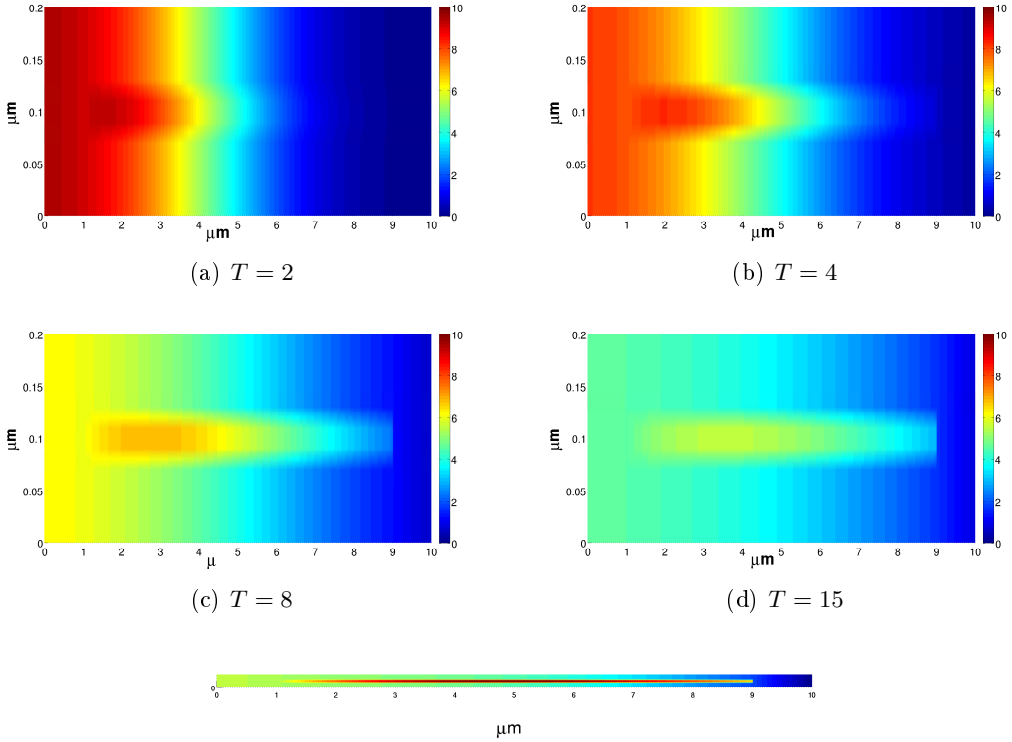

(a) $T = 2$

(b) $T = 4$

(c) $T = 8$

(d) $T = 15$

(e) realistic dimension

Figure 2.9: Spatial distribution of total concentration $u + v + w$ at different time steps. Parameters in Table 2.4. (e) A plot of the spatial distribution of the total concentration with the right proportion of the area modelled.

Using equations (2.27) we evaluate the total mass flow at the end of the domain, given by $F_u + F_v$. To compare the flow due to motor-assisted transport with the flow due to diffusion alone, we assume that the cargo proteins do not associate with dynein and we simulate system (2.6) setting $k = 0$. The flow due to diffusion and to motor transport is greater than the diffusive flow alone. Figure 2.10(a) shows this result: the black curve is the mass that at time t, traverses the segment at the end of the domain, fixed by the definition of equations (2.26). The blue curve is the mass flow due to diffusion, when the attachment to dynein is blocked. When the microtubule operates, enhanced transport towards the nucleus is evident.

Next, we perform the same simulations using different diffusion coefficients and we compare the results obtained when only diffusion is allowed, and when microtubule transport is active. As Figure 2.10(b) shows, for values of diffusion $< 4\mu m^2 s^{-1}$, microtubule activity enhances the total flow. If the diffusion coefficient of the cargo protein is set to $4\mu m^2 s^{-1}$ the flow with active transport is equal to the flow due to diffusion. Our results confirm that cytoplasmic transport of big molecules or organelles is increased by the use

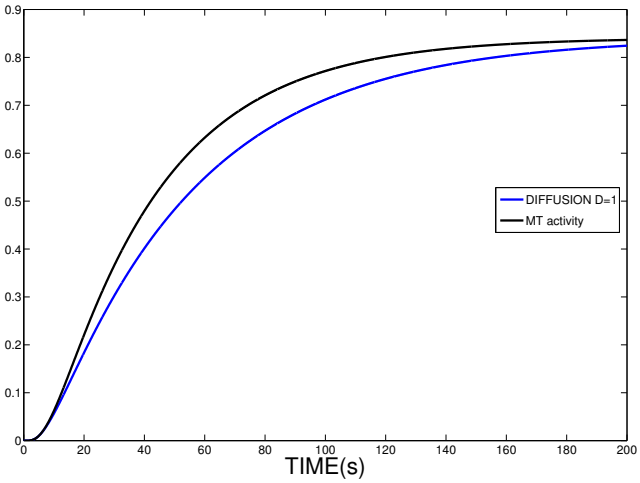

(a)

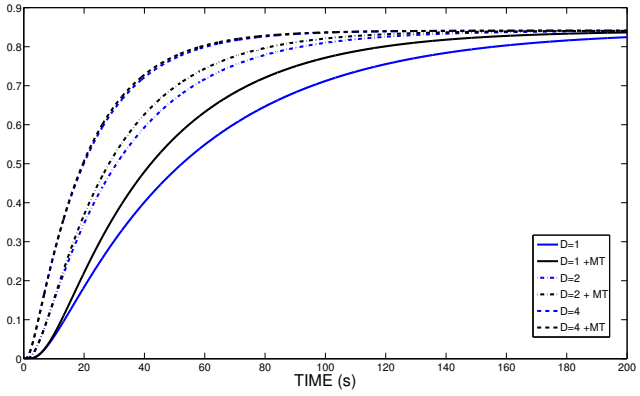

(b)

Figure 2.10: (a): Total flow with microtubule activity (black curve) and total flow due to diffusion alone. Diffusion coefficients are set to $1\mu m^2 s^{-1}$. (b)Comparison of the total flow calculated for different diffusion values: $d_u = d_v = 1, 2, 4\mu m^2/s$. The blue curves are the flow calculated when the activity of microtubules is blocked; the black curves are the flow relative to the MT activity. The flow is calculated using equations (2.27).

of microtubules. For example, a protein having a molecular mass $\sim 500kD$ would have a diffusion coefficient of $\sim 2.5\mu m^2 s^{-1}$ [117].

We conclude by some remarks. The mean attachment time of the cargo-dynein complex to the microtubule and the mean diffusive time of the cargo-dynein complex are

given by:

$$\tau_{on} = \frac{1}{k_{-1}}, \qquad \tau_{off} = \frac{1}{k_1}.$$

Using the values listed in Table 2.4, we can evaluate these values: $\tau_{on} = 2s$, and $\tau_{off} = 2s$. During this reference time, the distance travelled *on* the microtubule is $x_c(\tau_{on}) = 2\mu m$, while the displacement due to diffusion is $r_D(\tau_{off}) = 2\sqrt{2}$. A variation of these coefficients could improve further the benefit due to microtubule activity, since it would result in an increase of the time spent on the filament. We will analyse these possibilities in the next section.

2.3.2 Detachment and attachment rates from the MT increase the total flow

In section 2.3.1 we have shown that molecules having a diffusion coefficient up to $4\mu m^2 s^{-1}$ benefit of active transport. However, a protein like p53, which has a molecular mass $\sim 50kD$, has a diffusion coefficient $\sim 15\mu m^2 s^{-1}$ [58]. The results of Roth *et al.* [113] show that proteins like p53 and pRb (molecular mass $\sim 110kD$ [61]) benefit of microtubule activity in their way towards the nucleus. What can explain this discrepancy?

One possible explanation is that the attachment rate of dynein to microtubules is changeable and depends on the the microtubule length and motor concentration [135].The detachment rate is also variable and depends on the load. For instance, when unloaded, dynein detaches rapidly from the microtubule [135].

Suppose that the cargo in question is able to attach to more than one motor protein. On the one hand, this assumption would imply that the cargo spends a longer time *on* the microtubule. On the other hand, we can imagine that several motor proteins increase the probability to attach to the microtubule in such a way to decrease the time spent *off* the filament. We test how the attachment and the detachment rates from the microtubule influences its ability to enhance protein transport.

First, we fix the attachment rate k_1 of the cargo to the filament and we perform simulations for different values of k_{-1}. We fix $k_1 = 0.5$ in such a way that the diffusive mean time of a cargo-dynein complex is $\tau_{off} = 2s$, as in Section 2.3.1. We perform numerical simulations for values of $k_{-1} = 0.5$, 0.05 and $0.005s^{-1}$. The results indicate that the lower the rate of detachment, the greater the increase of the corresponding flow of molecules, that is, the greater the time spent on the microtubule, the greater the flow observed. Figure 2.11 illustrates the flows relative to different k_{-1}, when the diffusion coefficients of the cargo and of the cargo-dynein complex, are set to $1\mu m^2 s^{-1}$. We observe a remarkable increase of the total flow when k_{-1} passes from the value of $0.5s^{-1}$ to $0.05s^{-1}$. On the contrary, the difference between the cases $k_{-1} = 0.05s^{-1}$ and $k_{-1} = 0.005s^{-1}$ is very small. This result is not surprising, since the time needed to a motor protein to walk the whole filament is of 8 seconds. The values $k_{-1} < 1/8$, which give an average time of attachment greater than 8 seconds do not guarantee better results. In Figures 2.13 we plot the flows corresponding to diffusion coefficients of $2\mu m^2 s^{-1}$ and $4\mu m^2 s^{-1}$. We can observe that if $k_{-1} \leq 0.05$ then the microtubule influence slightly

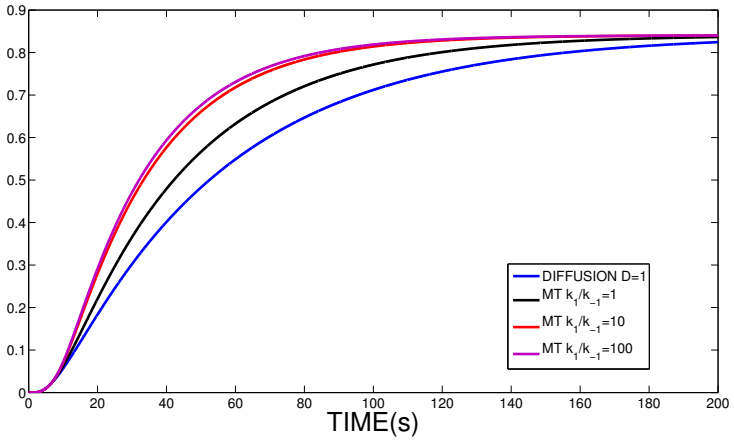

Figure 2.11: Diffusion is set to $1\mu m^2 s^{-1}$. Blue curve: flow due to diffusion with no MT activity. Other curves: total flow with MT for different values of $k_{-1} = 0.5$, 0.005, 0.005 ($k_1 = 0.5$ is a fixed value).

increases the flow for the diffusion coefficient of $4\mu m^2 s^{-1}$. In conclusion, we observed an increment of the flow for diffusion values up to $\sim 5\mu m^2 s^{-1}$ for values of $k_{-1} \leq 0.05$.

Second, we fix the detachment rate k_{-1} to $0.1 s^{-1}$ and we perform simulations for values of $k_1 = 1$ and $k_1 = 10$ in such a way to reduce the mean diffusive time τ_{off} of the cargo-dynein complex. In this second scenario, the influence of microtubule is greater: the total flow increases more rapidly and reaches its maximum in a lower time. Figure 2.13(a) shows the different flows for a diffusion value fixed to $4\mu m^2 s^{-1}$. Figure 2.13(b) shows the total flow for the diffusion coefficient $d_v = 6 m^2 s^{-1}$. It illustrates that for the values of k_1 and k_{-1} set to 0.5 and $0.005 s^{-1}$ respectively (dotted curve) the flow with microtubule activity corresponds to the flow due to diffusion only (blue curve). On the contrary, the flow obtained when setting $k_1 = 10$ and $k_{-1} = 0.1$ is slightly higher than the flow due to diffusion. In conclusion, diminishing the mean diffusive time of the cargo-dynein complex, further increases the total flow due to microtubule. In particular, with this choice of parameters ($k_1 = 10$ and $k_{-1} = 0.1$), we have shown that proteins having a diffusion coefficient up to $6\mu m^2 s^{-1}$ benefit of microtubule transport.

Finally, we could not explain the enhanced transport towards the nucleus of molecules having a diffusion coefficient $> 6\mu m^2 s^{-1}$. Proteins having a diffusion coefficient $\sim 10\mu m^2 s^{-1}$ have been shown to benefit of motor-assisted transport. However, we could reveal a strong difference on the total flow, for proteins having low diffusion coefficient, thus confirming the influence of microtubules in cytoplasmic transport.

2.4 Summary and further directions

We introduced this simple model with the aim to reproduce a mechanical behaviour of signal transport in the cytoplasm and to highlight the importance of microtubule

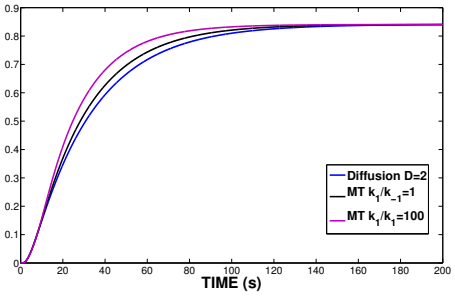

(a) $d_v = 2\mu m^2 s^{-1}$

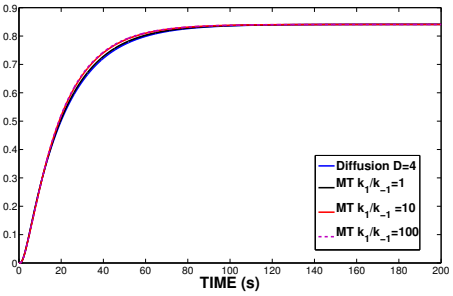

(b) $d_v = 4\mu m^2 s^{-1}$

Figure 2.12: (a),(b): Comparison of the total flow, with and without MT, for different diffusion values. Blue curves: flow due to diffusion when k is set to zero (no MT activity). Other curves: total flow with MT activity ($F_u + F_v$). (a) $d_u = d_v = 2\mu m^2 s^{-1}$; (b) $d_u = d_v = 4\mu m^2 s^{-1}$.

activity. It is still unknown why some proteins but others use the MTs. We found a clear difference in the results (total net flux enhanced thanks to microtubule based transport) for low-mobility cargoes that use this mechanism to move faster towards the nucleus. Our purpose was to point out the importance of this mechanism that has recently been explored as a nuclear protein trafficking support. Using a PDEs system of equation, with a two dimensional spatial representation of the free cargo concentration, and one dimensional representation of the transported cargo, we could compare the diffusion mechanism against the advection one. Our multidimensional approach was a tool to stress the difference in the two types of transport, which will be compared in the future to more data in the literature.

We could verify with this model that the mobility of molecules having a diffusion coefficient up to $6\mu m^2 s^{-1}$ is enhanced by motor assisted transport. Depending on the choice of the attachment and detachment rates (to and from the microtubule), we have shown that different cargoes take advantages of microtubule transport. In particular, if we assume that the cargo-dynein complex is attached to the microtubule for 2 seconds and that it also diffuses for 2 seconds, then the cargoes that benefit of motor assisted transport are those that have a diffusion coefficient $\leq 4m^2 s^{-1}$. On the contrary, if we assume that proteins have higher attachment rates and lower detachment rates, then bigger proteins, that have a diffusion coefficient up to $6\mu m^2 s^{-1}$, take advantage of microtubule activity. We remark also that the threshold on the diffusivity could be increased by a higher velocity of the motor proteins that here we fixed to $1\mu m/s$, that is the mean value observed in literature.

Our interest was relied on little proteins with higher diffusion coefficients, that need to be imported to the nucleus. In the next chapter we will explore the more complete setting, where all the import pathway of proteins to the nucleus is considered. We will couple our model with the model of the RAN import pathway proposed by Cangiani and Natalini in [15]. We will add the nuclear compartment in order to quantify the total

amount of imported proteins. This improvement of the model will permit us to take into account the realistic reaction times of the import pathway. In fact, cargo proteins do not traverse the nuclear membrane by themselves but they need to be actively imported in the nucleus.

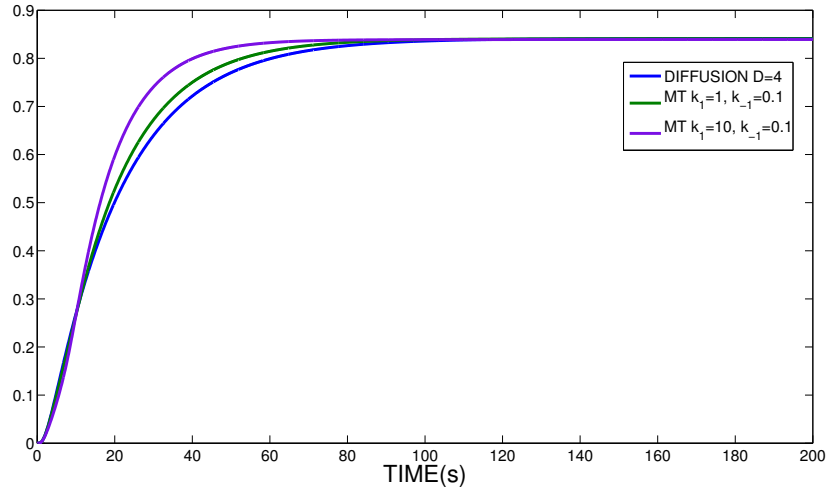

(a) $d_v = 4\mu m^2 s^{-1}$

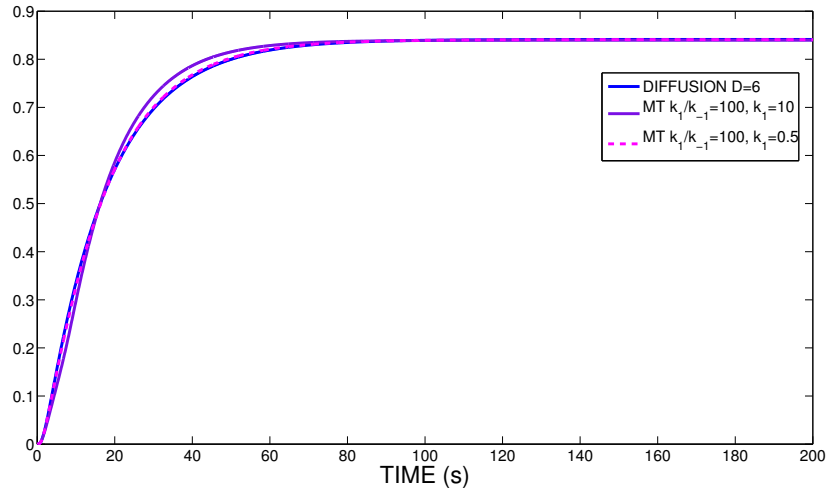

(b) $d_v = 6\mu m^2 s^{-1}$

Figure 2.13: (a),(b): Comparison of the total flow, with and without MT, for different diffusion values. Blue curves: flow due to diffusion when k is set to zero (no MT activity). Other curves: total flow with MT activity ($F_u + F_v$). (a) $d_u = d_v = 4\mu m^2 s^{-1}$; (b) $d_u = d_v = 6\mu m^2 s^{-1}$.

Chapter 3

Nucleocytoplasmic transport: including the whole pathway

In the previous Chapter we have introduced a simplified model of cytoplasmic transport. We have considered a sub-domain of the cytoplasm where we assumed that a unique microtubule is present. We have located the microtubule and have reduced its area of attraction to a sub-strip of the entire domain. Our results show that molecules having a diffusion coefficient up to $6\mu m^2 s^{-1}$ benefit of microtubule enhanced import.

In this Chapter we couple the model introduced in Chapter 2 with the model presented by Cangiani and Natalini in [15]. Our aim is to take into account all the reactions network that regulate protein import in order to evaluate, in this more realistic setting, which nuclear proteins benefit of motor assisted transport. In Section 3.1 we introduce the biological network of the Ran pathway, modelled by Cangiani and Natalini. We describe their mathematical model and we couple it with our model of motor-assisted transport. In Section 3.2 we give the details about the numerical treatment of the simulated system. In Section 3.3 we present the numerical results and we show that the import of nuclear proteins is enhanced by microtubule activity. Finally in Section 3.4 we discuss the main features of the model, its limitations and the possible future extensions.

Contents

3.1 A model for Ran

Fundamentals of Biology

Nuclear proteins carry out their functions within the nucleus. After synthesis in the cytoplasm they need to translocate to the nuclear compartment where they are able to perform their tasks. In order to get the access to the nucleus they bear a tag, the Nuclear Localization Signal (NLS) [27], through which they are able to bind to proteins of the importin family. Importins operate the translocations from cytoplasm to nucleus. Two types of importins exist: importin-α and importin-β. Members of the first family bind to nuclear proteins with high affinity [46]. Members of the importin-β family, mediate the interactions with the nuclear pore and actually shuttle their cargo from one compartment to the other [45]. Directionality of transport is assured by the Ran gradient. The molecule Ran can be found in two different forms within the cell: a GTP bound form that is mostly nuclear and a GDP bound form that is cytoplasmic. Ran-GTP, located near the nuclear pores, binds to the importin-cargo complex and delivers the cargo inside the nucleus. The newly formed complex importin-RanGTP shuttles back to the cytoplasm where it is disrupted after RanGTP hydrolysis, mediated by the cytoplasmic RanGap [7]. In the nucleus chromatin-bound RCC1 promotes the exchange of Ran-bound GDP by GTP [9]. RanGDP is transported to the nucleus by the receptor NTF2. The existence of a Ran gradient is thus assured and the directionality of transport follows. See Figure 3.1 for a schematic view of the Ran cycle. In Section 1.3 the import pathway of nuclear proteins has been explained in more details.

Modelling choices

The reaction network of the nuclear import pathway has been modelled by several authors [48, 111, 121]. Cangiani *et al.* , following Kopito *et al.* [65], keep the reaction network to the essentials. Following the authors [15] we introduce the modelled species, and we assign the names of the corresponding variables:

$$\begin{aligned} &RanGTP = R_t, \\ &RanGDP = R_d, \\ &Imp = T, \\ &Cargo = C, \\ &Imp\text{-}Cargo = T_c, \\ &Imp\text{-}RanGTP = T_r, \end{aligned} \tag{3.1}$$

where, for the sake of simplicity, the importin T represents the complex importin-α, importin-β and no distinction between the receptor, importin-α, and the transporter, importin-β, is made. In the same vein, the RanGDP is supposed to be in a complex with its chaperone NTF2. The nuclear import process begins with the recognition of the cargo C by the receptor T, that is able to shuttle across the membrane. The formation

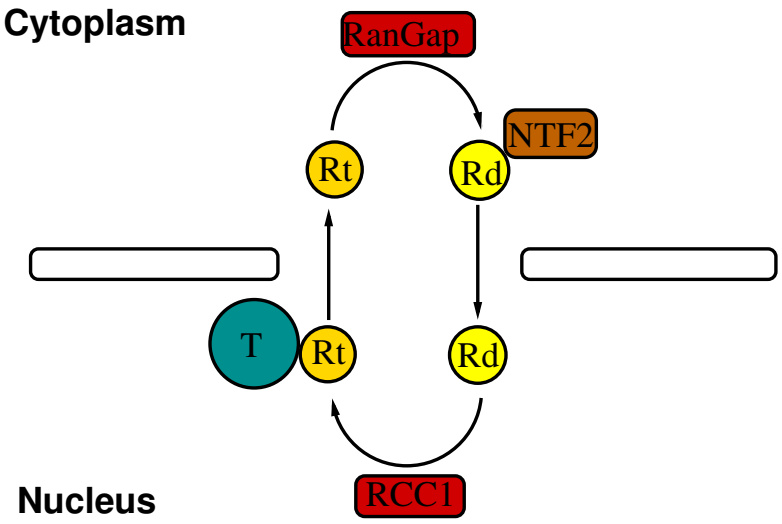

Figure 3.1: Sketch of the Ran cycle: the molecule Ran, in its GTP bound form, R_t is mostly nuclear. In the nucleus, it binds to the receptor T and delivers the transported cargo (see Figure 3.2). The complex RanGTP-receptor shuttles in the cytoplasm. Here the hydrolysis mediated by RanGap transforms RanGTP into RanGDP. RanGDP, R_d, is carried to the nucleus by the chaperone NTF2. In the nucleus RanGDP is converted into RanGTP through the action of RCC1.

of this complex is supposed to be only cytoplasmic. On the contrary, the receptor-cargo complex T_c is disrupted in the nuclear compartment by the action of RanGTP that binds to the receptor and shuttles to the cytoplasm. In the cytoplasm RanGTP is transformed into RanGDP. Cytoplasmic RanGDP can shuttle between the two compartments, as it is assumed to be in a complex with its chaperone NTF2. Nuclear RanGDP, interacts with the nuclear RCC1 which catalyses the exchange between nucleotide GDP and GTP forming the nuclear RanGTP. These reactions are summarized in Table 3.1 and the pathway summarized in Figure 3.2.

Cytoplasm	**Nucleus**
$RanGTP \overset{RanGAP}{\longrightarrow} RanGDP$	$RanGDP \overset{RCC1}{\longrightarrow} RanGTP$
Import Cycle	**Import Cycle**
$Imp + Cargo \longrightarrow Imp\text{-}Cargo$	$Imp\text{-}Cargo + RanGTP \longrightarrow$
(Imported into the nucleus)	$Cargo + Imp\text{-}RanGTP$

Table 3.1: Import model [15]

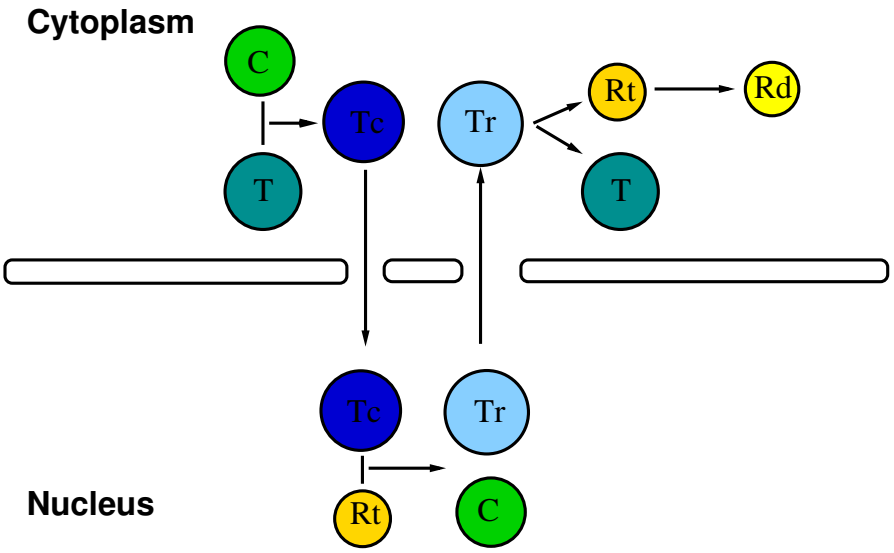

Figure 3.2: Model of the import pathway designed by [15]. The receptor T form a complex with the cargo C. The T_c complex crosses the nuclear envelope and, once in the nucleus, the cargo is released by the binding with RanGTP, R_t. The newly formed complex, T_r (the receptor T and the Ran molecule, R_t) shuttles back to the cytoplasm where it is disrupted. A new cycle starts over.

3.1.1 Mathematical formulation

The model is a system of six coupled semilinear parabolic PDEs set on two compartments: cytoplasm and nucleus. We introduce the following notations. Let Ω be the whole cell domain and $\partial\Omega$ its exterior boundary. Furthermore let Ω_c and Ω_n be respectively the cytoplasmic and nuclear domain and Γ_{nc} the common boundary of the two sub-compartment (the nuclear envelope). Each species is supposed to freely diffuse within each compartment and diffusion is modelled by Fickian Law. The membrane is assumed to be a porous medium and the translocation through each Nuclear Pore is modelled averaging the single processes. The inclusion of the membrane is thus made by assigning a permeability coefficient for each molecular species and permeability conditions are imposed using Kedem-Katchalsky boundary conditions [62]. See [13, 15, 118, 121] for a numerical and mathematical discussion about this type of conditions. All the reaction terms are modelled following the Law of Mass Action and they are summarized in Table 3.2. We obtain the following system of coupled semilinear parabolic equations, in the

cytoplasm Ω_c:

$$\begin{cases} \frac{\partial R_t}{\partial t} = d_{rt}\Delta R_t - m_1(R_t) - r_1(R_t, T) + r_{-1}(T_r), \\ \frac{\partial R_d}{\partial t} = d_{rd}\Delta R_d + m_1(R_t), \\ \frac{\partial T_r}{\partial t} = d_{tr}\Delta T_r + r_1(R_t, T) - r_{-1}(T_r), \\ \frac{\partial C}{\partial t} = d_c\Delta C - r_2(C, T), \\ \frac{\partial T}{\partial t} = d_t\Delta T - r_1(R_t, T) + r_{-1}(T_r) - r_2(C, T), \\ \frac{\partial T_c}{\partial t} = d_{tc}\Delta T_c + r_2(C, T), \end{cases} \tag{3.2}$$

and in the nucleus, Ω_n:

$$\begin{cases} \frac{\partial R_t}{\partial t} = d_{rt}\Delta R_t + m_2(R_d) - r_1(R_t, T) + r_{-1}(T_r) - r_3(R_t, T_c) \\ \frac{\partial R_d}{\partial t} = d_{rd}\Delta R_d - m_2(R_d), \\ \frac{\partial T_r}{\partial t} = d_{tr}\Delta T_r + r_1(R_t, T) - r_{-1}(T_r) + r_3(R_t, T_c) \\ \frac{\partial C}{\partial t} = d_c\Delta C + r_3(R_t, T_c), \\ \frac{\partial T}{\partial t} = d_t\Delta T - r_1(R_t, T) + r_{-1}(T_r), \\ \frac{\partial T_c}{\partial t} = d_{tc}\Delta T_c - r_3(R_t, T_c). \end{cases} \tag{3.3}$$

The transmission conditions couple system (3.2) and (3.3) on Γ_{nc}:

$$\begin{cases} d_{rt}\frac{\partial R_t^{(c),(n)}}{\partial \mathbf{n}} = 0 \\ d_{rd}\frac{\partial R_d^{(c)}}{\partial \mathbf{n}} = p_d(R_d^{(c)} - R_d^{(n)}) = d_{rd}\frac{\partial R_d^{(n)}}{\partial \mathbf{n}} \\ d_{tr}\frac{\partial T_r^{(c)}}{\partial \mathbf{n}} = p_{tr}(T_r^{(c)} - T_r^{(n)}) = d_{tr}\frac{\partial T_r^{(n)}}{\partial \mathbf{n}} \\ d_c\frac{\partial C^{(c),(n)}}{\partial \mathbf{n}} = 0 \\ d_t\frac{\partial T^{(c)}}{\partial \mathbf{n}} = p_t(T^{(c)} - T^{(n)}) = d_t\frac{\partial T^{(n)}}{\partial \mathbf{n}} \\ d_{tc}\frac{\partial T_c^{(c)}}{\partial \mathbf{n}} = p_{tc}(T_c^{(c)} - T_c^{(n)}) = d_{tc}\frac{\partial T_c^{(n)}}{\partial \mathbf{n}} \end{cases} \tag{3.4}$$

where $\cdot^{(c)}$ and $\cdot^{(n)}$ represent nuclear and cytoplasmic concentrations, respectively. The normal vector $\mathbf{n}$ is the one relative to the nuclear compartment. Notice that, at each side of the membrane, the fluxes are continuous, but there can be a jump in the concentrations. Remark also that the RanGTP, R_t, and the cargo C are unable to traverse the nuclear membrane if not in a complex with the chaperone T. Therefore, the corresponding flux at the nuclear membrane Γ_{nc}, is imposed to be zero. At the plasma membrane, $\partial\Omega$, homogeneous Neumann boundary conditions are imposed for each species. Thus, no mass exchange with the exterior is allowed.

Microtubule Activity

In the model of Ran mediated import presented above, the authors include also active transport along microtubules. The microtubules are modelled as a vector field that span the whole cytoplasm. Therefore, at each point of the cytoplasm, except for a narrow area

Cytoplasm	**Nucleus**
$R_t \xrightarrow{R_g} R_d$: $m_1(R_t) = K_c^t R_g \frac{R_t}{K_m^t + R_t}$	$R_d \xrightarrow{C1} R_t$: $m_2(R_d) = K_c^d C_1 \frac{R_d}{K_m^d + R_d}$
Import Cycle	**Import Cycle**
$T + R_t \underset{k_{-2}}{\overset{k_2}{\rightleftharpoons}} T_r$: $r_1(T, R_t) = k_2 T R_t$ and $r_{-1} = k_{-2} T_r$	
$T + C \xrightarrow{k_3} T_c$: $r_2(T, C) = k_3 TC$	$T_c + R_t \xrightarrow{k_4} C + T_r$: $r_3(T_c, R_t) = k_4 T_c R_t$

Table 3.2: Import model: reactions [15]. The Law of Mass Action is applied to represent the kinetic processes.

that surround the nucleus, cargo molecules can bind to microtubules, through the dynein action, and be actively transported. The advection field is considered as a radial field pointing to a point inside the nucleus and the field module is assumed constant and equal to 1, to account for the constant velocity of the motor dynein, $\sim 1 \mu m s^{-1}$ (see Section 1.2). In this light, an equation for the free dynein is added to system (3.3). The binding of the cargo-importin complex to dynein is allowed and, the resulting product, is assumed already bound to microtubules. Therefore the equation for the dynein-cargo-importin complex is an advection equation. Let $\mathbf{b}$ be the velocity field and D and D_c the two new species: dynein and the dynein-cargo-importin complex. The binding and unbinding of every molecule, is modelled following the Law of Mass Action and the resulting reactions are:

$$T_c + D \underset{k_d}{\overset{k_a}{\rightleftharpoons}} D_c \tag{3.5}$$

$$r_a(T_c, D) = k_a T_c D, \quad r_d(D_c) = k_d D_c \tag{3.6}$$

The equations for D and D_c, confined in the cytoplasm, read:

$$\begin{cases} \frac{\partial D}{\partial t} = d_d \Delta D - r_a(T_c, D) + r_d(D_c), \\ \frac{\partial D_c}{\partial t} = -\nabla \cdot (\mathbf{b} D_c) + r_a(T_c, D) - r_d(D_c), \end{cases} \tag{3.7}$$

while the equation for the cargo-importin complex T_c is accordingly modified, yielding:

$$\frac{\partial T_c}{\partial t} = d_{tc} \Delta T_c + r_2(C, T) - r_a(T_c, D) + r_d(D_c).$$

3.1.2 Mathematical coupling

The semi-linear parabolic PDEs system introduced in the previous Section, has become, with the addition of microtubule transport, a system of eight coupled semi-linear parabolic/hyperbolic equations. However, in the following, we consider only the classical import pathway, i.e. systems (3.2) and (3.3) coupled by the boundary conditions (3.4) and we introduce a single microtubule, as in Chapter 2.

First of all, we introduce the simulations domain. We consider a rectangular area, as in Chapter 2, but we expand it, in order to include the nuclear domain. Following the

notations of Cangiani *et al.* we set Ω as the whole simulation domain, Ω_c the cytoplasmic compartment and Ω_n the nuclear one. The two sub-domains, nucleus and cytoplasm, have a common boundary Γ_{nc}, as in Figure 3.3. We include, in Ω_c, the microtubule filament, positioning it from point (x_{In}, y_0) to point (x_{Fi}, y_0), parallel to the x-axis. We establish an attraction area for the microtubule, denoted $\mathbf{I} \times \mathbf{J}$, as in Section 2.1.2.

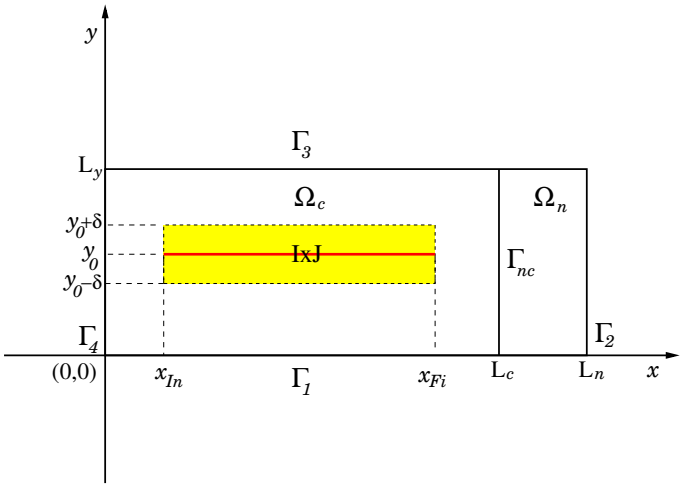

Figure 3.3: Area of the cell where intracellular transport is modelled: $\Omega_c \cup \Omega_n$, cytoplasm and nucleus. $\Gamma_{nc} = \partial\Omega_c \cap \partial\Omega_n$ is the common boundary of the two compartments. The yellow rectangle ($\mathbf{I} \times \mathbf{J} = [x_{In}, x_{Fi}] \times [y_0 - \delta, y_0 + \delta]$) represents the attraction area of the microtubule filament, the red strip is the microtubule, positioned in y_0.

We remind the species and reactions introduced in the previous chapter: we have considered a cargo molecule C, a cargo+dynein complex P_f. We have defined P_t as the result of the attachment of P_f to the microtubule. We have supposed all the interactions to be kinetic reactions and modelled them applying the Law of Mass Action. Therefore, we have obtained:

$$C + D \underset{k_-}{\overset{k'}{\rightleftharpoons}} P_f, \tag{3.8}$$

yielding:

$$\frac{dC}{dt} = -k' DC + k_- P_f, \tag{3.9}$$

and we fixed $k := k'D$, since we assumed the dynein concentration D constant. Similarly we have written:

$$P_f \underset{k_{-1}}{\overset{k_1}{\rightleftharpoons}} P_t, \tag{3.10}$$

and, for the Law of Mass Action:

$$\frac{dP_f}{dt} = kC + k_- P_f - k_1 P_f + k_{-1} P_t. \tag{3.11}$$

Finally, for the microtubule species, we have obtained the following equation:

$$\frac{dP_t}{dt} = k_1 P_f - k_{-1} P_t. \tag{3.12}$$

Every species is supposed to have a spatial dynamics: C and P_f diffuse, while P_t is attached to the microtubule and moves along it, at the constant speed $c = 1$. Thus, $C = C(x, y, t)$, $P_f = P_f(x, y, t)$, for $(x, y) \in \Omega$, $t \geq 0$. The microtubule attached species $P_t = P_t(x, t)$ is defined for $x \in]x_{In}, x_{Fi}[$, $t \geq 0$ and reaction 3.10 is allowed only in the attraction area $\mathbf{I} \times \mathbf{J}$. We assume that the cargo C interacts with the receptor T of model (3.2), (3.3,) (3.4) and we get the following coupled model of ran mediated import including transport along a single microtubule, in Ω_c:

$$\begin{cases} \frac{\partial R_t}{\partial t} = d_{rt}\Delta R_t - m_1(R_t) - r_1(R_t, T) + r_{-1}(T_r), \\ \frac{\partial R_d}{\partial t} = d_{rd}\Delta R_d + m_1(R_t), \\ \frac{\partial T_r}{\partial t} = d_{tr}\Delta T_r + r_1(Rt, T) - r_{-1}(T_r), \\ \frac{\partial C}{\partial t} = d_c\Delta C - r_2(C, T) \overbrace{-kC + k_- P_f}^{\text{coupling terms}}, \\ \frac{\partial T}{\partial t} = d_t\Delta T - r_1(R_t, T) + r_{-1}(T_r) - r_2(C, T), \\ \frac{\partial T_c}{\partial t} = d_{tc}\Delta T_c + r_2(C, T), \\ \frac{\partial P_f}{\partial t} = d_c\Delta P_f + kC - k_- P_f - k_1 P_f \mathbb{1}_{\mathbf{I}\times\mathbf{J}} + k_{-1} P_t \frac{\mathbb{1}_{\mathbf{I}\times\mathbf{J}}}{|\mathbf{J}|} \\ \qquad\qquad + cP_t(x_{Fi})\delta_0(x - x_{Fi}, y - y_0), \end{cases} \tag{3.13}$$

and the equation for P_t valid in $]x_{In}, x_{Fi}[$:

$$\frac{\partial P_t}{\partial t} + c\frac{\partial P_t}{\partial x} = k_1 P_f - k_{-1} \int_J dy P_t. \tag{3.14}$$

In the nucleus the equations relative to nuclear import stay unchanged:

$$\begin{cases} \frac{\partial R_t}{\partial t} = d_{rt}\Delta R_t + m_2(R_d) - r_1(R_t, T) + r_{-1}(T_r) - r_3(R_t, T_c) \\ \frac{\partial R_d}{\partial t} = d_{rd}\Delta R_d - m_2(R_d), \\ \frac{\partial T_r}{\partial t} = d_{tr}\Delta T_r + r_1(R_t, T) - r_{-1}(T_r) + r_3(R_t, T_c) \\ \frac{\partial C}{\partial t} = d_c\Delta C + r_3(R_t, T_c), \\ \frac{\partial T}{\partial t} = d_t\Delta T - r_1(R_t, T) + r_{-1}(T_r), \\ \frac{\partial T_c}{\partial t} = d_{tc}\Delta T_c - r_3(R_t, T_c). \end{cases} \tag{3.15}$$

Indeed, we suppose that the cargo-dynein complex is not allowed to enter the nucleus, since dynein is not a nuclear protein. The transmissions terms that couple systems (3.13)

and 3.15 are, as in [15]:

$$\begin{cases} d_{rt}\frac{\partial R_t^{(c),(n)}}{\partial \mathbf{n}} = 0 \\ d_{rd}\frac{\partial R_d^{(c)}}{\partial \mathbf{n}} = p_d(R_d^{(c)} - R_d^{(n)}) = d_{rt}\frac{\partial R_d^{(n)}}{\partial \mathbf{n}} \\ d_{tr}\frac{\partial T_r^{(c)}}{\partial \mathbf{n}} = p_{tr}(T_r^{(c)} - T_r^{(n)}) = d_{tr}\frac{\partial T_r^{(n)}}{\partial \mathbf{n}} \\ d_c\frac{\partial C^{(c),(n)}}{\partial \mathbf{n}} = 0 \\ d_t\frac{\partial T^{(c)}}{\partial \mathbf{n}} = p_t(T^{(c)} - T^{(n)}) = d_t\frac{\partial T^{(n)}}{\partial \mathbf{n}} \\ d_{tc}\frac{\partial T_{tc}^{(c)}}{\partial \mathbf{n}} = p_{tc}(T^{(c)} - T^{(n)}) = d_{tc}\frac{\partial T_{tc}^{(n)}}{\partial \mathbf{n}} \\ d_r\frac{\partial P_f^{(c),(n)}}{\partial \mathbf{n}} = 0, \end{cases} \tag{3.16}$$

at Γ_{nc}, where we included a zero-flux boundary condition for the species P_f. The boundary conditions on Γ_1 and Γ_3 are periodic while on Γ_2 and Γ_4 we impose homogeneous Neumann boundary conditions. We also impose a boundary condition for the transport equations and we fix, as in Chapter 2:

$$P_t(x_{In}) = 0, \tag{3.17}$$

assuming that the dynein-cargo complex cannot attach at the extremity of the MT. Finally we consider initial conditions for every species: an initial cargo concentration of $2\mu M$ supposed to only cytoplasmic. RanGTP is only nuclear and its total concentration is fixed to $1.2\mu M$. RanGDP initial concentration is only cytoplasmic, as for the receptor T and both total concentrations are fixed to $1.2\mu M$. The initial condition for all the other species is set to zero, since we suppose the cell to be at rest (no reactions occur before the simulations).

3.2 Numerical treatment of the model

The numerical method used to approximate the mathematical model (3.13), (3.14), (3.15), closed by the boundary conditions (3.16) and (3.17), is similar to the method introduced in Section 2.2. We denote by Δx, Δy the discretization steps in the x and y directions respectively and we divide the intervals $[0, L_c]$, $[L_c, L_n]$ and $[0, L_y]$ in $N_c + 1$, $N_n + 1$ and $N_y + 1$ points (see Figure 3.3). The mesh points will be $(x_i, y_j) = (i\Delta x, j\Delta y)$ with $0 \leq i \leq N_c + N_n + 1$, $0 \leq j \leq N_y + 1$. Let Δt be the time discretization step and t_n the n^{th} step, i.e. $t_n = n\Delta t$, $n \in \mathbb{N}$. Let us set u, a general species concentration in the domain Ω. According to these notations $u_{i,j}^n$ will be the numerical approximation of the solution of u in (x_i, y_j) at time t^n. Only P_t will be denoted by W_i^n, to be consistent with the notations of Section 2.2. Remark that P_t lies in $[x_{In}, x_{Fi}]$ so that W_i^n is well defined only for i satisfying $x_{In}/\Delta x \leq i \leq x_{Fi}/\Delta x$.

We first solve the equation for P_t and we refer to Section 2.2 for the numerical approximation of the transport equation. The approximation of systems (3.13), and (3.15) is done using an IMEX midpoint scheme of order 2. Let us write in a general form

the equation for the generic species u:

$$\frac{\partial u}{\partial t} = d_u \Delta u + R_u, \tag{3.18}$$

where R_u represents the reactions terms relative to the equation. We treat explicitly all the reactions terms and implicitly the contribution of the diffusion term. This yields:

$$u_{i,j}^{(1)} = u_{i,j}^n + d_u \frac{\Delta t}{2} \left(\frac{\delta_x^2 u^{(1)}}{\Delta x^2} + \frac{\delta_y^2 u^{(1)}}{\Delta y^2} \right) + \frac{\Delta t}{2} R_u^n, \tag{3.19}$$

$$u_{i,j}^{n+1} = u_{i,j}^n + d_u \Delta t \left(\frac{\delta_x^2 u^{(1)}}{\Delta x^2} + \frac{\delta_y^2 u^{(1)}}{\Delta y^2} \right) + \Delta t R_u^{(1)}, \tag{3.20}$$

where

$$\frac{\delta_x^2 u^{(1)}}{\Delta x^2} = \frac{u_{i+1,j}^{(1)} - 2u_{i,j}^{(1)} + u_{i-1,j}^{(1)}}{\Delta x^2}$$

and

$$\frac{\delta_y^2 u^{(1)}}{\Delta y^2} = \frac{u_{i,j+1}^{(1)} - 2u_{i,j}^{(1)} + u_{i,j-1}^{(1)}}{\Delta y^2}$$

Since u satisfy Neumann boundary conditions on Γ_2 and Γ_4, we use the second order derivative approximation to calculate the boundary values:

$$\frac{\partial u}{\partial n}(0, y_j) = \frac{1}{2\Delta x}(-3u_{0,j}^n + 4u_{1,j}^n - u_{2,j}^n), \quad \frac{\partial u}{\partial n}(L_n, y_j) = \frac{1}{2\Delta x}(3u_{N,j}^n - 4u_{N-1,j}^n + u_{N-2,j}^n),$$

to yield:

$$u_{0,j}^n = (\frac{4}{3}u_{1,j}^n - \frac{1}{3}u_{2,j}^n),$$

$$u_{N,j}^n = (\frac{4}{3}u_{N,j}^n - \frac{1}{3}u_{N-1,j}^n),$$

with $N = N_c + N_n + 1$. At the interior boundary Γ_{nc} we have to fix:

$$d_u \frac{\partial u^{(c)}}{\partial n}(Lc, y_j) = p_u(u^{(c)}(Lc, y_j) - u^{(n)}(Lc, y_j)) = \frac{\partial u^{(n)}}{\partial n}(Lc, y_j)$$

which gives

$$u^{(c)}(N_c, y_j) = \frac{\alpha}{\beta}(\frac{4}{3}u^{(c)}(N_c{-}1, y_j) - \frac{1}{3}u^{(c)}(N_c{-}2, y_j)) + \lambda\frac{\alpha^2}{\beta}(\frac{4}{3}u^{(n)}(N_c{+}1, y_j) - \frac{1}{3}u^{(n)}(N_c{+}2, y_j))$$

and

$$u^{(n)}(N_c, y) = \frac{\alpha}{\beta}(\frac{4}{3}u^{(n)}(N_c{+}1, y_j) - \frac{1}{3}u^{(n)}(N_c{+}2, y_j)) + \lambda\frac{\alpha^2}{\beta}(\frac{4}{3}u^{(c)}(N_c{-}1, y_j) - \frac{1}{3}u^{(c)}(N_c{-}2, y_j));$$

α, β and λ are defined as follows: $\lambda := \frac{2}{3}\frac{\Delta x p_u}{d_u}$, $\alpha := (1+\lambda)^{-1}$ and $\beta = 1 - (\alpha\lambda)^2$ and the approximations in terms of $u_{i,j}^n$ follow.

3.3 Simulations results

In Section 3.1.1 we have introduced the model developed by Cangiani and Natalini [15] for cellular molecular trafficking, which simulates the nuclear import of all NLS proteins. In Section 3.1.2 we coupled the model introduced with the model for active transport along microtubules proposed in Chapter 2. Our goal is to evaluate the influence of motor-assisted transport on the whole nuclear import pathway. The same study has already been done by Cangiani and Natalini, through the use of a vector field that spans the whole cytoplasmic compartment and represents the microtubules filaments. However, we test here a different approach, considering a single microtubule and localizing it inside the cytoplasm. Compared to the model of Ran import (3.2), (3.3), (3.4) and (3.7) [15], we also add a new species, by distinguishing between cargo+motor and cargo+motor *on the microtubule*. Finally we assume that the cargo, namely C, binds to the motor protein and not the complex cargo+importin, T_c, as done in [15]. The values of all parameters are set in Table 3.3

A single microtubule does not enhance nuclear import

In this section we compare the simulation results of model (3.2), (3.3), (3.4) to the results of model (3.13), (3.14), (3.15), (3.16). Namely, we compare, respectively, the nuclear accumulation of the cargo C without microtubule activity to the accumulation with microtubule. In both cases we calculate the evolution of nuclear cargo concentration. To do this, we set the initial concentration value of the cargo protein in the nucleus to 0 and, since the cargo is only allowed to get inside the nucleus, we calculate its accumulation in the nucleus over time.

Our results show that nuclear import is not enhanced by motor-assisted transport. Figure 3.4 illustrates the temporal evolution of the nuclear concentrations of cargo proteins having different diffusion coefficients. Diffusion coefficients are set to $d_c = 1\mu m^2 s^{-1}$ (Figure 3.4(a)) and to $d_c = 10\mu m^2 s^{-1}$ (Figure 3.4(b)). The blue curves show the nuclear accumulation of the cargo C when $k = 0$, i.e. when the cargo is not assumed to interact with the motor dynein. The black curves depict the cargo accumulation for $k > 0$, that is, the motor assisted transport is allowed. In both cases, the accumulation in the nucleus is greater without microtubule activity. In the fixed period of 180 seconds, if only the Ran pathway is used, the cargo completely accumulates inside the nucleus when $d_c = 10\mu m^2 s^{-1}$. On the contrary, with the microtubule, only the 95% of the total cargo has entered the nucleus. When $d_c = 1\mu m^2 s^{-1}$, 85% of the total cargo has got into the nucleus without microtubule activity and the $\sim 79\%$ with microtubule activity. Therefore, we also observe that the rate of nuclear accumulation depends on the diffusion coefficient, i.e. on the mobility of the nuclear protein. It is thus surprising that the microtubule does not improve nuclear import. To understand better, we represent in Figure 3.5 the spatial distribution of the cargo protein, at the initial time $T = 0$ and at the final time $T = 180$, when $d_c = 1$. In Figure 3.5(a) we plot the initial condition: the whole cargo concentration is enclosed in the cytoplasmic compartment. Figures 3.5(b) and 3.5(c) show the cargo concentration at $T = 180s$. Figure 3.5(b) illustrates the case with microtubule

Parameter	Unit	Description	Value	Reference(s)
		MT model chapter 2		
k	s^{-1}	dynein attach. rate	0.2	[15, 97]
k_-	s^{-1}	dynein detach. rate	0.2	[15, 97]
k_1	s^{-1}	attach. rate to MT	0.5	[122]
k_{-1}	s^{-1}	detach. rate from MT	0.05	section 2.3
		RAN model (reactions terms)		
K_c^t	s^{-1}	$m_1(R_t)$	10.6	[15]
K_m^t	μM	$m_1(R_t)$	0.7	[15]
R_g	μM	$m_1(R_t)$	0.5	[15]
K_c^d	s^{-1}	$m_2(R_d)$	8	[15]
K_m^d	μM	$m_2(R_d)$	1.1	[15]
C_1	μM	$m_1(R_t)$	0.7	[15]
k_2	$(\mu Ms)^{-1}$	$r_1(R_t, T)$	0.1	[15]
k_{-2}	s^{-1}	$r_{-1}(T_r)$	0.3	[15]
k_3	$(\mu Ms)^{-1}$	$r_2(C, T)$	0.15	[15]
k_4	$(\mu Ms)^{-1}$	$r_3(R_t, T_c)$	0.1	[15]
		Spatial parameters		
c	μms^{-1}	Dynein velocity	1	[96, 81]
d_c	$\mu m^2 s^{-1}$	C diff. coeff.	1	[117]
d_{rt}	$\mu m^2 s^{-1}$	R_t diff. coeff.	22	[15]
d_{rd}	$\mu m^2 s^{-1}$	R_d diff. coeff.	20	[15]
d_t	$\mu m^2 s^{-1}$	T diff. coeff.	14	[15]
d_{tr}	$\mu m^2 s^{-1}$	T_r diff. coeff.	14	[15]
d_{tc}	$\mu m^2 s^{-1}$	T_c diff. coeff.	0.8	proposed
p_d	μms^{-1}	R_d (with NTF2) perm. coeff	3.73	[15]
p_t	μms^{-1}	T perm. coeff	1.87	[15]
p_{tr}	μms^{-1}	T_r perm. coeff	1.87	[15]
p_{tc}	μms^{-1}	T_c perm. coeff	1.87	[15]
MT length	μm	-	8	section 2.3
L_c, L_n, L_y	μm	-	10, 2 and 0.2	section 2.3
$\mathbf{I}$, $\mathbf{J}$	μm	MT attraction area	8 and 0.04	section 2.3

Table 3.3: Parameter values for system (3.13), (3.14), (3.15), (3.16) and corresponding references in literature.

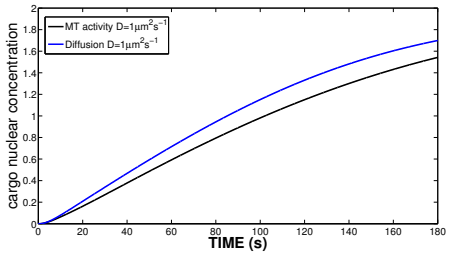

(a) $d_c = 1\mu m^2 s^{-1}$

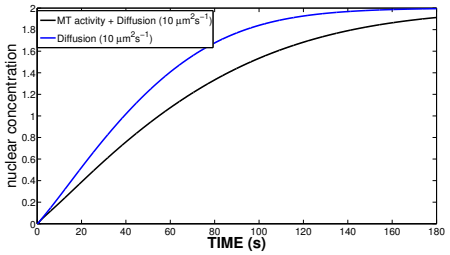

(b) $d_c = 10\mu m^2 s^{-1}$

Figure 3.4: Nuclear accumulation depends on the diffusion coefficient but it is not enhanced by the microtubule activity.

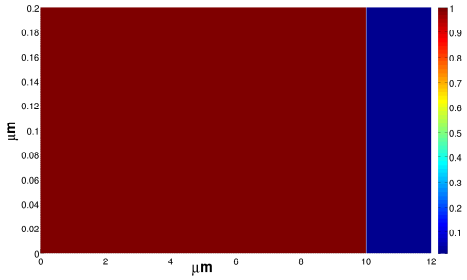

(a) $T = 0$

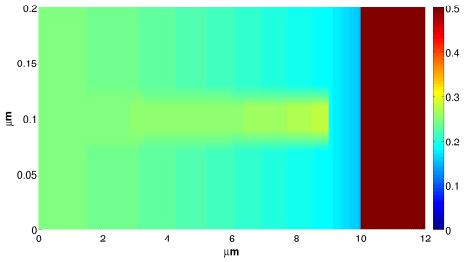

(b) $T = 180$, MT activity

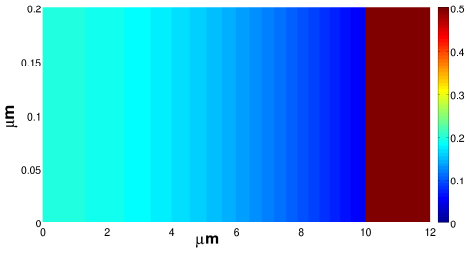

(c) $T = 180$, Ran cycle

Figure 3.5: Spatial distribution of the cargo concentration C and its complexes. (a) Initial concentration. (b): Spatial distribution of $C + T_c + P_f + P_t$ at $T = 180s$. (c): Spatial distribution of $C + T_c$ at $T = 180s$.

activity. We plot the spatial distribution of $C + T_c + P_f + P_t$ in 3.5(b), i.e. of the cargo and all the complexes it forms, with the dynein and the importin proteins. In Figure 3.5(c) we plot the simulation results with no microtubule activity. Therefore we plot the spatial distribution of $C + T_c$, since $P_f + P_t = 0$. Following the colour maps of both figures we can observe that, in the cytoplasm, the total concentration of cargo complexes with the microtubule is higher than the concentration of cargo complexes without the

microtubule. We can also observe that, if the cargo binds to the MT, the distribution of the cargo complexes has a lower gradient (i.e. the difference between the concentrations at the cytoplasmic and nuclear membrane is lower than in Figure 3.5(c)) and a higher concentration has accumulated at the nuclear envelope level. Therefore, we recognize the influence of the microtubule which causes a larger concentration to accumulate near the nuclear envelope. However, the gradient of the protein Ran handles the import pathway and it is sufficient for a efficient nuclear accumulation of the cargo protein.

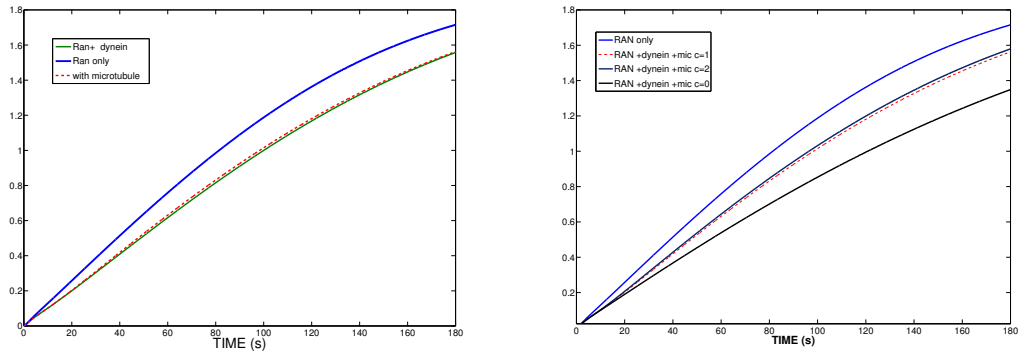

(a) (b)

Figure 3.6: Cargo nuclear accumulation. The blue curve shows the accumulation due to the ran import, without dynein activity ($k = 0$).(a) The green curve represents the cargo accumulation for $k > 0$ and $k_1 = 0$. The red dashed curve is the nuclear accumulation with microtubule activity. (b). Cargo accumulation with the microtubule activity for different velocities ($c = 0$, 1 and $2\mu m/s$). The diffusion coefficient of the cargo is set to $1\mu m^2/s$.

The difference between the results of model (3.13), (3.14), (3.15), (3.16) and those of model (3.2), (3.3), (3.4) might be due to the presence of the dynein protein. The motor dynein forms the complex P_f with the cargo C in such a way to compete with the formation of the importin-cargo complex T_c. To confirm this hypothesis, we perform numerical simulations setting $k > 0$ and $k_1 = 0$. This means that the cargo binds to dynein, but the cargo-dynein complex cannot attach the microtubule. As expected, the nuclear accumulation of the cargo is still lower than the nuclear accumulation obtained for $k = 0$ (no dynein concentration). Figure 3.6(a) illustrates this result. The blue curve shows the accumulation due to Ran import, without dynein activity ($k = 0$) and it is the curve that reaches the maximum value. The green curve represents the cargo accumulation for $k > 0$ and $k_1 = 0$. The nuclear accumulation in this second case is lower than the accumulation due to the exclusive use of the ran pathway. Furthermore it roughly coincides with the accumulation obtained with microtubule transport ($k > 0$ and $k_1 > 0$, red dashed curve in Fig. 3.6). We also test the effects of using different motor velocities. When the speed of the motor is set to zero ($c = 0$), i.e. the microtubule does not transport, but only hold the proteins in the same position, the nuclear import

is evidently decreased (black curve in Fig. 3.6(b)). If we set $c = 2$, the nuclear import increases, but slightly. The presence of the microtubule increases the competition for the formation of the complex T_c, since it takes away the complexes P_f. The increased competition seems to be balanced by the microtubule activity that releases the cargo next to the nuclear envelope. In conclusion, we cannot observe an increased nuclear import due to microtubule enhanced transport, neither for motor velocities $c > 1$.

3.4 Summary and further directions

Using the model of cytoplasmic transport on a single microtubule, introduced in Chapter 2, coupled with model of Cangiani *et al.* [15], we were unable to reproduce the experimental results of various authors that show that some specific nuclear proteins use microtubule transport to facilitate their way to the nucleus. These results have already been qualitatively reproduced in [15], where microtubule transport was modelled using a vector field. How can we explain the sharp difference of our results? One of the main differences with the model of Cangiani *et al.* compared to our approach, is that microtubule influence is averaged within the cytoplasmic area. This modelling choice yields two main consequences. The first one is "spatial": at each point of the cell the dynein-cargo-importin complex is trasported by microtubules and areas with no microtubule activity are thus suppressed. Even if the microtubule network can be dense, we consider this assumption too strong, furthermore in a three-dimensional domain: the distance between two single microtubules cannot be completely avoided. Or, at least, the motor velocity should not be kept constant, but should be adjusted to the assumptions of an over-crowding of filaments. The second consequence is "temporal": as soon as the dynein-cargo-importin complex is composed, transport along the avareged microtubules begins. Therefore, the attachment of the motor to the filament is not taken into account and the time spent on the microtubule is confused with the time the cargo spends bound to the molecular motor dynein. These modelling choices make transport along microtubules more efficient but are not necessarily more realistic. The comparison with real data can thus be misleading.

An other difference with respect the work of Cangiani *et al.* [15] is that we have chosen (see Section 2.1.2 and [26]) to represent the movement along microtubules as a one-dimensional process. This choice has been done to more accurately model motor-assisted transport that is, effectively, a one dimensional movement. Indeed, dynein walks along the filament in the unique possible direction of the nucleus. In this way we highlight the difference between the two considered type of motion: diffusion and advection.

We also remark that in [15], the authors assume that dynein binds to the cargo-importin complex. Instead, we have supposed, in the model proposed in Section 2.1.2, that dynein binds directly to the free cargo. The reason of our choice is linked to the experimental results of Salman and colleagues who have shown [114] that the NLS signal invokes active transport along microtubules. Thus we have supposed that cargo molecules can bind to dynein independently of the transport receptor. As we have shown, this choice leads to a competition between the dynein and the importin proteins to bind

to the cargo. This competition decreases the nuclear accumulation of the free cargo. Therefore it is necessary to test our model when the binding to dynein is allowed for the cargo-importin complexes, as done in [15]. Furthermore our model is very simple and different extensions are possible and necessary. Indeed we have simulated a thin area of a cell and we have considered a single microtubule. It would be interesting to test whether other observations could be done, changing the geometry of the model. The results could depend on the number of microtubule considered and on the distance between two single filaments.

Part II

A spatial model for p53 nuclear accumulation

Chapter 4

p53: a specific nucleocytoplasmic shuttling protein

In this chapter will be presented the network of a specific cargo protein, named "p53". It will be explained how this protein acts in the cell and what are its functions. Some models known from the literature will then be introduced and the mechanism used to reproduce the dynamical behaviour of p53 discussed.

Contents

History of p53

The protein p53 was isolated for the first time in 1979 (see [73] and Figure 4.1). Since its molecular mass was calculated to be $53kDa$ (one Dalton, expressed as Da, represents roughly the mass of one proton), scientists, unaware of the great interest that this protein would have aroused, named it "protein 53", or briefly p53.

At the beginning, biologists thought that p53 and its corresponding gene was an oncogene [108, 86], i.e., a gene that, when activated, can lead to uncontrolled proliferation of tumour cells. About ten years after its discovery, experiments have shown that p53 is a tumour suppressor [52]. Thus, instead of being an oncogene, p53 prevents cells with damaged DNA from dividing and passing the DNA damage to daughter cells. Furthermore, multiple studies have shown that the p53 gene is altered in about 50% of cancer cells. As a consequence, in cancer cells, the protein may not carry out its task of preventing from uncontrolled proliferation.

For all these reasons, p53 became *popular* among cell biologists. And since thirty years until now the functions, the network and the dynamics of p53 have been widely investigated, in the hope of developing clinical applications.

What is p53?

p53 is a protein that senses genotoxic stresses and prevents the cells from becoming tumoral. Protein p53 has multiple roles but in a general manner one can say that it acts as a controller. Indeed, following DNA damage, p53 blocks the cell cycle in order to avoid cell division, it starts repair pathways and, if needed, it triggers apoptosis (cell *suicide*). p53 is thus essential for healthy cell survival.

4.1 Mechanisms that regulate p53 activity

When a damage is detected, cells react in different ways depending on the type of stress undergone. The p53 pathway is activated in presence of damages due to ionising radiations, heat shock, cytotoxic drug insult and other forms of stress.

The protein p53 acts primarily as a transcription factor, so that it needs to accumulate

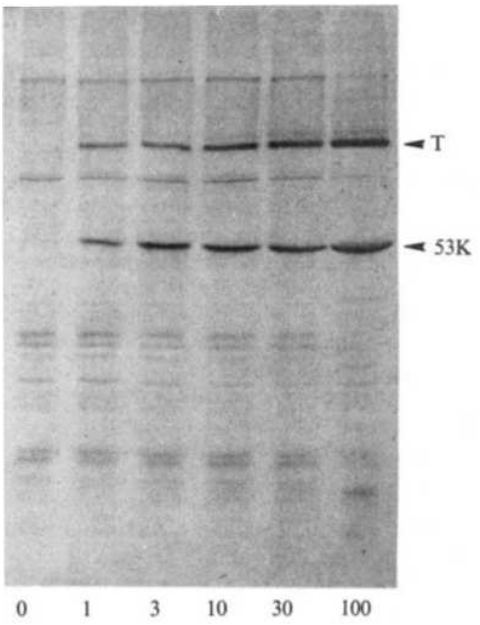

Figure 4.1: p53 discovery, image from [73], 1979. Immunoprecipitation of mouse cell lines transformed by the SV40 virus (simian virus 40) led to the isolation of a $53kDa$ protein. During the same year, p53 was also found to be expressed by tumor-induced cancer cells, see e.g. [24].

in the nucleus and bind to DNA to regulate the expression of proteins involved in the processes like cell cycle arrest, repair and apoptosis.

4.1.1 Healthy cells

In order to proceed normally towards cell division, healthy cells have a low level of nuclear p53. Even if a total loss of p53 can contribute to tumour development in mice [31], uncontrolled expression of p53 has been shown to be harmful for embryonic mouse cells. Indeed in the absence of the p53 major negative regulator, the protein Mdm2, mice embryos show early lethality. This premature lethality can be counteracted only by p53 knock-out [91].

Healthy cells regulate strictly the activity of p53 by post-translational modifications in order to orient the functions of the protein. The most important negative regulator of p53 is the protein Mdm2.

This protein inhibits p53 nuclear accumulation and resulting activity in several ways: it enhances p53 degradation, it blocks its transcriptional activity, it enhances p53 nuclear export and finally it reduces p53 nuclear import.

These multiple types of inhibition depend essentially on the enzymatic activity that Mdm2 exerts on p53. Indeed p53 is degraded by the ubiquitin-proteasome machinery of the cell and Mdm2 is a ubiquitin ligase for p53 [106, 33, 84]. Furthermore the conformational transformation due to the ubiquitination process also induces the masking of p53 principal NLS (Nuclear Localization Signal) [82], thus trapping p53 in the cytoplasm, where it cannot act as a transcription factor. At the same time the mono-ubiquitination step induced by Mdm2 improves the exposure of p53 NES (Nuclear Export Signal) [17], so that p53-Mdm2 interactions also result in an enhanced nuclear export [1]. Finally the binary complex p53−Mdm2 is inactive as a transcription factor [89, 120] and the binding of Mdm2 on p53 results in a loss on p53 activity.

Unexpected though it could be, Mdm2 is one of the target genes of p53 [37]. The existence of a negative feedback between these two proteins confirms the importance of the p53-Mdm2 auto-regulatory loop.

4.1.2 Activation of the p53 pathway

The p53 network can be activated by several independent pathways depending on the type of insult.

The activation pathway following DNA damage is regulated by ATM and Chk2 [16, 136]. ATM (Ataxia Telangiectasia Mutated gene) and Chk2 are two protein kinases that sense the damage and launch a signalling pathway that leads to p53 activation. In particular, ATM responds to damaging agents that produce double strand breaks in the DNA [74] and mediates the forthcoming phosphorylation events [25].

Aberrant growth signals, such as those resulting from the expression of oncogenes, activate the p53 network through the action of protein $p14^{ARF}$ [136].

[1] See Section 1.3 for a brief introduction about NLS, NES and nucleocytoplasmic transport

The third pathway is induced by a wide range of chemotherapeutic drugs, ultraviolet light, and protein-kinase inhibitors, and it may involve the ATR kinase [136].

All these different pathways generate a cascade of signals that lead to a decreased interaction between p53 and Mdm2. Both p53 and Mdm2 undergo post-translational modifications, as phosphorylation or sumoylation that reduce the ability of the two proteins to interact and thus elicit an increased p53 activity.

The activation process of p53 is highly complex and not fully controlled by any single phosphorylation site or protein [136] and mechanisms that control it have not yet been completely elucidated.

Just to show the complexity of the system we report in Fig. 4.2 the known sites of phosphorylation for p53, that is, as said before, only one of the possible post-translational transformations that p53 undergoes.

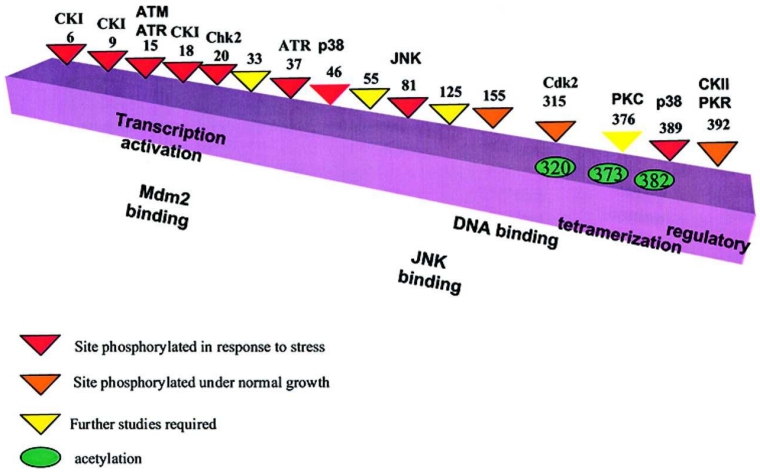

Figure 4.2: Phosphorylation known sites of protein p53 and the corresponding kinases implicated. Image from [2].

4.1.3 Stabilization and subcellular localization

An evidence of p53 activation is its stabilization. The term stabilization is referred to any process involved in maintaining the integrity of a protein and preventing it from degradation or aggregation (definition of the biological process from the Gene Ontology database at Ebi).

In response to stress stimuli p53 blocks cell growth, launches repair processes and triggers apoptosis. In order to accomplish these functions, p53 needs to stabilize and accumulate in the nucleus, where it can bind to DNA and starts the expression of its downstreaming genes.

Within a few minutes from start of a stress stimulus in the cell, the p53 protein accumulates in the nucleus [71] and its half-life rises significantly because of post-translational modifications, from twenty minutes to several hours [134, 109].

Several works demonstrate that p53 stabilization results from p53-Mdm2 blocked interaction. Indeed at least 11 post-translational modifications of p53 have been reported in response to DNA damage [16, 34]. These modifications allow on the one hand the stabilization of p53, on the other hand they regulate p53 transcriptional activity [34].

A first consequence of p53-Mdm2 reduced interaction is the reduced p53 degradation due to a lower ubiquitination. Secondly the subcellular localization of p53 is promptly readjusted. While in healthy cells Mdm2 sequesters p53 in the cytoplasm and improve p53 nuclear export, in stressed conditions these actions are reversed. Indeed, in order to regulate at best p53 nuclear functions, an appropriate subcellular localization is a crucial requirement.

Actually p53 NESs are easily masked by post-translational modifications and this make its export less efficient [82]. A first p53 NES is weak, localized in its tetramerization domain [125], and it is easily masked after DNA damage. A second NES, located at Mdm2-binding domain, is inhibited by phosphorylation induced by DNA damage [82].

Since nuclear export takes more than 3h to be achieved [125], also a promoted nuclear import is necessary for a fast stabilization. Interactions of p53 with proteins of the importin family is reduced by Mdm2-induced ubiquitination [82]. Conversely, cytoplasmic accumulation of ubiquitin-free p53 molecules, promotes the interaction with importin proteins and results in a rapid import and nuclear accumulation [82].

A sketch of these different processes is reported in Fig. 4.3 and 4.4.

The tumor suppressor p53 also performs some of its tasks in the cytoplasm. Indeed it is endowed with biological functions that are not all transcriptional-dependent, and it can directly activate the apoptotic pathway by translocating to mitochondria and triggering the release of pro-apoptotic factors [19]. Anyway the control of transcription by nuclear p53 decisively contributes to the function of cytoplasmic p53. Therefore without transcription, regulated by nuclear p53, endogenous cytoplasmic p53 may not function properly [49].

4.2 p53 temporal dynamics and existing models in literature

Within the regulatory circuit of p53, the existence of a negative feedback between p53 and Mdm2 has been clearly established [140]. The protein Mdm2 is the major p53 antagonist: it enhances p53 degradation [54], it blocks its entry into the nucleus [82] and inhibits p53 transcriptional activity [120]. Conversely, p53 activates Mdm2 transcription [37]. Through this negative feedback, and more generally as a result of the complex processes of p53 activation, it is possible to observe oscillations of p53 levels inside the cell under stress conditions.

Among the first to observe damped p53 peaks were Collister *et al.* in [22] who noticed a delayed and prolonged accumulation of p53 on cells treated with UV and ionizing radiations. But the first to point out the existence of clear oscillatory dynamics of p53 and Mdm2 (see Fig. 4.5) were Bar-Or *et al.* [3]. In their work the authors show the presence of damped oscillations in a human breast cancer epithelial cell population and in mouse fibroblasts submitted to ionizing radiations. Quantitative observations were made

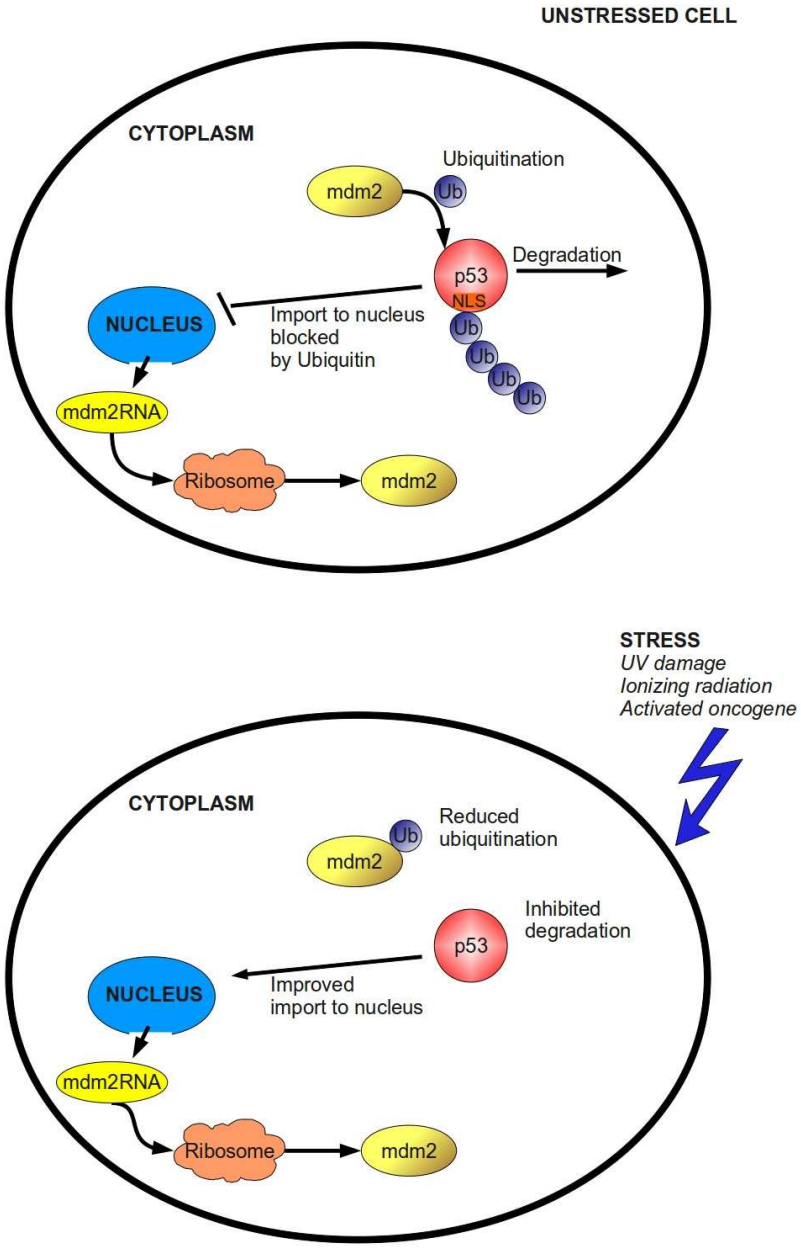

Figure 4.3: Scheme of p53-Mdm2 reactions in unstressed (up) and stressed (down) conditions, cytoplasmic compartment

on cell populations and the authors observed damped p53 oscillations. Further analysis demonstrated that the p53-Mdm2 system actually undergoes sustained oscillations after a

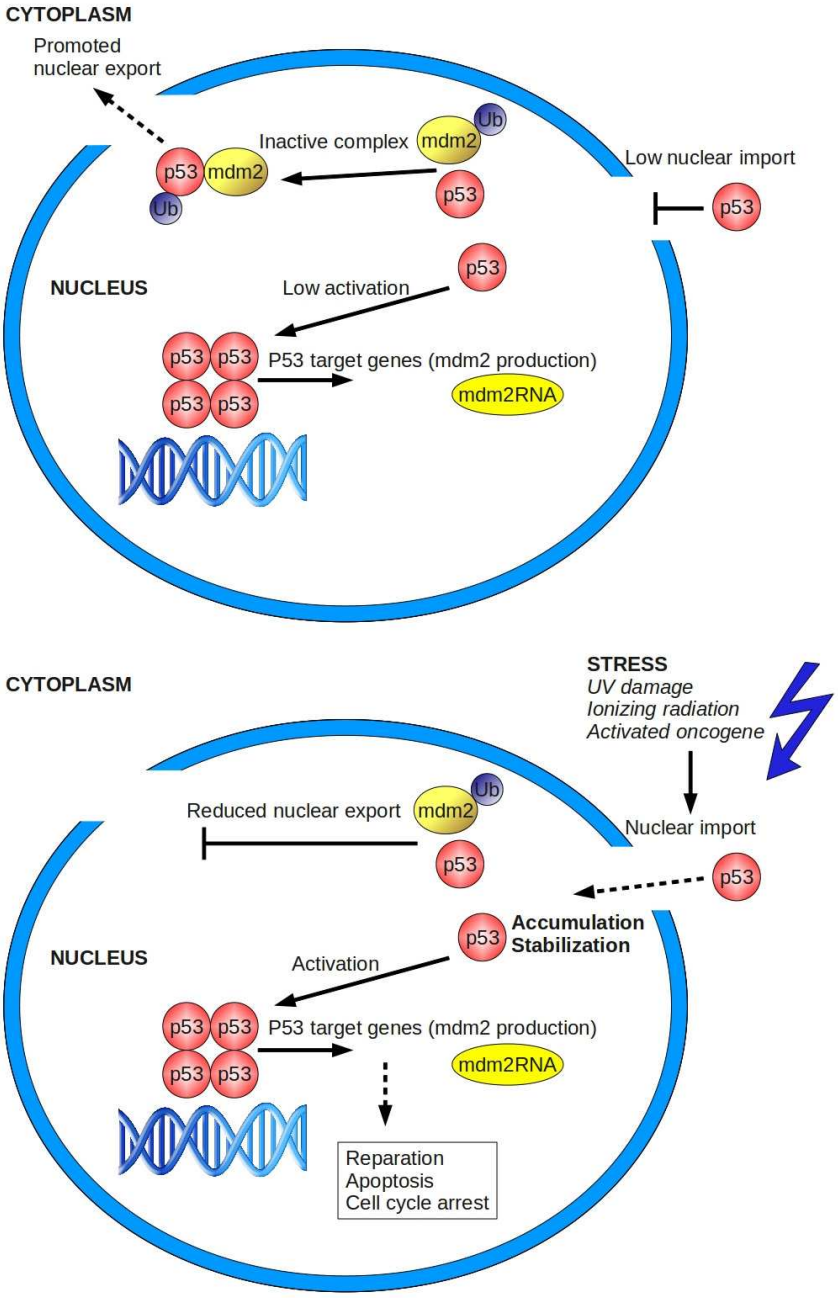

Figure 4.4: Scheme of p53-Mdm2 reactions in unstressed (up) and stressed (down) conditions, nuclear compartment. Improved nuclear import enhances p53 nuclear accumulation.

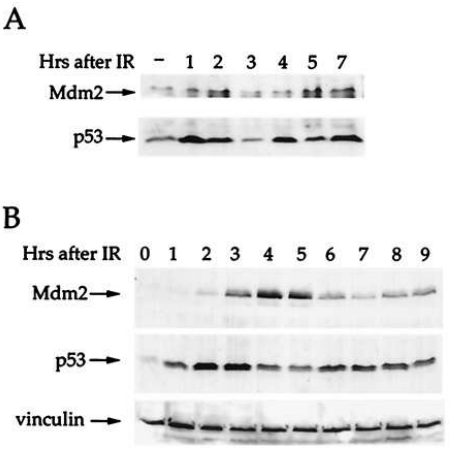

Figure 4.5: The authors of [3] observed an oscillatory behaviour of p53 and Mdm2 after irradiation damage. (A) Mouse fibroblasts NIH 3T3 cells expressing wild-type p53 and wild-type Mdm2 were irradiated with 5 Gy of IR and harvested at the indicated time points after irradiation. Total cell extracts were subjected to SDS/PAGE followed by Western blot analysis. (B) Human breast cancer epithelial MCF-7 cells, expressing wild-type p53 and wild-type Mdm2 were irradiated with 5 Gy of IR and harvested at the indicated time points after irradiation. Total cell extracts were subjected to SDS/PAGE followed by Western blot analysis [3].

damage signal [70]. Indeed experimental studies on single cells, made by Lahav *et al.* [70], showed that p53 levels start to oscillate after irradiation, following DNA damage. But *how* these oscillations depend on damage level? In their work, Lahav *et al.* observed that the total number of peaks of p53 concentration increases with damage level. However, identical cells exposed to the same amount of damage showed varying number of p53 pulses. Thus, the authors conclude that the possibility to see a series of pulses of p53 arises with the irradiation dose. The amplitude and the period of oscillations, on the other hand, do not depend on damage level.

The reason why Bar-Or *et al.* [3] observed only damped oscillations of p53 levels is that their analysis was made on cell populations. In this way, the number of peaks of single cells, was averaged on the total population, giving a global damped behaviour. This behaviour is schematically represented in Figure 4.6.

There are two main challenges about p53 oscillatory behaviour. The first one is to understand the biological meaning of these oscillations, i.e. how oscillations are linked to cell fate 'decision' (towards life or death). This problem is still the object of debates, but undoubtedly oscillations make decisions more flexible. According to a current interpretation [68], each pulse of these oscillations corresponds to an evaluation of the cell state, and an oscillatory response of the signalling pathway suggests that several evaluations of the system state can take place before the conclusive commitment towards one fate or the other.

Secondly, identifying the physiological mechanisms that underlie the observed oscillations, and how they can be altered in disease, is also a challenge with possible therapeutic implications (recalling that p53 is mutated and inefficient in about 50% of cancers). Thus is particularly a challenge to modellers. Indeed in recent years many models have appeared aiming at explaining how the two-protein system p53-Mdm2 can reproduce such sustained oscillations. In a model design perspective, a negative feedback is necessary to

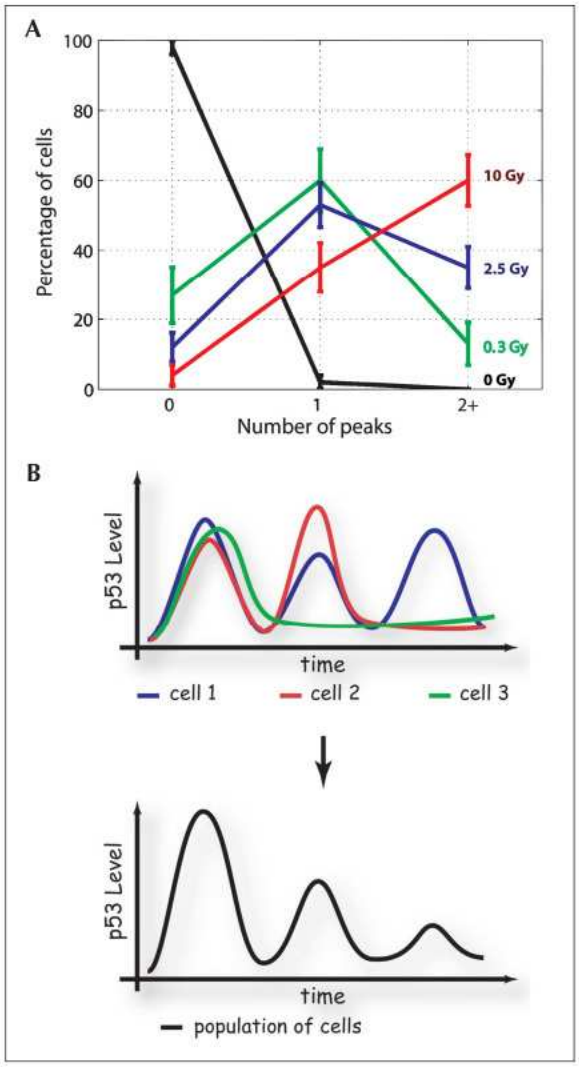

Figure 4.6: Single cell analysis of p53 oscillations. A) Fraction of cells with zero, one two or more pulses as a function of γ-irradiation dose. Taken from [68]. B) Schematic diagram showing the differential p53 oscillations in individual cells. When studying populations of cells, the amplitude of the pulses is averaged, and damped oscillations are observed [69].

obtain oscillations, but it is not sufficient by itself [98]. Other mechanisms need to be identified in order to understand and reproduce the dynamics of p53.

4.2.1 Oscillations in a negative feedback system

An interesting review on how to get suitable oscillations in simple reaction networks has been made by Tyson and Novák [98]. The authors give some clear examples and briefly sum up how simple networks generate oscillations if accurate conditions are satisfied.

The first requirement is the existence of a negative feedback that make the system step back to its initial state. But sustained oscillations do not appear through a single negative feedback, other conditions are necessary. Time delay, nonlinearity and time scale constraints are the ingredients which, if "well mixed", make oscillations appear. We report here the first of the examples discussed in [98], as it shows that a single variable system can reproduce oscillatory dynamics if the negative feedback, always required, is enriched with a time delay. Let us consider a system composed of the single variable Y and suppose that it represents the concentration of a protein that inhibits its own transcription. The corresponding equation reads:

$$\frac{dY(t)}{dt} = k_1 S \frac{K_d^p}{K_d^p + Y^p} - k_d E_t \frac{Y}{K_m + Y}, \tag{4.1}$$

where the first member of the right end side is the protein production rate, a decreasing function of Y, the blue curve in Fig. 4.7. The second term is the degradation term that is supposed to be a bounded function, increasing with Y (the green curve in Fig. 4.7). Both terms depend also on source (S), enzymes (E_t) and rate constants that are assumed to be constant. As can be seen in Fig. 4.7 there is a unique equilibrium point, that is stable, so that no oscillations can appear, whatever the values of parameters. Let us now

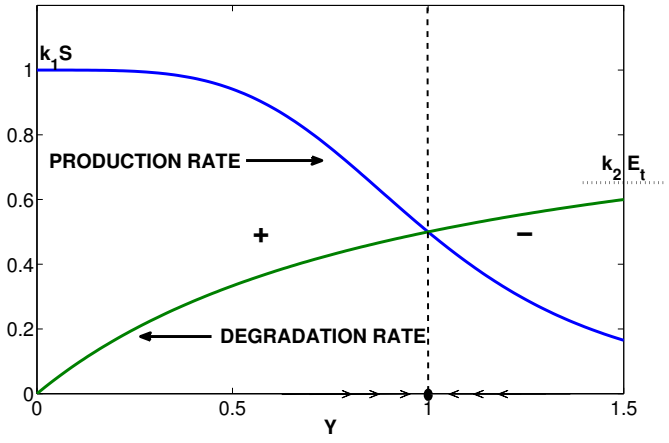

Figure 4.7: A negative feedback alone does not generate oscillations

use an explicit time delay and take into account the time needed for transcription and

translation. Protein production at time t depends, in this case, on its concentration at $t-\tau$ for a fixed delay τ, and the equation reads:

$$\frac{dY}{dt}(t) = k_1 S \frac{K_d^p}{K_d^p + Y^p(t-\tau)} - k_d E_t \frac{Y(t)}{K_m + Y(t)}. \tag{4.2}$$

The nonlinearity of the equation and the delay introduced allow sustained oscillations, according to specific constraints on τ, p , K_m, and S (the signal strength). Let us show briefly how to obtain a periodic solution to this equation. Let us start by writing the equation in dimensionless form:

$$\frac{dy}{d\hat{t}} = \frac{\sigma}{1 + [y(\hat{t}-\hat{\tau})]^p} - \frac{y}{\kappa + y}$$

where $\hat{t} = \frac{k_2 E_t}{K_d} t$, $y = Y/K_d$, $\sigma = k_1 S/(k_2 E_t)$, $\kappa = K_m/K_d$, $\hat{\tau} = \frac{k_2 E_t}{K_d}\tau$. The steady state solution is the solution of the equation

$$f(y) := y^{p+1} + y(1-\sigma) - \sigma\kappa = 0.$$

It is straightforward to see that there is a unique positive root y_0 to this equation. Assuming the solution to have oscillatory dynamics, thus to be of the form $\hat{y}(\hat{t}) = y_0 + ce^{i\omega\hat{t}}$ and substituting this solution in equation 4.2, it is possible to find convenient conditions on τ, p , K_m and S for the existence of this solution. Examples of p53-Mdm2 models with an explicit time delay will be introduced in the next subsection.

Another classical example of network that reproduces oscillatory dynamics are systems that present positive and negative feedback together. Examples of such modelling choice will be given below.

Finally it is interesting to take into account space and spatial constraints. Indeed within a cell, every protein needs to be translocated from the nucleus to the cytoplasm in order to be synthesized and, depending on its functional activities, need to be transported to the right compartment (nucleus, nucleolus, mitochondria, etc.). Many ODE models exist to represent the p53-Mdm2 oscillations but few consider the spatial variable as an element involved in the generation of oscillations. We will discuss in a more detailed manner the first examples of models that include a spatial description for p53 evolution.

The basic ideas that brought us to the model and to the results presented in this thesis are based on the idea that physical constraints cannot be dodged. Certainly it is useful and important to study the dynamics of molecular systems considering averaged cellular concentrations of molecules, as it is done in ODE models. However, we believe that an important step in the modelling process is to take into account the main physical features of the system we deal with. In the specific case of eukaryote cells, the most eye-catching physical feature that has to be considered is the separation between the nucleus and the cytoplasm. As explained in Section 1.3, the processes that regulate the access to the two compartments are strictly controlled and the functions that proteins carry out strongly depend on their location. Therefore, in a modelling perspective, we believe that integrating the spatial variable, as constraint and as functional information, is an important direction to follow.

Models introducing a delay

Here we present two examples of models of p53 where the authors use delay differential equations (DDE) to reproduce the oscillatory dynamics of the p53-Mdm2 network. The

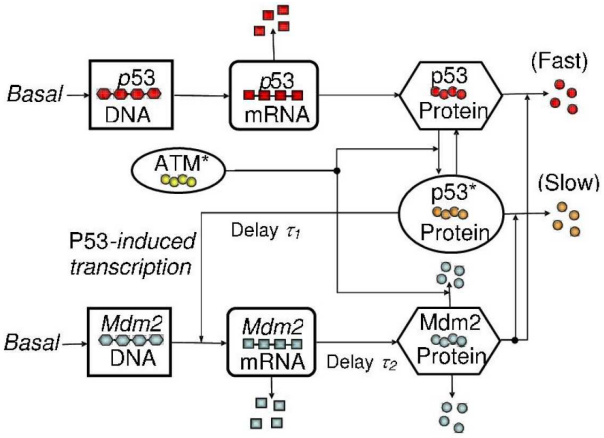

Figure 4.8: Diagram of the oscillator in the Wagner model, [78]

model was proposed by Wagner *et al* in 2005 [78]. In figure 4.8 we can see the scheme of the model proposed by the authors. The second model of DDE system is Monk's model [90] and the corresponding scheme is reported in Fig. 4.9.

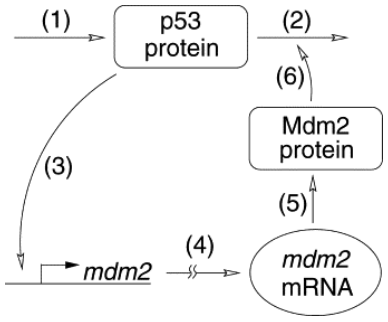

Figure 4.9: Scheme of Monk's Model reproducing p53 oscillations, [90].

Both these works reproduce the oscillatory behaviour of p53 and Mdm2. They model the negative feedback $p53 \rightarrow Mdm2 \dashv p53$ and add a delay that allows oscillations to occur. In both cases an intermediate variable is introduced. This intermediate represents the mRNA of Mdm2. As established by [3] the use of a third equation in the p53-Mdm2 feedback is mandatory to obtain the oscillations.

In [78] the authors take into account two different delays, τ_1 and τ_2. The first one represents the delay due to transcription of Mdm2 mRNA, while the second one, represents the delay due to translation of Mdm2 mRNA into the Mdm2 protein (see Fig. 4.8). The authors also model the activation of p53 due to the ATM kinase (see Section 4.1.2)

and consider p53 in two distinct states: active and inactive ($p53$ and $p53^*$ respectively in Fig. 4.8). Only nuclear concentrations are considered. A constraint is imposed in order to get stable oscillatory dynamics: $\tau_1 + \tau_2 > 16$ min. But the switch that make oscillations appear is due to the increased degradation rate of Mdm2, as a consequnece of ATM activity. Finally, the authors couple these equations with a DNA damage repair module and an ATM activation module, thus modelling all steps of the p53 pathway.

In the work of Monk, [90], a unique delay τ is taken into account. It stands for the time due to transcription of Mdm2 (steps 3 and 4 of Fig. 4.9). The authors obtain oscillations of p53 and Mdm2 levels in good agreement with experimental data. However, no bifurcation analysis is done and no mathematical details about the existence of a stable limit cycle are given.

Models of p53 oscillatory behaviour: positive and negative feedback

Here we will describe three different models that reproduce p53 oscillatory dynamics, obtained by introducing a negative and a positive feedback. Indeed biological evidence shows that p53 inhibits Mdm2 nuclear entry through its interaction with protein PTEN [84]. Also, various authors suggest an auto-catalytic nature for p53 transcription [5]. Therefore there are two possible positive feedbacks that can be taken into account in order to generate oscillations (see Fig. 4.10).

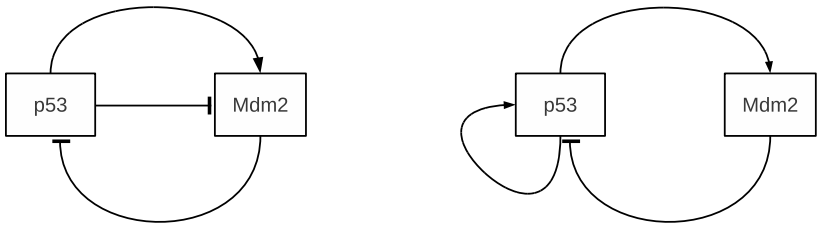

(a) (b)

Figure 4.10: Motifs for the p53-Mdm2 network; (a): Negative and Positive Feedback (NPF) due to inhibition of Mdm2 nuclear entry, as in [20, 100]. (b): the NPF is obtained by taking into account an auto-catalysis of p53, as in [18]

Ciliberto [20] and Ouattara [100] consider the first scenario of Fig. 4.10. Both models describe nuclear and cytoplasmic levels of p53 and Mdm2. Furthermore they both take into account the DNA damage process thus describing an active and an inactive state of the network. Ciliberto and collaborators in [20] analyse the question whether the oscillations are due to the existence of a positive feedback or if the delay alone is the unique necessary condition. To this purpose, the authors conceive an experimental study that

could empirically prove which is the right mechanism (positive and negative feedback or negative feedback+delay). They propose to remove experimentally the negative feedback and induce p53 synthesis. Since the positive feedback creates a bistable state, the removal of the negative feedback would make the system step in a new state, without traversing the oscillatory regime. If, instead, the positive feedback does not influence p53 dynamics, then the p53 level should increase, after induction of p53 synthesis, and then come back to its initial state, once the signal is off.

In [100] the authors introduce a simple model composed of four elements: p53, nuclear and cytoplasmic Mdm2 and DNA damage. In this model, DNA damage enhances the Mdm2 degradation rate, thus weakening the Mdm2 negative control on p53. Nuclear Mdm2 affects p53 degradation rate and reduces p53 functional activity. On the other hand p53 acts as a transcription factor for Mdm2 and inhibits the nuclear entry of cytoplasmic Mdm2. Finally p53 promotes DNA damage repair (see the scheme of the model on Fig. 4.11).

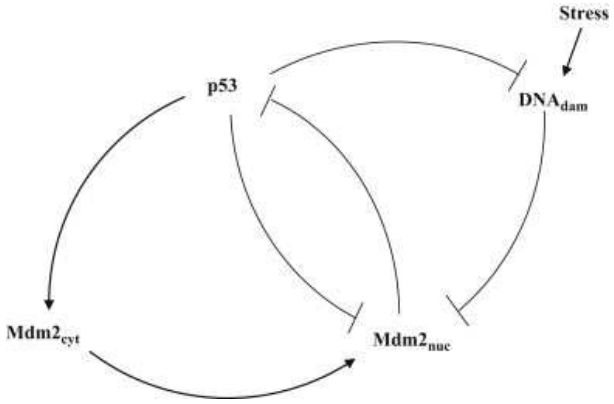

Figure 4.11: Reaction network scheme p53/Mdm2 dynamics from the model proposed in [100]

Here is the system of equations they consider:

$$\begin{cases} \frac{d[P]}{dt} = k_P \frac{K_P^4}{K_P^4+[M_n]^4} - (d_P + d_P'[M_n])[P], \\ \frac{d[M_n]}{dt} = V_r(k_{in} - k_{in}' \frac{[P]^4}{K_{M_n}^4+[P]^4})[M_c] - k_{out}[M_n] - d_{M_n}[M_n], \\ \frac{d[M_c]}{dt} = k_{M_c} + k_{M_c}' \frac{[P]^4}{K_{M_c}^4+[P]^4} - (k_{in} - k_{in}' \frac{[P]^4}{K_{M_n}^4+[P]^4})[M_c] + \frac{1}{V_r} k_{out}[M_n] - d_{M_c}[M_c], \\ \frac{d[DNA_{dam}]}{dt} = k_{Ir}\mathbf{Ir} - k_{dam} \frac{[P]^4}{K_{dam}^4+[P]^4}[DNA_{dam}], \end{cases} \tag{4.3}$$

where **Ir** is the irradiation dose. Here $[P]$, $[M_n]$ and $[M_c]$ represents respectively the p53, nuclear Mdm2 and cytoplasmic Mdm2 concentrations. The degradation rate of $[M_n]$,

d_{M_n}, is controlled by DNA damage by imposing $d_{M_n} = d'_{M_n} + d''_{M_n} \frac{[DNA_{dam}]}{K'_{M_n}+[DNA_{dam}]}$, where d'_{M_n},d''_{M_n} and K'_{M_n} are fixed parameters.

Ouattara and colleagues analyse several bifurcation scenarios corresponding to different parameter sets. They choose the most relevant parameters by performing a logical analysis of the dynamic network [1].

In particular they use as a bifurcation parameter the degradation rate of nuclear Mdm2 (d_{M_n}), that depends on DNA damage. And they study the response of the system to variations of the ratio K_{M_c}/K_{M_n}. This value represents the p53-Mdm2 binding affinity: K_{M_c} is the dissociation constant of p53 from Mdm2 target gene, while K_{M_n} is the dissociation constant of p53 to the target genes that are responsible for the down-regulation of Mdm2 import (see equations 4.3). If the ratio $K_{M_c}/K_{M_n} < 1$ the negative feedback prevails and the bifurcation scenarios are similar to those of models discussed in the previous section. On the contrary, for high values of K_{M_c} the binding affinity of p53 to the Mdm2 target gene is low and the positive feedback prevails. We can thus observe a bistable behaviour which, coupled to the negative feedback loop, results in a relaxation oscillator (see Fig. 4.12). The oscillatory modes differ in periods, mean levels of p53 and amplitude. This study shows the dependence of the type of response of the network on characteristics such as p53 affinity to target genes. The authors suggest that the p53-Mdm2 network is able to modulate its behaviour in order to better respond to different types of DNA damage.

Finally we recall the model proposed by Chickarmane [18] who proposed the autocatalysis of p53 positive feedback in the p53-Mdm2 network. The authors couple the module of the p53-Mdm2 oscillator (Fig. 4.10(b)) with a bistable switch that represents the damage sensor. The switch is turned on when damage occurs and oscillations arise. The authors show that the interaction between the bistable switch and the oscillator is one way to obtain pulsatile behaviour. Furthermore they show that this system exhibits robust oscillatory behaviour in the presence of noise.

Spatial models

We conclude this section about models of p53 dynamics with the description of the works that include the spatial variable in the description of the p53-Mdm2 network. To our knowledge Chaplain and his colleagues are the only authors who recently developed *in silico* experimental cases where the oscillatory regime of p53 is reproduced through the description of the spatial environment of a single cell. The first work that goes in this direction is the model of Gordon *et al.* [44]. The authors suggest a simplified model of the p53 network that takes into account the p53-Mdm2 negative feedback loop and they introduce a time delay associated to the transcription and translation of Mdm2. They also represent a DNA damage term that decreases the Mdm2-dependent degradation rate of p53 and enhances the p53-dependent transcription rate of Mdm2. The most important aspect of this work is that for the first time the spatial component was introduced in order to describe p53 dynamics. However the spatial component of the model is very simplified: a unique compartment is designed and no difference between nucleus and cytoplasm are

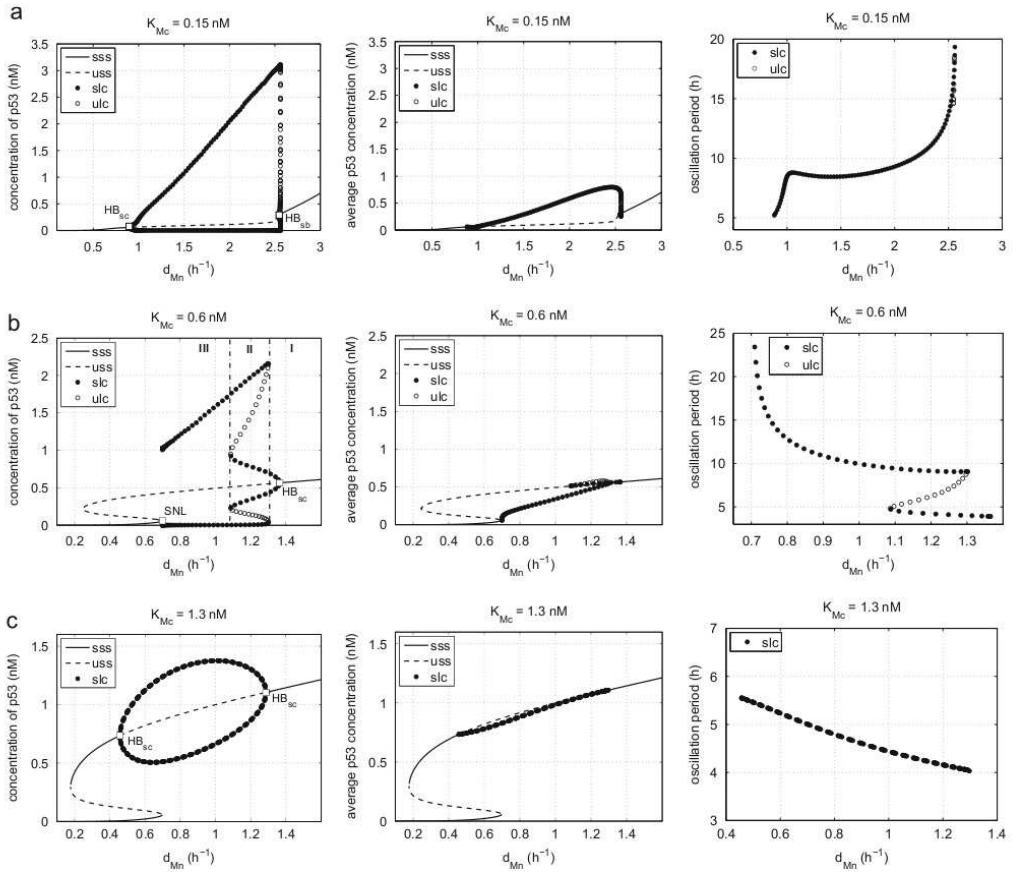

Figure 4.12: Different bifurcation scenarios for low and high values of K_{M_c} [100]. **sss** stands for Stable Steady State, **uss** Unstable Steady State, **slc** Stable Limit Cycle and **ulc** Unstable Limit Cycle. The type of bifurcations are respectively a sub critical and a super critical Hopf bifurcation.

imposed on the spatial domain. The cytoplasm is indeed modelled through a weight function that represents the location where proteins are translated. Furthermore all the reactions but one, translation, are not localized and the nuclear activity of p53 as a transcription factor is shifted to the cytoplasm. The spatial component is not completely exploited or, at least, characterized. However this work has the merit of introducing for the first time, in the study of p53 dynamics, the spatial variable and to ask new questions about how the environment of the cell can contribute to the generation, maintenance and quality of the oscillations of the p53 network.

From the same group, two new studies about p53 dynamics with space have appeared in the last years. In these works the spatial component is an essential ingredient to explain the dynamics of p53. Thus the spatial environment of the cell has been further characterised. The first one, [128], plunges the equations of Monk's model [90] in a spatial environment and removes its explicit delay. Two domains are considered, a nuclear and

a cytoplasmic one. Each represented species is modelled in a cytoplasmic and nuclear form. Proteins are supposed to diffuse freely in the cytoplasm and in the nucleus and the reactions are localized. Thus, protein transcription take place in the nucleus and protein translation in the cytoplasm. Furthermore the authors characterize spatially the location of ribosomes within the cytoplasm and study the robustness of oscillations with respect to it. The greatest interest of this work is that the authors manage to reproduce p53-Mdm2 oscillations by neither adding a positive feedback nor a delay, but by using the spatial description of the cellular environment and the well-known negative feedback.

Recently, an extended version of the model analysed in [128] has been proposed by the same authors [129] and the spatial details further analysed. In particular the authors model the nuclear membrane, that was not considered in the previous work. This choice represents a significant improvement of their work, since the nuclear membrane plays a pivotal role in regulating the access to the nucleus and protein levels are not continuous at the two sides of the membrane (for further biological details see Section 1.3). This aspect was not taken into account in [128] and protein concentration was assumed to be continuous at the membrane level. Beyond the diffusivity of proteins, the authors also suppose that transport of p53 and Mdm2 is enhanced by microtubule activity. They model microtubules through a vector field and transport with a convection term, as done in [15] (see Section 1.2 and 1.4). The extended model is a more robust oscillator over parameter changes with respect to the previous one. However there is no direct evidence that Mdm2 uses microtubules to be transported throughout the cytoplasm. Furthermore the diffusivity (and permeability) coefficients used in this model do not correspond to the known values of p53 and Mdm2 diffusion (and permeability), and oscillations disappear for the 'right' values of diffusivity, i.e. biological identified. To conclude, the work proposed in [129] provides an analysis of p53 dynamics in a detailed and realistic spatial environment. However, in our opinion, some biological assumptions are premature and need further evidence to be considered (relevance of the role of microtubules). Furthermore the use of spatial mechanisms as diffusion, permeability and microtubule velocity of transport, is distorted by the choice of coefficients 2-3 fold orders of magnitude lower than the experimentally calculated ones.

4.3 Conclusions and Outline of the Work

The most common instruments used to describe the dynamics of p53 protein are ODE systems of equations. And, as discussed above, the main strategies used to reproduce oscillations are 1) positive feedback and 2) delays. As regards the former, additional biological hypotheses on the p53 network need to be introduced. Furthermore, as pointed out by Puszyński [104], the positive feedback used by [20] (and others, see e.g. [138]) is mediated by other proteins, PTEN, PIP3 and Akt, but the authors do not consider any of these intermediates explicitly nor introduce any time delay to account for this part of the pathway. This simplification introduces a direct feedback between p53 and Mdm2 that is not observed in experiments and produces non-physiological dynamics.

On the other side, implicit delays, that imply the use of DDE models, are untrust-

worthy. Indeed a DDE model cannot characterize the physiological mechanisms that underlie the introduced delay, so that key mechanisms might be hidden behind the delay.

Finally a few studies [128, 129] used the spatial description of the cellular environment to reproduce the oscillations of the p53 network. Indeed, as it has been shown by Sturrock *et al.* [128], the negative feedback and the localization of p53 and Mdm2 processes give rise to oscillations. Through the spatial characterization of the biological processes, the delay due to transcription and translation can be explicitly taken into account and the delay due to transport is also considered.

In this second part of this thesis we will introduce a new model that considers activation of p53, its degradation due to Mdm2 action, and its activity as a transcription factor. The negative feedback between Mdm2 and p53 will also be taken into account in terms of directionality of transport.

In Chapter 5 a simplified version of this model will be given in terms of ODEs. We will study the temporal dynamics of the p53 core network. It will be shown that the existence of oscillations is dependent on the negative feedback and on the distinction between nucleus and cytoplasm that naturally provide together the physiological delay responsible for oscillations. A detailed bifurcation analysis will be done and different scenarios considered. Then in Chapter 6 we will introduce the spatial component and we will discuss in a detailed manner the properties of the system in this 'new' spatial environment. We start its analysis by studying the behaviour of the system in a simplified one-dimensional domain. Then we analyse, using numerical simulations, the behaviour of the system in a more realistic two dimensional domain. In this environment, we vary all the spatial parameters of the system (diffusion and permeability coefficients, volume and shape of the cell) and we observe the qualitative change in the response of the system (existence of oscillations, amplitude and period of oscillations). We end the chapter with a discussion about our findings and the possible extensions of the model.

Chapter 5

A physiological model for p53 intracellular dynamics

Protein p53 regulates essential cellular pathways, as the ones controlling cell cycle arrest, DNA repair and apoptosis, and thereby it has a decision-making role for the cell, choosing between death and survival, and such 'decision' is strictly regulated by specialised cell signalling pathways.

Because of the central role that p53 has in cell survival, the network that controls its stabilization is rich and complex, so that modelling the dynamics of p53 is a challenge to mathematicians.

An interesting aspect of p53 dynamics is its oscillatory behaviour. While in healthy cells p53 concentration is low and at steady state, in damaged cells, where p53 is activated, the protein concentration rises and sustained oscillations appear [40, 70]. Identifying the physiological mechanisms that underlie the observed oscillations, is a challenge with possible therapeutic implications (knowing that p53 is mutated and inefficient in about 50% of cancers). We introduce in this chapter a physiological model that take into account only the basic signalling pathways of the p53 protein. Our aim is to reach a better understanding of the mechanisms which generate the oscillations in the p53 network and allow the nuclear accumulation of the protein.

This chapter is organized as follows: in Section 5.1 we introduce the biological model that we designed and we explain our modelling choices. Then, we give the mathematical formulation of the model in an ODE form. In Section 5.2 we analyse the mathematical model through equilibrium study and numerical bifurcation theory. Finally we propose a biological explanation of the oscillations showing that they occur only if the relative concentrations of active and inactive p53 overcome some threshold.

Contents

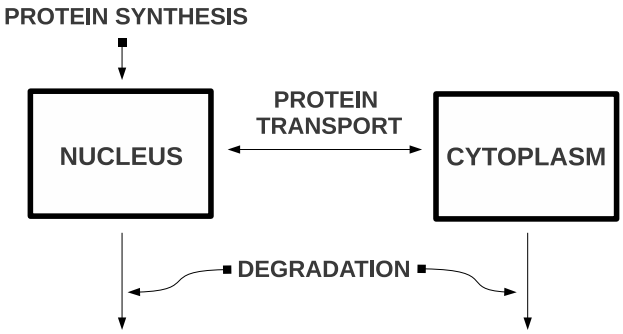

Figure 5.1: The compartmental model: we suppose protein concentrations to be homogeneous in each compartment and we fix exchange rules between them.

5.1 Model formulation

In this section we introduce the model we analyse in this part of the thesis. We design a compartmental ODE differential system by assuming that the concentrations of proteins are homogeneous in each compartment. We determine which reactions are allowed in each compartment and we fix rules for the exchange of mass between them (see figure 5.1).

The model involves two distinct states of p53 (an active and an inactive one), its primary inhibitor Mdm2, and the mRNA of Mdm2, whose synthesis is promoted by p53. Every species of the model exists in a nuclear and in a cytoplasmic form. If necessary, to avoid confusion between the two compartments, we denote by $[\cdot]^{(n)}$ and $[\cdot]^{(c)}$, respectively, the nuclear and cytoplasmic concentration of each species.

Protein p53 undergoes several conformational changes. In our model we represent the ubiquitination process, i.e. the enzymatic action of Mdm2 on p53 by which p53 is

marked for degradation. Even if ubiquitination is more complicated than other enzymatic processes, we choose, for the sake of simplicity, to model it as a classical enzymatic reaction. Thus we write:

$$[Mdm2] + [p53] \underset{k_-}{\overset{k}{\rightleftharpoons}} [Complex] \overset{k_1}{\to} [p53_U] + [Mdm2] \tag{5.1}$$

where $p53_U$ represents the ubiquitinated form of p53. Then, following the Quasi Steady State Approximation [63, 116], the associated differential equation describing the chemical kinetics in (5.1) is given by:

$$\frac{d[p53]}{dt} = -k_1[Mdm2]\frac{[p53]}{K_1 + [p53]}, \tag{5.2}$$

where $K_1 = \dfrac{k_1 + k_-}{k}$ is the Michaelis constant and $k_1[Mdm2]$ represents the maximum velocity of the reaction. In our model we do not include an equation for $p53_U$. Indeed, since through ubiquitination p53 is marked for degradation, we suppose that the right term of equation (5.2) is a loss of mass in our system. In order to be detected by the proteasome, p53 actually needs to be ubiquitinated several times (see [89] and reference therein for a review on Mdm2-mediated p53 ubiquitination). Anyway, we choose not to describe all the single ubiquitination steps, but rather a global one, because we are more interested in the activation process. Furthermore we want to represent the simplest possible network.

We also take into account the phosphorylation and dephosphorylation processes of p53. As reviewed in Chapter 4, a single conformational change cannot uniquely determine the activity of the p53 protein. Several post-translational transformations decide how p53 will be activated [34] and stabilised. Since p53 phosphorylation is particularly important for its regulation in response to DNA damage [30], we represent only this transformation and we treat the phosphorylated form of p53 as a generic 'active' species. Furthermore, although we are aware of the fact that different kinases are activated and are able to phosphorylate p53 depending on the type of damage, we choose to model here only the ATM kinase, that is thus here meant to roughly represent a DNA damage sensor. For the sake of simplicity we treat ATM as a parameter and consider simple enzymatic kinetics. We consider the following reactions:

$$[ATM] + [p53] \underset{k_{-2}}{\overset{k_2}{\rightleftharpoons}} [Complex] \overset{k_3}{\to} [p53_p] + [ATM], \tag{5.3}$$

$$[E] + [p53_p] \underset{k_{-4}}{\overset{k_4}{\rightleftharpoons}} [Complex] \overset{k_5}{\to} [p53] + [E], \tag{5.4}$$

where $p53_p$ is the phosphorylated form of p53, while $[E]$ is a generic phosphatase that removes a phosphate group from its substrate $p53_p$. Again by the quasi Steady State Approximation we obtain the following equations:

$$\frac{d[p53]}{dt} = k_{dph}\frac{[p53_p]}{K_{dph} + [p53_p]} - k_3[ATM]\frac{[p53]}{K_{ATM} + [p53]}, \tag{5.5}$$

$$\frac{d[p53_p]}{dt} = k_3[ATM]\frac{[p53]}{K_{ATM} + [p53]} - k_{dph}\frac{[p53_p]}{K_{dph} + [p53_p]}, \tag{5.6}$$

where k_{dph} is the maximum velocity of the dephosphorylation process, $K_{dph} = \frac{k_5+k_{-4}}{k_4}$ and $K_{atm} = \frac{k_3+k_{-2}}{k_2}$, the Michaelis constants. We assume that the phosphorylated form of p53, that is the product of the reaction in equation (5.3), is unable to interact with Mdm2, so that after DNA damage, a pool of p53 is not subject to Mdm2 control and is active in the nucleus as a transcription factor.

Next, we model protein transcription and translation: a part of the mRNA of Mdm2 is produced in the nucleus at a constant rate, but a fraction is also produced as a function of p53. Since p53 is known to be active as a transcription factor when it is in a tetrameric form (formed up by four sub-units), we represent this reaction as is classically done in modelling cooperative processes [57], by using a Hill function with coefficient 4:

$$\frac{d[Mdm2_{RNA}]}{dt} = k_{Sm} + k_{Sp}\frac{([p53_p])^4}{([p53_p])^4 + K_{Sp}^4}\,, \tag{5.7}$$

these reactions being located only in the nucleus. The mRNA of Mdm2 is then translated in the cytoplasm by the ribosomes. We assume a constant production rate for the synthesis of p53 in the cytoplasmic compartment. Although recent studies [39] show that p53 transcription could be enhanced after a damage, we choose not to represent explicitly its mRNA.

We include degradation terms as linear functions of each protein concentration. Since it has been proved that p53 degradation occurs mainly in the cytoplasm [82], we add, besides the ubiquitination term, a classical degradation term for p53, in the cytoplasm. Actually, p53 is known to be degraded also in the nucleus ([36, 141]), but in normal growth conditions this is not the preferential way chosen by the cell [54]. Phosphorylated p53 poorly interacts with Mdm2 and thus it is not marked for degradation by Mdm2. We assume that it is not be degraded at all and do not consider any degradation term for it. Following Ciliberto *et al.* in [20], we model the exchanges between compartments as a linear contribution of a difference between averaged nuclear and cytoplasmic concentrations and we multiply the nuclear flux by V_r, a nondimensional quantity representing the volume ratio between cytoplasm and nucleus. It is known that p53 and Mdm2 can shuttle between nucleus and cytoplasm [37, 82]. On the contrary, nuclear export of phosphorylated p53, that represents active p53, is inhibited after DNA damage [125, 143]. Therefore, basing our modelling hypotheses on these biological observations, we assume here that p53 and Mdm2 can traverse the different compartments. The phosphorylated form of p53 is assumed to move from cytoplasm to nucleus but not backwards. On the other hand, we assume that the mRNA of Mdm2 only moves from the nucleus, where it is transcribed, to the cytoplasm, where it is translated. See Figure 5.2.

Based on our assumptions we obtain the following differential system for the activity

of the coupled oscillator p53-Mdm2 in the nucleus:

$$\begin{cases} \dfrac{d[p53]^{(n)}}{dt} = k_{dph}\dfrac{[p53_p]^{(n)}}{K_{dph}+[p53_p]^{(n)}} - k_1[Mdm2]^{(n)}\dfrac{[p53]^{(n)}}{K_1+[p53]^{(n)}} \\ \qquad\qquad -k_3[ATM]\dfrac{[p53]^{(n)}}{K_{ATM}+[p53]^{(n)}} - p_pV_r([p53]^{(n)}-[p53]^{(c)}), \\ \dfrac{d[Mdm2]^{(n)}}{dt} = -\delta_m[Mdm2]^{(n)} - p_mV_r([Mdm2]^{(n)}-[Mdm2]^{(c)}), \\ \dfrac{d[Mdm2_{RNA}]^{(n)}}{dt} = k_{Sm} + k_{Sp}\dfrac{([p53_p]^{(n)})^4}{([p53_p]^{(n)})^4+K_{Sp}^4} - \delta_{mRNA}[Mdm2_{RNA}]^{(n)} \\ \qquad\qquad -p_{mRNA}V_r[Mdm2_{RNA}]^{(n)}, \\ \dfrac{d[p53_p]^{(n)}}{dt} = p_{pp}V_r[p53_p]^{(c)} + k_3[ATM]\dfrac{[p53]^{(n)}}{K_{ATM}+[p53]^{(n)}} - k_{dph}\dfrac{[p53_p]^{(n)}}{K_{dph}+[p53_p]^{(n)}}, \end{cases} \tag{5.8}$$

and the following one in the cytoplasm:

$$\begin{cases} \dfrac{d[p53]^{(c)}}{dt} = k_S + k_{dph}\dfrac{[p53_p]^{(c)}}{K_{dph}+[p53_p]^{(c)}} - k_1[Mdm2]^{(c)}\dfrac{[p53]^{(c)}}{K_1+[p53]} \\ \qquad\qquad -k_3[ATM]\dfrac{[p53]^{(c)}}{K_{ATM}+[p53]^{(c)}} - p_p([p53]^{(c)}-[p53]^{(n)}) - \delta_p[p53]^{(c)}, \\ \dfrac{d[Mdm2]^{(c)}}{dt} = k_{tm}[Mdm2_{RNA}]^{(c)} - p_m([Mdm2]^{(c)}-[Mdm2]^{(n)}) - \delta_m[Mdm2]^{(c)}, \\ \dfrac{d[Mdm2_{RNA}]^{(c)}}{dt} = p_{mRNA}[Mdm2_{RNA}]^{(n)} - k_{tm}[Mdm2_{RNA}]^{(c)} \\ \qquad\qquad -\delta_{mRNA}[Mdm2_{RNA}]^{(c)}, \\ \dfrac{d[p53_p]^{(c)}}{dt} = k_3[ATM]\dfrac{[p53]^{(c)}}{K_{ATM}+[p53]^{(c)}} - k_{dph}\dfrac{[p53_p]^{(c)}}{K_{dph}+[p53_p]^{(c)}} - p_{pp}[p53_p]^{(c)}. \end{cases} \tag{5.9}$$

5.2 Analysis of the model

In this section we study model (5.8)-(5.9) in order to capture the temporal dynamics of the system [107]. To simplify our notations, let us set $u_0 = [p53]$, $u_1 = [Mdm2]$, $u_2 = [Mdm2_{RNA}]$ and $u_3 = [p53_P]$. In the sequel we denote the nuclear and cytoplasmic concentrations by the superscripts (n) and (c). The autonomous differential system

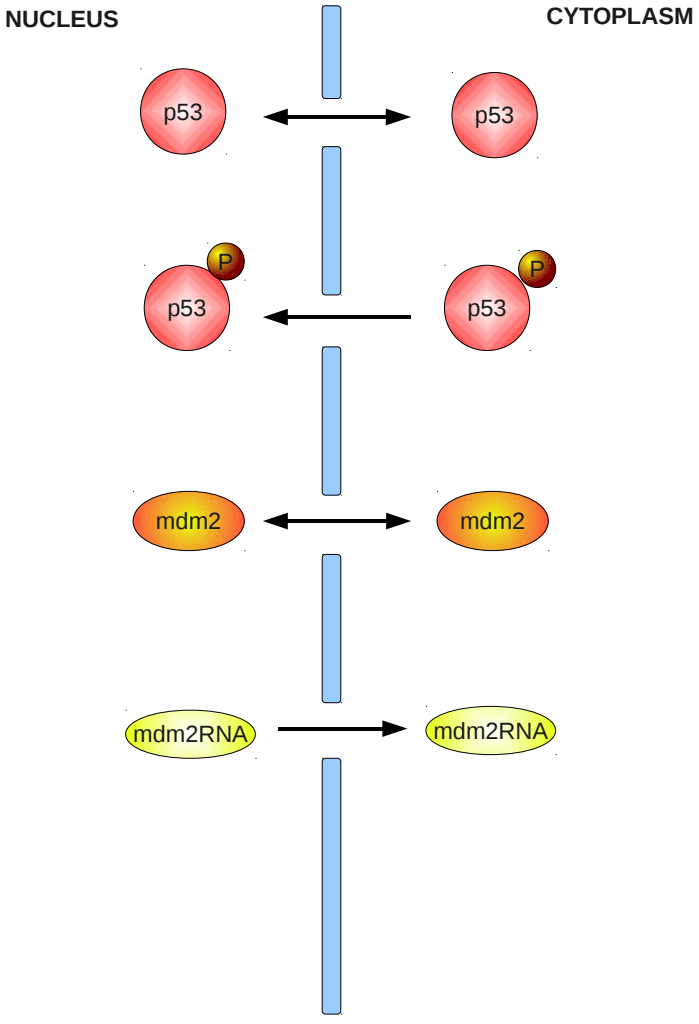

Figure 5.2: Schematic view of the import-export abilities of p53 and Mdm2: modelling choices.

resulting from the model presented in Section 5.1 may be rewritten as:

$$\begin{cases} \frac{du_0^{(n)}}{dt} = -k_1 u_1 \frac{u_0^{(n)}}{(K_{m1}+u_0^{(n)})} - k_3 ATM \frac{u_0^{(n)}}{(K_{atm}+u_0^{(n)})} + k_{dph} \frac{u_3^{(n)}}{(K_{dph}+u_3^{(n)})} - V_r p_0 (u_0^{(n)} - u_0^{(c)}), \\ \frac{du_1^{(n)}}{dt} = -V_r p_1 (u_1^{(n)} - u_1^{(c)}) - d_1 u_1^{(n)}, \\ \frac{du_2^{(n)}}{dt} = k_{pm} + k_{Sp} (\frac{u_3^{(n)4}}{(K_{Sp}^4+u_3^{(n)4})}) - V_r p_2 u_2^{(n)} - d_2 u_2^{(n)}, \\ \frac{du_3^{(n)}}{dt} = k_3 ATM \frac{u_0^{(n)}}{(K_{atm}+u_0^{(n)})} - k_{dph} \frac{u_3^{(n)}}{(K_{dph}+u_3^{(n)})} + V_r p_3 u_3^{(c)}, \\ \frac{du_0^{(c)}}{dt} = k_{tp} - k_1 u_1^{(c)} (\frac{u_0^{(c)}}{(K_{m1}+u_0^{(c)})}) - k_3 ATM \frac{u_0^{(c)}}{(K_{atm}+u_0^{(c)})} + k_{dph} \frac{u_3^{(c)}}{(K_{dph}+u_3^{(c)})} \\ \qquad\qquad + p_0 (u_0^{(n)} - u_0^{(c)}) - d_0 u_0^{(c)}, \\ \frac{du_1^{(c)}}{dt} = k_{tm} u_2^{(c)} + p_1 (u_1^{(n)} - u_1^{(c)}) - d_1 u_1, \\ \frac{du_2^{(c)}}{dt} = -k_{tm} u_2^{(c)} + p_2 u_2^{(n)} - d_2 u_2^{(c)}, \\ \frac{du_3^{(c)}}{dt} = k_3 ATM \frac{u_0^{(c)}}{(K_{atm}+u_0^{(c)})} - k_{dph} \frac{u_3^{(c)}}{(K_{dph}+u_3^{(c)})} - p_3 u_3^{(c)}. \end{cases} \tag{5.10}$$

Here the first four equations represent the nuclear concentrations and the others the cytoplasmic ones. Notice that, accordingly to the new notations, we denote by p_i and d_i the permeability and degradation coefficients of the i-th species.

Nondimensionalisation

First of all we adimensionalise the system by writing

$$\bar{u}_0(\tau) = \frac{u_0(t)}{\alpha_0}, \ldots, \bar{u}_3(\tau) = \frac{u_3(t)}{\alpha_3}$$
$$\tau = \frac{t}{t^\star}$$

where the α_i are concentrations of the i-th species (expressed in μM) and $t^\star$ is a time constant, expressed in minutes. We fixed $\alpha_0 = \alpha_3$ as p53 reference concentrations and

$\alpha_1 = \alpha_2$ as Mdm2 reference concentrations and we rewrite the system as follows:

$$\begin{cases} \frac{d\bar{u}_0^{(n)}}{d\tau} = -k_4 t^\star \alpha_1 \bar{u}_1^{(n)} \frac{\bar{u}_0^{(n)}}{(K_{m1}+\alpha_0 \bar{u}_0^{(n)})} - k_3 ATM t^\star \frac{\bar{u}_0^{(n)}}{(K_{atm}+\alpha_0 \bar{u}_0^{(n)})} + k_{dph} \frac{t^\star}{\alpha_0} \frac{\alpha_3 \bar{u}_3^{(n)}}{(K_{dph}+\alpha_3 \bar{u}_3^{(n)})} \\ \qquad\qquad -V_r p_0 t^\star (\bar{u}_0^{(n)} - \frac{\alpha_0}{\alpha_0} \bar{u}_0^{(c)}), \\ \frac{d\bar{u}_1^{(n)}}{d\tau} = -V_r p_1 t^\star (\bar{u}_1^{(n)} - \frac{\alpha_1}{\alpha_1} \bar{u}_1^{(c)}) - d_1 t^\star \bar{u}_1^{(n)}, \\ \frac{d\bar{u}_2^{(n)}}{d\tau} = \frac{t^\star}{\alpha_2} k_{pm} + \frac{t^\star}{\alpha_2} k_{Sp} (\frac{(\alpha_3 \bar{u}_3^{(n)})^4}{K_{Sp}^4 + (\alpha_3 \bar{u}_3^{(n)})^4}) - V_r p_2 t^\star \bar{u}_2^{(n)} - d_2 t^\star \bar{u}_2^{(n)} \\ \frac{d\bar{u}_3^{(n)}}{d\tau} = \frac{t^\star}{\alpha_3} k_3 ATM \frac{\alpha_0 \bar{u}_0^{(n)}}{(K_{atm}+\alpha_0 \bar{u}_0^{(n)})} - k_{dph} t^\star \frac{\bar{u}_3^{(n)}}{(K_{dph}+\alpha_3 \bar{u}_3)^{(n)}} + V_r p_3 \frac{t^\star}{\alpha_3} \alpha_3 \bar{u}_3^{(c)}, \\ \frac{d\bar{u}_0^{(c)}}{d\tau} = \frac{t^\star}{\alpha_0} k_{tp} - k_4 t^\star \alpha_1 \bar{u}_1^{(c)} (\frac{\bar{u}_0^{(c)}}{(K_{m1}+\alpha_0 \bar{u}_0^{(c)})}) - k_3 ATM t^\star \frac{\bar{u}_0^{(c)}}{(K_{atm}+\alpha_0 \bar{u}_0^{(c)})} + k_{dph} \frac{t^\star}{\alpha_0} \frac{\alpha_3 \bar{u}_3^{(c)}}{(K_{dph}+\alpha_3 \bar{u}_3^{(c)})} \\ \qquad\qquad +t^\star p_0 (\frac{\alpha_0}{\alpha_0} \bar{u}_0^{(n)} - \bar{u}_0^{(c)}) - d_3 t^\star \bar{u}_0^{(c)}, \\ \frac{d\bar{u}_1^{(c)}}{d\tau} = \frac{t^\star \alpha_2}{\alpha_1} k_{tm} \bar{u}_2^{(c)} + t^\star p_1 (\frac{\alpha_1}{\alpha_1} \bar{u}_1^{(n)} - \bar{u}_1^{(c)}) - d_1 t^\star \bar{u}_1^{(c)}, \\ \frac{d\bar{u}_2^{(c)}}{d\tau} = -t^\star k_{tm} \bar{u}_2^{(c)} + p_2 \frac{t^\star \alpha_2}{\alpha_2} \bar{u}_2^{(n)} - d_2 t^\star \bar{u}_2^{(c)}, \\ \frac{d\bar{u}_3^{(c)}}{d\tau} = \frac{t^\star}{\alpha_3} k_3 ATM \frac{\alpha_0 \bar{u}_0^{(c)}}{(K_{atm}+\alpha_0 \bar{u}_0^{(c)})} - k_{dph} t^\star \frac{\bar{u}_3^{(c)}}{(K_{dph}+\alpha_3 \bar{u}_3^{(c)})} - p_3 t^\star \bar{u}_3^{(c)}, \end{cases} \tag{5.11}$$

We collect the commun terms of equations (5.11):

$$\begin{cases} \frac{d\bar{u}_0^{(n)}}{d\tau} = -k_4 t^\star \frac{\alpha_1}{\alpha_0} \bar{u}_1^{(n)} \frac{\bar{u}_0^{(n)}}{(K_{m1}/\alpha_0+\bar{u}_0^{(n)})} - \frac{ATM}{\alpha_0} \frac{\bar{u}_0^{(n)}}{(1+\bar{u}_0^{(n)})} + k_{dph} \frac{t^\star}{\alpha_0} \frac{\bar{u}_3^{(n)}}{(K_{dph}/\alpha_3+\bar{u}_3^{(n)})} \\ \qquad\qquad -V_r p_0 t^\star (\bar{u}_0^{(n)} - \bar{u}_0^{(c)}) \\ \frac{d\bar{u}_1^{(n)}}{d\tau} = -V_r p_1 t^\star (\bar{u}_1^{(n)} - \bar{u}_1^{(c)}) - d_1 t^\star \bar{u}_1^{(n)} \\ \frac{d\bar{u}_2^{(n)}}{d\tau} = \frac{t^\star}{\alpha_2} k_{pm} + \frac{(\bar{u}_3^{(n)})^4}{(K_{Sp}^4/\alpha_3^4 + (\bar{u}_3^{(n)})^4)} - V_r p_2 t^\star \bar{u}_2^{(n)} - d_2 t^\star \bar{u}_2^{(n)} \\ \frac{d\bar{u}_3^{(n)}}{d\tau} = \frac{ATM}{K_{atm}} \frac{\bar{u}_0^{(n)}}{(1+\bar{u}_0^{(n)})} - \frac{k_{dph} t^\star}{\alpha_3} \frac{\bar{u}_3^{(n)}}{(K_{dph}/\alpha_3+\bar{u}_3^{(n)})} + V_r p_3 t^\star \bar{u}_3^{(c)} \\ \frac{d\bar{u}_0{}^{(c)}}{d\tau} = \frac{t^\star}{\alpha_0} k_{tp} - k_4 t^\star \frac{\alpha_1}{\alpha_0} \bar{u}_1^{(c)} (\frac{\bar{u}_0^{(c)}}{(K_{m1}/\alpha_0+\bar{u}_0^{(c)})}) - \frac{ATM}{K_{atm}} \frac{\bar{u}_0^{(c)}}{(1+\bar{u}_0^{(c)})} + k_{dph} \frac{t^\star}{\alpha_0} \frac{\bar{u}_3^{(c)}}{(K_{dph}/\alpha_3+\bar{u}_3^{(c)})} \\ \qquad\qquad +t^\star p_0 (\bar{u}_0^{(n)} - \bar{u}_0^{(c)}) - d_3 t^\star \bar{u}_0^{(c)} \\ \frac{d\bar{u}_1^{(c)}}{d\tau} = t^\star k_{tm} \bar{u}_2^{(c)} + t^\star p_1 (\bar{u}_1^{(n)} - \bar{u}_1^{(c)}) - d_1 t^\star \bar{u}_1^{(c)} \\ \frac{d\bar{u}_2^{(c)}}{d\tau} = -t^\star k_{tm} \bar{u}_2^{(c)} + p_2 t^\star \bar{u}_2^{(n)} - d_2 t^\star \bar{u}_2^{(c)} \\ \frac{d\bar{u}_3^{(c)}}{d\tau} = \frac{ATM}{\alpha_0} \frac{\bar{u}_0^{(c)}}{(1+\bar{u}_0^{(c)})} - \frac{k_{dph} t^\star}{\alpha_3} \frac{\bar{u}_3}{(K_{dph}/\alpha_3+\bar{u}_3^{(c)})} - p_3 t^\star \bar{u}_3^{(c)}. \end{cases} \tag{5.12}$$

We set: $k_{ub} := t^\star k_4 \frac{\alpha_1}{\alpha_0}$, $K_{ub} := \frac{K_{m1}}{\alpha_0}$, $A\bar{T}M := \frac{ATM}{\alpha_0}$, $\bar{k_{dph}} := \frac{k_{dph} t^\star}{\alpha_0}$, $\bar{K_{dph}} := \frac{K_{dph}}{\alpha_3}$, $\bar{k}_{pm} = \frac{t^\star k_{pm}}{\alpha_2}$, $\bar{K}_{Sp} := \frac{K_{Sp}}{\alpha_3}$,$\bar{k}_{tp} := \frac{t^\star k_{tp}}{\alpha_0}$, $\bar{k}_{tm} := t^\star k_{tm}$. We set $\bar{p}_i = t^\star p_i$ and $\bar{d}_i = t^\star d_i$ for $i = 0, \ldots, 3$. Then we choose $\alpha_0 = K_{atm}$, $t^\star = \frac{1}{k_3}$ and $\alpha_2 = \frac{k_{Sp}}{k_3}$. This scaling choice has been made in such a way that the term relative to the main bifurcation (with respect to the ATM parameter) depends on the smallest possible number of parameters. Other scaling choises are, of course, possible. Finally, the nondimensional system, which does

not depend on K_{atm}, k_3 and k_{Sp}, reads:

$$\begin{cases} \frac{d\bar{u}_0^{(n)}}{d\tau} = -k_{ub}\bar{u}_1^{(n)}\frac{\bar{u}_0^{(n)}}{(K_{ub}+\bar{u}_0^{(n)})} - \overline{ATM}\frac{\bar{u}_0^{(n)}}{(1+\bar{u}_0^{(n)})} + \bar{k}_{dph}\frac{\bar{u}_3^{(n)}}{(\bar{K}_{dph}+\bar{u}_3^{(n)})} - V_r\bar{p}_0(\bar{u}_0^{(n)} - \bar{u}_0^{(c)}), \\ \frac{d\bar{u}_1^{(n)}}{d\tau} = -V_r\bar{p}_1(\bar{u}_1^{(n)} - \bar{u}_1^{(c)}) - \bar{d}_1\bar{u}_1^{(n)}, \\ \frac{d\bar{u}_2^{(n)}}{d\tau} = \bar{k}_{pm} + \frac{\bar{u}_3^{(n)4}}{(\bar{K}_{Sp}^4+\bar{u}_3^{(n)4})} - V_r\bar{p}_2\bar{u}_2^{(n)} - \bar{d}_2\bar{u}_2^{(n)}, \\ \frac{d\bar{u}_3^{(n)}}{d\tau} = \overline{ATM}\frac{\bar{u}_0^{(n)}}{(1+\bar{u}_0^{(n)})} - \bar{k}_{dph}\frac{\bar{u}_3^{(n)}}{(\bar{K}_{dph}+\bar{u}_3^{(n)})} + V_r\bar{p}_3\bar{u}_3^{(c)}, \\ \frac{d\bar{u}_0^{(c)}}{d\tau} = \bar{k}_{tp} - k_{ub}\bar{u}_1^{(c)}(\frac{\bar{u}_0^{(c)}}{K_{ub}+\bar{u}_0^{(c)}}) - \overline{ATM}\frac{\bar{u}_0^{(c)}}{(1+\bar{u}_0^{(c)})} + \bar{k}_{dph}\frac{\bar{u}_3^{(c)}}{(\bar{K}_{dph}+\bar{u}_3^{(c)})} + \bar{p}_0(\bar{u}_0^{(n)} - \bar{u}_0^{(c)}) \\ \qquad\qquad -\bar{d}_0\bar{u}_0^{(c)}, \\ \frac{d\bar{u}_1^{(c)}}{d\tau} = \bar{k}_{tm}\bar{u}_2^{(c)} + \bar{p}_1(\bar{u}_1^{(n)} - \bar{u}_1^{(c)}) - \bar{d}_1\bar{u}_1^{(c)}, \\ \frac{d\bar{u}_2^{(c)}}{d\tau} = -\bar{k}_{tm}\bar{u}_2^{(c)} + \bar{p}_2\bar{u}_2^{(n)} - \bar{d}_2\bar{u}_2^{(c)}, \\ \frac{d\bar{u}_3^{(c)}}{d\tau} = \overline{ATM}\frac{\bar{u}_0^{(c)}}{(1+\bar{u}_0^{(c)})} - \bar{k}_{dph}\frac{\bar{u}_3^{(c)}}{(\bar{K}_{dph}+\bar{u}_3^{(c)})} - \bar{p}_3\bar{u}_3^{(c)}, \end{cases} \tag{5.13}$$

which we will refer to as

$$\frac{d\bar{u}}{dt} = F(\bar{u}), \quad \bar{u} = (\bar{u}_0^{(n)}, \ldots, \bar{u}_3^{(c)}) \in \mathbb{R}^8, \tag{5.14}$$

in the sequel.

Remark. All the simulations of the system have been done using the values of the parameters on column 2 of Table 5.1. Those values have been obtained by numerical data fitting, starting from values found in the biological or modelling literature on p53 [20, 103, 139]. We also found for each parameter a range of values for which the oscillations are present. To do this, we fixed all the parameters, except for one that we varied, to assess the response of the system. These ranges correspond in order of magnitude to the corresponding parameters of many other models [20, 103, 139].

5.2.1 Equilibrium points

Basic definitions

We begin this section by shortly recalling some general notions that will be useful in what follows. Theorems and definitions come from the book by Kuznetsov [67], Françoise [35] or Perko [102]. Let us consider a generic continuous-time dynamical system defined by

$$\dot{x} = f(x), \quad \forall x \in \mathbb{R}^n, \tag{5.15}$$

where f is smooth. Let x_0 be an equilibrium of the system, i.e. $f(x_0) = 0$ and let A denote the Jacobian matrix of f evaluated at x_0. Let n_-, n_0, n_+ be the numbers of eigenvalues of A (counting multiplicities) with negative, zero and positive real part, respectively.

Param.	Description	Chosen Value	Units	Ranges for osc.
k_{dph}	Dephosphorylation velocity	0.1	$\mu M/min$	$0.039 \leq k_{dph} \leq 1.73$
K_{dph}	Michaelis dephosporylation constant	0.05	μM	$0.0001 \leq K_{dph} \leq 2.2$
k_1	Ubiquitination velocity	100	min^{-1}	$30.5 \leq k_1 \leq 4180$
K_1	Michaelis ubiquination constant	1.01	μM	$0.023 \leq K_1 \leq 3.3$
k_3	Phosphorylation velocity	1	min^{-1}	*fixed*
K_{atm}	Michaelis phosphorylation constant	0.1	μM	*fixed*
δ_m	Mdm2 degradation rate	0.16	min^{-1}	$0.03 \leq \delta_m \leq 0.45$
k_{Sm}	basal Mdm2 mRNA transcription rate	0.005	$\mu M/min$	$0 \leq k_{Sm} \leq 0.19$
k_{Sp}	p53-dependent Mdm2 mRNA transcription velocity	1	min^{-1}	*fixed*
K_{Sp}	Michaelis p53-dependent Mdm2 mRNA transcription	0.1	μM	$0.06 \leq K_{Sp} \leq 0.9$
δ_{mRNA}	Mdm2 mRNA degradation rate	0.0001	min^{-1}	$0 \leq \delta_{mRNA} \leq 0.41$
k_S	p53 synthesis rate	0.015	$\mu M/min$	$0.001 \leq k_S \leq 0.02$
δ_{p53}	p53 degradation rate	0.2	min^{-1}	$0 \leq \delta_{p53} \leq 23$
k_{tm}	Mdm2 translation rate	1	min^{-1}	$\forall k_{tm} \geq 0.02$
V_r	Volume ratio	10	adim	$0.8 \leq V_r \leq 24.2$
p_0	$p53$ permeability	0.083	min^{-1}	$p_0 \geq 0$
p_1	Mdm2 permeability	0.04	min^{-1}	$p_1 > 0$
p_2	Mdm2 mRNA permeability	0.083	min^{-1}	$p_2 > 0$
p_3	$p53_p$ permeability	0.083	min^{-1}	$p_3 > 0.01$

Table 5.1: Parameter values for the model 5.10. Starting from values taken from [139, 103] and [20] we numerically obtained by data fitting, a complete set of parameter values that are used in the sequel for the simulations. For instance, in [20], $V_r = 15$, $k_S = 0.0055$ and $k_{Sm} = 0.0015$. Keeping all but one of these parameters fixed at these reference values, and varying the last one, we also calculated ranges of parameters (in projection on each parameter axis) for which sustained oscillations take place. Note that the parameters k_3, K_{atm} and k_{Sp} are presented in this table as *fixed* because they have been fixed to constant values by the change of variables occurring in the nondimensionalisation (see text in Section 5.2).

Definition 5.2.1. *An equilibrium is called* hyperbolic *if $n_0 = 0$, that is, if there are no eigenvalues on the imaginary axis. A hyperbolic equilibrium is called a* hyperbolic saddle *if $n_- n_+ \neq 0$.*

Let us also introduce the two invariant sets:

$$W^s(x_0) = \{x : \phi^t x \to x_0, t \to +\infty\}, \quad W^u(x_0) = \{x : \phi^t x \to x_0, t \to -\infty\},$$

where ϕ^t is the flow associated with 5.15.

Definition 5.2.2. *$W^s(x_0)$ is called the* stable set *of x_0, while $W^u(x_0)$ is called the* unstable set *of x_0.*

Proposition 5.2.1. *Globally the invariant sets W^s and W^u are* immersed *manifolds of dimensions n_- and n_+ , respectively, and have the same smoothness properties af f.*

Having these properties in mind, the sets W^s and W^u are called the stable *and* unstable invariant manifolds*, respectively, of the system at x_0.*

We also state the Hartman-Grobman Theorem:

Theorem 5.2.1. *Let $\mathbf{E}$ be an open subset of $\mathbb{R}^n$ containing the origin, let $f \in C^1(\mathbf{E})$, and let ϕ^t be the flow of system (5.15). Suppose that $f(0) = 0$ and that the matrix $A = Df(0)$ has no eigenvalues with zero real part. Then there exist a homeomorphism H of an open set U containing the origin onto an open set V containing the origin such that for each $\hat{x} \in U$, there is an open interval $\hat{I} \subset \mathbb{R}$ containing zero such that for all $\hat{x} \in U$ and $t \in \hat{I}$*

$$H \circ \phi_t(\hat{x}) = e^{At} H(\hat{x});$$

i.e., H maps trajectories of (5.15) near the origin onto trajectories of the system $\dot{x} = Ax$ near the origin and preserves the parametrization by time.

Otherwise said, the flow ϕ_t is topologically equivalent to (i.e. conjugated through a homeomorphism with) the exponential flow e^{At} of the linearised system in 0. See below definition 5.2.3. For a proof see [53].

Equilibrium points of system (5.13) when $\overline{ATM} = 0$

In healthy cells, p53 is targeted by Mdm2-mediated ubiquitination and it is highly degraded by the cell machinery. The damage sensor ATM is inactive and no oscillations are present, which our model reproduces accurately, as shown below. On the contrary, when a damage to the DNA occurs, conformational transformations of both Mdm2 and p53 release this tight control, a pool of active p53 can accumulate in the nucleus and oscillations start. In system (5.13) we set $p53_p = \bar{u_3}$ as the free and active species and the growth of its concentration is related to the phosphorylation process, exerted by ATM. Thus, if $\overline{ATM} = 0$, i.e. if ATM is inactive, $\bar{u_3}$ tends to zero and no oscillations appear, as is easily seen in system (5.13). Indeed the equations for $\bar{u}_3$ read, when $\overline{ATM} = 0$:

$$\frac{d\bar{u}_3^{(n)}}{d\tau} = -\bar{k}_{dph} \frac{\bar{u}_3^{(n)}}{(\bar{K}_{dph} + \bar{u}_3^{(n)})} + V_r \bar{p}_3 \bar{u}_3^{(c)}, \tag{5.16}$$

$$\frac{d\bar{u}_3^{(c)}}{d\tau} = -\bar{k}_{dph} \frac{\bar{u}_3^{(c)}}{(\bar{K}_{dph} + \bar{u}_3^{(c)})} - \bar{p}_3 \bar{u}_3^{(c)}. \tag{5.17}$$

We remark in equation (5.17) that $u_3^{(c)}$ tends to zero, and, as a consequence, $u_3^{(n)}$ too. Let us set $v_0^{(n)}, \ldots, v_3^{(n)}$ and $v_0^{(c)}, \ldots, v_3^{(c)}$ the values of the equilibrium points for system (5.13). We can calculate explicitly the equilibrium points of system (5.13), when $\overline{ATM} = 0$. Indeed, $v_3^{(n)} = 0$ and $v_3^{(c)} = 0$. Thus, the equation for $\bar{u}_2^{(n)}$ is uncoupled from the others seven and we can calculate the corresponding equilibrium:

$$v_2^{(n)} = \frac{\bar{k}_{pm}}{V_r \bar{p}_2 + \bar{d}_2}. \tag{5.18}$$

Substituting this value in the equation for $\bar{u}_2^{(c)}$ results in:

$$v_2^{(c)} = p_2(\frac{\bar{k}_{pm}}{V_r\bar{p}_2 + \bar{d}_2})\frac{1}{\bar{k}_{tm} + \bar{d}_2}. \tag{5.19}$$

We continue to substitute into the remaining equations, obtaining the values $v_1^{(c)}$ and $v_1^{(n)}$:

$$\begin{aligned} v_1^{(c)} &= \frac{\alpha}{\bar{d}_1 + \bar{p}_1 - \frac{\bar{p}_1^2 V_r}{\bar{d}_1 + \bar{p}_1 V_r}}, \\ v_1^{(n)} &= \frac{\bar{p}_1 V_r}{\bar{d}_1 + \bar{p}_1 V_r}\frac{\alpha}{\bar{d}_1 + \bar{p}_1 - \frac{\bar{p}_1^2 V_r}{\bar{d}_1 + \bar{p}_1 V_r}}, \end{aligned} \tag{5.20}$$

where $\alpha = \bar{p}_2(\frac{\bar{k}_{pm}}{V_r\bar{p}_2+\bar{d}_2})\frac{\bar{k}_{tm}}{\bar{k}_{tm}+\bar{d}_2}$. Notice that the value of $v_1^{(c)}$ and $v_1^{(n)}$ are both positive for any value of the parameters, since $\bar{d}_1 + \bar{p}_1 - \frac{\bar{p}_1^2 V_r}{\bar{d}_1+\bar{p}_1 V_r} \geq 0$, for all $(\bar{p}_1, \bar{d}_1, V_r) \in \mathbb{R}^3_+$. Let us set $\beta := v_1^{(n)}$. Finally we can calculate the values of the equilibria for the equations for $\bar{u}_0^{(c)}$ and $\bar{u}_0^{(n)}$. We set

$$v_0^{(n)} = v_0^{(c)} + \frac{\beta}{\bar{p}_0}\frac{v_0^{(c)}}{K_{ub} + v_0^{(c)}} - \frac{\bar{k}_{tp}}{\bar{p}_0}$$

and we substitute in the equation for $\bar{u}_0^{(c)}$. We obtain an implicit function of $v_0^{(c)}$ given by the following relation:

$$-\beta\frac{v_0^{(c)} + \frac{\beta}{p_0}\frac{v_0^{(c)}}{K_{ub}+v_0^{(c)}} - \frac{k_{tp}}{p_0}}{K_{ub} + v_0^{(c)} + \frac{\beta}{p_0}\frac{v_0^{(c)}}{K_{ub}+v_0^{(c)}} - \frac{k_{tp}}{p_0}} - p_0 V_r(\frac{\beta}{p_0}\frac{v_0^{(c)}}{K_{ub} + v_0^{(c)}} - \frac{k_{tp}}{p_0}) = 0. \tag{5.21}$$

We solve this relation to find two different solutions:

$$\begin{aligned} v_0^{(c),1} &= -\frac{\beta p_0 K_{ub} + 5V_r\beta - \beta k_{tp} + \beta^2 - 5p_0 V_r k_{tp} - \mathbf{A}}{2\beta p_0} \\ v_0^{(c),2} &= -\frac{\beta p_0 K_{ub} + 5V_r\beta - \beta k_{tp} + \beta^2 - 5p_0 V_r k_{tp} + \mathbf{A}}{2\beta p_0} \end{aligned}$$

where $\mathbf{A} = (10\beta^2 p_0^2 K_{ub} V_r + 2\beta^2 p_0 K_{ub} k_{tp} - 20 p_0 V_r \beta^2 k_{tp} - 50 p_0^2 V_r^2 \beta k_{tp} + 10\beta k_{tp}^2 p_0 V_r + 10\beta p_0^2 K_{ub} V_r k_{tp} + \beta^2 k_{tp}^2 - 2\beta^3 k_{tp} + \beta^4 + \beta^2 p_0^2 K_{ub}^2 + 2\beta^3 p_0 K_{ub} + 25 p_0^2 V_r^2 \beta^2 + 10 p_0 V_r \beta^3 + 25 p_0^2 V_r^2 k_{tp}^2)^{1/2}$. Therefore, there are two possible equilibrium states at $\overline{ATM} = 0$.

Using the values of the parameters given in Table 5.1, we calculate, using Maple, the coordinates of the equilibrium values of $v_0^{(c),1,2}$ for $\overline{ATM} = 0$. For the values of parameters chosen, only $v_0^{(c),2}$ is positive, while $v_0^{(c),1}$ is strictly negative. We can thus

calculate (using a built-in function of Matlab that implements a Newton method) or formally (using Maple) the equilibrium point whose coordinates are non-negative:

$$v = [0.2364, 0.0024, 0.0125, 0, 0.3028, 0.0029, 0.0005, 0], \tag{5.22}$$

where $v = [v_0^{(n)}, v_1^{(n)}, \dots v_3^{(c)}]$. This equilibrium point represents the equilibrium concentration of each species when no damage is detected by the cell.

We calculate the Jacobian matrix of system (5.13):

$$J(\bar{u}) = \begin{bmatrix} \frac{-k_{ub}\bar{u}_1^{(n)}K_{ub}}{(K_{ub}+\bar{u}_0^{(n)})^2} - \frac{ATM}{(1+\bar{u}_0^{(n)})^2} - V_r p_0 & -k_{ub}\frac{\bar{u}_0^{(n)}}{(K_{ub}+\bar{u}_0^{(n)})} & 0 & \frac{k_{dph}K_{dph}}{(K_{dph}+\bar{u}_3^{(n)})^2} \\ 0 & -V_r p_1 - d_1 & 0 & 0 \\ 0 & 0 & -V_r p_2 - d_2 & \frac{hk_{Sp}K_{Sp}^h(\bar{u}_3^{h-1})}{(K_{Sp}^h+\bar{u}_3^{(n)h})^2} \\ \frac{\overline{ATM}}{(1+\bar{u}_0^{(n)})^2} & 0 & 0 & -k_{dph}\frac{K_{dph}}{(K_{dph}+\bar{u}_3^{(n)})^2} \\ p_0 & 0 & 0 & 0 \\ 0 & p_1 & 0 & 0 \\ 0 & 0 & p_2 & 0 \\ 0 & 0 & 0 & 0 \end{bmatrix}$$

$$\begin{bmatrix} V_r p_0 & 0 & 0 & 0 \\ 0 & V_r p_1 & 0 & 0 \\ 0 & 0 & 0 & 0 \\ 0 & 0 & 0 & V_r p_3 \\ \frac{-k_{ub}\bar{u}_1^{(c)}K_{ub}}{(K_{ub}+\bar{u}_0^{(c)})^2} - \frac{ATM}{(1+\bar{u}_0^{(c)})^2} - p_0 - d_3 & -\frac{k_{ub}\bar{u}_0^{(c)}}{(K_{ub}+\bar{u}_0^{(c)})} & 0 & \frac{k_{dph}K_{dph}}{(K_{dph}+\bar{u}_3^{(c)})^2} \\ 0 & -p_1 - d_1 & k_{tm} & 0 \\ 0 & 0 & -k_{tm} - d_2 & 0 \\ \frac{ATM}{(1+\bar{u}_0^{(c)})^2} & 0 & 0 & -k_{dph}\frac{K_{dph}}{(K_{dph}+\bar{u}_3^{(c)})^2} - p_3 \end{bmatrix}$$

and we evaluate its eigenvalues at the equilibrium point (5.22). All the eigenvalues of the matrix J, evaluated in v have negative real parts. Therefore the equilibrium point is hyperbolic. Since the vector field relative to system (5.13) is smooth, we can apply the Hartman-Grobman theorem and conclude that v is a stable equilibrium point.

Equilibrium points for $\overline{ATM} > 0$

The nonlinear nature of system (5.13) implies the existence of several equilibrium points, for each value of the parameter $\overline{ATM}$. Using the software Maple, we tried to evaluate formally the expression of those equilibria, but the software was unable to do it. Assigning the value of all but $\overline{ATM}$ of the parameters in Table 5.1, Maple gave as a result a polynomial expression of degree 17, whose coefficients depends on $\overline{ATM}$, unusable to obtain more information about the values of the equilibria.

However, we can state a general results about their nature. Let us remind that $F : \mathbb{R}^8 \to \mathbb{R}^8$ is the vector field associated to system (5.13):

Proposition 5.2.2. *The solutions of $F(\bar{u}) = 0$ depend on the values of the solutions of the following system of three equations:*

$$\begin{cases} -\dfrac{k_{ub}\bar{u}_1^{(n)}\bar{u}_0^{(n)}}{K_{ub}+\bar{u}_0^{(n)}} - \dfrac{\overline{ATM}\bar{u}_0^{(n)}}{1+\bar{u}_0^{(n)}} + \dfrac{\bar{k}_{dph}\bar{u}_3^{(n)}}{\bar{K}_{dph}+\bar{u}_3^{(n)}} - V_r\bar{p}_0\bar{u}_0^{(n)} + V_r\bar{p}_0\bar{u}_0^{(c)} = 0 \\ -V_r\bar{p}_1\bar{u}_1^{(n)} - d_1\bar{u}_1^{(n)} + V_r\bar{p}_1\bar{u}_1^{(c)} = 0 \\ \bar{k}_{sp} - \dfrac{k_{ub}\bar{u}_1^{(c)}\bar{u}_0^{(c)}}{K_{ub}+\bar{u}_0^{(c)}} - \dfrac{\overline{ATM}\bar{u}_0^{(c)}}{1+\bar{u}_0^{(c)}} + \dfrac{\bar{k}_{dph}\bar{u}_3^{(c)}}{\bar{K}_{dph}+\bar{u}_3^{(c)}} + \bar{p}_0\bar{u}_0^{(n)} - \bar{p}_0\bar{u}_0^{(c)} - \bar{d}_0\bar{u}_0^{(c)} = 0 \end{cases} \tag{5.23}$$

in the three unknowns $\bar{u}_0^{(n)}$, $\bar{u}_1^{(n)}$ and $\bar{u}_3^{(n)}$, once the following solutions are made:

$$\begin{aligned} v_2^{(c)} &= v_2^{(n)}\frac{\bar{p}_2}{\bar{k}_{tm}+\bar{d}_2}, \\ v_1^{(c)} &= \frac{\bar{k}_{tm}v_2^{(c)}+\bar{p}_1v_1^{(n)}}{\bar{p_1}+\bar{d}_1}, \\ v_0^{(c)} &:= \frac{\bar{k}_{dph}v_3^{(c)}+\bar{p}_3v_3^{(c)}(\bar{K}_{dph}+v_3^{(c)})}{\overline{ATM}\bar{K}_{dph}+\overline{ATM}v_3^{(c)}-\bar{k}_{dph}v_3^{(c)}-\bar{p}_3v_3^{(c)}(\bar{K}_{dph}+v_3^{(c)})}, \\ v_3^{(c)} &:= \frac{1}{V_r\bar{p}_3}\left(-\overline{ATM}\frac{v_0^{(n)}}{1+v_0^{(n)}}+\frac{\bar{k}_{dph}v_3^{(n)}}{\bar{K}_{dph}+v_3^{(n)}}\right), \\ v_2^{(n)} &:= \frac{1}{V_r\bar{p}_2+\bar{d}_2}\left(k_{pm}+\frac{(v_3^{(n)})^4}{K_{Sp}^4+(v_3^{(n)})^4}\right). \end{aligned}$$

This system has a finite number of solutions.

Proof. Let us set $v = [v_0^{(n)}, v_1^{(n)}, \ldots, v_3^{(c)}]$ a generic equilibrium point of system $F(\bar{u}) = 0$. Using the single equations of the system $F(\bar{u}) = 0$ we can explicit the value of the equilibrium point for $v_2^{(c)}$ as a function of $v_2^{(n)}$:

$$v_2^{(c)} = v_2^{(n)}\frac{\bar{p}_2}{\bar{k}_{tm}+\bar{d}_2};$$

then we write $v_1^{(c)}$ as a function of $v_2^{(c)}$ and $v_1^{(n)}$

$$v_1^{(c)} = \frac{\bar{k}_{tm}v_2^{(c)}+\bar{p}_1v_1^{(n)}}{\bar{p_1}+\bar{d}_1}.$$

In a similar way we write $v_0^{(c)}$ as a function of $v_3^{(c)}$ and $v_3^{(c)}$ as a function of $v_0^{(n)}$ and $v_3^{(n)}$:

$$v_0^{(c)} := \frac{\bar{k}_{dph}v_3^{(c)}+\bar{p}_3v_3^{(c)}(\bar{K}_{dph}+v_3^{(c)})}{\overline{ATM}\bar{K}_{dph}+\overline{ATM}v_3^{(c)}-\bar{k}_{dph}v_3^{(c)}-\bar{p}_3v_3^{(c)}(\bar{K}_{dph}+v_3^{(c)})},$$

$$v_3^{(c)} := \frac{1}{V_r \bar{p}_3} \left(-\overline{ATM} \frac{v_0^{(n)}}{1 + v_0^{(n)}} + \frac{\bar{k}_{dph} v_3^{(n)}}{\bar{K}_{dph} + v_3^{(n)}} \right)$$

and finally:

$$v_2^{(n)} := \frac{1}{V_r \bar{p}_2 + \bar{d}_2} \left(k_{pm} + \frac{(v_3^{(n)})^4}{K_{Sp}^4 + (v_3^{(n)})^4} \right)$$

Thus all the equilibrium points of the nonlinear system $F(\bar{u}) = 0$ depend on the values of $v_0^{(n)}$, $v_1^{(n)}$ and $v_3^{(n)}$. By substituting in $F(\bar{u}) = 0$ all the expressions written above, we obtain system (5.23). □

We verified numerically the existence of at least one positive solution of system (5.23)

Positivity of solutions for $\overline{ATM} > 0$

In the previous subsection we stated a theorem that gives us a general form for the equilibria. However, we cannot write explicitly the values of those equilibria. Therefore, we still need to show the existence of a positive equilibrium for our system, when $\overline{ATM} > 0$. As above, we refer to the values of the equilibrium points as $v = (v_1^{(n)}, v_2^{(n)}, \ldots, v_3^{(c)})$.

Proposition 5.2.3. *The equilibrium values of $\bar{u}_1^{(n)}$, $\bar{u}_2^{(n)}$, $\bar{u}_1^{(c)}$ and $\bar{u}_2^{(c)}$ are positive for all positive values of the parameter $\overline{ATM}$.*

Proof. It is easy to see from the second and seventh equations of system (5.13) that the equilibrium values of $v_1^{(c)}$ and $v_1^{(n)}$ and of $v_2^{(c)}$ and $v_2^{(n)}$ have the same sign. We observe also that the sign of the equilibrium value of $v_2^{(c)}$ is concordant with the sign of $v_1^{(c)}$. Indeed, using the sixth equation of system (5.13) we can write

$$v_2^{(c)} = \frac{1}{\bar{k}_{tm}} \left(\bar{d}_1 + \bar{p}_1 - \frac{V_r \bar{p}_1^2}{V_r \bar{p}_1 + \bar{d}_1} \right) v_1^{(c)},$$

where we have substituted the value for $v_1^{(n)}$ obtained from the second equation of system (5.13), $v_1^{(n)} = \dfrac{V_r \bar{p}_1 v_1^{(c)}}{V_r \bar{p}_1 + \bar{d}_1}$. Therefore, we need to evaluate the positivity of only one of the four equilibria $v_1^{(n),(c)}$ and $v_2^{(n),(c)}$. Using the equation for $\bar{u}_2^{(n)}$, we can write the value of the relative equilibrium point, as a function of $v_3^{(n)}$:

$$v_2^{(n)} = \frac{1}{V_r \bar{p}_2 + \bar{d}_2} \left(\bar{k}_{pm} + \frac{(v_3^{(n)})^4}{\bar{K}_{Sp}^4 + (v_3^{(n)})^4} \right) \geq 0,$$

since we only consider positive values of the parameters. Thus the existence of an equilibrium of system (5.13) implies that the values of $v_1^{(n),(c)}$ and $v_2^{(n),(c)}$ are positive. □

The expression of the equilibrium points, relative to the variables $\bar{u}_0^{(n),(c)}$ and $\bar{u}_3^{(n),(c)}$, are more difficult to be written explicitly, since the corresponding equations are non-linear. For this reason, it is more reasonable to study the evolutionary problem. We state the following proposition:

Proposition 5.2.4. *The positive quadrant is invariant for the flow of system (5.13) if* $\overline{ATM} > 0$.

Proof. Let us suppose, one by one, that the values of the variable $\bar{u}_0^{(n),(c)}$ and $\bar{u}_3^{(n),(c)}$ drop to zero. If $\bar{u_0}^{(n)} = 0$ the values of the corresponding derivative is :

$$\frac{d\bar{u}_0^{(n)}}{d\tau} = \bar{k}_{dph}\frac{\bar{u}_3^{(n)}}{(\bar{K_{dph}} + \bar{u}_3^{(n)})} + V_r\bar{p}_0\bar{u}_0^{(c)} \geq 0,$$

thus the solution $\bar{u}_0^{(n)}$ stays positive. Secondly, we consider the derivative of $\bar{u}_3^{(n)}$. Setting $\bar{u}_3^{(n)} = 0$ we obtain:

$$\frac{d\bar{u}_3^{(n)}}{d\tau} = \overline{ATM}\frac{\bar{u}_0^{(n)}}{(1 + \bar{u}_0^{(n)})} + V_r\bar{p}_3\bar{u}_3^{(c)} \geq 0,$$

which is positive. In the same way, the derivatives of the equations for $\bar{u_0}^{(c)}$ and $\bar{u}_3^{(c)}$ are positive when (respectively) $\bar{u}_{0,3}^{(c)} = 0$:

$$\frac{d\bar{u}_0^{(c)}}{d\tau} = \bar{k}_{tp} + \bar{k}_{dph}\frac{\bar{u}_3^{(c)}}{(\bar{K}_{dph} + \bar{u}_3^{(c)})} + \bar{p}_0\bar{u}_0^{(n)} \geq 0,$$

and

$$\frac{d\bar{u}_3^{(c)}}{d\tau} = \overline{ATM}\frac{\bar{u}_0^{(c)}}{(1 + \bar{u}_0^{(c)})} \geq 0$$

It is easy to verify the same property for each variable of the system. Therefore we can conclude that, for every value of the parameter $\overline{ATM} > 0$, if the initial value of system (5.13) is positive, meaning that each component of the vector of initial values is positive, then the solution will remain positive . □

5.2.2 Basis of Bifurcation analysis

In this section we detail a numerical bifurcation study of system (5.13). Let us introduce some preliminary definitions. What follows comes from the book by Kuznetsov [67]. We consider a dynamical system that depends on a parameter:

$$\dot{x} = f(x, \alpha), \quad x \in \mathbb{R}^n \text{ and } \alpha \in \mathbb{R}^m, \tag{5.24}$$

where x represents the variable while α is the parameter. If the parameters vary the phase portrait varies, too. Upon these variations, the system could remain topologically equivalent to the original one, or its topology could change.

Example 5.2.1. *Consider the two dimensional differential system*

$$\begin{cases} \dot{x_1} = \alpha x_1 - x_2 - x_1(x_1^2 + x_2^2), \\ \dot{x_2} = x_1 - \alpha x_2 - x_2(x_1^2 + x_2^2), \end{cases} \tag{5.25}$$

that in polar coordinates takes the form:

$$\begin{cases} \dot{\rho} = \rho(\alpha - \rho^2), \\ \dot{\theta} = 1, \end{cases} \tag{5.26}$$

The origin of the phase portrait is, $\forall \alpha$, the unique equilibrium point of (5.25). For $\alpha \leq 0$ the equilibrium is stable since $\dot{\rho} < 0$ and $\rho(t) \to 0$ if we start from any initial point. For $\alpha > 0$ we have $\dot{\rho} > 0$ for $\rho < \sqrt{\alpha}$ and $\dot{\rho} < 0$ if $\rho > \sqrt{\alpha}$. Moreover the system has a periodic orbit for any $\alpha > 0$ of radius $\sqrt{\alpha}$ and this orbit is stable. Therefore, $\alpha = 0$ is a bifurcation parameter value. The phase portrait changes: it has a stable equilibrium for $\alpha \leq 0$ that becomes unstable for $\alpha > 0$ while a stable periodic orbit appears. This type of bifurcation is called an Andronov-Hopf bifurcation*, or simply a* Hopf bifurcation *[67].*

In order to classify different types of bifurcations and to combine dynamical systems that can be considered qualitatively similar, some definitions are needed.

Definition 5.2.3. *Two systems of the form (5.24) are called* locally topologically equivalent *near the origin, if there exist a map $(x, \alpha) \mapsto (h_\alpha, p(\alpha))$, defined in a small neighbourhood of $(x, \alpha) = (0, 0)$ in the direct product $\mathbb{R}^n \times \mathbb{R}^m$ and such that*

1. *$p : \mathbb{R}^m \to \mathbb{R}^m$ is a homeomorphism defined in a small neighbourhood of $\alpha = 0$, $p(0) = 0$;*

2. *$h_\alpha : \mathbb{R}^n \to \mathbb{R}^n$ is a parameter-dependent homeomorphism defined in a small neighbourhood U_α of $x = 0$, $h_0(0) = 0$, and mapping orbits of the first system in U_α onto orbits of the second system in $h_\alpha(U_\alpha)$, preserving the direction of time.*

An important issue in bifurcation theory is the classification of all possible bifurcation scenarios of generic systems. For local bifurcation of equilibria, universal bifurcation diagrams are provided by *topological normal forms*. Consider a simple system, polynomial in ξ_i

$$\dot{\xi} = g(\xi, \beta; \sigma), \quad \xi \in \mathbb{R}^n, \beta \in \mathbb{R}^k, \sigma \in \mathbb{R}^l, \tag{5.27}$$

which has at $\beta = 0$ an equilibrium $\xi = 0$ satisfying k bifurcation conditions determining a codim k bifurcation of this equilibrium. Here σ is a vector of the coefficients σ_i, $I = 1, 2, \ldots, l$, of the polynomials involved in (5.27). Together with system (5.27), let us consider a system

$$\dot{x} = f(x, \alpha), \quad x \in \mathbb{R}^n, \alpha \in \mathbb{R}^k, \tag{5.28}$$

having at $\alpha = 0$ an equilibrium $x = 0$.

Definition 5.2.4. *System (5.27) is called a* topological normal form *for the bifurcation if any generic system (5.28) with the equilibrium $x = 0$ satisfying the same bifurcation conditions at $\alpha = 0$ is locally topologically equivalent near the origin to (5.27) for some values of the coefficients σ_i.*

By *generic* system we intend a system that satisfies a finite number of *genericity conditions*. These conditions have the form of nonequalities:

$$N_i[f] \neq 0, \qquad i = 1, \ldots, s,$$

where each N_i is some algebraic function of certain partial derivatives of $f(x, \alpha)$ with respect to x and α evaluated at $(x, \alpha) = (0, 0)$. Actually, the value of σ is determined by the values of N_i, $i = 1, \ldots, s$. Two types of conditions exist: the *nondegeneracy conditions*, expressed in terms of partial derivatives of $f(x, 0)$, and the *transversality conditions*, in which the derivatives of $f(x, \alpha)$ with respect to α are involved. All these conditions take the form of nonequalities. The role of these two types of conditions is different. The nondegeneracy conditions guarantee that the critical equilibrium is not too degenerate, while the transversality conditions assure that the parameters 'unfold' this singularity in a generic way. We will give now the topological normal form of any generic two dimensional system undergoing a Hopf bifurcation, since it is the bifurcation we will encounter for system (5.13). These results can be applied also to systems having a dimension > 2.

Theorem 5.2.2. *Consider a two dimensional system*

$$\frac{dx}{dt} = f(x, \alpha), \quad x \in \mathbb{R}^2, \alpha \in \mathbb{R} \tag{5.29}$$

with f smooth, and assume that if $|\alpha|$ is sufficiently small, the point $x = 0$ is an equilibrium with eigenvalues

$$\lambda_{1,2}(\alpha) = \mu(\alpha) \pm i\omega(\alpha),$$

where $\mu(0) = 0$, $\omega(0) = \omega_0 > 0$.

Let the following conditions be satisfied:

1. *$l_1(0) \neq 0$, where l_1 is the first Lyapunov coefficient (*nondegeneracy*);*

2. *$\mu'(0) \neq 0$ (*transversality*).*

Then, system (5.29) is topologically equivalent near the origin to one of the following normal forms:

$$\begin{pmatrix} \dot{y_1} \\ \dot{y_2} \end{pmatrix} = \begin{pmatrix} \beta & -1 \\ 1 & \beta \end{pmatrix} \begin{pmatrix} y_1 \\ y_2 \end{pmatrix} \pm (y_1^2 + y_2^2) \begin{pmatrix} y_1 \\ y_2 \end{pmatrix}. \tag{5.30}$$

where $\beta = \beta(\alpha) = \dfrac{\mu(\alpha)}{\omega(\alpha)}$.

Remarks. The first Lyapunov coefficient l_1 is a real function that is expressed by a certain combination of Taylor coefficients of the right-hand sides of the system. Furthermore, the sign before the cubic part of (5.30) is given by the sign of l_1 and determines the nature of the Hopf bifurcation. If $l_1(0) < 0$, the bifurcation is *supercritical*. In this case a stable equilibrium point becomes unstable after the bifurcation, and a stable periodic orbit, surrounding the equilibrium point, appears. Otherwise the bifurcation is *subcritical*: a stable equilibrium is surrounded by an *unstable* limit cycle that shrinks as α goes towards zero. When $\alpha = 0$ the equilibrium becomes unstable and remain unstable for $\alpha > 0$. The limit cycle disappears when α crosses 0 from negative to positive values.

Let us now give an analytical expression of the first Lyapunov coefficient for the general case of systems of n variables undergoing a Hopf bifurcation. In order to do this, let us introduce some notations. Consider a system $\dot{x} = f(x)$, with $x \in \mathbb{R}^n$, f sufficiently smooth and $f(0) = 0$. Suppose it can be written in the form:

$$\dot{x} = Ax + F(x), \quad x \in \mathbb{R}^n, \tag{5.31}$$

where $F(x) = O(||x||^2)$ is a smooth function. Let us write its Taylor expansion near $x = 0$ as

$$F(x) = \frac{1}{2}B(x,x) + \frac{1}{6}C(x,x,x) + O(||x||^4), \tag{5.32}$$

where $B(x,y)$ and $C(x,y,z)$ are multilinear functions:

$$B_i(x,y) = \sum_{j,k=1}^{n} \frac{\partial^2 F_i(\xi)}{\partial\xi_j\partial\xi_k}\Big|_{\xi=0} x_i y_k, \qquad i = 1,\dots,n,$$

the Hessian form, and

$$C_i(x,y,z) = \sum_{j,k,l=1}^{n} \frac{\partial^3 F_i(\xi)}{\partial\xi_j\partial\xi_k\partial\xi_l}\Big|_{\xi=0} x_j y_k z_l, \qquad i = 1,\dots,n,$$

the third derivative of F. Suppose that A has a simple pair of complex eigenvalues on the imaginary axis, $\lambda_{1,2} = \pm i\omega_0$, $\omega_0 > 0$, and these eigenvalues are the only eigenvalues with $\mathrm{Re}\lambda = 0$. Let $q \in \mathbb{C}^n$ be a complex eigenvector corresponding to λ_1 and consider also the adjoint eigenvector $p \in \mathbb{C}^n$ having the properties

$$A^T p = -i\omega_0 p,\ A^T \bar{p} = i\omega_0 \bar{p},$$

and satisfying the normalization condition

$$\langle p, q\rangle = 1,$$

where $\langle p, q\rangle = \sum_{i=1}^{n} \bar{p}_i q_i$ is the standard Hermitian product in $\mathbb{C}^n$.

Then, it can be proved [67] that the expression of the first Lyapunov coefficient is given by the formula:

$$l_1(0) = \frac{1}{2\omega_0^2}\mathrm{Re}\left[\langle p, C(q,q,\bar{q})\rangle - 2\langle p, B(q, A^{-1}B(q,\bar{q},\bar{q}))\rangle \right. \\ \left. + \langle p, B(\bar{q}, (2i\omega_0 I_n - A)^{-1}B(q,q))\rangle\right] \tag{5.33}$$

where I_n is the identity matrix in $\mathbb{R}^n$. In order to calculate this coefficient numerically, we will use an algorithm, detailed in [67], that we report in the Appendix of this Chapter.

5.2.3 Bifurcations of system (5.13) with respect to changes on the parameter $\overline{ATM}$

System (5.13) depends over more than one parameter. In the remainder of this chapter, we analyse numerically the bifurcation scenarios studying the behaviour of the system with respect to the variations of several parameters. The first, and more important one, is $\overline{ATM}$, because it represents the sensor of DNA damage and activates p53 in our system. Indeed our model writes:

$$[p53] \overset{ATM}{\longrightarrow} [p53_p],$$

where $p53_p$ stands for the active form of p53 and it is supposed to be able to transcribe Mdm2.

Let us rewrite system (5.13) in a different way, to make explicit the dependence on $\overline{ATM}$:

$$\frac{d\bar{u}}{dt} = G(\bar{u}, \overline{ATM}), \quad \bar{u} \in \mathbb{R}^8, \ \overline{ATM} \in \mathbb{R}, \tag{5.34}$$

where $G : \mathbb{R}^9 \to \mathbb{R}^8$. As detailed in section 5.2.1, at $\overline{ATM} = 0$, system (5.13) has a *hyperbolic* equilibrium point v, whose components, strictly positive, are given in formula (5.22). Starting from this equilibrium point, we determined numerically the *equilibrium curve* of (5.34), using a classical continuation method [67]. This curve, defined by the nonlinear system

$$G(y) = 0, \quad y = (\bar{u}, \overline{ATM}), \tag{5.35}$$

exists, since the rank of the Jacobian matrix of (5.35), $J_G = G_y$, evaluated in $y = (v, 0)$ is equal to 8 and we can apply the Implicit Function Theorem. The equilibrium curve lays in $\mathbb{R}^9$ and depends on the parameter $\overline{ATM}$.

The equilibrium points corresponding to the values of $\overline{ATM} < 1.4$ are hyperbolic. Indeed, we evaluated, at each computed equilibrium point, the Jacobian matrix of system (5.13) and its relative eigenvalues, whose real parts are strictly negative [102]. Furthermore, there exist a couple of complex conjugate eigenvalues of our system. Denote by

$$\lambda_{1,2}(\overline{ATM}) = \mu(\overline{ATM}) \pm i\omega(\overline{ATM}),$$

these eigenvalues. What follows is the result of numerical simulations. At $\overline{ATM} \sim 1.4$, $\mu(1.4)$ drops to zero while $\omega(1.4) = \omega_0 > 0$: the system exhibits a *supercritical Hopf*

bifurcation. The real part of the eigenvalues $\mu(\overline{ATM})$ crosses the imaginary axis with a nonzero velocity, as it can been clearly seen in Figure 5.3 and verified numerically by an approximation of $\mu'(\overline{ATM})$. Using the algorithm detailed in Appendix 5.4, we evaluated the first Lyapunov coefficient finding $l_1(1.4) < 0$. Thus all the genericity conditions given in theorem 5.2.2 are satisfied and a unique attractive limit cycle appears under variations of $\overline{ATM}$. At $\overline{ATM} \sim 97.5$ a second supercritical Hopf bifurcation occurs. For higher

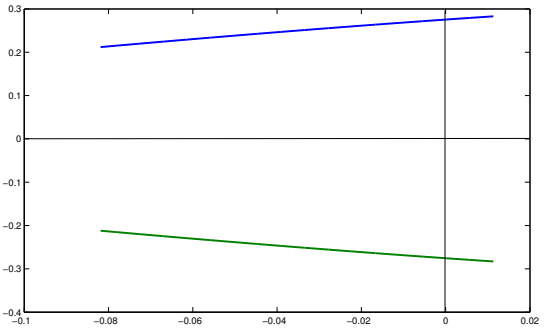

Figure 5.3: $\overline{ATM} = [1, 2]$. The two conjugate eigenvalues $\lambda_{1,2}$ in the complex plane.

values of $\overline{ATM}$ the real part of the eigenvalues $\lambda_{1,2}$ decreases towards zero. It crosses again the imaginary axis at $\overline{ATM} \sim 97.5$ with $l_1(97.5) < 0$. For $\overline{ATM} > 97.5$ the equilibrium points are stable again.

In Figure 5.4 we represent the bifurcation diagram of $\bar{u}_3^{(n)}$ and $\bar{u}_1^{(n)}$. The dotted curves stand for the value of the unstable equilibrium for each of the variables. The +-marked curves represent the amplitude of oscillations that, as we can observe, varies slightly. In order to calculate the period of each limit cycle, we counted the number of local maxima of each computed numerical solution, at different values of $\overline{ATM}$. Once fixed the time interval of the simulations, the number of local maxima corresponds to the number of peaks of the solution and we were able to evaluate an approximation of the period of oscillations. Figure 5.5 shows the (integer) number of peaks corresponding to solutions at different values of $\overline{ATM}$. In our simulations, the period of oscillations varies slightly, between 25 and 33 min, for values of $\overline{ATM} \in [1.4, 97.5]$. The amplitude of oscillations can be very small, for $\overline{ATM}$ next to the bifurcation values, or be significantly wider depending on the bifurcation parameter value, as figure 5.4 shows. This observation is consistent with biological experiments which show that for low and high values of damage, the period of oscillations is roughly the same. On the other hand, the amplitude of oscillations is more changeable [40]. The characteristic period of these numerical simulations is shorter than the experimental one which is around $\sim 4 - 5h$ [40]. However, the exact values of the parameters used here and collected in Table 5.1) are not easy to be determined physiologically, and we will perform such physiological interpretation only in the PDE case with the introduction of space coordinates.

In Figure 5.6(a) we draw the temporal evolution of the nuclear concentrations of phosphorylated p53 and Mdm2 (respectively $\bar{u_3}^{(n)}$ and $\bar{u_1}^{(n)}$). We can observe sustained

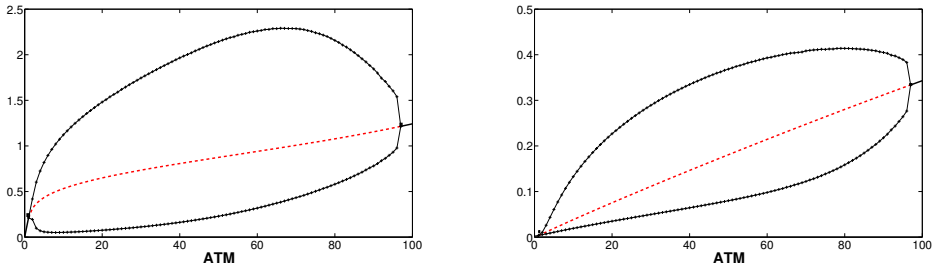

(a) Bifurcation diagram of $u_3^{(n)}$ (b) Bifurcation diagram of $u_1^{(n)}$

Figure 5.4: Bifurcation diagrams (ODE system) for nuclear $p53_p$ and nuclear $Mmd2$. The equilibrium of the system is stable for values of $\overline{ATM}$ lower than a threshold ($\overline{ATM} \sim 1.4$), then a supercritical Hopf bifurcations occurring, it becomes unstable and a limit cycle appears. The dotted curve represents the branch with unstable equilibrium and the $+$ marked curves represent the minimum and maximum values of the oscillations. When $\overline{ATM}$ becomes higher then at a second threshold the equilibrium becomes stable again through a second supercritical Hopf bifurcation ($\overline{ATM} \sim 97.5$).

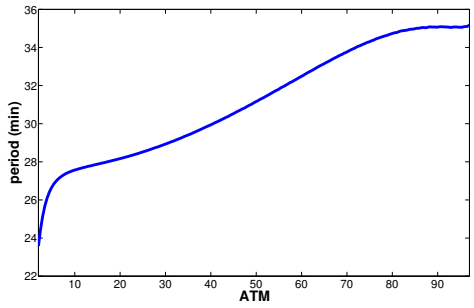

Figure 5.5: Period (in minutes) of p53 oscillations as function of $\overline{ATM}$

oscillations of their concentrations. In 5.6(b) we show the phase plane relative to the same simulation, where we can observe the corresponding limit cycle in the $(\bar{u_3}^{(n)}, \bar{u_1}^{(n)})$ plane (respectively nuclear $p53_p$ and $Mdm2$).

In conclusion, we found that for all values of $\overline{ATM}$ in the interval [1.4, 97.5], the equilibrium point of system (5.13) is unstable and a stable limit cycle exist. Thus, in this range of values for the parameter $\overline{ATM}$, the system oscillates and reproduces the observed biological behaviour. As proposed in [78], our results can be interpreted as follows. If the damage is too low, the cell does not need to activate the p53 pathway in order to repair. When the damage is high enough, the p53 pathway needs to be launched and the oscillations begin. On the contrary, if the damage is too big, the cell does not start repair processes, but directly launches apoptosis. Furthermore, the period of oscillations does not change significantly with the damage ($\sim$ 30 min), reproducing once again the behaviour observed experimentally.

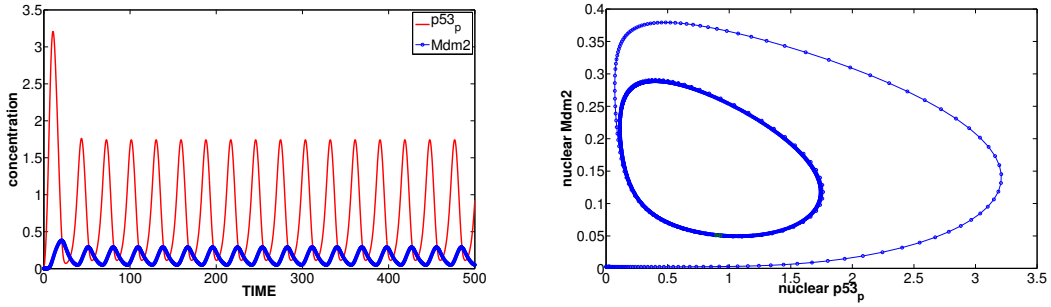

(a) (b)

Figure 5.6: ODE Model. Simulations results. (a): Evolution of nuclear concentrations of $Mmd2$ and $p53_p$ for $\overline{ATM} = 30$, a value in the range [1.4, 97.5], giving rise to sustained oscillations) . (b): Phase plane relative to the variable $\bar{u_1}^{(n)}$ and $\bar{u_3}^{(n)}$ (nuclear $Mmd2$ and nuclear $p53_p$). The orbit of the solution tends towards a stable limit cycle.

5.2.4 Bifurcations with respect to degradation values with fixed $\overline{ATM}$

The values of degradation parameters have been shown to be determinant in other works about p53. For example Ciliberto *et al.* [20] (but see also [40]) use the degradation rate of Mdm2 as a bifurcation parameter and observe the appearance of oscillations in the p53-Mdm2 system, over variations of this parameter. Thus we changed, one by one, the degradation rates of each species and we observed how the behaviour of the system is affected. We set $\overline{ATM} = 3$ in such a way that a limit cycle exist for the values of parameters fixed in Table 5.1.

If we analyse the system over different values of $\bar{d_1}$, the Mdm2 degradation rate, we obtain, as in the ATM case, two supercritical Hopf bifurcation. But the system looses its stability after the second bifurcation. The first supercritical Hopf bifurcation occurs at $\bar{d_1} \sim 0.03$ and the second one at $\bar{d_1} \sim 0.43$. If the parameter goes over the threshold of ~ 0.8 the system looses stability. In particular, $\bar{u_3}^{(n)}$ tends to $+\infty$. See figure 5.7.

We notice that the system oscillates for very low values of the mRNA degradation constant $\bar{d_2} \sim 0$. The system exhibits a supercritical Hopf bifurcation at $\bar{d_2} \sim 0.41$ after which the equilibrium point is stable. The equilibrium is stable for $0.41 < \bar{d_2} < 0.85$. Then the system looses stability and the solution for u_3 tends to $+\infty$ for high values of the parameter $\bar{d_2}$. We conclude that, if the degradation rate of Mdm2 or mRNA is too high, p53 degradation by ubiquitination is not controlled and the system does not reproduce any biologically observed data.

Over changes on the $\bar{u}_0$ degradation rate, namely $\bar{d_3}$ we do not see significant variation of the system. A stable limit cycle exists $\forall \bar{d_3} \in [0\,, 21]$. No changes at all in period and a smooth change in amplitude of oscillations is observed, as it can be seen in Figure 5.8.

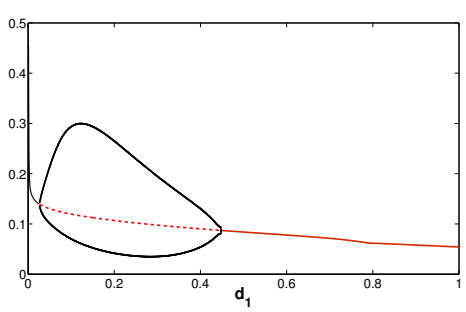

(a) bifurcation relative to the Mdm2 degradation rate

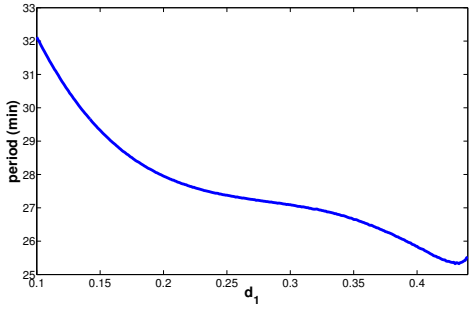

(b) period relative to the Mdm2 degradation rate

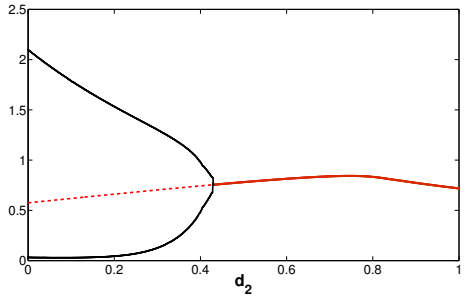

(c) bifurcation relative to the mRNA degradation rate

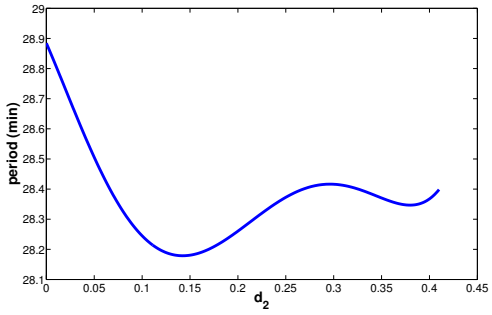

(d) period relative to the mRNA degradation rate

Figure 5.7: (a) Bifurcation diagram for $u_1^{(n)}$. Two supercritical Hopf bifurcations at $\bar{d_1} = 0.03$ and $\bar{d_1} = 0.43$, the Mdm2 degradation rate. A stable limit cycle exists for $0.03 < \bar{d_1} < 0.43$. (b) Period of the oscillations, in minutes. (c): Bifurcation diagram for $u_2^{(n)}$. A supercritical Hopf Bifurcation occurs: a stable limit cycle exist for $\bar{d_2} < 0.41$, the Mdm2 mRNA degradation rate. The red dotted curve is the unstable equilibrium for $u_2^{(n)}$. (d) Period of the oscillations as a function of $\bar{d_2}$.

5.2.5 p53 degraded in both compartments

As reported in [82] p53 degradation is more efficient in the cytoplasm. Other works, however, see [141], prove that p53 can be degraded in the nucleus. In our model we added a degradation term *only* in the cytoplasmic compartment. In order to test whether this assumption was not too strong, we added a nuclear degradation term for p53. In system (5.13) only the equation for $u_0^{(n)}$ changes and reads:

$$\frac{d\bar{u}_0^{(n)}}{d\tau} = -k_{ub}\bar{u}_1^{(n)}\frac{\bar{u}_0^{(n)}}{(K_{ub}+\bar{u}_0^{(n)})} - \overline{ATM}\frac{\bar{u}_0^{(n)}}{(1+\bar{u}_0^{(n)})} + \bar{k}_{dph}\frac{\bar{u}_3^{(n)}}{(\bar{K}_{dph}+\bar{u}_3^{(n)})} - V_r\bar{p}_0(\bar{u}_0^{(n)} - \bar{u}_0^{(c)}) - \bar{d}_0\bar{u}_0^{(n)}$$

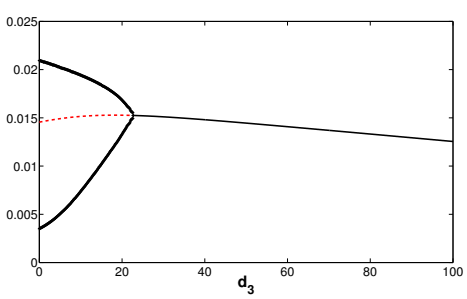

(a) bifurcation for p53 degradation rate

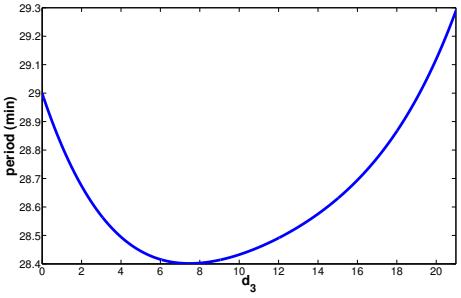

(b) period for p53 degradation rate

Figure 5.8: (a): Bifurcation diagram for $\bar{u}_0^{(n)}$. A supercritrical Hopf bifurcation occurs: a stable limit cycle exist for $\bar{d}_3 < 21$, the p53 degradation rate. The red dotted curve is the unstable equilibrium for $\bar{u}_0^{(c)}$. The black curve is the stable equilibrium and black $+$ are the maxima and minima of oscillations for $\bar{u}_0^{(c)}$. (b): Period of the oscillations, expressed as a function of $\bar{d}_3$. The period is given in minutes.

We calculated the bifurcation diagram as a function of $\overline{ATM}$ and we observed that there are no significant differences with the response of our original system. Thus we confirmed that our assumption was reasonable. We found again two supercritical Hopf bifurcations. The bifurcation points have smoothly moved: we have a first supercritical Hopf bifurcation for $\overline{ATM} \sim 1.93$ while in the first case the bifurcation value was $\overline{ATM} \sim 1.4$. The second Hopf supercritical bifurcation is at $\overline{ATM} \sim 98.5$ while in the previous case the second point was at $\overline{ATM} \sim 97.5$, see Figure 5.9.

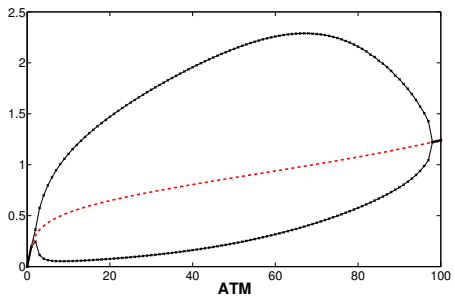

(a) bifurcation relative to $\overline{ATM}$

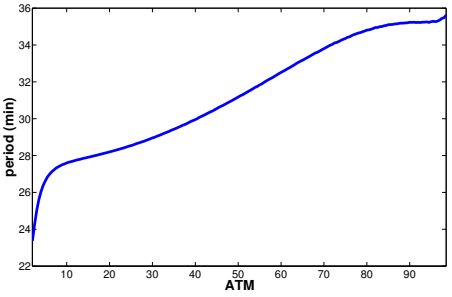

(b) period relative to $\overline{ATM}$

Figure 5.9: System with symmetrical degradation. Similarly to figure 5.5 we plotted the bifurcation diagram of $\bar{u}_3^{(n)}$ (a), and the period (in minutes) of the corresponding oscillations (b). Compare (a) with Figure 5.4(a) and (b) with Figure 5.5.

We also calculated the bifurcation diagrams over the degradation rate of each variable. We observe the same behaviour as in the original system (5.13). Only the bifurcation

relative to $\bar{d}_3$ differs from previous scenario: the bifurcation point in this second scenario is $\bar{d}_3 \sim 8$ instead of $\bar{d}_3 \sim 21$ (point which corresponds to the case when the degradation of u_0 is allowed exclusively in the cytoplasmic compartment). The relative bifurcation diagrams are plotted in Figure 5.10.

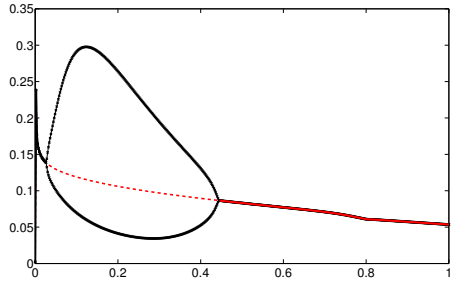

(a) Mdm2 degradation rate

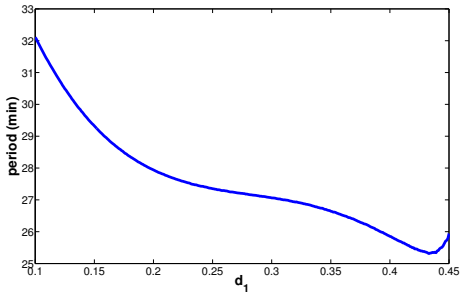

(b)

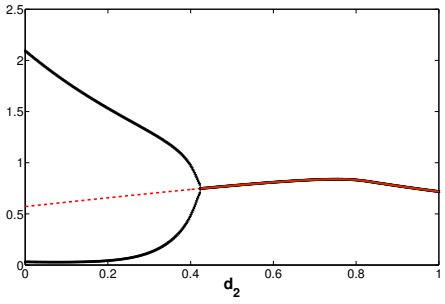

(c) mRNA degradation rate

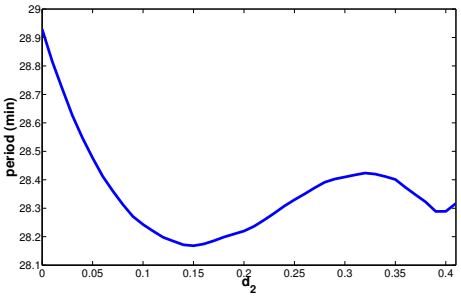

(d)

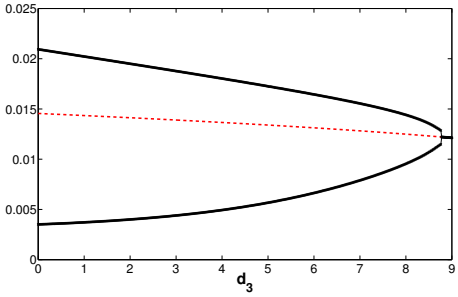

(e) p53 degradation rate

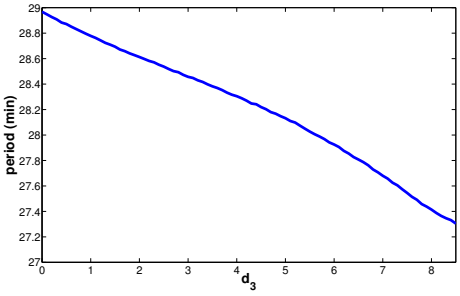

(f)

Figure 5.10: Bifurcation diagrams of $\bar{u_0}^{(n)}, \bar{u_1}^{(n)}, \bar{u_2}^{(n)}$ in the case of $\bar{u_0}$ nuclear and cytoplasmic degradation. (a): $\bar{u_1}^{(n)}$ bifurcation diagram over $\bar{d}_1$. (b): period of the oscillations as a function of $\bar{d}_1$, expressed in minutes. (c): $\bar{u_2}^{(n)}$ bifurcation diagram over d_2 and (d) period of the oscillations as a function of $\bar{d}_2$, expressed in minutes. In both cases for values of $\bar{d}_1$ and $\bar{d}_2$ bigger then ~ 0.6 the system loose equilibrium as in system (5.13). (e), (f): $\bar{u_0}^{(n)}$ bifurcation diagram over $\bar{d}_3$ and period of the oscillations.

5.3 Physiological interpretation of the rise of oscillations

What is the physiological explanation of the rise of oscillations? Is it possible to identify a physiological quantity that induces the start of oscillations? Here we show that oscillations are linked to the ratio of concentrations of p53 in its active and inactive state. We prove, on a simplified version of our system, that there is threshold value $\sigma > 0$, to be determined, such that, if

$$\frac{[p53_p]}{[p53]} > \sigma,$$

the system is in the oscillatory regime. Let us recall that $v = [v_0^{(n)}, \ldots, v_0^{(c)}, \ldots, v_3^{(c)}]$ stands for a general equilibrium point of system (5.13). Define the function $\phi_p : \mathbb{R} \to \mathbb{R}$,

$$\phi_p(\overline{ATM}) = \frac{v_3^{(n)} + v_3^{(c)}}{v_0^{(n)} + v_0^{(c)}},$$

that associate to $\overline{ATM}$ the ratio of the sum of the equilibrium values of $p53$ (nuclear and cytoplasmic) and $p53_p$, respectively. This function is well defined for all positive values of $\overline{ATM}$, since $v_0^{(n)} + v_0^{(c)} > 0$ as we have shown by the numerical computation of the equilibria done in the previous section, see Figure 5.11.

Proposition 5.3.1. *Assume that the function ϕ_p is strictly increasing. If system (5.13) is in its oscillatory regime for a fixed value of the parameter $\overline{ATM}$, then $\phi_p(\overline{ATM}) > \sigma$ where $\sigma = \phi_p(\overline{ATM}_0)$ and $\overline{ATM}_0$ is the bifurcation parameter value.*

Proof. If for a fixed $\overline{ATM}$, the system is in its oscillatory regime then $\phi_p(\overline{ATM}) > \phi_p(\overline{ATM}_0)$, i.e. $\phi_p(\overline{ATM}) > \sigma$, since ϕ_p is supposed to be strictly increasing. □

In order to apply Proposition 5.3.1 we have to show that ϕ_p is an increasing function of $\overline{ATM}$. Therefore, we need to write explicitly the equilibrium values corresponding to nuclear and cytoplasmic $p53$ and $p53_p$, as functions of $\overline{ATM}$. Let us rewrite system (5.13) in its compact formulation:

$$\frac{d\bar{u}}{dt} = F(\bar{u}), \quad \bar{u} = (\bar{u}_0^{(n)}, \ldots, \bar{u}_3^{(c)}) \in \mathbb{R}^8. \tag{5.36}$$

The problem is to evaluate the equilibrium values of system (5.14), namely the solutions $\bar{u}$ of the system of equations:

$$F(\bar{u}) = 0. \tag{5.37}$$

As we are interested in the values of $v_0^{(n)}, v_0^{(c)}, v_3^{(n)}, v_3^{(c)}$, we substitute in (5.37) the fol-

lowing expressions for $v_1^{(n)}, v_1^{(c)}, v_2^{(n)}, v_2^{(c)}$:

$$v_1^{(n)} = \frac{V_r \bar{p}_1 u_1^{(c)}}{\bar{d}_1 + V_r \bar{p}_1}, \quad v_1^{(c)} = \frac{\bar{k}_{tm}(\bar{d}_1 + V_r \bar{p}_1)}{\bar{d}_1(\bar{d}_1 + \bar{p}_1 + V_r \bar{p}_1)} v_2^{(c)},$$

$$v_2^{(n)} = \frac{1}{\bar{d}_2 + V_r \bar{p}_2} \left(\bar{k}_{pm} + \frac{(v_3^{(n)})^4}{\bar{K}_{Sp}^4 + (v_3^{(n)})^4} \right), \quad v_2^{(c)} = v_2^{(n)} \frac{\bar{p}_2}{\bar{k}_{tm} + \bar{d}_2},$$

obtained using system (5.37). Using the values of the parameters given in Table 5.1, we can write the following system of four equations:

$$\begin{cases} -\dfrac{\left(2.4 + \frac{483.5(v_3^{(n)})^4}{1+(v_3^{(n)})^4}\right) u_0^{(n)}}{10.1 + u_0^{(n)}} - \dfrac{\overline{ATM} u_0^{(n)}}{1 + u_0^{(n)}} + \dfrac{v_3^{(n)}}{0.5 + v_3^{(n)}} - 0.833 u_0^{(n)} + 0.833 u_0^{(c)} = 0, \\ \dfrac{\overline{ATM} u_0^{(n)}}{1 + u_0^{(n)}} - \dfrac{v_3^{(n)}}{0.5 + v_3^{(n)}} + 0.833 v_3^{(c)} = 0, \\ 0.15 - \dfrac{\left(2.9 + \frac{576.4(v_3^{(n)})^4}{1+(v_3^{(n)})^4}\right) u_0^{(c)}}{10.1 + u_0^{(c)}} - \dfrac{\overline{ATM} u_0^{(c)}}{1 + u_0^{(c)}} + \dfrac{v_3^{(c)}}{0.5 + v_3^{(c)}} + 0.0833 u_0^{(n)} - 0.0833 u_0^{(c)} = 0, \\ \dfrac{\overline{ATM} u_0^{(c)}}{1 + u_0^{(c)}} - \dfrac{v_3^{(c)}}{0.5 + v_3^{(c)}} - 0.0833 v_3^{(c)} = 0. \end{cases} \tag{5.38}$$

As already discussed in Section 5.2.1, the equilibria of system (5.13) and equivalently those of system 5.38 are hard to write in an explicit form. Using the software *Maple*, that allows formal computations, we obtain implicit expressions of the roots of system (5.38), not useful to further analysis. Since for low values of $\overline{ATM}$, the values of the equilibria v_0 and v_3, computed numerically, are 'small' and included in the interval [0, 0.3] (see Figure 5.11(a) and 5.11(c)), we linearize the system around $v_0, v_3 = 0$, and we obtain the simplified system:

$$\begin{cases} -0.24 u_0^{(n)} - \overline{ATM} u_0^{(n)} + 2 v_3^{(n)} - 0.833 u_0^{(n)} + 0.833 u_0^{(c)} = 0, \\ \overline{ATM} u_0^{(n)} - 2 v_3^{(n)} + 0.833 v_3^{(c)} = 0, \\ 0.15 - 0.28 u_0^{(c)} - \overline{ATM} u_0^{(c)} + 2 v_3^{(c)} + 0.0833 u_0^{(n)} - 0.0833 u_0^{(c)} = 0, \\ \overline{ATM} u_0^{(c)} - 2 v_3^{(c)} - 0.0833 v_3^{(c)} = 0. \end{cases} \tag{5.39}$$

This system being linear, it is easy to solve and solutions can be written explicitly:

$$\begin{aligned} v_0^{(n)} &= \frac{17.85(\overline{ATM}+2.0833)}{2.85\overline{ATM}+160}, \\ v_0^{(c)} &= \frac{47.8}{2.85\overline{ATM}+160}, \\ v_3^{(n)} &= \frac{8.9\overline{ATM}(\overline{ATM}+3.15)}{2.85\overline{ATM}+160}, \\ v_3^{(c)} &= \frac{23\overline{ATM}}{2.85\overline{ATM}+160}. \end{aligned} \tag{5.40}$$

We can now write the expression of the function $\phi_p(\overline{ATM}) = \dfrac{v_3^{(n)}+v_3^{(c)}}{v_0^{(n)}+v_0^{(c)}}$,

$$\phi_p(\overline{ATM}) = \frac{1.25(2.05+0.36\overline{ATM})}{42.5+8.9\overline{ATM}},$$

that is increasing for positive values of $\overline{ATM}$ since its derivative

$$\frac{d\phi_p}{d\overline{ATM}} = \frac{1.5(7.25+2.5\overline{ATM}+0.265\overline{ATM}^2)}{(4.25+0.89\overline{ATM}^2)} > 0.$$

Finally, we can apply Proposition 5.3.1. This results states that if the total concentration of active p53 is 'σ times bigger' than the concentration of inactive p53 then the system oscillates. We verified that the results due to the simplified system are in accordance with the data calculated solving numerically the original system (5.37). We remark that the range of values of the solutions are roughly the same and the behaviour of all variables is the same, except for $v_0^{(n)}$. In figures 5.11(a), 5.11(b),5.11(c) and 5.11(d) we plotted the values calculated numerically solving system (5.37) and the roots of the simplified system (5.38). We also evaluated numerically the function ϕ_p relative to the original system (5.37), verifying that it is a increasing function of $\overline{ATM}$ (see figure 5.11(e)).

Notice that the same proposition can be applied to the functions: $\phi_1(\overline{ATM}) = \dfrac{v_3^{(n)}}{v_0^{(n)}}$ and $\phi_2(\overline{ATM}) = \dfrac{v_3^{(c)}}{v_0^{(c)}}$ since both functions are strictly increasing, as it can be easily verified using the formulas (5.40). It would be interesting to verify experimentally if the crossing of a threshold of the ratios of $p53$ and $p53_p$ in the nucleus or in the cytoplasm (or the total quantity) determine the oscillations. It would be even more interesting to understand if the biological location of the 'unbalanced' concentration of active and inactive p53 has a role in the starting of oscillations.

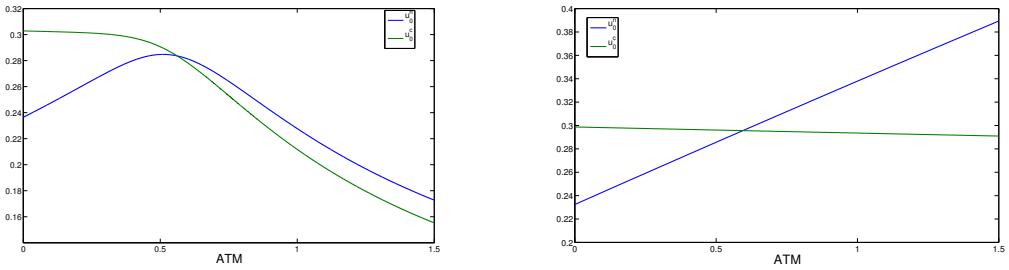

(a)

(b)

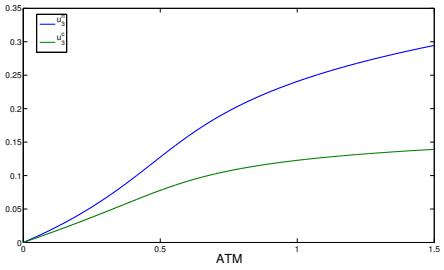

(c)

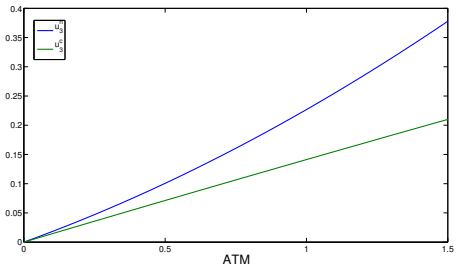

(d)

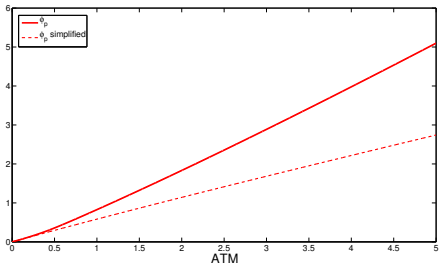

(e)

Figure 5.11: (a),(c): Numerically computed equilibrium values of system (5.13) relative to u_0 et u_3 in the nucleus (blue) and in the cytoplasm (green). (b),(d): Roots of the simplified system (5.39), computed using formulas (5.40). (e): The function ϕ_p computed with the numerical solution of system (5.13) (plain line) and computed formally using formulas (5.40) (dotted line).

5.4 Appendix: computation of the first Lyapunov coefficient

We summarize here the main steps which are useful to compute the first Lyapunov coefficient, following the algorithm presented in the book by Kuznetsov [67], to which we refer for a more detailed description of each step of the algorithm. We remember that we consider a dynamical system depending on one parameter α (the other parameters are considered fixed):

$$\dot{x} = f(x, \alpha), \quad x \in \mathbb{R}^n, \, \alpha \in \mathbb{R}, \tag{5.41}$$

where f is a smooth function of (x, α). Let us suppose that f exhibits a Hopf bifurcation at the equilibrium x_0 at the critical parameter value α_0. The formula giving the first Lyapunov coefficient, that determines if a Hopf bifurcation is *supercritical* or *subcrititcal*, reads:

$$\begin{aligned} l_1(0) = \frac{1}{2\omega_0^2} \mathrm{Re} \big[&\langle p, C(q, q, \bar{q}) \rangle - 2 \langle p, B(q, A^{-1} B(q, \bar{q})) \rangle \\ &+ \langle p, B(\bar{q}, (2i\omega_0 I_n - A)^{-1} B(q, q)) \rangle \big] \end{aligned} \tag{5.42}$$

where A is the Jacobian matrix of system (5.41), and q and p satisfy

$$Aq = i\omega_0 q, \quad A^T p = -i\omega_0 p,$$

and are normalized by setting $\langle p, q \rangle = 1$. Assume also that $\langle q, q \rangle = 1$ and $\langle \mathrm{Re}\, p, \mathrm{Im}\, q \rangle = 0$. We recall the definition of the bilinear function $B : \mathbb{R}^n \times \mathbb{R}^n \to \mathbb{R}^n$

$$B_i(x, y) = \sum_{j,k=1}^{n} \frac{\partial^2 f_i(\xi, \alpha_0)}{\partial \xi_j \partial \xi_k} \Big|_{\xi = x_0} x_j y_k, \quad i = 1, 2, \ldots, n, \tag{5.43}$$

and of the function $C : \mathbb{R}^n \times \mathbb{R}^n \times \mathbb{R}^n \to \mathbb{R}^n$

$$C_i(x, y, z) = \sum_{j,k,l=1}^{n} \frac{\partial^3 f_i(\xi, \alpha_0)}{\partial \xi_j \partial \xi_k \partial \xi_l} \Big|_{\xi = x_0} x_j y_k z_l, \quad i = 1, 2, \ldots, n. \tag{5.44}$$

In order to avoid the computations of the partial derivatives in (5.43) and (5.44), notice that it is possible to evaluate the vector $B(v, v)$ for $v \in \mathbb{R}^n$ by the formula

$$B(v, v) = \frac{d^2}{d\tau^2} f(x_0 + \tau v, \alpha_0)|_{\tau = 0} \,, \tag{5.45}$$

and similarly, the vector $C(v, v, v)$ for $v \in \mathbb{R}^n$ can be obtained using the formula:

$$C(v, v, v) = \frac{d^3}{d\tau^3} f(x_0 + \tau v, \alpha_0)|_{\tau = 0} \,. \tag{5.46}$$

These derivatives with respect the scalar variable τ can be easily approximated using finite differences. Therefore we can evaluate (5.42) using expressions computable via

(5.45) and (5.46). We denote the real and imaginary parts of the vector q by q_R and q_I, so that we have

$$\begin{aligned}
&B(q,q) = B(q_R,q_R) - B(q_I,q_I) + 2iB(q_R,q_I)\\
&B(q,\bar{q}) = B(q_R,q_R) + B(q_I,q_I)\\
&B(q,q,\bar{q}) = C(q_R,q_R,q_R) + C(q_R,q_I,q_I) + iC(q_R,q_R,q_I) + iC(q_I,q_I,q_I).
\end{aligned}$$

The formulas (5.45) and (5.46) let us compute some of the terms of the previous expression, namely $B(q_R,q_R)$, $B(q_I,q_I)$, $C(q_R,q_R,q_R)$ and $C(q_I,q_I,q_I)$. B being a bilinear form, this lead to the following identity:

$$B(v+w) = \frac{1}{4}\left(B(v+w,v+w) - B(v_w,v-w)\right).$$

Similarly we can obtain the following expression for $C(v,v,w)$:

$$C(v,v,w) = \frac{1}{6}\left(C(v,v,v) - C(v-w,u-v,v-w)\right) - \frac{1}{3}C(w,w,w),$$

which permits to evaluate all the terms involving B and C in the expression for l_1.

Let us summarize all the principal steps useful to compute the Lyapunov coefficient l_1.

Step 0. Evaluate the Jacobian matrix $A = f_x(x_0,\alpha_0)$ of (5.41).

Step 1. Find four vectors $q_R, q_I, p_R, p_I \in \mathbb{R}^n$ satisfying the systems

$$\begin{cases} Aq_R + \omega_0 q_I = 0,\\ -\omega_0 q_R + Aq_I = 0, \end{cases}$$

and

$$\begin{cases} A^T p_R - \omega_0 q_I = 0,\\ \omega_0 p_R + A^T p_I = 0, \end{cases}$$

and normalize according to

$$\begin{aligned}
\langle q_R, q_R\rangle + \langle q_I, q_I\rangle = 1, \quad \langle q_R, q_I\rangle = 0,\\
\langle p_R, q_R\rangle + \langle p_I, q_I\rangle = 1, \quad \langle p_R, q_I\rangle - \langle p_I, q_R\rangle = 0.
\end{aligned}$$

Step 2. Compute the following vectors by the directional differentiation:

$$\begin{aligned}
a &= \frac{d^2}{d\tau^2} f(x_0 + \tau q_R, \alpha_0)|_{\tau=0},\\
b &= \frac{d^2}{d\tau^2} f(x_0 + \tau q_I, \alpha_0)|_{\tau=0}
\end{aligned}$$

and

$$c = \frac{1}{4}\frac{d^2}{d\tau^2}\left[f(x_0 + \tau(q_R+q_I),\alpha_0) - f(x_0+\tau(q_R-q_I),\alpha_0)\right]|_{\tau=0}.$$

Step 3. Solve the linear systems for r and (s_R, s_I):

$$Ar = a + b,$$

and

$$\begin{cases} -As_R - 2\omega_0 s_I = a - b, \\ 2\omega_0 s_R - As_I = 2c. \end{cases}$$

Step 4. Compute the following numbers:

$$\sigma_1 = \frac{1}{4}\frac{d^2}{d\tau^2}\langle p_R, f(x_0 + \tau(q_R + r), \alpha_0) - f(x_0 + \tau(q_R - r), \alpha_0)\rangle|_{\tau=0},$$
$$\sigma_2 = \frac{1}{4}\frac{d^2}{d\tau^2}\langle p_I, f(x_0 + \tau(q_I + r), \alpha_0) - f(x_0 + \tau(q_I - r), \alpha_0)\rangle|_{\tau=0},$$

and evaluate their sum $\Sigma_0 = \sigma_1 + \sigma_2$.
Step 5. Compute

$$\delta_1 = \frac{1}{4}\frac{d^2}{d\tau^2}\langle p_R, f(x_0 + \tau(q_R + s_R), \alpha_0) - f(x_0 + \tau(q_R - s_R), \alpha_0)\rangle|_{\tau=0},$$
$$\delta_2 = \frac{1}{4}\frac{d^2}{d\tau^2}\langle p_R, f(x_0 + \tau(q_I + s_I), \alpha_0) - f(x_0 + \tau(q_I - s_I), \alpha_0)\rangle|_{\tau=0},$$
$$\delta_3 = \frac{1}{4}\frac{d^2}{d\tau^2}\langle p_I, f(x_0 + \tau(q_R + s_I), \alpha_0) - f(x_0 + \tau(q_R - s_I), \alpha_0)\rangle|_{\tau=0},$$
$$\delta_4 = \frac{1}{4}\frac{d^2}{d\tau^2}\langle p_I, f(x_0 + \tau(q_I + s_R), \alpha_0) - f(x_0 + \tau(q_I - s_R), \alpha_0)\rangle|_{\tau=0},$$

and evaluate $\Delta_0 = \delta_1 + \delta_2 + \delta_3 - \delta_4$.
Step 6. Compute the numbers

$$\gamma_1 = \frac{d^3}{d\tau^3}\langle p_R, f(x_0 + \tau q_R, \alpha_0)\rangle|_{\tau=0},$$
$$\gamma_2 = \frac{d^3}{d\tau^3}\langle p_I, f(x_0 + \tau q_I, \alpha_0)\rangle|_{\tau=0},$$
$$\gamma_3 = \frac{d^3}{d\tau^3}\langle p_R + p_I, f(x_0 + \tau(q_R + q_I), \alpha_0)\rangle|_{\tau=0},$$
$$\gamma_4 = \frac{d^3}{d\tau^3}\langle p_R - p_I, f(x_0 + \tau(q_R - q_I), \alpha_0)\rangle|_{\tau=0},$$

and evaluate $\Gamma_0 = \frac{2}{3}(\gamma_1 + \gamma_2) + \frac{1}{6}(\gamma_3 + \gamma_4)$.
Step 7. Finally, compute

$$l_1(0) = \frac{1}{2\omega_0}(\Gamma_0 - 2\Sigma_0 + \Delta_0).$$

If $l_1(0) \neq 0$ and the eigenvalues cross the imaginary axis with nonzero velocity, a unique limit cycle appears under variation of α.

5.5 Conclusion and Outline of the Work

From this preliminary study of the ODE compartmental model, we verified, in a simplified setting, that the system proposed reproduces the expected behaviour, with no need of any artificial mechanism. The parameter that activates the system and gives rise to the

oscillations is $\overline{ATM}$. This parameter represents the protein ATM that phosphorylates p53 in the cell, after a damage. We established the existence of two supercritical Hopf bifurcations through which the system passes. Oscillations arise for low values of $\overline{ATM}$ ($\overline{ATM} \sim 1.4$) and disappear for higher values ($\overline{ATM} \sim 97$). We evaluated the period of oscillations following variations $\overline{ATM}$ and we verified that it does not depend strongly on the damage undergone (value of $\overline{ATM}$ in our model). This result reproduces the behaviour of p53, experimentally observed [40]. However the period of the oscillations of our simulations is shorter than the period observed experimentally. We will show in the next Chapter how we obtained more realistic periods of our model by the addition of a spatial variable. Finally we have given a physiological interpretation of the rise of oscillations, based on the concentration ratio of active and inactive p53. We have shown, using a simplified model, that if the concentration of active p53 is σ times higher than the concentration of inactive p53, the system must be in its oscillatory regime. It would be interesting to further investigate this aspect and to have an experimental confirmation of our results. The possibility that the *location* of the unbalanced concentration of p53 in its two states could play a role, makes this aspect of the problem even more interesting to us.

Chapter 6

A spatial model of p53 nuclear accumulation

In this Chapter we continue the study of the model of p53 introduced in Chapter 5. We analyse the behaviour of a modified version of the model, to which we add the spatial variability. We keep the same reaction network, as in Chapter 5, but we take into account the distances that molecules have to cover to pass from a compartment to the other. We assume that all the molecules are able to diffuse within each compartment and we add a transmission condition between the nucleus and the cytoplasm that models the nuclear membrane. We obtain a reaction-diffusion system of equations, defined on two subdomains having a common boundary. We analyse the behaviour of this extended system, testing the effects of the variations of the spatial coefficients, on the temporal dynamics of p53.

Contents

6.1 Some remarks about the spatial distribution of p53

Here we introduce the few notions about p53 spatial distribution in damaged or undamaged cells. Depending on the state of a cell (damaged or undamaged), but also on the

type of the cell, p53 can be mostly nuclear or cytoplasmic. For instance, in mouse stem cells, p53 is cytoplasmic, as figure 6.1(a) shows. In this figure we can observe a population of stem cells (D3), where p53 is labelled by a green GFP tag, and the nucleus is visualized using a fluorescent (blue) DNA-interactive agent (Draq5). In healthy cells, the protein p53 is exported from the nucleus and degraded in the cytoplasm, thus, generally the total concentration of p53 both in the nucleus and in the cytoplasm is very low and not always detectable. When the damage is sensed by the cell, the network of p53 is activated and the protein undergoes several modifications that allow its accumulation in the nucleus. Figure 6.1(b) shows the cases of stem cells, where a gradual p53 stabilization in the whole cell can be observed. In irradiated cells, nuclear p53 is detected half an hour after irradiation [82]. The correct location of p53 has a direct impact on the functioning of the protein. Many tumour types that have mutations on the p53 gene (classically p53 cytoplasmic confinement) are less responsive to genotoxic stress induced by radiotherapy or chemotherapy [99]. Import and export of p53 need to be tightly regulated for an effective response in case of DNA damage. Moreover we recall that nuclear import and export signals of p53 are easily masked or unmasked, depending on the necessities of the cell and play an important role in p53 activation (see Section 4.1.2).

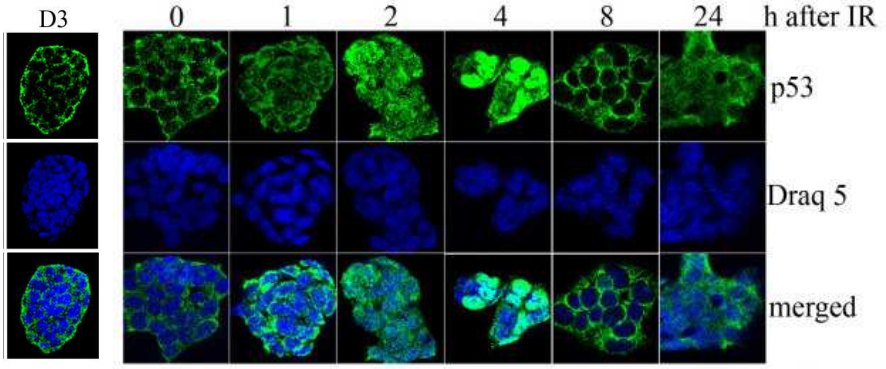

(a) (b)

Figure 6.1: (a) p53 is localized to the cytoplasm of mouse embryonic stem cells. (b): p53 accumulates in the nucleus of irradiated embryonic stem cells. GFP-tagged p53 is expressed in green. To visualize the nuclei, cover slips were incubated with Draq5 (blue) [123]

6.2 Mathematical formulation

Consider the p53 model, introduced in Chapter 5. We cast system (5.13) in a two-dimensional domain divided into a nuclear and a cytoplasmic compartment as shown in Figure 6.2. We set Ω as the entire domain of the cell and we define Ω_1 as the nuclear compartment and Ω_2 as the cytoplasmic one. We set $\Gamma_{12} := \partial\Omega_1 \cap \partial\Omega_2$ for the common

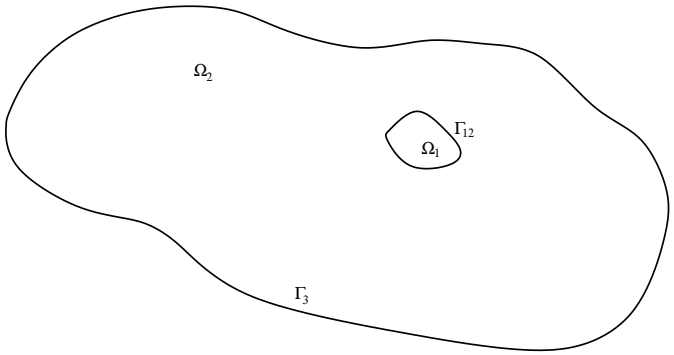

Figure 6.2: Domain of the PDE system: we represent the two different compartments, Ω_1 for the nucleus and Ω_2 for the cytoplasm. Γ_{12} is the common boundary between the two compartments; Γ_3 is the exterior boundary, representing the cellular membrane.

boundary and $\Gamma_3 := \partial\Omega \backslash \Gamma_{12}$. Each species is a function of time t and position $\mathbf{x} = (x, y)$; we suppose that each species is able to diffuse in the cytoplasm and in the nucleus. We include permeability conditions at the common boundary Γ_{12} that take into account nuclear membrane. As for the ODE case, we nondimensionalise the system. Setting

$$\bar{u}_0(\xi,\eta,\tau) = \frac{u_0(x,y,t)}{\alpha_0}, \ldots, \bar{u}_3(\tau) = \frac{u_3(x,y,t)}{\alpha_3},$$
$$\tau = \frac{t}{t^\star},\ \xi = \frac{x}{L},\ \eta = \frac{y}{L},$$

where L, expressed in μm, is some one-dimensional space parameter related to cell size, we obtain in Ω_1:

$$\begin{cases} \frac{\partial \bar{u}_0}{\partial \tau} = \bar{D}_0 \Delta \bar{u}_0 - k_{ub}\bar{u}_1 \frac{\bar{u}_0}{(K_{ub}+\bar{u}_0)} - \overline{ATM}\frac{\bar{u}_0}{(1+\bar{u}_0)} + \bar{k}_{ph}\frac{\bar{u}_3}{(\bar{K}_{ph}+\bar{u}_3)}, \\ \frac{\partial \bar{u}_1}{\partial \tau} = \bar{D}_1 \Delta \bar{u}_1 - \bar{d}_1 \bar{u}_1, \\ \frac{\partial \bar{u}_2}{\partial \tau} = \bar{D}_2 \Delta \bar{u}_2 + \bar{k}_{pm} + \frac{\bar{u}_3^h}{(\bar{K}_{Sp}^h+\bar{u}_3^h)} - \bar{d}_2 \bar{u}_2, \\ \frac{\partial \bar{u}_3}{\partial \tau} = \bar{D}_3 \Delta \bar{u}_3 + \overline{ATM}\frac{\bar{u}_0}{(1+\bar{u}_0)} - \bar{k}_{ph}\frac{\bar{u}_3}{(\bar{K}_{ph}+\bar{u}_3)}, \end{cases} \tag{6.1}$$

and in Ω_2:

$$\begin{cases} \frac{\partial \bar{u}_0}{\partial \tau} = \bar{D}_0 \Delta \bar{u}_0 + \bar{k}_{tp} - k_{ub}\bar{u}_1 \frac{\bar{u}_0}{(K_{ub}+\bar{u}_0)} - \overline{ATM}\frac{\bar{u}_0}{(1+\bar{u}_0)} + \bar{k}_{ph}\frac{\bar{u}_3}{(\bar{K}_{ph}+\bar{u}_3)}, \\ \frac{\partial \bar{u}_1}{\partial \tau} = \bar{D}_1 \Delta \bar{u}_1 + \bar{k}_{tm}\bar{u}_2 - \bar{d}_1 \bar{u}_1, \\ \frac{\partial \bar{u}_2}{\partial \tau} = \bar{D}_2 \Delta \bar{u}_2 - \bar{k}_{tm}\bar{u}_2 - \bar{d}_2 \bar{u}_2, \\ \frac{\partial \bar{u}_3}{\partial \tau} = \bar{D}_3 \Delta \bar{u}_3 + \overline{ATM}\frac{\bar{u}_0}{(1+\bar{u}_0)} - \bar{k}_{ph}\frac{\bar{u}_3}{(\bar{K}_{ph}+\bar{u}_3)}, \end{cases} \tag{6.2}$$

where we used the same notations as in the previous chapter. Notice that, as in [15], we used Fick's Law to model the diffusion of each species concentration. We defined $\bar{D}_i = \frac{t^\star D_i}{L^2}$, $i = 0, \ldots, 3$, as the nondimensional diffusion coefficients, where D_i is the dimensional diffusion parameter of the $i-th$ species, expressed in $\mu m^2/min$. Finally, following [15] and [121], and consistently with the assumptions of the ODE model, we

fix Kedem-Katchalsky [62] boundary conditions at the common boundary Γ_{12} for the species that cross the nuclear membrane from both sides:

$$\begin{cases} \frac{\partial \bar{u_0}^n}{\partial \mathbf{n}} = \frac{\bar{p_0}}{D_0}(\bar{u_0}^c - \bar{u_0}^n) = \frac{\partial \bar{u_0}^c}{\partial \mathbf{n}} & \text{on } \Gamma_{12}, \\ \frac{\partial \bar{u_1}^n}{\partial \mathbf{n}} = \frac{\bar{p_1}}{D_1}(\bar{u_1}^c - \bar{u_1}^n) = \frac{\partial \bar{u_1}^c}{\partial n} & \text{on } \Gamma_{12}, \end{cases} \tag{6.3}$$

meaning that the flux of each species through the nuclear envelope is proportional to the difference between the concentrations at the two sides of the membrane. Notice that the normal vector $\mathbf{n}$ is pointing outwards from the nucleus and that fluxes are continuous. We fix the following boundary conditions for $\bar{u}_2$ and $\bar{u}_3$:

$$\begin{cases} \frac{\partial \bar{u_2}^n}{\partial \mathbf{n}} = \frac{\bar{p_2}}{D_2}(-\bar{u_2}^n) = \frac{\partial \bar{u_2}^c}{\partial \mathbf{n}} & \text{on } \Gamma_{12}, \\ \frac{\partial \bar{u_3}^n}{\partial \mathbf{n}} = \frac{\bar{p_3}}{D_3}\bar{u_3}^c = \frac{\partial \bar{u_3}^c}{\partial \mathbf{n}} & \text{on } \Gamma_{12}, \end{cases} \tag{6.4}$$

that include the directionality of transport: $\bar{u_2}$, the mRNA of Mdm2, is only able to exit the nucleus, while $\bar{u_3}$, phosphorylated p53, traverses the nuclear membrane only towards the nucleus. Again notice that the fluxes are continuous. The constants $\bar{p}_i$ are the permeability coefficients relative to each species and are expressed, in the dimensional model, in $\mu m/min^{-1}$. We also assume that proteins are not able to exit the cell and we use Neumann homogeneous boundary conditions on Γ_3 (zero-flux) for all species:

$$\frac{\partial u_i}{\partial \mathbf{n}} = 0 \text{ on } \Gamma_3, i = 0, \dots, 3. \tag{6.5}$$

Since nuclear pores are homogeneously distributed on the nuclear envelope and far from saturation [121], the choice of Kedem-Katchalsky boundary conditions, to model membrane permeability [62], is consistent with our environment; see [15] and references therein for more details on Kedem-Katchalsky conditions in the case of the nuclear membrane. We emphasize here that the choice of the boundary condition is coherent with the choice of the ODE model, where we fixed an exchange rule between compartments as the linear contribution of the difference of the mean concentrations in each compartment. Let us consider a simplified system for one generic species u that can only diffuse in the domain Ω:

$$\begin{cases} \frac{\partial u^{(n)}}{\partial t} = D_n \Delta u^{(n)} & \text{in } \Omega_1, \\ \frac{\partial u^{(c)}}{\partial t} = D_c \Delta u^{(c)} & \text{in } \Omega_2, \end{cases} \tag{6.6}$$

and let us couple this system by using the boundary conditions:

$$D_n \frac{\partial u^{(n)}}{\partial \mathbf{n}} = p(u^{(c)} - u^{(n)}) = D_c \frac{\partial u^{(c)}}{\partial \mathbf{n}} \qquad \text{on } \Gamma_{12}, \tag{6.7}$$

closed by the continuity of the flux: $D_n \frac{\partial u^{(n)}}{\partial \mathbf{n}} = D_c \frac{\partial u^{(c)}}{\partial \mathbf{n}}$. Here again the normal vector $\mathbf{n}$ is the same on both sides. If we integrate over the whole region and apply Green's formula, we obtain:

$$\begin{cases} \frac{du^{(n)}}{dt} = \frac{p}{|\Omega_1|} \int_{\Gamma_{12}} (u^{(c)} - u^{(n)}) d\sigma, \\ \frac{du^{(c)}}{dt} = \frac{p}{|\Omega_2|} \int_{\Gamma_{12}} (u^{(n)} - u^{(c)}) d\sigma, \end{cases} \tag{6.8}$$

thus reducing the initial system (6.6) to system (6.8) above, in agreement with equations:

$$\frac{du^{(n)}}{dt} = pV_r(u^{(c)} - u^{(n)}), \qquad \frac{du^{(c)}}{dt} = pV_r(u^{(n)} - u^{(c)}), \tag{6.9}$$

which corresponds to our choices in the ODE model (5.13).

6.3 Numerical approximation

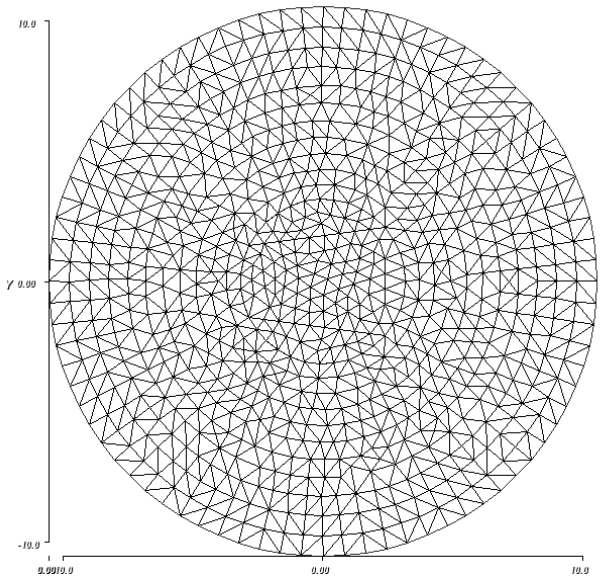

Figure 6.3: Mesh example.

All simulations have been performed using the open source tool *FreeFem++*. *FreeFem++* (http://www.freefem.org/ff++/) is a computer language dedicated to the finite element method, developed at Jacques-Louis Lions Laboratory, Pierre et Marie Curie University (UPMC), Paris.

Weak formulation

To simplify notations, and introduce the weak formulation of our problem, let us rewrite the equations in vectorial form. We set $V = (v_1, \ldots, v_n)^{\mathbf{T}}$ that is defined as a vector function $V : \Omega_1 \cup \Omega_2 \to \mathbb{R}^n$, with $n = 8$. We look for solutions of (6.1)-(6.2),(6.3)-(6.4) in the space $H^1(\Omega_1) \cup H^1(\Omega_2)$, $\forall t \in [0, T]$ where T represents a final time. We define $\nabla V : \Omega_1 \cup \Omega_2 \to \mathbb{R}^{n,d}$ as the gradient of vector V, where d is the dimension where the system lies: $\forall \mathbf{x} \in \Omega_1 \cup \Omega_2$, $\nabla v_i(\mathbf{x}) \in \mathbb{R}^d$. We also define the divergence of a tensor $\mathbf{Q} : \Omega_1 \cup \Omega_2 \to \mathbb{R}^{n,d}$, with rows Q_i, $i = 1, \ldots, n$, as $\nabla \cdot \mathbf{Q} := (\nabla \cdot Q_1, \ldots, \nabla \cdot Q_n)^{\mathbf{T}}$.

We define the diagonal tensors $A = \mathrm{diag}(d_1, d_2, \ldots, d_n)$ and $P = \mathrm{diag}(p_1, p_2, \ldots, p_n)$ where the d_i and p_i, $i = 1, \ldots, n$, are respectively the diffusivity and permeability coefficients of each considered species.

We define a vector field $R(V)$ that collects all the reaction terms and we set $V_0 \in [L^2(\Omega)]^n$ as the initial conditions. Finally we state the problem in vector form: find the solution $V \in L^2(0,T;[H^1(\Omega_1 \cup \Omega_2)]^n)$ of the following initial and boundary value problem

$$\begin{cases} \partial_t V = \nabla \cdot (A \nabla V) + R(V) & \text{in } [0,T] \times (\Omega_1 \cup \Omega_2), \\ V(0,\mathbf{x}) = V_0(\mathbf{x}) & \text{on } \{0\} \times (\Omega_1 \cup \Omega_2), \\ (A\nabla V)\mathbf{n} = \mathbf{0} & \text{on } \Gamma_3, \\ (A\nabla V)\mathbf{n}|_{\Omega_1} = P(V|_{\Omega_2} - V|_{\Omega_1}) & \text{on } \Gamma_{12}, \\ (A\nabla V)\mathbf{n}|_{\Omega_2} = P(V|_{\Omega_1} - V|_{\Omega_2}) & \text{on } \Gamma_{12}, \end{cases} \tag{6.10}$$

where, here, $\mathbf{n}$ corresponds to the normal vector is relative to each compartment. Let us consider a test function $\hat{V} \in [H^1(\Omega_1 \cup \Omega_2)]^n$. The weak formulation is given by:

$$\int_{\Omega_1 \cup \Omega_2} \partial_t V \hat{V} d\mathbf{x} + \int_{\Omega_1 \cup \Omega_2} A\nabla V \cdot \nabla \hat{V} d\mathbf{x} - \int_{\Gamma_{12}} (A\nabla V)\mathbf{n} \cdot \hat{V} d\sigma = \int_{\Omega_1 \cup \Omega_2} R(V)\hat{V} d\mathbf{x}. \tag{6.11}$$

In order to describe clearly the contribution due to the flux between the two compartments, we can re-write the border term as it follows:

$$\begin{gathered} \textstyle\int_{\Gamma_{12}} (A\nabla V)\mathbf{n} \cdot \hat{V} d\sigma = \\ \textstyle\int_{\Gamma_{12}} P(V|_{\Omega_2} - V|_{\Omega_1}) \cdot \hat{V}^{(n)} d\sigma + \int_{\Gamma_{12}} P(V|_{\Omega_1} - V|_{\Omega_2}) \cdot \hat{V}^{(c)} d\sigma \end{gathered} \tag{6.12}$$

where we ordered the terms of $\hat{V}$ as "nuclear" and "cytoplasmic": $\hat{V} = (\hat{V}^{(n)}, \hat{V}^{(c)})^{\mathbf{T}}$.

The finite element method

We use finite elements for the spatial discretization of problem (6.1)-(6.2), (6.3)-6.4). The triangularization of the domain is created by FreeFem++ built-in function. Let $\mathbf{\Lambda_h}$ a C^0 finite element subspace of $[H^1(\Omega_1 \cup \Omega_2)]^n$ defined on a regular mesh parametrized by h (e.g see Figure 6.3) . The numerical solution is calculated using a backward Euler scheme in time and a Newton iteration for the nonlinear terms. Le $t_0 = 0$ and $t_{n+1} = t_n + \Delta t$ where Δt is the step size in time. For $n = 0, 1, \ldots,$ we let

$$\begin{gathered} \textstyle\int_{\Omega_1 \cup \Omega_2} V^{n+1} \hat{V} d\mathbf{x} + \Delta t \int_{\Omega_1 \cup \Omega_2} A\nabla V^{n+1} \cdot \nabla \hat{V} d\mathbf{x} - \Delta t \int_{\Gamma_{12}} (A\nabla V^{n+1})\mathbf{n} \cdot \hat{V} d\sigma \\ \textstyle -\Delta t \int_{\Omega_1 \cup \Omega_2} R(V^{n+1,k})\hat{V} d\mathbf{x} = 0. \end{gathered} \tag{6.13}$$

The term $V^{n+1,k}$ is the approximation of the term V^{n+1} solved by the Newton iteration step. The algorithms goes as follows: at t_0 we set $V^{1,0} = V^0$ and we solve equation (6.13). After solving the equation, we calculate the L^2 distance $\|V^{1,1} - V^{1,0}\|_{L^2(\Omega_1 \cup \Omega_2)^n}$

Parameter	Description	Value	Reference
d_p	p53 Diffusion coefficient	$600\mu m^2/min$	[15]
d_m	Mdm2 Diffusion coefficient	$600\mu m^2/min$	[15]
d_{mRNA}	Mdm2 mRNA Diffusion coefficient	$6\mu m^2/min$	[38, 119]
$d_{p'}$	$p53_P$ Diffusion coefficient	$600\mu m^2/min$	[15]
p_{p53}	p53 permeability coefficient	$10\mu m \cdot min^{-1}$	obtained
p_{mdm2}	Mdm2 permeability coefficient	$10\mu m \cdot min^{-1}$	obtained
p_{mRNA}	Mdm2 mRNA permeability coefficient	$0.1\mu m \cdot min^{-1}$	obtained
p_{pp}	$p53_p$ permeability coefficient	$10\mu m \cdot min^{-1}$	obtained

Table 6.1: Parameter values for the dimensional model. The permeability coefficients are obtained by numerical data fitting. A more accurate description of the choice of the permeability parameter is done in section 6.4.3.

and we proceed until $\|V^{1,1} - V^{1,0}\|_{L^2(\Omega_1 \cup \Omega_2)^n} < \varepsilon$, for a fixed ε. Once calculated the numerical solution V^1 we set $V^{2,0} = V^1$ and we calculate the solution for the following time step with a new Newton iteration.

6.4 Simulations Results

6.4.1 Spatial parameters

In this new setting, the number of parameters of the system has increased. Diffusion and permeability coefficients need to be set accordingly to the biophysical knowledge of the cellular environment and molecular species. Since, according to [15], the diffusion coefficient of a general protein with a mass of about $40kDa$ is roughly $600\mu m^2/min$, we take this value as a reference for all the protein species, p53 and Mdm2, in the nucleus and in the cytoplasm. Using single molecule tracking and statistical analysis, recent works managed to calculate the mRNA diffusion coefficient [38, 119, 50] and found that the coefficient of a single mRNA particle is $\sim 6 - 30 \times \mu m^2/min$, i.e., the ratio between mRNA and protein diffusion coefficients is about $1 : 100$. Concerning the permeability coefficient, we supposed, to tie in with this diffusion coefficient ratio, that the ratio between the mRNA and the protein permeability coefficient is $1 : 100$. In the sequel, all the simulations will be done for values of parameters listed in Table 6.1.

6.4.2 Simulations results in a 1-dimensional domain

We begin the study of the system in a simplified one-dimensional domain, plotted in Figure 6.4. This domain is given by two adjoining segments that represent the cytoplasmic and nuclear compartments. We fix an interval $[a, c] = [0\,, 10]$ (in μm), $[a, c] = [a, b] \cup [b, c]$, with $[a, b] = [0\,, 9]$ the cytoplasmic compartment, and $[b, c] = [9\,, 10]$ the nucleus, as shown on Figure 6.4. We performed all simulations using finite differences

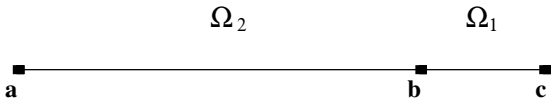

Figure 6.4: A 1-dimensional simplified domain of the cell.

schemes and we used a basic IMEX numerical scheme. For further details see [60]. Even if the geometry is oversimplified, there is a striking difference with the ODE case. The protein flux from one compartment to the other is not given, as in the ODE case, by an average of the total concentration over the whole compartment, but by the protein concentration that actually exists at the membrane location. In order to test whether the system reproduces the oscillatory behaviour observed in the ODE case, first we analyse it by following the variations of the ATM parameter. As explained above, this parameter is meant to represent the DNA damage and it is the switch that turns on the system, giving rise to robust oscillations. In the sequel we fix a time duration of 500 min to compare the results for different values of the parameters. We observed, see Figure 6.5(a), that for values of $ATM < 2$, first the system tends towards a stable equilibrium, then starts to produce damped oscillations (Figures 6.5(c) and 6.5(e)). Oscillations become undamped and their amplitude rises when $ATM > 2$, see Figures 6.5(d), 6.5(f) . It is known from *in vitro* observations [70, 40] that the period of oscillations is stable over different irradiation doses and consequent damages. The same behaviour may be observed on our simulation results that show that once the undamped oscillations occur, the period varies slightly and stabilises around a value of 35 min. See Figure 6.5(b) where we plotted the number of peaks of the sustained oscillations observed in 500 min, against ATM variations.

The response of the system is robust upon changes of the diffusion coefficients.

Once the oscillatory regime is established, we can vary the spatial parameters, namely diffusion and permeability, to understand how the system responds to spatial perturbations. In Section 6.4.1 we pointed out that the physiological ratio between protein and mRNA diffusion is about 100:1. Keeping this ratio fixed, we performed simulations, varying only the diffusion coefficient. Our results show that the oscillatory behaviour is highly robust over a wide range of variation for the diffusion coefficient. Oscillations arise for very low diffusion coefficient (see Fig. 6.6) and remain active for very large values of the parameters. The amplitude of oscillations decreases slightly with the diffusion coefficient but the period of oscillations is almost constant. We can observe damped oscillations for values of protein diffusion lower than $10\mu m^2/min$, but once this threshold is crossed, undamped oscillations arise with a period of about 35 minutes (lower than the period observed in biological experiments [40, 70]). Conversely, if simulations are performed with a 1:1 ratio between mRNA and protein diffusion, oscillations disappear quickly, for diffusion values $D \geq 100$, as shown on Figure 6.7. This suggests that the difference between mRNA and protein diffusion coefficients is crucial to the oscillations of the system.

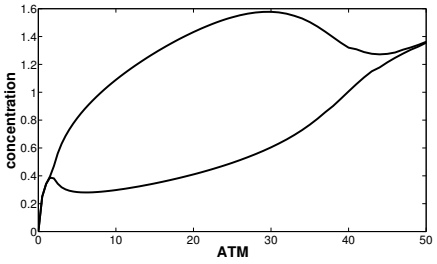

(a) Bifurcation diagram of $u_3^{(n)}$

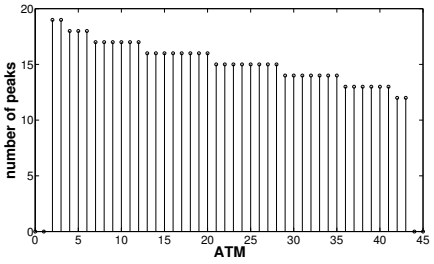

(b) Number of observed peaks in 500 min

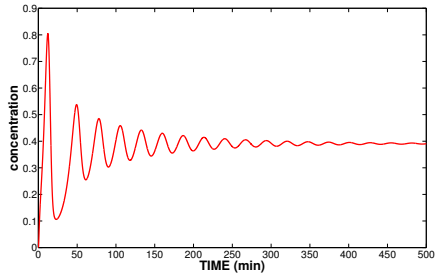

(c) Nuclear $p53$ over time, $ATM = 1.5$

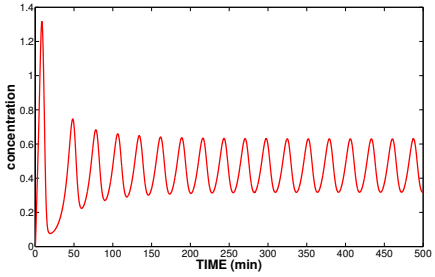

(d) Nuclear $p53$ over time, $ATM = 2.5$

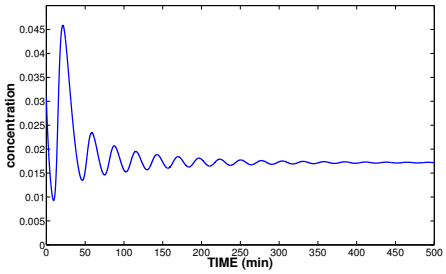

(e) Nuclear $Mdm2$ over time, $ATM = 1.5$

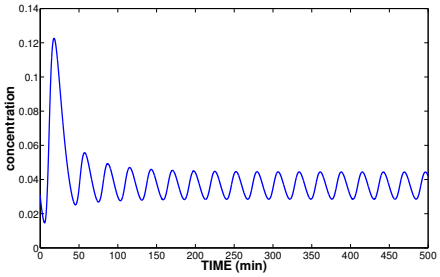

(f) Nuclear $Mdm2$ over time, $ATM = 2.5$

Figure 6.5: 1-dimensional PDE model. (a): Bifurcation diagram of $u_3^{(n)}$ as a function of ATM. (b): Number of sustained oscillations peaks observed in a fixed duration of 500 minutes. Oscillations in the 1-dimensional case: (c),(d) evolution of p53 concentration, nuclear compartment. (e) (f): evolution of Mdm2 concentration, nuclear compartment. Undamped oscillations occur only for value of $ATM > 2$ ($\overline{ATM} = 0.2$).

Low permeability is essential for oscillations in the 1-D case.

We analysed the behaviour of the system under variations of the permeability coefficient. In order to cross the nuclear membrane, proteins and RNAs need to pass through large protein channels, called nuclear pore complexes (NPCs), that let only authorised molecules to pass through. Even though a nuclear pore can be up to 100 nm long [110] and the access to the pore is highly controlled, the translocation pathway is impressively

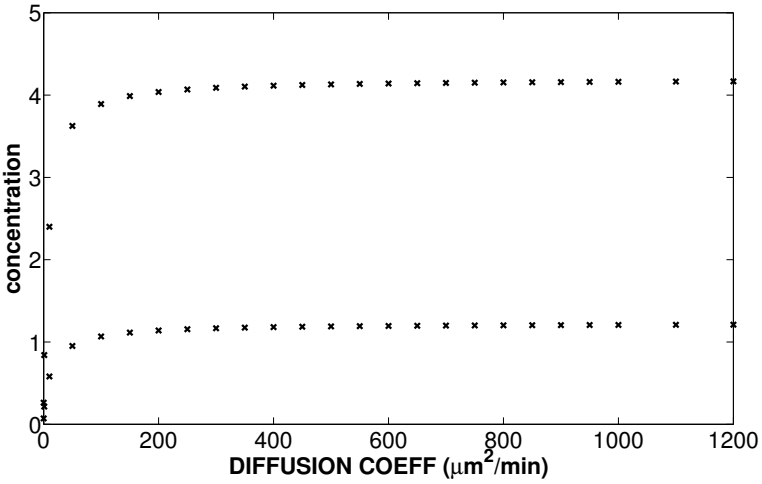

(a)

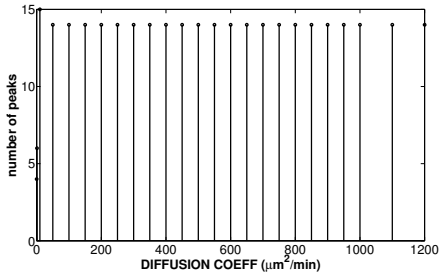

(b)

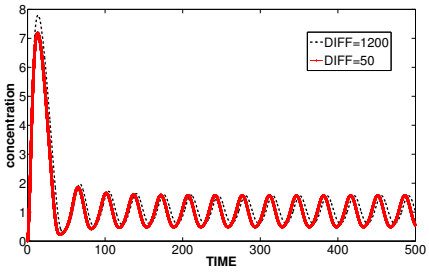

(c)

Figure 6.6: Oscillations in the one-dimensional PDE case. If the ratio between protein to mRNA diffusion is kept 100:1, varying the diffusion coefficient do not compromise the oscillatory behaviour of the system. (a): oscillation amplitudes over the diffusion coefficient for $u_3^{(n)}$.(b) Number of peaks of the sustained oscillations during 500 min for each diffusion coefficient value. (c) Evolution of $u_3^{(n)}$ over time, for a diffusion coefficient equal to 50 and $1200 \mu m^2/min$.

efficient. The mass flow through a single NPC can be up to 80 MDa/s [111] and the time needed for translocation through the pore lasts only 5-7ms [23]. In order to understand whether the permeability parameter is determinant for the model behaviour, we performed numerical simulations for different permeability values. As in Section 6.4.2, the ratio between the diffusion coefficients of protein and mRNA has been set to 100:1. In the 1-dimensional case, undamped oscillations occur for values of the permeability p_i included between 3 and 20 μm/min. Some damped oscillations still appear for values of the parameter $p_i \in [20, 40]$, as shown in Figure 6.8. We also notice that, unlike in the previous experiments on diffusion coefficients, the period of the oscillations depends

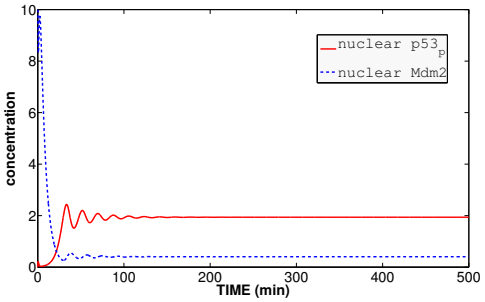

Figure 6.7: 1-dimensional PDE model. Temporal evolution of nuclear $p53_p$ and $Mdm2$ concentrations. For homogeneous values of the diffusion coefficient (ratio 1:1) only damped oscillations occur. Here we fixed $D_i = 200$, $\forall i = 0, \ldots, 3$. All the other parameter values are fixed to the reference ones reported in Table 5.1 and 6.1.

highly on permeability variations. Figure 6.8(b) shows the number of peaks of p53 level observed in 500 minutes.

These first results bring out the importance of the spatial variable: analysing variations of the system with respect to coefficients that could not be studied in the ODE case, we have pointed out the strong dependence of the solution upon the permeability coefficient. However, the range of values over which we can observe the expected oscillatory behaviour is lower than the permeability values proposed in the literature (see e.g. [121]), that range around 100 $\mu m/\text{min}^{-1}$. We also noticed that different diffusion coefficients did not influence - neither qualitatively nor quantitatively - the behaviour of the system. Since the one-dimensional case is an oversimplified model of the cell, where the nuclear membrane is reduced to a single point and diffusion is too fast to allow for significantly different behaviours, we will now analyse the behaviour of the model in a still simple, but more realistic, two-dimensional domain.

6.4.3 Results in the 2-Dimensional domain

In this section we analyse the system in a two-dimensional cell-shaped domain. For our simulations we chose the domain represented in Fig. 6.9, where the total area is of about 300 μm^2, while the ratio between cytoplasmic and nuclear areas is $10:1$. These values will be varied only when specified. References values for spatial parameters have been reported in Table 6.1.

We reproduced the spatial dynamics of the p53-Mdm2 system, as observed in [70, 40]. As can be observed on Figure 6.10, 30 min after damage sensing, the p53 protein accumulates in the nucleus. A first peak of p53 concentration appears 1 hour after the start of simulations. Then the cytoplasm and the nucleus empty and a second cycle starts. Oscillations of Mdm2 follow, see Figure 6.11. The period of oscillations is about 300 min and corresponds to the actual period experimentally observed [70, 40].

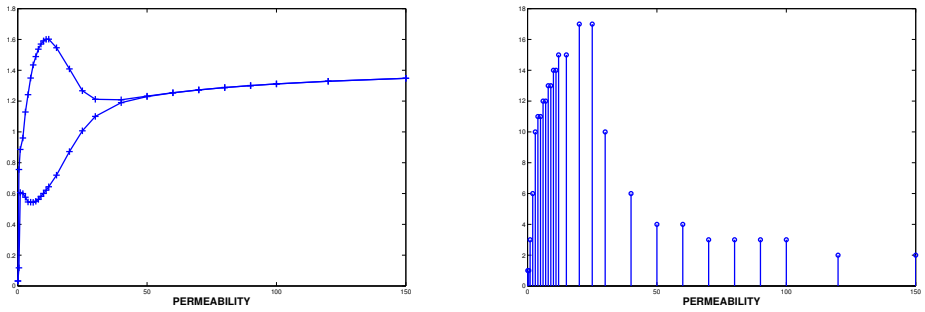

(a) (b)

Figure 6.8: 1-dimensional PDE model. (a): Bifurcation diagram for non homogeneous permeability coefficient: protein permeability:RNA permeability fixed to 100:1. All the other parameter values are fixed to the reference ones reported in Table 5.1 and 6.1. (b) Corresponding number of oscillations in 500 min.

Oscillations exist for realistic protein and mRNA diffusion values.

Following the results of [38, 119] and the numerical results of the previous section, we fixed the protein to mRNA diffusion coefficient ratio to $100:1$. As in section 6.4.2, we observe a robust oscillatory behaviour, with sustained oscillations occurring for diffusion values ranging in $[10, 1000]\mu m^2$/min (see Table 6.2 and Figure 6.12). Comparing these results with the one-dimensional case, we remark that diffusion values play a more important role. Indeed in Section 6.4.2 we obtained an oscillatory behaviour for all diffusion values > 10 μm^2/min. Adding the second dimension to the system, we remark instead that oscillations disappear for values of the diffusion coefficient higher than 1000 μm^2/min, which implies that very fast diffusion of molecules prevents the occurrence of oscillations. This emphasizes the importance in the 2D model of spatial diffusion, with physiological values for the diffusion cefficients. As shown in [59] experimentally observed p53 mobility reduces drastically after DNA damage, and its diffusion coefficient passes from $\sim$ 18 $\mu m^2/s$ to $\sim$ 3 $\mu m^2/s$ (1000 μm^2/min- 180 μm^2/min), within 8 hours. This reduced mobility is probably due to increased protein-protein interactions and DNA binding of active p53. Interestingly, the oscillatory dynamics is captured by our model for all those different values. Nevertheless, we did not consider the diffusion of p53 as a function of time and DNA damage, which is an open option left for future work.

Period depends on permeability, but sustained oscillations are always present.

We tested again the robustness of the system towards perturbations of the permeability coefficients. We know, from the previous section, that in the one-dimensional case the response of the system is sensitive to permeability variations. In the one-dimensional setting, oscillations disappear for permeability values lower than the realistic ones (see [121]). In the two-dimensional model the system reacts in a different way, and we can

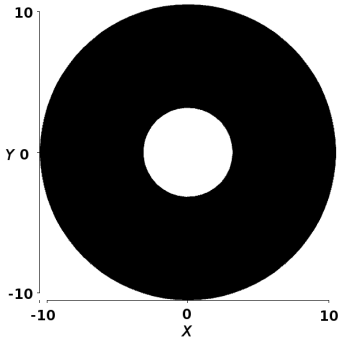

Figure 6.9: Simulation domain of the bi-dimensional PDE model, Volume ratio: $(C : N) = 10 : 1$

observe oscillations over a much larger range of the permeability coefficient. We set the diffusion constant to $600\mu m^2$/min for proteins and to $6\mu m^2$/min for the variable u_2, representing the mRNA and we varied the permeability coefficient.

In the two-dimensional case the system is much more robust and oscillations arise for permeability values strictly higher than 5 μm/min. We notice that the amplitude of oscillations is almost constant (see Figure 6.13(a)), whereas, again, it is the period of oscillations that exhibits the most remarkable variations. It varies from 250 min for permeability values of $10\mu m$/min to about 40 min when the permeability is set to 200 μm/min (and 2 μm/min for the mRNA), see Fig 6.13(b) and Table 6.2.

We notice that, in the two-dimensional setting, the period of oscillations strongly depends on these spatial coefficients. For high permeability constants the frequencies of oscillations are high, while for lower permeabilities we can reproduce the period of *in vitro* observations (about 4-5h, [70]).

The discrepancy between our values and those found in the literature could be due to the simplification of the transport machinery done in our model. We supposed indeed that proteins could traverse the nuclear membrane by themselves, which is not the case. Proteins like p53 or Mdm2 need to be carried by a chaperon through the membrane and then be released in the destination compartment. The translocation process imply a number of reactions, like the recognition by the importin and exportin proteins and the binding (and unbinding) to the small GTPase RAN, that handle the directionality of the transport. The time needed for these events to occur is not taken into account by our model and this led us to set low permeability values, namely $10\mu m$/min instead of $100\mu m$/min [121], in order to get oscillations with the period observed in the literature. Note that this point is more extensively commented in Section 6.6.

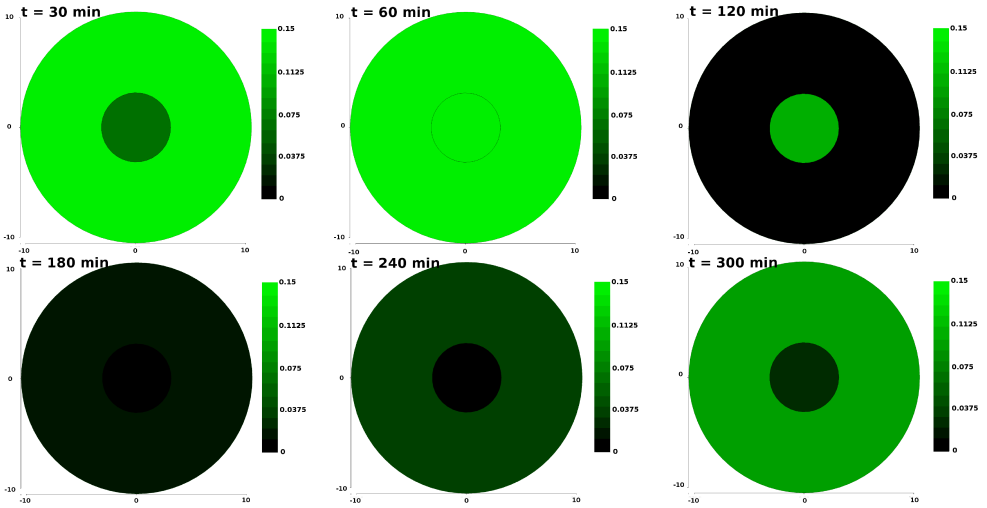

Figure 6.10: Bi-dimensional PDE model. Spatial distribution of $p53_p$ at different time-step on the reference domain. Phosphorylated p53 spatial distribution and temporal evolution. As observed in biological experiments [40, 70] p53 accumulates in the nucleus. The peak of p53 protein is observed at 1h from damage sensing. Then the level of p53 steps back towards the initial state.

Period depends on the total volume of the cell rather than on cytoplasmic to nuclear volume ratio.

The spatial treatment of the problem allow us to analyse the response of the model in different domains. Numerical simulations have been performed over a large range of domains having different total area, while the ratio between cytoplasmic and nuclear area was kept fix at $10:1$. Our results show that the oscillatory dynamics is the constant response of the system. However the period of oscillations depends on the total volume of the *in silico* cell, see Fig. 6.14(b). For smaller volumes, the period is shorter and it rises with the volume. We observed variations between 55 and 1000 min.

We also analysed how the nuclear:cytoplasmic volume ratio affects the response of

Parameter	Description	Ref. values	values for oscillations
Vol	Total area of the simulations domain	$300\mu m^2$	$Vol > 0(\mu m^2)$
V_r	Volume ratio Cytoplasm:Nucleus	10	$2 \leq V_r \leq 100$
p_i	Protein permeabilities	$10\mu m/\text{min}$	$5 \leq p_i \leq 5000(\mu m/\text{min})$
D_i	Protein diffusion coefficients	$600\mu m^2/\text{min}$	$10 \leq D_i \leq 1000(\mu m^2/\text{min})$

Table 6.2: Parameter ranges of spatial values for which oscillations occurs. Remark: As explained within the text, the ratio "protein diffusion:mRNA diffusion" has been fixed to 100:1. Consistently to this choice also the ratio "protein permeability:mRNA permeability" has been fixed to 100:1. Range of parameters obtained as in Table 5.1.

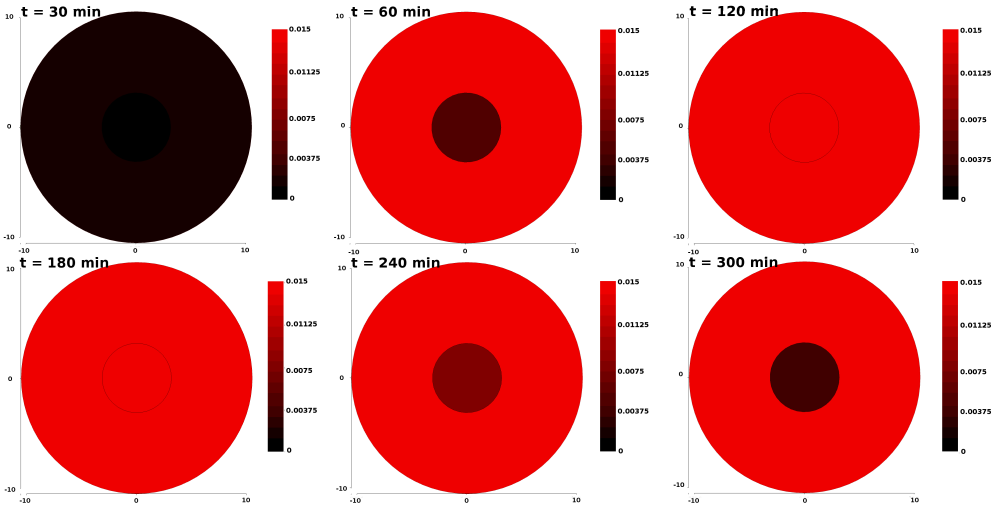

Figure 6.11: Bi-dimensional PDE model. Mdm2 evolution in time and space. As shown in biological experiments, the peak level of Mdm2 follows the peak of p53 [40]. The peak of nuclear Mdm2 takes place at t=2h, while p53 peaks at t=1h. To compare with p53 evolution, see Figure 6.10.

the system. In this case, we fixed the total area to $300\mu m^2$ (Figure 6.9), and we varied the nuclear area. Here again, the temporal dynamics of the system is oscillatory and oscillations do not depends on the volume ratio. The period of sustained oscillations varies between 175 and 400 min. Two or three peaks of p53 level (in the fixed time lapse of 500 minutes) can be observed on Figure 6.15(b) for volume ratios varying between 2 and 100. See Figures 6.14 and 6.15 below and Table 6.2 for more quantitative details.

One can remark that the dynamics of the system is robust as sustained oscillations can be observed over different domains. This information let us speculate that the role of oscillations is crucial for the p53-Mdm2 system. Indeed, even if we change drastically the physical environment, or the cell shape (as we will see in the next section), sustained oscillations are always present.

The geometry of the domain does not change the dynamics of the system.

We analysed the behaviour of the system over different geometric domains: rectangular, elliptic and 'cell-shaped' domains. In accordance with Terry *et al* [132] we conclude that the geometry of the domain does not influence the dynamic response of the system. In Figure 6.16, we reported the cellular domain used in simulations and the corresponding temporal evolution of nuclear and cytoplasmic levels of p53, all three domains having approximately the same area and same volume ratio. As can be seen, the reproduced temporal dynamics of the three systems are the same. Furthermore, the spatial dynamics does not depend on the shape of the domain, as can be observed on Figure 6.18 where we reported the simulations results in two different domains.

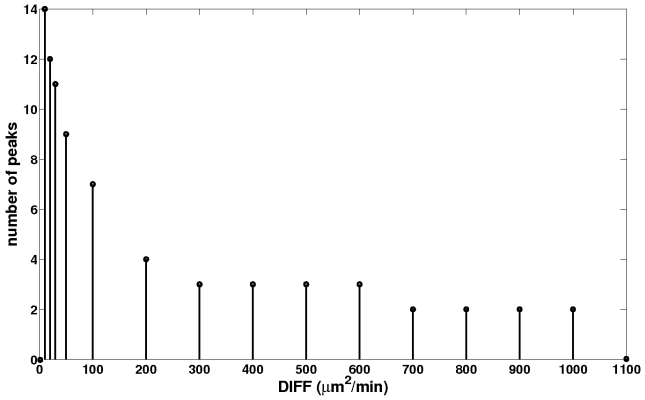

Figure 6.12: 2-dimensional PDE model. Number of peaks of sustained oscillations observed in the fixed time laps of 500 min. On the x-axis the values of the corresponding diffusion coefficient expressed in $\mu m^2/\text{min}$.

We also performed simulations locating the ribosomes, the big protein complexes, scattered within the cytoplasm, that translate the mRNAs into proteins. We designed the spatial distribution of ribosomes in such a way that their total concentration did not change, varying only their location. To do this, we considered different functions defined on the domain of Figure 6.9, all having the same mean. No influence of the ribosome location could be observed and we could conclude that the oscillatory behaviour is robust upon changes on the location of ribosomes. This result differs from [128] where the authors stated that the p53 oscillatory response was dependent on ribosome location. However the same authors in [129], studying the spatial distribution of ribosomes in a more precise spatial setting, observed a lower influence of this location.

Oscillations depends on the localization of the damage signal.

Finally we were interested in understanding whether the location of the damage signal, triggered by ATM, and not only its strength, was responsible of generating the oscillations. To do this, we have changed the equations relative to $p53_p^{(n)}$ and $p53_p^{(c)}$, i.e. $\bar{u}_3^{(n),(c)}$. In a first experiment we have set:

$$\frac{\partial \bar{u}_3^{(n)}}{\partial \tau} = \bar{D}_3 \Delta \bar{u}_3^{(n)} - \bar{k}_{ph} \frac{\bar{u}_3^{(n)}}{\bar{K}_{ph} + \bar{u}_3^{(n)}},$$
$$\frac{\partial \bar{u}_3^{(c)}}{\partial \tau} = \bar{D}_3 \Delta \bar{u}_3^{(c)} + \overline{ATM} \frac{\bar{u}_0^{(c)}}{1 + \bar{u}_0^{(c)}} - \bar{k}_{ph} \frac{\bar{u}_3^{(c)}}{\bar{K}_{ph} + \bar{u}_3^{(c)}}.$$

so that $p53_p$ is *produced* only in the cytoplasm. In a second experiment, we have assumed the opposite, i.e. the damage signal is triggered only in the nuclear compartment. In

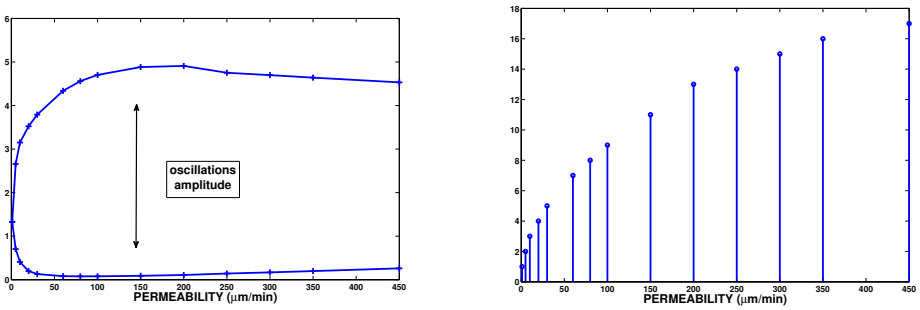

(a) Amplitude of oscillations

(b) Number of oscillations in 500 minutes

Figure 6.13: Bi-dimensional PDE model. Oscillations in the 2-dimensional case. Variations according to the permeability coefficient: in the 2-dimensional domain, undamped oscillations appear for a wide range of permeability values (see Table 6.2). In (a) we plotted the amplitude of oscillations, while in (b) we plotted the number of oscillations in 500 min. The protein to mRNA permeabilty ratio is fixed to 100:1.

this case, the equations for $\bar{u_3}$ write:

$$\frac{\partial \bar{u}_3^{(n)}}{\partial \tau} = \bar{D}_3 \Delta \bar{u}_3^{(n)} + \overline{ATM} \frac{\bar{u}_0^{(n)}}{1+\bar{u}_0^{(n)}} - \bar{k}_{ph} \frac{\bar{u}_3^{(n)}}{\bar{K}_{ph}+\bar{u}_3^{(n)}},$$
$$\frac{\partial \bar{u}_3^{(c)}}{\partial \tau} = \bar{D}_3 \Delta \bar{u}_3^{(c)} - \bar{k}_{ph} \frac{\bar{u}_3^{(c)}}{\bar{K}_{ph}+\bar{u}_3^{(c)}},$$

We left unchanged the corresponding boundary condition on $\Gamma_{1,2}$, that we recall:

$$\frac{\partial \bar{u_3}^n}{\partial \mathbf{n}} = \frac{\bar{p_3}}{\bar{D_3}} \bar{u_3}^c = \frac{\partial \bar{u_3}^c}{\partial \mathbf{n}} \qquad \text{on } \Gamma_{12}.$$

In both cases, no oscillations are observed. It is clear that the concentration of $p53_p$, in the compartment where it is not produced, is very low. Indeed, in both cases, in at least one compartment, the only reaction term for u_3 is of degradation. If p53 is phosphorylated only in the nucleus, its cytoplasmic concentration tends to zero. Indeed, $p53_p$ moves from the cytoplasm to the nucleus but not back. Thus, no boundary sources at all are present. Depending on the location of the signal, $p53_p$ accumulates mostly in the nucleus or in the cytoplasm. However, in both cases a fraction of $p53_p$ reaches the nucleus so that the mdm2 production increases. Anyhow, no oscillations occur and a equilibrium between p53 and Mdm2 concentrations is found. The temporal evolution of the total concentrations, nuclear and cytoplasmic, are plotted in figure 6.17. We have also repeated the same experiments, without considering in one of the compartment, neither the production term for $p53_p$, nor the degradation one. In this way, one of the two equations for $\bar{u}_3$ (nuclear or cytoplasmic), is reduced to a diffusion equation. The results are qualitatively similar to the previous case and no oscillations are observed. These

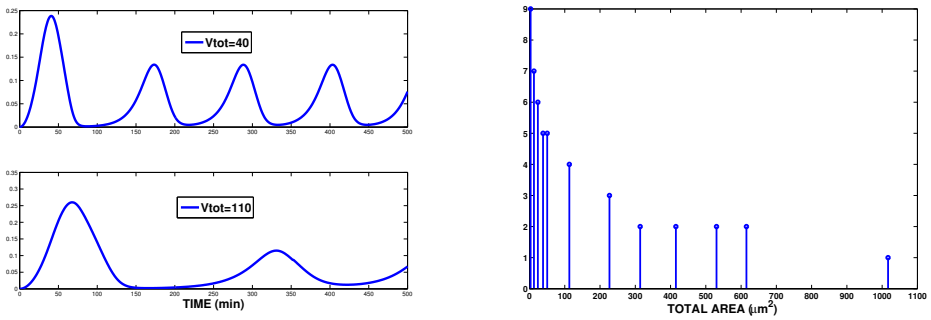

(a) (b)

Figure 6.14: Bi-dimensional PDE model. (a): Oscillations of nuclear p53 (avarage concentrations) for different total volume (V_{tot}) and fixed volume ratio (V_r). (b): number of oscillations occurring in 500 min for different total volumes.

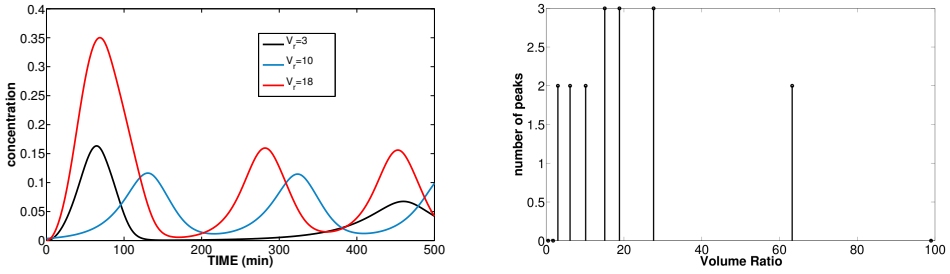

(a) (b)

Figure 6.15: Bi-dimensional PDE model. (a) Oscillations of nuclear p53 (average concentrations) for different volume ratios (V_r) and fixed total area, $V_r = \frac{\text{cytoplasmic area}}{\text{nuclear area}}$. (b): number of oscillations occurring in 500 min for different volume ratio.

results seem to show that oscillations depends on the nuclear import of cytoplasmic p53. In fact, when the damage is triggered in the nucleus, active p53 accumulates and produces the mRNA of Mdm2. Thus, the negative feedback is 'on' and should triggers the oscillations. The fact that it doesn't happened could mean that the import to the nucleus of activated p53 is necessary to cause the oscillations and that an active p53 species exclusively nuclear, is unable to generate an oscillatory behaviour. A deeper understating of these results is clearly needed.

6.5 Summary of the results

In this chapter we studied a new model for p53 which describes both its temporal and spatial dynamics. We were able to reproduce oscillations with the period observed in *in*

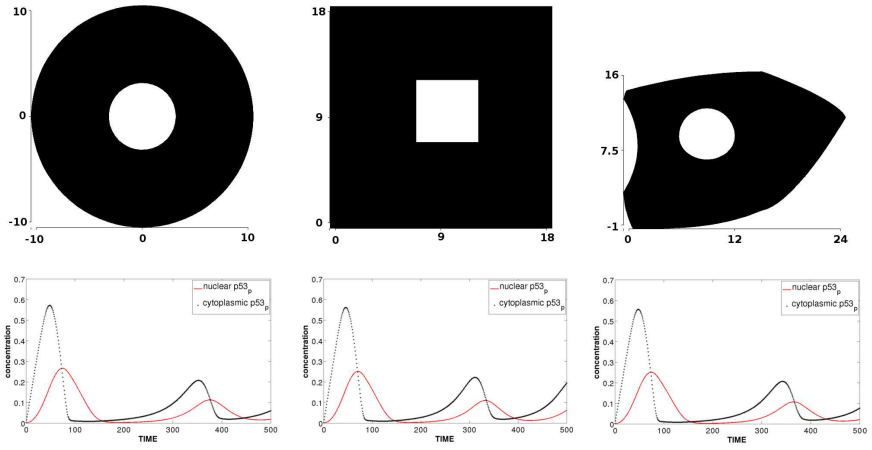

Figure 6.16: Bi-dimensional PDE model. Different simulation domains having the same total volume and same nucleus to cytoplasmic volume ratio, lead to similar oscillatory behaviours of the system.

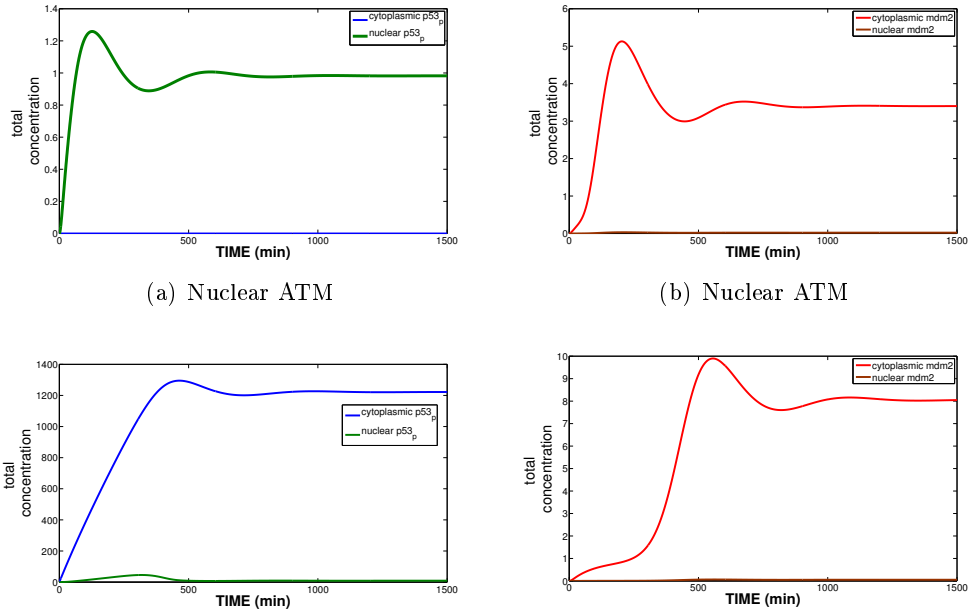

(a) Nuclear ATM

(b) Nuclear ATM

(c) Cytoplasmic ATM

(d) Cytoplasmic ATM

Figure 6.17: (a), (b): nuclear and cytoplasmic total concentrations of $p53_p$ and Mdm2, respectively, as functions of time when ATM is blocked into the nucleus. (c), (d): nuclear and cytoplasmic total concentrations of $p53_p$ and Mdm2, respectively, as functions of time when ATM is blocked into the cytoplasm.

vitro experiments, namely 4 - 5 hours [70], using realistic diffusion coefficients, by the addition of a spatial variable. Moreover we have shown that these oscillations are present for all known values of p53 diffusivity [59] (knowing that p53 mobility is reduced after DNA damage).

We observed that the response of the system strongly depends on the spatial coefficients of the system (diffusion, permeability, total volume of the cell), which points out the significant role of space in the p53 system.

We have also studied how the system responds to variations in permeability coefficients, total volume and nuclear to cytoplasmic volume ratio. We have shown that the oscillatory response is robust towards such variations, and that the period of oscillations depends on the permeability coefficient, and also on the total volume of the cell.

The distinction between nucleus and cytoplasm is the characteristic feature of eukaryotic cells. We think that a model of signal transduction needs to consider this basic and simple distinction in order to be consistent with common knowledge of the intracellular biology and topology.

6.6 Conclusions and Perspectives - Part II

We have proposed a model for p53 nuclear accumulation. We have shown that the negative p53-Mdm2 feedback reproduces the oscillatory behaviour observed in cultured cells, if the distinction between the nuclear and cytoplasmic compartments is taken into account. This implies locating the main cellular processes and making explicit the delays due to transcription, translation and translocation between compartments. Firstly, we have studied the response of the ODE differential system, and we have verified that the dynamics of the network proposed was the expected one. We have reproduced undamped oscillations against ATM variations showing the existence of a Hopf supercritical bifurcation. Then we have introduced a spatial variable and numerically analysed the simulation results in the new PDE setting. Our choice to develop a spatial model of the p53 network has led us to remark that taking into account physiological phenomena within the cellular space explains in biologically relevant details the expected oscillations. We have shown that the experimental diffusion values fit our model and reproduce the oscillatory behaviour with a good estimation of the period observed *in vitro*. We have provided evidence that the oscillatory behaviour of the system is also robust towards variations of the nuclear to cytoplasmic ratio and of cell shapes. This allows us to speculate that such a robust response of the system towards changes in physical coefficients, as cell volume, diffusion coefficient or volume ratios, testifies the crucial role of oscillations in the p53 system.

It is worth nothing that the permeability values that reproduce the physiological behaviour in our model are lower than the values proposed in other works [15, 121]. We believe that, taking into account more signalling pathways involved in the import and export nucleocytoplasmic machinery should permit to consider more realistic permeability values. Indeed, it is known that the translocation rate is given by the nucleocytoplasmic transport machinery [50], and not by the translocation through the nuclear pore com-

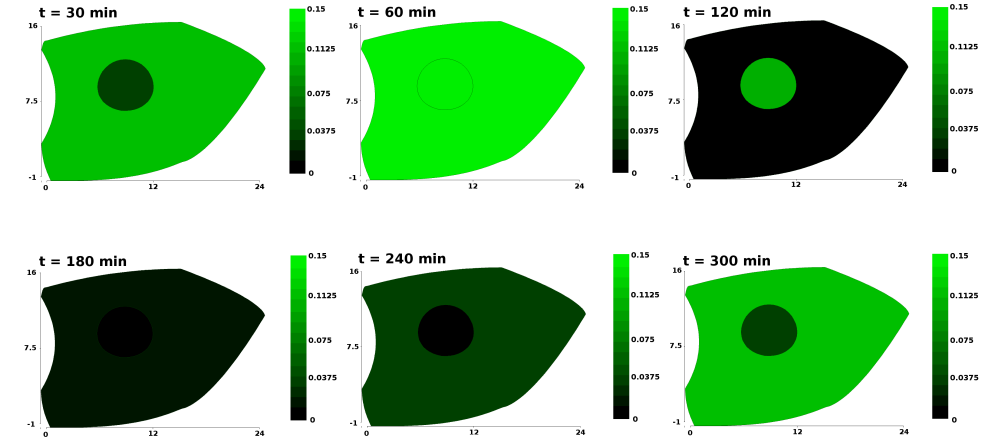

(a)

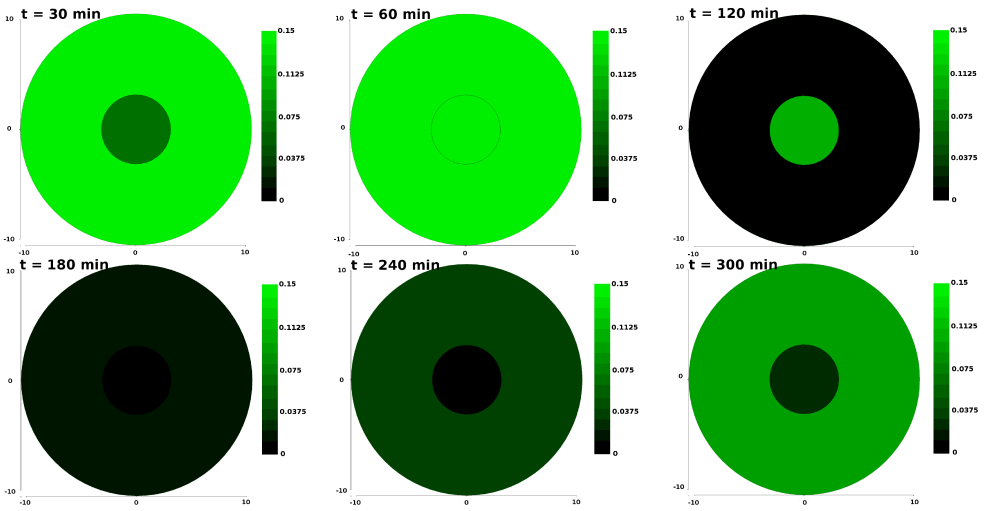

(b)

Figure 6.18: Bi-dimensional PDE model. (a): p53 oscillations in the two-dimensional case: after 30 minutes the concentration of the molecule accumulates in the whole cell. Then the nucleus fills up and the cytoplasmic concentration decreases. The cycle starts again. (b): spatial dynamics of p53 in the reference domain. The spatial and temporal dynamics do not depend on cell shape.

plexes, since the time during which molecules bind to the central region of the nuclear pore is very low [23]. Thus to take into account more realistic transport timing it would be important to couple the model we have designed with the model of nucleocytoplasmic transport studied in [15]. It would also be interesting to model the cytoskeloton activity in the transport mechanism, as done in [129, 15]. It has indeed been shown that p53 uses the microtubule filaments in order to get faster to the nucleus [113, 41]. However, there is still no experimental evidence for a role of microtubules in Mdm2 cytosolic transport.

To conclude on a medically oriented note, the simplicity of the network considered in this work may offer in the future an effective tool to understand the effects of known mutations of p53 with respect to the different mechanisms that we represent in our model, as nuclear import, translation, or phosphorylation. Indeed p53 is known to be mutated in more than 50% of cancer cells and it is a future goal with possible pharmacological and clinical consequences for us to understand how these mutations influence the spatio-temporal dynamics of p53.

Chapter 7

Conclusions and Perspectives

In this thesis we have dealt with the transmission of molecular signals within a cell. In particular we were interested in the exchange of information between the two major compartments of the eukaryotic cells, the nucleus and the cytoplasm. Proteins undergo transformations that have a specific meaning for the cell, and move inside the cell in order to transmit their message to the required location. Often, several proteins and molecules are involved in signal transmission, and long sequence of transformations, e.g. a phosphorylation cascade, is necessary in order to transmit a signal. Therefore, the delivery of a message depends not only on chains of reactions, but also on the distances that molecules have to cover in the intracellular space.

Most of the current models of signal transduction take into account only the first issue: the chemical reactions. Those models focus on the biological networks in order to reproduce the dynamics of the considered system. The use of ordinary differential equations is straightforward, since they are a powerful means that permit to explore the temporal dynamics of complex systems. In this thesis our aim was to consider both the network and the space. On the one hand, we are interested in the physiology of the biological system studied, on the other hand, we wanted to reproduce the spatial dynamics of the networks we considered.

In the first part of the thesis the necessity of dealing with a spatial distribution was crucial. The problem is *spatial* in its own definition. We have proposed a model of transport of proteins along a single microtubule with the aim to evaluate what kind of proteins benefit of motor-assisted transport in their way towards the nucleus. Therefore we have compared the mass flow due to diffusion, by which proteins naturally move, with the flow given by the combined action of the microtubule and the diffusion. We have found that transport towards the nucleus, of proteins having a diffusion coefficient up to $6\mu m^2/s$, is enhanced by the interactions with motor proteins, that allow the attachment to the microtubule. Then, we have coupled our model with a model of nucleo-cytoplasmic transport, proposed in [15], and we have quantified the nuclear accumulation of a generic cargo protein. Our results show that the classical import mechanism is efficient and that the addition of a 'microtubule-bound species' reduces the import rate. This result is quite surprising, since on the one hand, some experimental works show the opposite

result for some specific proteins. On the other hand, the work of Cangiani *et al.* [15], that models in a three-dimensional environment the transport between nucleus and cytoplasm with the addition of microtubules, presents a divergent result, that emphasizes the benefit of microtubule activity. The main difference with our model, that partially explains the difference in the results, is that in [15] the authors consider a vector field that averages the influence of many single microtubules. In our model we have located the microtubule, defining a specific attraction area, that corresponds roughly to the width of a microtubule. The transport on the microtubule is uni-directional and uni-dimensional, while the diffusive particles move in two directions. Moreover, we have defined a diffusive species attached to the motor proteins and a species that is only transported along the filament. In this way we have located spatially all the reactions that are needed to perform microtubule transport at a macromolecular level. It is clear that our understanding of these phenomena is still incomplete and further research will be necessary.

In the second part of this thesis, we have introduced a physiologically based model for the activity of the tumour suppressor protein p53. As a first step, we have studied and analysed the temporal dynamics of the p53 network. The main idea was to separate, using an ODE compartmental model, nuclear and cytoplasmic reactions. We have introduced, for each considered species, its nuclear and cytoplasmic forms. This approach marks the main difference with respect to other existing ODE models in the literature, since it has allowed us to consider the physiological and spatial aspects of the p53 network. For instance, p53 in its active form is able to reach the nucleus, but unable to get out of it. The two compartment model that we have proposed, has allowed us to take into account the directionality of transport. We have analysed this model by a numerical bifurcation analysis. First with respect to the parameter that activates the network usually triggered by DNA damage, for which we have shown the existence of two supercritical Hopf bifurcations that explain the oscillations; then we have considered other possible parameters and analysed the response of the system to their variations. Finally by the addition of a spatial variable, we have studied the behaviour of the system in a PDE form, assuming that all the proteins can diffuse within the cytoplasm and the nucleus. Moreover we added a membrane-like boundary condition (Kedem-Katchalsky condition) between the two compartments in order to model the nuclear envelope. In this setting, we have verified the existence of oscillations, and we have shown that the system is robust with respect to variations of the spatial parameters. We have reproduced the experimental data coming from the literature, showing a nuclear accumulation of p53 half an hour after the damage signal and the periodicity of nuclear and cytoplasmic accumulation already shown in [123]. Finally we have reproduced oscillations occurring at the period experimentally observed. Other works share this approach [129, 132] explaining the temporal oscillations of biological systems using PDE systems of equations. We believe that this is a direction to follow and that the analysis of biological networks must include the treatment of the spatial component.

Both topics covered in this thesis have a broad range of perspectives. Concerning the first part of the thesis, it should be important to extend the model in terms of the geometry of the system. We should consider a domain of the size of a cell, in order

to allow comparisons with data of the literature. Also a comparison with models that use velocity fields, instead of localized microtubules, would be interesting and could explain the difference in the qualitative results of the two types of model. Finally, a more theoretical study could allow us to establish an optimal setting for the use of microtubules, that would depend on the distance between two microtubules (that do not have to congest or overcrowd the cytoplasmic area) and on the size of a cell.

The model of the p53 protein dynamics has possible extensions of different natures. From a mathematical point of view, it would be interesting to consider a three-dimensional environment and test the system in a cell-like domain.

Concerning the extension of the model from a biological point of view, we think that this model should be coupled with a model of nucleo-cytoplasmic transport that should take into account import and export from the nucleus, dependent on the Ran cycles. This would make a more realistic model, but, first of all, it would also allow to study the impact that the variation on the timing of import and export, have on the oscillations. On the other hand, it should allow the analysis of two biological models that explain the stabilization of p53 in the nucleus. In fact, according to some authors [36], the accumulation of p53 in the nucleus is due to a decreased export of the protein from the nucleus. According to other authors [82, 83], the reason why p53 accumulates in the nucleus after DNA damage is the increased import rate triggered by post-translational modifications. Since the import and the export cycles occur on two different time scales, it would be possible to test which of the two mechanisms allows the accumulation of the protein in the observed time, using a mathematical model.

An expansion of the model that would include the mRNA of p53, could allow us to test the latest scientific results of Gajjar *et al.* [39] that show that the interaction between the p53 mRNA and Mdm2 are necessary for p53 stabilization. These observations demonstrate the existence of a direct positive feedback between p53 and Mdm2, which has never been translated into a mathematical model. It would be interesting to analyse the impact of this extension, in terms of the period and the nature of the oscillations.

Finally this model may have medical applications. Since the network of the model is reduced to the essential, simple extensions would permit to study the effects of genetic mutations of p53 on the nuclear accumulation of the protein.

To conclude we remark that a comparison of all our numerical results with a larger set of experimental data would allow to support the validity of our results and it remains a necessary step to fully validate our models.

Bibliography

[1] W. Abou-Jaoudé, D. A. Ouattara, and M. Kaufman. From structure to dynamics: frequency tuning in the p53-mdm2 network i. logical approach. *J Theor Biol*, 258(4):561–577, Jun 2009.

[2] D. Alarcon-Vargas and Z. Ronai. p53-mdm2–the affair that never ends. *Carcinogenesis*, 23(4):541–547, Apr 2002.

[3] R. L. Bar-Or, R. Maya, L. A. Segel, U. Alon, A. J. Levine, and M. Oren. Generation of oscillations by the p53-mdm2 feedback loop: a theoretical and experimental study. *Proc Natl Acad Sci U S A*, 97(21):11250–11255, Oct 2000.

[4] P. Bastiaens, M. Caudron, P. Niethammer, and E. Karsenti. Gradients in the self-organization of the mitotic spindle. *Trends Cell Biol*, 16(3):125–134, Mar 2006.

[5] V. Benoit, A. C. Hellin, S. Huygen, J. Gielen, V. Bours, and M. P. Merville. Additive effect between nf-kappab subunits and p53 protein for transcriptional activation of human p53 promoter. *Oncogene*, 19(41):4787–4794, Sep 2000.

[6] H. C. Berg. *Random Walks in Biology*. Princeton University Press, 1993.

[7] F. R. Bischoff, C. Klebe, J. Kretschmer, A. Wittinghofer, and H. Ponstingl. Ran-gap1 induces gtpase activity of nuclear ras-related ran. *Proc Natl Acad Sci U S A*, 91(7):2587–2591, Mar 1994.

[8] F. R. Bischoff, H. Krebber, E. Smirnova, W. Dong, and H. Ponstingl. Co-activation of rangtpase and inhibition of gtp dissociation by ran-gtp binding protein ranbp1. *EMBO J*, 14(4):705–715, Feb 1995.

[9] F. R. Bischoff and H. Ponstingl. Catalysis of guanine nucleotide exchange on ran by the mitotic regulator rcc1. *Nature*, 354(6348):80–82, Nov 1991.

[10] M. Briani, R. Natalini, and G. Russo. Implicit-explicit numerical schemes for jump-diffusion processes. *Calcolo*, 44:33–57, 2007.

[11] S. A. Burgess, M. L. Walker, H. Sakakibara, P. J. Knight, and K. Oiwa. Dynein structure and power stroke. *Nature*, 421(6924):715–718, Feb 2003.

[12] D. Cai, K. J. Verhey, and E. Meyhöfer. Tracking single kinesin molecules in the cytoplasm of mammalian cells. *Biophys J*, 92(12):4137–4144, Jun 2007.

[13] F. Calabró and P. Zunino. Analysis of parabolic problems on partitioned domains with nonlinear conditions at the interface: Application to mass transfer through semi-permeable membranes. *Mathematical Models and Methods in Applied Sciences (M3AS)*, 16(4):479–501, 2006.

[14] E. M. Campbell and T. J. Hope. Role of the cytoskeleton in nuclear import. *Adv Drug Deliv Rev*, 55(6):761–771, Jun 2003.

[15] A. Cangiani and R. Natalini. A spatial model of cellular molecular trafficking including active transport along microtubules. *J Theor Biol*, Sep 2010.

[16] A. M. Carr. Cell cycle. piecing together the p53 puzzle. *Science*, 287(5459):1765–1766, Mar 2000.

[17] S. Carter, O. Bischof, A. Dejean, and K. H. Vousden. C-terminal modifications regulate mdm2 dissociation and nuclear export of p53. *Nat Cell Biol*, 9(4):428–435, Apr 2007.

[18] V. Chickarmane, A. Ray, H. M. Sauro, and A. Nadim. A model for p53 dynamics triggered by dna damage. *SIAM Journal on Applied Dynamical Systems*, 1:61–78, 2007.

[19] J. Chipuk, U. Maurer, D. R. Green, and M. Schuler. Pharmacologic activation of p53 elicits bax-dependent apoptosis in the absence of transcription. *Cancer Cell*, 4(5):371–81, Nov 2003.

[20] A. Ciliberto, B. Novak, and J. J. Tyson. Steady states and oscillations in the p53/mdm2 network. *Cell Cycle*, 4(3):488–493, Mar 2005.

[21] P. R. Clarke and C. Zhang. Spatial and temporal coordination of mitosis by ran gtpase. *Nat Rev Mol Cell Biol*, 9(6):464–477, Jun 2008.

[22] M. Collister, D. P. Lane, and B. Kuehl. Differential expression of p53, p21waf1/cip1 and hdm2 dependent on dna damage in bloom's syndrome fibroblasts. *Carcinogenesis*, 19(12):2115–20, Dec 1998.

[23] T. Dange, D. Grünwald, A. Grünwald, R. Peters, and U. Kubitscheck. Autonomy and robustness of translocation through the nuclear pore complex: a single-molecule study. *J Cell Biol*, 183(1):77–86, Oct 2008.

[24] A. B. DeLeo, G. Jay, E. Appella, G. C. Dubois, L. W. Law, and L. J. Old. Detection of a transformation-related antigen in chemically induced sarcomas and other transformed cells of the mouse. *Proc Natl Acad Sci U S A*, 76(5):2420–2424, May 1979.

[25] F. A. Derheimer and M. B. Kastan. Multiple roles of atm in monitoring and maintaining dna integrity. *FEBS Lett*, 584(17):3675–3681, Sep 2010.

[26] L. Dimitrio, R. Natalini, and L. Milanesi. A mathematical model for the enhanced cytoplasmic transport - how to get (faster) to the nucleus. In *BIOINFORMATICS*, pages 39–46. SciTePress, Jan. 2011.

[27] C. Dingwall and R. A. Laskey. Nuclear targeting sequences–a consensus? *Trends Biochem Sci*, 16(12):478–481, Dec 1991.

[28] A.-T. Dinh, T. Theofanous, and S. Mitragotri. A model for intracellular trafficking of adenoviral vectors. *Biophys J*, 89(3):1574–1588, Sep 2005.

[29] A.-T. Dinh, T. Theofanous, and S. Mitragotri. Modeling of pattern regulation in melanophores. *J Theor Biol*, 244(1):141–153, Jan 2007.

[30] K. M. Dohoney, C. Guillerm, C. Whiteford, C. Elbi, P. F. Lambert, G. L. Hager, and J. N. Brady. Phosphorylation of p53 at serine 37 is important for transcriptional activity and regulation in response to dna damage. *Oncogene*, 23(1):49–57, Jan 2004.

[31] L. A. Donehower, M. Harvey, B. L. Slagle, M. J. McArthur, C. A. Montgomery, J. S. Butel, and A. Bradley. Mice deficient for p53 are developmentally normal but susceptible to spontaneous tumours. *Nature*, 356(6366):215–221, Mar 1992.

[32] W. F. Doolittle. A paradigm gets shifty. *Nature*, 392(6671):15–16, Mar 1998.

[33] S. Fang, J. P. Jensen, R. L. Ludwig, K. H. Vousden, and A. M. Weissman. Mdm2 is a ring finger-dependent ubiquitin protein ligase for itself and p53. *J Biol Chem*, 275(12):8945–8951, Mar 2000.

[34] L. Feng, T. Lin, H. Uranishi, W. Gu, and Y. Xu. Functional analysis of the roles of posttranslational modifications at the p53 c terminus in regulating p53 stability and activity. *Mol Cell Biol*, 25(13):5389–5395, Jul 2005.

[35] J.-P. Françoise. *Oscillations en Biologie, Analyse qualitative et Modèles*. Springer, 2005.

[36] D. A. Freedman and A. J. Levine. Nuclear export is required for degradation of endogenous p53 by mdm2 and human papillomavirus e6. *Mol Cell Biol*, 18(12):7288–7293, Dec 1998.

[37] D. A. Freedman, L. Wu, and A. J. Levine. Functions of the mdm2 oncoprotein. *Cell Mol Life Sci*, 55(1):96–107, Jan 1999.

[38] D. Fusco, N. Accornero, B. Lavoie, S. M. Shenoy, J. M. Blanchard, R. H. Singer, and E. Bertrand. Single mrna molecules demonstrate probabilistic movement in living mammalian cells. *Curr Biol*, 13(2):161–167, Jan 2003.

[39] M. Gajjar, M. M. Candeias, L. Malbert-Colas, A. Mazars, J. Fujita, V. Olivares-Illana, and R. Fåhraeus. The p53 mrna-mdm2 interaction controls mdm2 nuclear trafficking and is required for p53 activation following dna damage. *Cancer Cell*, 21(1):25–35, Jan 2012.

[40] N. Geva-Zatorsky, N. Rosenfeld, S. Itzkovitz, R. Milo, A. Sigal, E. Dekel, T. Yarnitzky, Y. Liron, P. Polak, G. Lahav, and U. Alon. Oscillations and variability in the p53 system. *Molecular Systems Biology*, 2, 2006.

[41] P. Giannakakou, M. Nakano, K. C. Nicolaou, A. O'Brate, J. Yu, M. V. Blagosklonny, U. F. Greber, and T. Fojo. Enhanced microtubule-dependent trafficking and p53 nuclear accumulation by suppression of microtubule dynamics. *Proc Natl Acad Sci U S A*, 99(16):10855–10860, Aug 2002.

[42] N. W. Goehring, P. K. Trong, J. S. Bois, D. Chowdhury, E. M. Nicola, A. A. Hyman, and S. W. Grill. Polarization of par proteins by advective triggering of a pattern-forming system. *Science*, 334(6059):1137–1141, Nov 2011.

[43] X. Gong, X. Ming, P. Deng, and Y. Jiang. Mechanisms regulating the nuclear translocation of p38 map kinase. *J Cell Biochem*, May 2010.

[44] K. Gordon, I. van Leeuween, S. Lain, and M. Chaplain. Spatio-temporal modelling of the p53-mdm2 oscillatory system. *Math. Model. Nat. Phenom.*, 4(3):97–116, 2009.

[45] D. Görlich. Nuclear protein import. *Curr Opin Cell Biol*, 9(3):412–419, Jun 1997.

[46] D. Görlich, S. Kostka, R. Kraft, C. Dingwall, R. A. Laskey, E. Hartmann, and S. Prehn. Two different subunits of importin cooperate to recognize nuclear localization signals and bind them to the nuclear envelope. *Curr Biol*, 5(4):383–392, Apr 1995.

[47] D. Görlich and I. W. Mattaj. Nucleocytoplasmic transport. *Science*, 271(5255):1513–1518, Mar 1996.

[48] D. Görlich, M. J. Seewald, and K. Ribbeck. Characterization of ran-driven cargo transport and the rangtpase system by kinetic measurements and computer simulation. *EMBO J*, 22(5):1088–1100, Mar 2003.

[49] D. R. Green and G. Kroemer. Cytoplasmic functions of the tumour suppressor p53. *Nature*, 458:1127–1130, April 2009.

[50] D. Grünwald, R. H. Singer, and M. Rout. Nuclear export dynamics of rna-protein complexes. *Nature*, 475(7356):333–341, Jul 2011.

[51] D. D. Hackney. The kinetic cycles of myosin, kinesin, and dynein. *Annu Rev Physiol*, 58:731–750, 1996.

[52] O. Halevy, D. Michalovitz, and M. Oren. Different tumor-derived p53 mutants exhibit distinct biological activities. *Science*, 250(4977):113–116, Oct 1990.

[53] P. Hartman. *Ordinary Differential Equations*. Siam, second edition, 2002.

[54] Y. Haupt, R. Maya, A. Kazaz, and M. Oren. Mdm2 promotes the rapid degradation of p53. *Nature*, 387(6630):296–299, May 1997.

[55] L. He and B. Niemeyer. A novel correlation for protein diffusion coefficients based on molecular weight and radius of gyration. *Biotechnol Prog*, 19(2):544–548, Mar/Apr 2003.

[56] R. Heinrich, B. G. Neel, and T. A. Rapoport. Mathematical models of protein kinase signal transduction. *Mol Cell*, 9(5):957–970, May 2002.

[57] A. Hill. Proceedings of the physiological society. *The Journal of Physiology*, 40:i–vii, 1910.

[58] P. Hinow, C. E. Rogers, C. E. Barbieri, J. A. Pietenpol, A. K. Kenworthy, and E. DiBenedetto. The dna binding activity of p53 displays reaction-diffusion kinetics. *Biophys J*, 91(4):330–342, Jul 2006.

[59] S. Hong, Y.-N. Wang, H. Yamaguchi, H. Sreenivasappa, C.-K. Chou, P.-H. Tsou, M.-C. Hung, and J. Kameoka. Measurement of protein 53 diffusion coefficient in live hela cells using raster image correlation spectroscopy (rics). *J Biomater Nanobiotechnol*, 1(1):31–36, Oct 2010.

[60] W. Hundsdorfer and J. Verwer. *Numerical Solution of Time-Dependent Advection-Diffusion-Reaction Equations*, volume 33 of *Springer Series in Computational Mathematics*. Springer-Verlag, 2003.

[61] A. Inoue, T. Torigoe, K. Sogahata, K. Kamiguchi, S. Takahashi, Y. Sawada, M. Saijo, Y. Taya, S. Ishii, N. Sato, and K. Kikuchi. 70-kda heat shock cognate protein interacts directly with the n-terminal region of the retinoblastoma gene product prb. identification of a novel region of prb-mediating protein interaction. *J Biol Chem*, 270(38):22571–22576, Sep 1995.

[62] O. Kedem and A. Katchalsky. Thermodynamic analysis of the permeability of biological membranes to non-electrolytes. *Biochim Biophys Acta*, 27(2):229–246, Feb 1958.

[63] J. P. Keener and J. Sneyd. *Mathematical physiology*. Springer, second edition, 1998.

[64] B. N. Kholodenko. Spatially distributed cell signalling. *FEBS Lett*, 583(24):4006–4012, Dec 2009.

[65] R. B. Kopito and M. Elbaum. Reversibility in nucleocytoplasmic transport. *Proc Natl Acad Sci U S A*, 104(31):12743–12748, Jul 2007.

[66] T. Krouglova, J. Vercammen, and Y. Engelborghs. Correct diffusion coefficients of proteins in fluorescence correlation spectroscopy. application to tubulin oligomers induced by mg2+ and paclitaxel. *Biophys J*, 87(4):2635–2646, Oct 2004.

[67] Y. A. Kuznetsov. *Elements of Applied Bifurcation Theory*. Springer-Verlag, third edition, 2004.

[68] G. Lahav. The strength of indecisiveness: oscillatory behavior for better cell fate determination. *Sci STKE*, 2004(264):pe55, Dec 2004.

[69] G. Lahav. Oscillations by the p53-mdm2 feedback loop. *Adv Exp Med Biol.*, 641:28–38, Feb. 2008.

[70] G. Lahav, N. Rosenfeld, A. Sigal, N. Geva-Zatorsky, A. J. Levine, M. B. Elowitz, and U. Alon. Dynamics of the p53-mdm2 feedback loop in individual cells. *Nat Genet*, 36(2):147–150, Feb 2004.

[71] N. D. Lakin and S. P. Jackson. Regulation of p53 in response to dna damage. *Oncogene*, 18(53):7644–7655, Dec 1999.

[72] M. H. C. Lam, R. J. Thomas, K. L. Loveland, S. Schilders, M. Gu, T. J. Martin, M. T. Gillespie, and D. A. Jans. Nuclear transport of parathyroid hormone (pth)-related protein is dependent on microtubules. *Mol Endocrinol*, 16(2):390–401, Feb 2002.

[73] D. P. Lane and L. V. Crawford. T antigen is bound to a host protein in sv40-transformed cells. *Nature*, 278(5701):261–263, Mar 1979.

[74] M. F. Lavin and S. Kozlov. Atm activation and dna damage response. *Cell Cycle*, 6(8):931–942, Apr 2007.

[75] M.-S. Liou. A generalized procedure for constructing an upwind-based tvd scheme. *AIAA Paper 87-0355*, 1987.

[76] H. Lodish, A. Berk, S. L. Zipursky, P. Matsudaira, D. Baltimore, and J. Darnell. *Molecular Cell Biology*. W. H. Freeman, 4th edition, 2000.

[77] R. Loughlin, R. Heald, and F. Nédélec. A computational model predicts xenopus meiotic spindle organization. *J Cell Biol*, 191(7):1239–1249, Dec 2010.

[78] L. Ma, J. Wagner, J. J. Rice, W. Hu, A. J. Levine, and G. A. Stolovitzky. A plausible model for the digital response of p53 to dna damage. *Proc Natl Acad Sci U S A*, 102(40):14266–14271, Oct 2005.

[79] S. Ma and R. L. Chisholm. Cytoplasmic dynein-associated structures move bidirectionally in vivo. *J Cell Sci*, 115(Pt 7):1453–1460, Apr 2002.

[80] I. G. Macara. Transport into and out of the nucleus. *Microbiol Mol Biol Rev*, 65(4):570–94, table of contents, Dec 2001.

[81] R. Mallik, D. Petrov, S. A. Lex, S. J. King, and S. P. Gross. Building complexity: an in vitro study of cytoplasmic dynein with in vivo implications. *Curr Biol*, 15(23):2075–2085, Dec 2005.

[82] N. D. Marchenko, W. Hanel, D. Li, K. Becker, N. Reich, and U. M. Moll. Stress-mediated nuclear stabilization of p53 is regulated by ubiquitination and importin-alpha3 binding. *Cell Death Differ*, 17(2):255–267, Feb 2010.

[83] J.-C. Marine. p53 stabilization: the importance of nuclear import. *Cell Death Differ*, 17(2):191–192, Feb 2010.

[84] L. D. Mayo and D. B. Donner. A phosphatidylinositol 3-kinase/akt pathway promotes translocation of mdm2 from the cytoplasm to the nucleus. *Proc Natl Acad Sci U S A*, 98(20):11598–11603, Sep 2001.

[85] J. L. McGrath. Dynein motility: four heads are better than two. *Curr Biol*, 15(23):R970–R972, Dec 2005.

[86] W. E. Mercer, C. Avignolo, and R. Baserga. Role of the p53 protein in cell proliferation as studied by microinjection of monoclonal antibodies. *Mol Cell Biol*, 4(2):276–281, Feb 1984.

[87] A. Mesika, V. Kiss, V. Brumfeld, G. Ghosh, and Z. Reich. Enhanced intracellular mobility and nuclear accumulation of dna plasmids associated with a karyophilic protein. *Hum Gene Ther*, 16(2):200–208, Feb 2005.

[88] J. Meyers, J. Craig, and D. J. Odde. Potential for control of signaling pathways via cell size and shape. *Curr Biol*, 16(17):1685–1693, Sep 2006.

[89] D. Michael and M. Oren. The p53-mdm2 module and the ubiquitin system. *Semin Cancer Biol*, 13(1):49–58, Feb 2003.

[90] N. A. M. Monk. Oscillatory expression of hes1, p53, and nf-kappab driven by transcriptional time delays. *Curr Biol*, 13(16):1409–1413, Aug 2003.

[91] R. Montes de Oca Luna, D. S. Wagner, and G. Lozano. Rescue of early embryonic lethality in mdm2-deficient mice by deletion of p53. *Nature*, 378(6553):203–206, Nov 1995.

[92] Y. Mori, A. Jilkine, and L. Edelstein-Keshet. Wave-pinning and cell polarity from a bistable reaction-diffusion system. *Biophys J*, 94(9):3684–3697, May 2008.

[93] J. Murray. *Mathematical Biology: An Introduction*, volume 3. Springer-Verlag, 2002.

[94] P. Nalbant, L. Hodgson, V. Kraynov, A. Toutchkine, and K. M. Hahn. Activation of endogenous cdc42 visualized in living cells. *Science*, 305(5690):1615–1619, Sep 2004.

[95] G. Naldi, L. Pareschi, and G. Toscani. Hyperbolic relaxation approximation to nonlinear parabolic problems. In I. S. of Num. Math. Birkhauser Verlag Basel, editor, *Proceedings 7th Int. Conf. on Hyperbolic Problems: Theory, Numerics, Application ETH Zurich 1998*, volume 130, page 747756, 1999.

[96] X. Nan, P. A. Sims, P. Chen, and X. S. Xie. Observation of individual microtubule motor steps in living cells with endocytosed quantum dots. *J Phys Chem B*, 109(51):24220–24224, Dec 2005.

[97] F. Nédélec, T. Surrey, and A. C. Maggs. Dynamic concentration of motors in microtubule arrays. *Phys Rev Lett*, 86(14):3192–3195, Apr 2001.

[98] B. Novák and J. J. Tyson. Design principles of biochemical oscillators. *Nat Rev Mol Cell Biol*, 9(12):981–991, Dec 2008.

[99] A. O'Brate and P. Giannakakou. The importance of p53 location: nuclear or cytoplasmic zip code? *Drug Resist Updat*, 6(6):313–322, Dec 2003.

[100] D. A. Ouattara, W. Abou-Jaoudé, and M. Kaufman. From structure to dynamics: frequency tuning in the p53-mdm2 network. ii differential and stochastic approaches. *J Theor Biol*, 264(4):1177–1189, Jun 2010.

[101] M. A. Peletier, H. V. Westerhoff, and B. N. Kholodenko. Control of spatially heterogeneous and time-varying cellular reaction networks: a new summation law. *J Theor Biol*, 225(4):477–487, Dec 2003.

[102] L. Perko. *Differential Equations and Dynamical Systems*. Springer-Verlag, second edition, 1996.

[103] T. Pu, X.-P. Zhang, F. Liu, and W. Wang. Coordination of the nuclear and cytoplasmic activities of p53 in response to dna damage. *Biophys J*, 99(6):1696–1705, Sep 2010.

[104] K. Puszyński, B. Hat, and T. Lipniacki. Oscillations and bistability in the stochastic model of p53 regulation. *J Theor Biol*, 254(2):452–465, Sep 2008.

[105] J. P. Qi, S. H. Shao, J. Xie, and Y. Zhu. A mathematical model of p53 gene regulatory networks under radiotherapy. *Biosystems*, 90(3):698–706, Nov/Dec 2007.

[106] H. R., T. H., and Y. H. Oncoprotein mdm2 is a ubiquitin ligase e3 for tumor suppressor p53. *FEBS Lett*, 420(1):25–7, Dec 1997.

[107] P. Rangamani and R. Iyengar. Modelling spatio-temporal interactions within the cell. *J Biosci*, 32(1):157–167, Jan 2007.

[108] N. C. Reich and A. J. Levine. Growth regulation of a cellular tumour antigen, p53, in nontransformed cells. *Nature*, 308(5955):199–201, Mar 1984.

[109] N. C. Reich, M. Oren, and A. J. Levine. Two distinct mechanisms regulate the levels of a cellular tumor antigen, p53. *Mol Cell Biol*, 3(12):2143–2150, Dec 1983.

[110] R. Reichelt, A. Holzenburg, E. L. Buhle, M. Jarnik, A. Engel, and U. Aebi. Correlation between structure and mass distribution of the nuclear pore complex and of distinct pore complex components. *J Cell Biol*, 110(4):883–894, Apr 1990.

[111] K. Ribbeck and D. Görlich. Kinetic analysis of translocation through nuclear pore complexes. *EMBO J*, 20(6):1320–1330, Mar 2001.

[112] P. Roe. Approximate riemann solver, parameter vectors, and difference schemes. *J. Comp. Phys.*, 43:357–372, 1981.

[113] D. M. Roth, G. W. Moseley, D. Glover, C. W. Pouton, and D. A. Jans. A microtubule-facilitated nuclear import pathway for cancer regulatory proteins. *Traffic*, 8(6):673–686, Jun 2007.

[114] H. Salman, A. Abu-Arish, S. Oliel, A. Loyter, J. Klafter, R. Granek, and M. Elbaum. Nuclear localization signal peptides induce molecular delivery along microtubules. *Biophys J*, 89(3):2134–2145, Sep 2005.

[115] A. R. Sedaghat, A. Sherman, and M. J. Quon. A mathematical model of metabolic insulin signaling pathways. *Am J Physiol Endocrinol Metab*, 283(5):E1084–E1101, Nov 2002.

[116] L. A. Segel and M. Slemrod. The quasi-steady-state assumption: A case study in perturbation. *SIAM Review*, 31(3), 1989.

[117] O. Seksek, J. Biwersi, and A. S. Verkman. Translational diffusion of macromolecule-sized solutes in cytoplasm and nucleus. *J Cell Biol*, 138(1):131–142, Jul 1997.

[118] A. Serafini. *Mathematical models for intracellular transport phenomena.* PhD thesis, Dottorato di Ricerca in Modelli e Metodi Matematici per la tecnologia e la società, Università degli Studi di Roma "Sapienza", 2007.

[119] Y. Shav-Tal, X. Darzacq, S. M. Shenoy, D. Fusco, S. M. Janicki, D. L. Spector, and R. H. Singer. Dynamics of single mrnps in nuclei of living cells. *Science*, 304(5678):1797–1800, Jun 2004.

[120] K.-X. Shu, B. Li, and L.-X. Wu. The p53 network: p53 and its downstream genes. *Colloids Surf B Biointerfaces*, 55(1):10–18, Mar 2007.

[121] A. E. Smith, B. M. Slepchenko, J. C. Schaff, L. M. Loew, and I. G. Macara. Systems analysis of ran transport. *Science*, 295(5554):488–491, Jan 2002.

[122] D. A. Smith and R. M. Simmons. Models of motor-assisted transport of intracellular particles. *Biophys J*, 80(1):45–68, Jan 2001.

[123] V. Solozobova, A. Rolletschek, and C. Blattner. Nuclear accumulation and activation of p53 in embryonic stem cells after dna damage. *BMC Cell Biol*, 10:46, Jun 2009.

[124] M. Stewart. Molecular mechanism of the nuclear protein import cycle. *Nat Rev Mol Cell Biol*, 8(3):195–208, Mar 2007.

[125] J. M. Stommel, N. D. Marchenko, G. S. Jimenez, U. M. Moll, T. J. Hope, and G. M. Wahl. A leucine-rich nuclear export signal in the p53 tetramerization domain: regulation of subcellular localization and p53 activity by nes masking. *EMBO J*, 18(6):1660–1672, Mar 1999.

[126] C. Strambio-De-Castillia, M. Niepel, and M. P. Rout. The nuclear pore complex: bridging nuclear transport and gene regulation. *Nat Rev Mol Cell Biol*, 11(7):490–501, Jul 2010.

[127] J. C. Strikwerda. *Finite Difference Schemes And Partial Differential Equations*. Siam, 2004.

[128] M. Sturrock, A. J. Terry, D. P. Xirodimas, A. M. Thompson, and M. A. J. Chaplain. Spatio-temporal modelling of the hes1 and p53-mdm2 intracellular signalling pathways. *J Theor Biol*, 273(1):15–31, Mar 2011.

[129] M. Sturrock, A. J. Terry, D. P. Xirodimas, A. M. Thompson, and M. A. J. Chaplain. Influence of the nuclear membrane, active transport, and cell shape on the hes1 and p53-mdm2 pathways: insights from spatio-temporal modelling. *Preprint submitted to Bulletin of Mathematical Biology*, 2012.

[130] K. Svoboda and S. M. Block. Force and velocity measured for single kinesin molecules. *Cell*, 77(5):773–784, Jun 1994.

[131] P. Sweeby. High resolution schemes using flux-limiters for hyperbolic conservation laws. *SIAM J. Num. Anal.*, 21:995–1011, 1984.

[132] A. J. Terry and M. A. J. Chaplain. Spatio-temporal modelling of the nf-κb intracellular signalling pathway: the roles of diffusion, active transport, and cell geometry. *J Theor Biol*, 290:7–26, Dec 2011.

[133] A. Veglio, A. Gamba, M. Nicodemi, F. Bussolino, and G. Serini. Symmetry breaking mechanism for epithelial cell polarization. *Phys Rev E Stat Nonlin Soft Matter Phys*, 80(3 Pt 1):031919, Sep 2009.

[134] M. P. Vierboom, S. Zwaveling, B. GMJ, M. Ooms, G. M. Krietemeijer, C. J. Melief, and R. Offringa. High steady-state levels of p53 are not a prerequisite for tumor eradication by wild-type p53-specific cytotoxic t lymphocytes. *Cancer Res*, 60(19):5508–5513, Oct 2000.

[135] S. K. Vogel, N. Pavin, N. Maghelli, F. Jülicher, and I. M. Tolić-Nørrelykke. Self-organization of dynein motors generates meiotic nuclear oscillations. *PLoS Biol*, 7(4):e1000087, Apr 2009.

[136] B. Vogelstein, D. Lane, and A. J. Levine. Surfing the p53 network. *Nature*, 408(6810):307–310, Nov 2000.

[137] K. M. Wagstaff and D. A. Jans. Importins and beyond: non-conventional nuclear transport mechanisms. *Traffic*, 10(9):1188–1198, Sep 2009.

[138] K. B. Wee and B. D. Aguda. Akt versus p53 in a network of oncogenes and tumor suppressor genes regulating cell survival and death. *Biophys J*, 91(3):857–865, Aug 2006.

[139] K. B. Wee, U. Surana, and B. D. Aguda. Oscillations of the p53-akt network: implications on cell survival and death. *PLoS One*, 4(2):e4407, Feb 2009.

[140] X. Wu, J. H. Bayle, D. Olson, and A. J. Levine. The p53-mdm-2 autoregulatory feedback loop. *Genes Dev*, 7(7A):1126–1132, Jul 1993.

[141] D. P. Xirodimas, C. W. Stephen, and D. P. Lane. Cocompartmentalization of p53 and mdm2 is a major determinant for mdm2-mediated degradation of p53. *Exp Cell Res*, 270(1):66–77, Oct 2001.

[142] L. Xu and J. Massagué. Nucleocytoplasmic shuttling of signal transducers. *Nat Rev Mol Cell Biol*, 5(3):209–219, Mar 2004.

[143] Y. Zhang and Y. Xiong. A p53 amino-terminal nuclear export signal inhibited by dna damage-induced phosphorylation. *Science*, 292(5523):1910–1915, Jun 2001.

[144] Z. Zhang and D. Thirumalai. Dissecting the kinematics of the kinesin step. *Structure*, 20(4):628–640, Apr 2012.